Discovery and Development of Small Molecule Adrenomedullin-1 Receptor Antagonists

By:

Robert Anthony Hathway

A thesis submitted in partial fulfilment of the requirements for the degree of Doctor of Philosophy

The University of Sheffield
Faculty of Medicine, Dentistry and Health.
Division of Clinical Medicine (Oncology and Metabolism)

Submission Date

August 2023

Acknowledgements

I would firstly like to say a massive thank you to my excellent supervisors Dr Gareth Richards and Professor Joe Harrity. I feel very privileged to have been given the opportunity to work on this exciting, multi-disciplinary project and your in-depth knowledge of your respective fields has helped me develop into a well-rounded drug discovery scientist. It hasn't always been smooth sailing, especially with the Covid-19 pandemic making the project to be a little stop-start in the beginning, but your support and guidance has always been present throughout, and for that I am grateful. I would further like to thank Professor Tim Skerry for this opportunity and for your contributions and guidance for the project.

A special thanks also goes to Dr Paris Avgoustou for your guidance and patience whilst teaching me, the resident chemist, the practical side of biology. Your knowledge of the assay enabled me to confidently carry it out and you were always around to answer any questions. Additionally, a special thanks goes to Dr Jean-Olivier Zirimwabagabo for helping me settle into the chemistry lab and for being on hand to help with any chemistry based problems. I would also like to express a big thank you to my collaborator and friend Joe Egan. It's been a pleasure working alongside you for the past couple of years and you have made some very valuable contributions to the project in this time. I will look back fondly at the fun times we had, particularly the Schrodinger conference in Lisbon!

A big thank you also goes to my lab mates in both the Department of Chemistry and the Department of Oncology and Metabolism. I would like to say thank you to current Harrity group members Dr Dan Crossley, Wenzheng Gao, Jiaxin Han, Salah Obaida and Nada Elhajj, as well as every former member I've had the privilege of working alongside, for your support and encouragement during my time here. I will miss our random lab/office chats and occasional trips to the pub. Additionally, in the medical school lab, I would like to thank Dr Ameera Jailani and Dr Karan Shah who always went out of their way to help me when I needed it, as well as current PhD students Georgia Taylor-Vine and Josie Cadman for creating a friendly, encouraging environment.

Additionally I would like to thank the EPSRC for funding my PhD, to Sharon Spey for the Mass Spectrometry service and to Dr Craig Robertson for the X-ray diffraction analysis.

Last but certainly not least, I would like to say a big thank you to my family for your unceasing love, encouragement and support, as well as my friends for all the fun times and memories that I will cherish for many years to come. All of you have provided me with positive motivation throughout my PhD which has got me through some challenging days and I genuinely couldn't have done this without you. Finally I would like to express my thanks to anyone who has directly or indirectly lent their knowledge and help in this project.

Abstract

Adrenomedullin (AM) is a potent vasodilatory peptide hormone implicated in many physiological processes, as well as pathophysiological processes such as septic shock. The Adrenomedullin 1 (AM_1) receptor is a heteromeric receptor comprising of a calcitonin-like receptor (CLR), a class B GPCR, and Receptor Activity Modifying Protein 2 (RAMP2). Association of the CLR with RAMP1 and RAMP3 forms the CGRP and AM_2 receptors respectively. It has previously been revealed that AM exerts is vasodilatory properties through signalling from the AM_1 receptor. Therefore, antagonizing this receptor with small molecules can arrest and reverse the dangerously low blood pressure levels observed in septic shock patients. Therefore the aim was to develop the first potent small molecule AM_1 antagonist

The initial strategy involved designing compounds based on antagonists previously discovered for AM_2 and CGRP, by keeping the CLR binding motif but modifying the RAMP binding motif to target RAMP2 residues. None of the compounds produced using this strategy showed any significant AM_1 activity.

A high throughput screening generated a series of hit compounds, from which a promising, potent lead compound, SHF1556, was discovered (IC50 = 100 nM). The more active enantiomer of this compound has been successfully isolated and identified. The compound displays modest selectivity over the CGRP and AM_2 receptors. SAR studies on the compound identified the sulfoxide and nitro groups to be crucial to the activity of the compound, enabling room for further optimisation of the structure.

Studies have also revealed a lower molecular weight fragment of the lead compound, SHF1572 which retains the majority of the potency. SAR on this compound has revealed the nitrile group to be important to potency, whilst the selectivity over CGRP and AM_2 has improved compared to SHF1556.

In conclusion, a promising lead AM_1 antagonist has been discovered displaying sub-micromolar potency, with plenty of opportunity to optimise the structure and to increase the potency. The *in vivo* efficacy of this compound will be evaluated.

Table of Content

List of Figures

Chapter 1

Chapter 2

Chapter 3

Chapter 4

Chapter 5

Chapter 6

List of Tables

Chapter 1

Chapter 2

Chapter 3

Chapter 4

Chapter 5

Chapter 7

List of Schemes

Chapter 2

Chapter 3

Chapter 4

Chapter 5

Abbreviations

ADME: Absorption, Distribution, Metabolism, Excretion

Ala: Alanine

AM: Adrenomedullin

AM_1: Adrenomedullin-1

AM_2: Adrenomeduulin-2

AMY: Amylin

Arg: Arginine

Asn: Asparagine

Asp: Aspartic Acid

ATP: Adenosine Triphosphate

BRET: Bioluminescence Resonance Energy Transfer

BSA: Bovine Serum Albumin

cAMP: Cyclic Adenosine Monophosphate

CGRP: Calcitonin Gene Related Peptide

CHO-K1 – Chinese Hamster Ovary Cells

CLR: Calcitonin-like Receptor

CRHR1: Corticotropin-releasing Hormone Receptor 1

Cryo-EM: Cryogenic Electron Microscopy

CT: Calcitonin

CTR: Calcitonin Receptor

Cys: Cysteine

DCC: *N*-*N*'-Dicyclohexylcarbodiimide

DG: Diglycerol

DMAP: 4-Dimethylaminopyridine

DMF: Dimethylformamide

DMSO: Dimethyl Sulfoxide

DNA: Deoxyribonucleic Acid

EC50: Half Maximal Excitation Concentration

ECD: Extracellular Domain

ECL: Extracellular Loop

ELF: European Lead Factory

ER: Endoplasmic Reticulum

FBS: Foetal Bovine Serum

GCGR: Glucagon Receptor

GDP: Guanosine Diphosphate

Glu: Glutamic Acid

Gly: Glycine

GPCR: G Protein-coupled Receptor

GTP: Guanosine Triphosphate

HATU: Hexafluorophosphate Azabenzotriazole Tetramethyl Uronium

HBSS: Hanks Balanced Salt Solution

HEPES: 4-(2-hydroxyethyl)-1-piperazineethanesulfonic acid

His: Histidine

HPLC: High Performance Liquid Chromatography

HRMS: High Resolution Mass Spectrometry

HTS: High Throughput Screening

IBMX: 3-isobutyl-1-methylxanthine

IC50: Half Maximum Inhibitory Concentration

ICL: Intracellular Loop

Ile: Isoleucine

IMD: Intermedin

IP_3: Inositol Triphosphate

K_i: Inhibition Constant

LC-MS: Liquid Chromatography-Mass Spectrometry

Leu: Leucine

Log P: Partition Coefficient

Lys: Lysine

mCPBA: meta-Chloroperoxybenzoic Acid

Met: Methionine

mRNA: Messenger Ribonucleic Acid

NMM: *N*-methylmorpholine

NMR: Nuclear Magnetic Resonance

PBS: Phosphate Buffered Saline

PDB: Protein Data Bank

Phe: Phenylalanine

PIP_2: Phosphatidylinsositol

PKA: Protein Kinase A

PKC: Protein Kinase C

Pro: Proline

RAMP: Receptor Activity Modifying Protein

RNA: Ribonucleic Acid

RT: Room Temperature

SAR: Structure Activity Relationships

SEM: 2-(trimethylsilyl)ethoxymethyl

Ser: Serine

STAB: Sodium Triacetoxyborohydride

TM: Transmembrane

TMD Transmembrane Domain

Thr: Threonine

TLC: Thin Layer Chromatography

TPSA: Topological Polar Surface Area

TR-FRET: Time-resolved Fluorescent Resonance Energy Transfer

Trp: Tryptophan

Tyr: Tyrosine

UV: Ultraviolet

Val: Valine

VIPR1: Vasoactive Intestinal Polypeptide Receptor 1

VIPR2: Vasoactive Intestinal Polypeptide Receptor 2

Amino Acid Single Letter Abbreviations

A: Alanine	C: Cysteine
D: Aspartic Acid	E: Glutamic Acid
F: Phenylalanine	G: Glycine
H: Histidine	I: Isoleucine
K: Lysine	L: Leucine
M: Methionine	N: Asparagine
P: Proline	Q: Glutamine
R: Arginine	S: Serine
T: Threonine	V: Valine
W: Tryptophan	Y: Tyrosine

Chapter 1 - General Introduction

Chapter 1: General Introduction

1.1 Introduction to Sepsis

Sepsis, or systemic inflammatory response syndrome, is a life-threatening inflammatory syndrome caused by a dysregulated host immune response to a bacterial, fungal or viral infection (Singer, Deutschman et al., 2016). Septic shock is an extreme case of this, defined by increased lactate levels and vasopressor requirement to maintain sufficient blood pressure levels. The pathogenesis of sepsis is complex, but one of the hallmarks is the dysfunction of the vascular endothelium, a protective barrier involved in the maintenance of vascular integrity (Ince, Mayeux et al., 2016) The extreme inflammatory response causes the dysfunction of the vascular endothelium, which leads to endothelial cell death and loss of vascular resistance (Angus and van der Poll, 2013). This result is an edema, a dramatic decrease in blood pressure and subsequent organ failure, leading to a high mortality rate (Gotts and Matthay, 2016). Despite the pathogenesis of sepsis being relatively well understood, there is currently a lack of a single, effective therapy (Geven, Kox et al., 2018). Therefore there is a great need for new therapeutic options to treat this syndrome.

1.2 General introduction to Adrenomedullin and CLR/RAMP Receptors

1.2.1 Adrenomedullin and Calcitonin Peptide Family

Adrenomedullin (AM) is a 52 amino acid residue containing peptide. It is a potent vasodilator and is expressed in the human body as a paracrine hormone, mainly in endothelial cells and vascular smooth muscle cells, meaning high concentrations are found in the placenta, lungs, heart and kidneys (Lenhart and Caron, 2012). AM was first discovered in 1993 by Kitamura et al. in human pheochromocytoma (*Kitamura, 1993*). Upon its discovery it was suggested that this new peptide was involved in blood pressure control and indicated a novel system for circulation control. It has since been found that AM is also linked to a variety of biological processes.

AM is encoded in humans by a gene in chromosome 11, consisting of 4 exons and 3 introns (Ishimistsu, 1994). Translation of AM mRNA initially leads to the synthesis of an 185 amino acid peptide known as preprohormoneAM (preproAM) (Beltowski, 2004). Cleavage of a 21 amino acid N-terminal signalling peptide from this structure leads to an 164 amino acid peptide known as proAM (Kitaruma, 1994). ProAM is then converted to mature AM by conversion of proAM to a glycine extended 53 amino acid (Nagatomo, 1996), before enzymatic amidation converts to the mature 52 amino acid peptide.

AM is a member of the calcitonin peptide family, which also includes peptides such as Calcitonin Gene Related Peptide (CGRP) (alpha and beta), Amylin (AMY) Calcitonin (CT) and Adrenomedullin 2/Intermedin (IMD) (Hay and Pioszak, 2016). The CGRP family of peptides are grouped together despite showing limited sequence homology. As they cannot be grouped by amino acid sequence, they are instead grouped by similarities in secondary structure (Figure **1.1**). These structural similarities includes a cyclic peptide formed by a single intramolecular disulphide bond at the N-terminus of each member of the CGRP family, an α-helical conformation with a C-terminus structured around a β-turn and a C-terminal amide (Hay, Garelja et al., 2018). The peptides in this family are between 32-52 amino acids long, with AM and AM2 being the largest members.

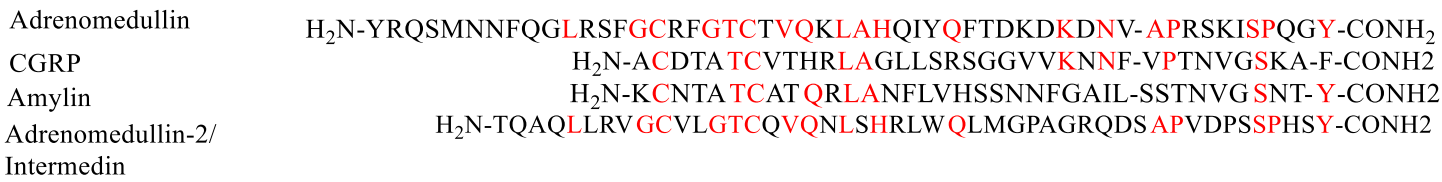

Figure 1.1 – Amino acid sequences of Adrenomedullin (AM), Calcitonin gene-related peptide (CGRP), Amylin and Adrenomedullin-2/intermedin. Residues highlighted in red indicate common amino acid residues within two or more of the peptides.

1.2.2 Physiological properties of AM

As mentioned above, one of the first discovered effects of AM was it's role in blood pressure control. AM is a potent vasodilator, with these effects predominantly as a result of AM binding to its receptors on endothelial cells and vascular smooth muscle cells (Kitaruma, 1993). AMs role in decreasing blood pressure have been shown *in vitro*, demonstrating

vasodilation of blood vessels and organs (Passaglia, Gonzaga et al., 2014), and *in vivo* in which direct AM infusion saw a decrease in blood pressure and a compensatory increase in cardiac output in various mammalian species (Lainchbury, 2000). AM can induce it's effects either directly on vascular smooth muscle cells by reducing intracellular calcium levels via a cAMP/Protein Kinase A pathway (Yoshimoto, Mitsui-Saito et al., 1998) or via the endothelium from the release of nitric oxide (NO) from the phosphatidylinositol-4.5-biphosphate 3 protein kinase B (PI3K/Akt) pathway (Shimikake, 1995).

AM also plays a key role in endothelial barrier protection, which is a single cell vascular barrier that makes up the inner layer of all blood vessels. AM is crucial for endothelial barrier stability and integrity, with knockout studies deleting parts of the AM signalling pathway showing the development of lethal hydrops fetalis (Dackor, Fritz-Six et al., 2006). Further studies in which AM production from endothelial cells was deleted, increased vascular permeability was observed, resulting in edema formation. The cAMP/PKA pathway has been shown to play a huge role in AM-induced endothelial protection, resulting in the inhibition of RhoA GTPase (Eguchi, Hirata et al., 1994).

Other physiological roles of AM include that in the cardiovascular system. From models of hypertension and myocardial infarction, it was shown that AM production from cardiac ventricles and atria is induced during these conditions, and further *in vitro* studies have shown that AM release from these cells can act in a paracrine or autocrine manner to supress fibroblast proliferation (Tsuruda et al., 1999) Studies using rat models for conditions such as myocardial infarction showed that AM can decrease the mortality rate of these diseases as well as inhibit deterioration of cardiac function, implying a role for AM in protection of the heart studies.

1.2.3 Role of AM in Pathophysiology

AM levels in plasma are shown to increase during the onset of tumours, and is strongly upregulated in several different tumour types, especially in hypoxic conditions (Hay et al., 2011; Ishikawa et al., 2003). Increased levels of AM do not lead to cancer but can lead to its pathogenesis. It can do this by stimulating cell growth and inhibiting apoptosis in tumour cells. AM can also alter the phenotype of some cells, causing them to exhibit tumourigenic behaviour. In addition, AM promotes blood and lymphatic angiogenesis of tumours, providing materials to allow tumours to spread such as oxygen and nutrients, and can even

reduce the ability of the immune system to destroy tumours by protecting them from immune surveillance (Garayoa et al., 2000). Studies have shown that AM antagonists can significantly reduce the in vivo growth of pancreatic cells (Ishikawa et al., 2003), indicating that lowering AM levels can lead to a reduction in the size and mass of tumours.

In addition to the role of AM in tumour progression, large increases of AM are observed in patients with sepsis. A sepsis response is triggered by circulating bacteria in the bloodstream by triggering a systematic inflammatory response syndrome (SIRS) in blood vessels. The highest increases of plasma AM levels in the body occur during sepsis, with AM levels up to 40-fold higher than normal values (Gibbons et al., 2007). AM is linked to the immune response observed in sepsis and has been found to be beneficial in the early hyperdynamic stage. Experiments involving AM-overexpressing mice have shown that AM can provide anti-inflammatory and bactericidal effects due to it's vasodilatory properties, as well as limit hypoxic injury of tissues (Allaker et al., 1999; Isumi et al., 1999). It has also been shown that AM even displays antimicrobial properties, with studies displaying AMs ability to inhibit bacterial growth *in vitro*. However, due to the hemodynamic properties of AM, it is also involved in decreased peripheral vascular resistance in the hypodynamic phase of sepsis, causing increased vascular permeability and vasodilation, leading to organ failure (Wang et al., 1998). Therefore care must be taken when using antagonists such as AM(22-52) therapeutically, as the pharmacological effects might not always be beneficial depending on the phase of sepsis (Hyvelin et al., 2001).

1.2.4 G Protein Coupled Receptors

G protein-coupled receptors (GPCRs) are a family of membrane proteins that are the largest in the human genome and have emerged as one of the primary classes of drug targets (Alexander et al., 2017). The GPCR family all share a common structure, consisting of a 7-transmembrane polypeptide helix containing an extracellular N-terminus and an intracellular C-terminus. The transmembrane domains are linked by three intracellular loops and three extracellular loops (Hauser et al., 2017) (Figure **1.2**).

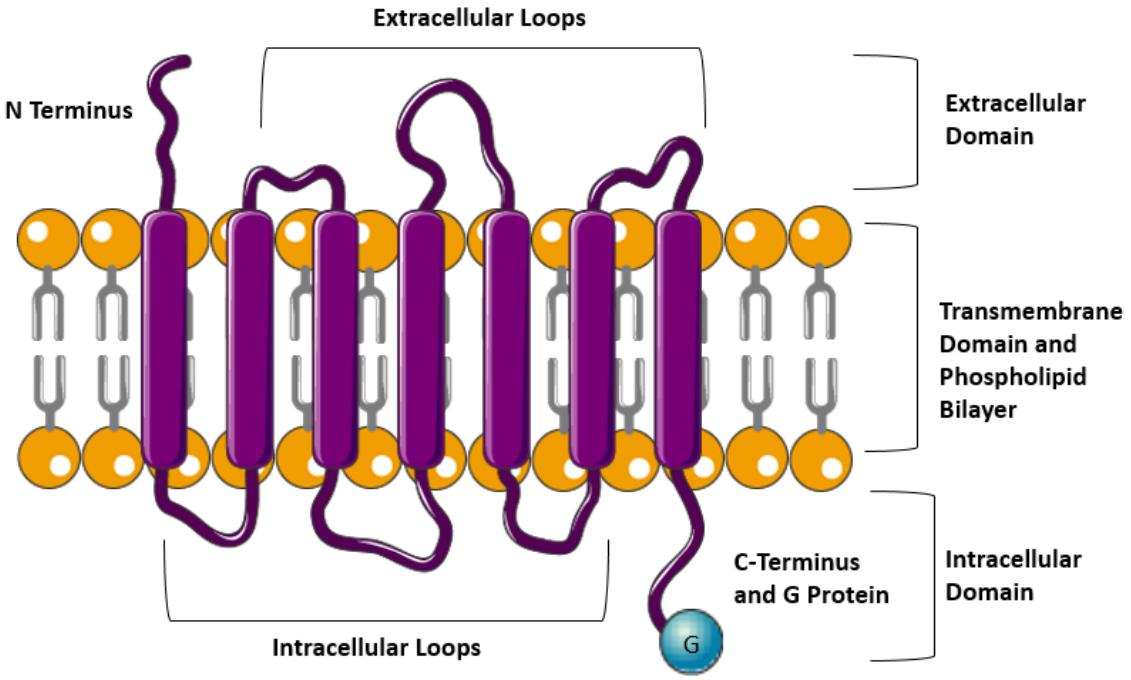

Figure 1.2 General Structural Features of GPCRs. The extracellular, transmembrane and intracellular domains are outlined. The N-terminus, C-terminus and G-protein are annotated. Image created using Sevier Medical Art under the creative commons licence.

There are six different classes of GPCR, and they are categorised on the basis of their sequence homology (Frderiksson, 2003). Class A GPCRs are known as the rhodopsin family. Receptors in this family are also divided into various sub groups but all rhodopsin GPCRs contain relatively short N-terminal domains and respond to agonist ligands such as small molecules, peptides and glycoproteins (Tuteja, 2009). Class B GPCRs are known as the secretin family. These receptors are activated by medium-length peptide ligands (between 27-141 amino acid residues) (Tuteja, 2009). Class C GPCRs are known as the glutamate family. The glutamate family contains a large orthosteric N-terminal binding domain, with some receptors in this family additionally containing an allosteric binding site within the 7-transmembrane domain. Other GPCR families include the adhesion family, which are often involved in controlling processes such as cell migration (Lagerstorm, 2008), and the Fzd family, which are crucial to cell proliferation and embryonic development (Tuteja, 2009).

GPCRs are activated by external peptides such as peptide hormones or nerotransmitters. Agonist binding to a GPCR results in a conformational change, which activates the G protein and enables the GDP molecule to be exchanged for guanine triphosphate (GTP). This causes the G protein to split into two subunits: a single α subunit and a βγ dimer. The α subunit can then initiate various signalling pathways (Figure **1.3**).

One of the key mechanisms of the activation of GPCRs is the increase in concentrations of intracellular cyclic adenosine monophosphate (cAMP) from a $G_{\alpha\text{-}s}$ pathway, during which the $G_{\alpha\text{-}s}$ unit allosterically activates the enzyme adenylyl cyclase which catalyses the conversion of adenosine triphosphate (ATP) into cAMP. cAMP can then go on to activate protein kinase A (PKA) which can result in the activation of transcription factors, leading to the expression of particular genes (Wu, Yeerna et al., 2019) (Figure **1.3**). Detection of cAMP in biochemical assays is a commonly used method to study class B GPCRs in more detail. Physiological functions resulting from the $G_{\alpha\text{-}s}$ protein include the synthesis of estrogen and progesterone, as well as contractility in the cardiovascular system (Syrovatkina, Alegre et al., 2016).

Alternatively, if the $G_{\alpha\text{-}i}$ pathway is activated the production of cAMP is hindered, inhibiting the signalling pathway (Figure **1.3**). $G_{\alpha\text{-}i}$ control the opening of ion channels, as well as activate phospholipases and phosphodiesterases (Wu, Yeerna et al., 2019). Physiological functions of this pathway also include cardiac activation, as well as regulation of immune cells and renal function (Syrovatkina, Alegre et al., 2016).

Another major signalling pathway for GPCRs include the $G_{\alpha\text{-}q}$ pathway, which leads to activation or inactivation of phospholipase C depending on the $G_{\alpha\text{-}q}$ subtype. When activated, phospholipase C catalyses the hydrolysis of phosphatidylinsositol diphosphate (PIP_2) into diclycerol (DG) and inositol triphosphate (IP_3), both of which act as secondary messengers. DG can then go on to activate protein kinase C, whilst IP_3 can open calcium ion channels to increase intracellular Ca^{2+} (Wu, Yeerna et al., 2019) (Figure **1.3**). Physiological functions of this pathway include platelet activation and insulin secretion by β-cells (Syrovatkina, Alegre et al., 2016).

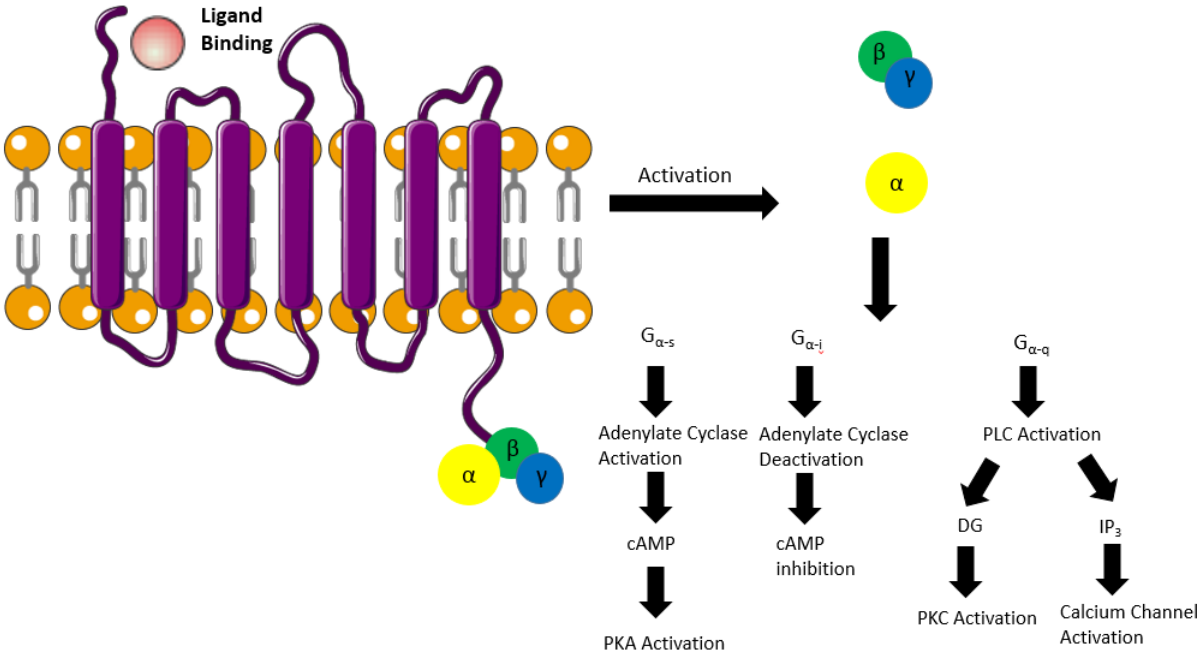

Figure 1.3 – Basic signal pathways resulting from the activation of GPCRs. Activation of GPCRs causes the G-protein α subunit to dissociate from the βγ dimer. A signalling cascade is induced depending on the nature of the α subunit. The various signalling pathways are highlighted. Image created using Sevier Medical Art under the creative commons licence

The C-terminal tail of an active GPCR can be phosphorylated by GPCR kinases (GRKs). This phosphorylated C-terminal region can then be bound by adapter/signalling molecules known as β-arrestins. Binding of β-arrestins to GPCRs primarily "switch off" G-protein signalling, and thus can be involved in mediating signalling cascades resulting from GPCR activation. Arrestins can additionally promote GPCR trafficking and internalisation pathways, as well as initiate alternative signalling pathways (Gurevich and Gurevich, 2019).

1.2.5 Introduction to CLR/RAMP receptors

Receptor activity modifying proteins (RAMPs) are single transmembrane spanning proteins. They were first identified by McLatchie et al in 1998, resulting from an expression cloning strategy when identifying the receptor which is activated by the CGRP peptide. (McLatchie, 1998). There are three known RAMPs in existence, RAMP1, RAMP2 and RAMP3, and are characterised by structured extracellular N-termini and short intracellular C-terminal tails. There are currently 46 GPCRs which are known to couple to a RAMP, and coupling of GPCRs to RAMPs can have profound effects on their pharmacology, including ligand selectivity,

GPCR trafficking and G protein signalling. The effects of RAMP coupling to selective GPCRs are summarised in Table **1.1**.

Table 1.1 – Selected GPCRs known to interact with RAMPs and the effects of these interactions

GPCR	RAMP Interactions	Effects	Reference
CLR (CGRP, AM_1, AM_2)	RAMP1-3	Receptor trafficking and modulation of ligand pharmacology	(McLachtlie, 1999)
CTR (AMY_1, AMY_2, AMY_3)	RAMP1-3	Modulation of ligand pharmacology	(Poyner, 2002)
VIPR1	RAMP1-3	Modulation of receptor signalling	(Christopoulos, Christopoulos et al., 2003)
VIPR2	RAMP1-3	Modulation of receptor signalling	(Wootten, Lindmark et al., 2013)
GCGR	RAMP2	Modulation of ligand pharmacology	(Weston, Lu et al., 2015)
CRHR1	RAMP2	Receptor trafficking and modulation of receptor signalling	(Wootten, Lindmark et al., 2013)
Secretin	RAMP3	Receptor trafficking	(Harikumar, Simms et al., 2009)

As mentioned above, the calcitonin-like receptor (CLR) is a class B GPCR. The 7 transmembrane CLR domains can form a heteromeric receptor by coupling to a single receptor activity modifying protein (RAMP) (Hay & Pioszak, 2016). The co-expression of the CLR with RAMP1 gives the CGRP receptor (Figure **1.4**). The CGRP receptor is stimulated by the CGRP peptide, although other Calcitonin family peptides have also been shown to bind to this receptor (Weston, Winfield et al., 2016) (Table **1.2**). CGRP binding to the CGRP receptor has been implicated in blood flow regulation and pain modulation, whilst research has shown that CGRP receptor stimulation has a primary role in migraine stimulation (Hansen, Hauge et al., 2010).

Co-expression of CLR with RAMP2 and RAMP3 give the adrenomedullin receptors AM_1 and AM_2, respectively (Figure **1.4**). The AM_1 receptor is primarily stimulated by the AM peptide, although other Calcitonin family peptides including CGRP, AMY, and CT can also bind here with relatively strong affinity (Table **1.2**). The AM_2 receptor is also primarily stimulated by AM, although IMD has been shown to bind with almost equal affinity for this receptor (Table **1.2**). AM signalling through AM_1 and AM_2 has shown to be implicated in promoting vascular integrity, angiogenesis and many other physiological processes mentioned above. The AM receptors, however, have been implicated in tumour development.

It has been shown that receptor coupling to the RAMPs is crucial for cell surface expression of the CLR, and therefore can't function as a receptor on its own. The RAMPs can additionally be linked to the calcitonin receptor (CT), to form amylin receptors AMY_1, AMY_2 and AMY_3 when the CT is linked to RAMP1, RAMP2 and RAMP3, respectively (Hargreaves & Olesen, 2019). It is also worth noting that the CT receptor doesn't require RAMPs for cell surface expression and can function independently as a GPCR, highlighting the complexity of the effects RAMP coupling has on GPCR pharmacology.

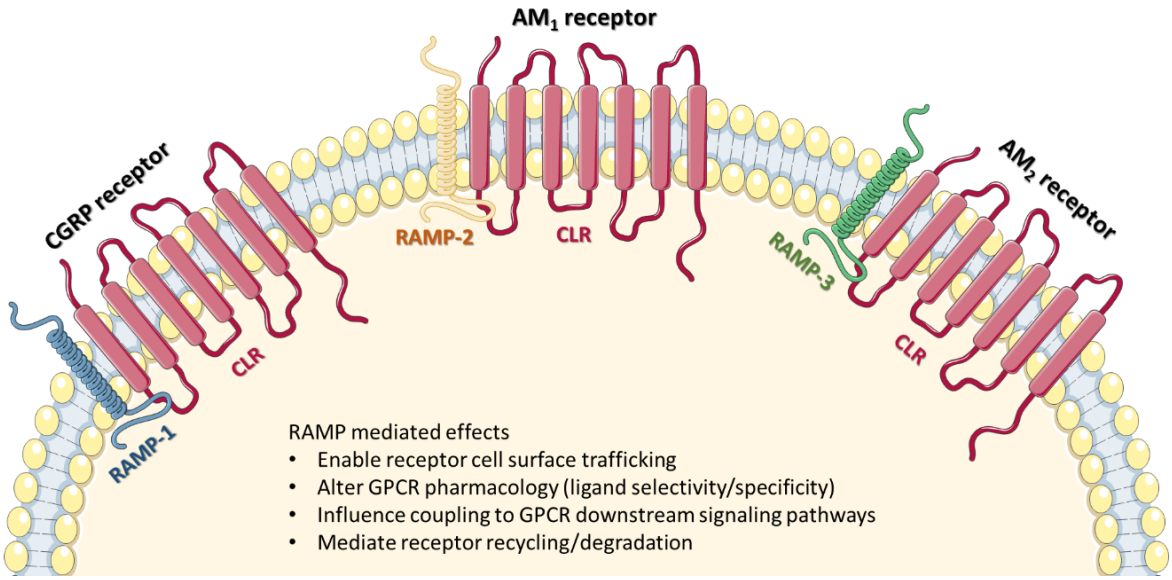

Figure 1.4 – Composition and classification of CLR/RAMP receptors. Combination of CLR with RAMP1 (blue) forms the CGRP receptor, CLR and RAMP2 (yellow) forms the AM_1 receptor and CLR/RAMP3 (green) forms the AM_2 receptor. The three different RAMPs forms three pharmacologically different receptors and RAMP mediated effects are summarised. Image taken from Avgoustou, 2020.

Table 1.2 – Rank order of potency of Calcitonin family peptides on CLR/RAMP receptors. Data from Hay et al, 2018 Weston et al, 2016 and Moore and Salvatore, 2012.

Receptor	Composition	Rank order of agonist potency
CGRP	CLR-RAMP1	αCGRP > AM, AM2 > AMY > CT
AM_1	CLR-RAMP2	AM > AM2 > αCGRP > AMY > CT
AM_2	CLR-RAMP3	AM, AM2 > αCGRP > AMY > CT

1.3 Structural Characteristics of CLR/RAMP receptors

1.3.1 Structural Characteristics of RAMPs

The crystal structure of the RAMP1 extracellular domain (ECD) was resolved by Kusano et al in 2008. The protein consists of 3 α-helices (α1-3), with a 3_{10} helix between α1 and α2 (Figure **1.5**). The helices are arranged in a three helix bundle, with the α2 helix aligned in an antiparallel manner relative to α1 and α3. An interesting feature in the α1 helix is that the structure contains a "kink" at the Leu39 position (Kusano, Kukimoto-Niino et al., 2008). As a result, there is an absence of an expected hydrogen bond between the carbonyl group of Leu39 and the Gln43 amino group. Further abnormal hydrogen bonds around Leu39 include those between the Leu36 carbonyl and Leu41 amino, Arg37 carbonyl and Thr42 amino, and Glu38 carbonyl and Thr42 sidechain.

There are three disulfide bonds within the structure; between Cys40 and Cys72 between α1 and α2, Cys57 and Cys104 connecting the α1-α2 loop to the C-terminus, and Cys27-Cys82 connecting the N-terminus to the α2-α3 loop (Figure **1.5**). The Cys40-Cys72 and Cys57-Cys104 disulfide bonds have been shown to be crucial for stabilisation of the RAMP1 structure, with individual alanine mutations of these residues impairing expression of the CLR:RAMP1 dimer at the cell surface (Kuwasako, Kitamura et al., 2003) (Simms, Hay et al., 2006). It is thought that the Cys40-Cys72 disulfide bond also stabilises the kink at Leu39 in the α1 helix. Additionally, there are hydrophobic interactions between Tyr32, Leu35, Leu41,

Phe44, Met48, and Val51 in the α1 helix and Val89, Phe92, Phe93, Val96, Tyr100 and Phe101. It is likely that these interactions also play a role in structure stabilisation.

The electrostatic potential of the RAMP1 ECD revealed a hydrophobic patch in the concave area between α2 and α3, consisting of the residues Phe93, His97, Tyr100 and Phe101. This patch is highly conserved across all three RAMPs. Mutagenesis studies on these residues have shown that aniline substitution has lead to a significant loss of cell surface expression and CGRP binding (Kuwasako, Kitamura et al., 2003), suggesting that these residues form a binding interface with the CLR ECD. This is backed up by previous modelling studies (Simms, Hay et al., 2006).

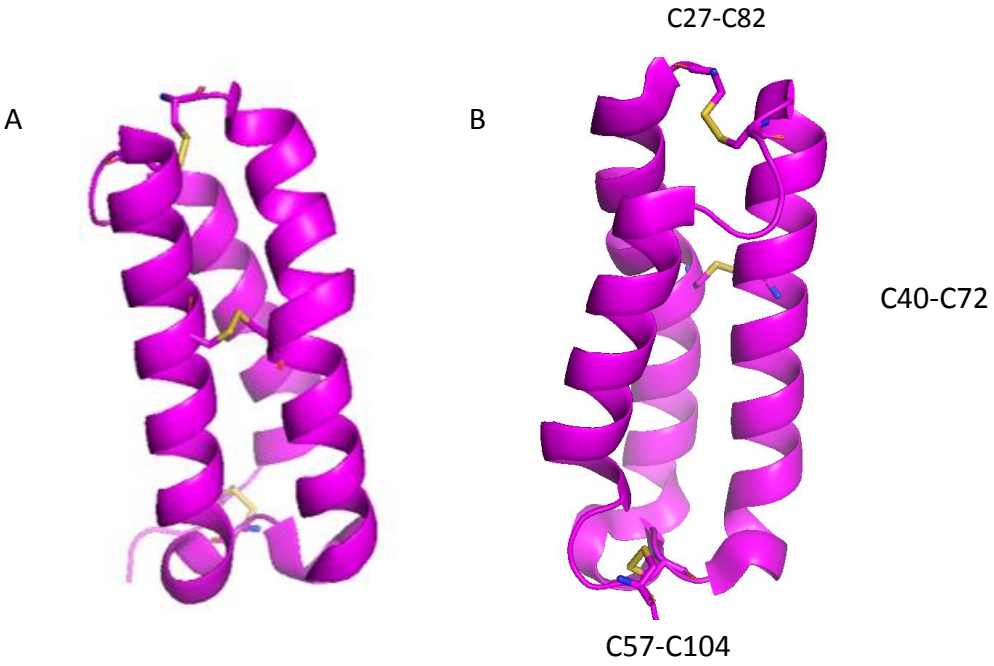

Figure 1.5 – Structure of the RAMP1 ECD. (A) RAMP1 ECD (PDB: 2YX8) (magenta) is comprised of 3 α-helices, with α2 aligned in an antiparallel manner compared to α1 and α3. **(B)** Reverse view. 3 cysteine disulfide bonds are highlighted in yellow and labelled. Image was generated using PyMol Molecular Graphics System, Version 1.7.4.5- Educational Product, Schrodinger.

1.3.2 Structural Characteristics of RAMP2

The RAMP2 ECD was first resolved by Kusano et al 2012. Despite there being only 30% sequence homology between RAMP1 and RAMP2, they exhibit a very similar structure. As with RAMP1, RAMP2 contains three α-helices, with the α2 helix aligned in an antiparallel manor with respect to α1 and α3 (Figure **1.6**). The key difference between the RAMP1 and

RAMP2 proteins is the lack of kink in the α1 helix, leading to a straight α1 helix and making the two proteins easily distinguishable (Kusano, Kukimoto-Niino et al., 2012).

Additionally, RAMP2 contains two disulfide bonds. These include the Cys68-Cys99 bond between the α1 and α2 helices and the Cys84-Cys131 bond, which links loop 1 with the C-terminal tail (Figure **1.6**). As in RAMP1, these bonds are crucial to the structural stability of the ECD, with mutagenesis of these four cysteine residues leading to a reduction of AM affinity for AM_1 . The Cys27-Cys82 bond in RAMP1 that connects the loop between α2 and α3 and the N-terminal tail is absent in RAMP2 (Kusano, Kukimoto-Niino et al., 2012).

Futhermore there is a hydrophobic patch between the α2 and α3 helices, similar to that of RAMP1, this time including Tyr93, His124 and Phe128. As with the equivalent residues in the hydrophobic patch of RAMP1, these RAMP2 residues form interactions with CLR residues contribute to CLR binding, and therefore cell surface trafficking (Kusano, Kukimoto-Niino et al., 2012) (ter Haar, Koth et al., 2010).

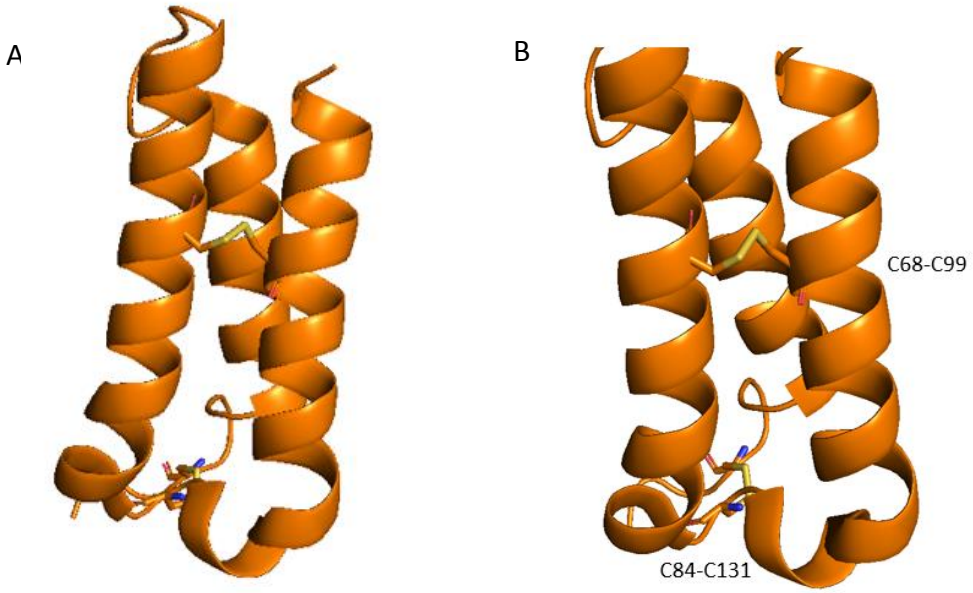

Figure 1.6 – Structure of RAMP2 ECD. (A) The RAMP2 ECD (PDB: 3AQF) (orange) consists of 3 α-helices with α2 aligned in an antiparallel manner to α1 and α3. **(B)** Cysteine disulfide bonds are highlighted in yellow and are labelled. Image was generated using PyMol Molecular Graphics System, Version 1.7.4.5- Educational Product, Schrodinger.

1.3.3 Predicted Structural Features of RAMP3 ECD

The structure of RAMP3 has yet to be resolved on it's own but Cyro-EM studies on the AM_2 receptor have resolved it in complexation with the CLR (Liang, Belousoff et al., 2020) (see later). There was a low resolution around this structure at the N-terminus, however, making the specific structure of the RAMP3 ECD unclear. However, the general structure indicates that, like RAMP1 and RAMP2, RAMP3 contains 3 α-helices with α2 aligned in an antiparallel manner compared to RAMP1 and RAMP2.

Structural predictions about the RAMP3 ECD can also be made by aligning the sequences of RAMP1, RAMP2 and RAMP3 (Figure **1.7**). The Leu39 residue, which forms a kinked structure in RAMP1, is also present in RAMP3. This could suggest that the kinked structure in the RAMP1 α1 helix is also present in RAMP3. The absence of this residue in RAMP2 leads to the absence of this kinked structure in the α1 helix. Sequence alignment also shows the conservation of cysteine residues in RAMP3 compared with RAMP1. It is therefore likely that the RAMP1 disulfide bonds between the α1 and α2 helices (Cys40-Cys72), the α1-α2 loop and the C-terminal tail (Cys57-Cys104), and the α2-α3 loop and the N-terminus are also present in RAMP3.

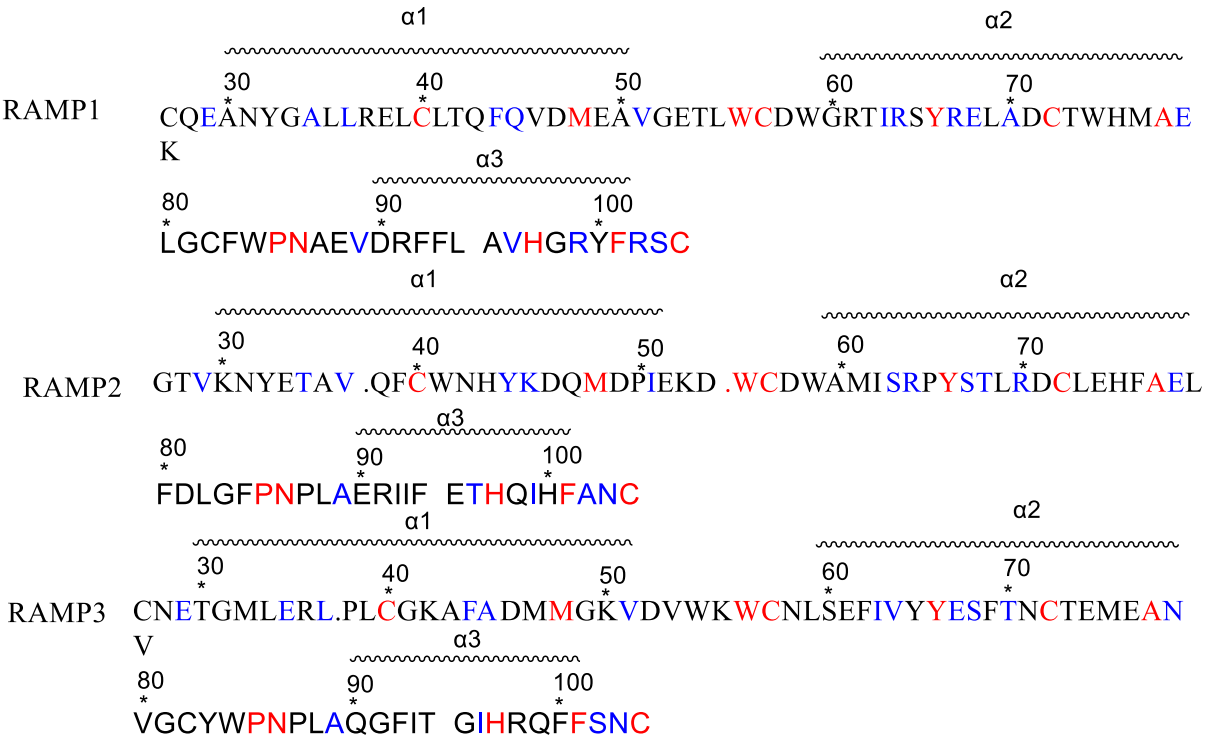

Figure 1.7 – Amino acid sequences of the ECDs in RAMP1, RAMP2 and RAMP3. Residues highlighted in red indicate common residues found in all three RAMPs, and residues highlighted in blue indicate similar residues. Curly lines indicate regions of secondary structure.

1.3.4 Structural Characteristics of CLR and Receptor Binding Sites

Ter Haar et al have published the crystal structure of the unliganded CLR-RAMP1 ECD complex. The CLR forms an α helix from residues 35-51 which packs against the RAMP1 α1 and α2 helices (Figure **1.8 A**). The RAMP1 3 helix bundle sits perpendicular to this structure. There is then a long, finger-like irregular secondary structure from residues 65-81 in the CLR, with the Trp72 residue at the tip of the finger, forming the so called Trp shelf, which forms a key part of the binding site (ter Haar, Koth et al., 2010). This structure is stabilised by disulfide bonds between Cys48-Cys74, and Cys65-Cys105. Mutation of Cys48 has shown to significantly reduce CGRP potency and receptor cell surface expression, highlighting the importance of this interaction in structural stability of the protein (ter Haar, Koth et al., 2010) (Barwell, Miller et al., 2010).

There are numerous interactions between CLR and RAMP1 that help stabilize the dimer, with these interactions mostly occurring between CLR αC1 helix and α2 and α3 of the RAMP1 C-terminal region (Figure **1.8 B**) (Table **1.3**). There are several hydrogen bonds involving CLR glutamic acid residues, including Gln54 with the backbone amide of RAMP1

Arg102 and Cys104, and Gln 50 with His97 and Phe101 sidechains and Pro105 amide backbone (Ter Haar, 2010) (Table **1.3**). RAMP1 His97 and Phe101 interactions are consistent with predictions reported previously (Kusano, Kukimoto-Niino et al., 2008) and from mutagenesis studies (Kuwasako, Kitamura et al., 2003) (Table **1.4**). Additional hydrogen bonds include those between the sidechains of CLR Tyr49 and RAMP1 Asp90, and between CLR Gln45 and RAMP1 Tyr60. CLR Tyr49 and Gln45 have previously been shown to be crucial for receptor cell surface expression from mutagenesis studies (Barwell, Miller et al., 2010). There are also further hydrophobic interactions between CLR Tyr46 and RAMP1 Trp59 and Phe101.

Table 1.3 – Key amino acid residue interactions between CLR and RAMP1 proteins in the CGRP receptor

CLR Residue	RAMP1 Residue	Interaction
Met42	Tyr66, Arg67, Ala70,	Hydrophobic
Gln45	Tyr60	Hydrogen Bond
Tyr46	Trp59, Phe101	Hydrophobic
Tyr49	Asp90	Hydrogen Bond
Gln50	His97, Phe101, Pro105	Hydrogen Bond
Gln54	Arg102, Cys104	Hydrogen Bond

Table 1.4 – Effect of mutating key CLR amino acid residues in the CGRP receptor

Residue Interaction Between CLR and RAMP1	Effect After Mutagenesis
CLR Gln54 – RAMP1 Arg102, Cys104	Reduced cell surface expression of CLR-RAMP1 dimer
CLR Gln50 – RAMP1 His97, Phe101, Pro105	Reduced cell surface expression, impaired CGRP binding

The CGRP receptor binding site consist of a pocket and a hydrophobic patch separated by the Trp72 shelf. The patch extends from the base of CLR loop4 to loop3 and contains CLR residues Trp72, Phe92, Phe95 and Try124 (Booe, Walker et al., 2015). The pocket is much larger and extends from the base of CLR loop4 to loop2 and RAMP1, containing CLR residues

Trp72, Asp70, Gly71, Trp121, Thr122, Tyr124 and RAMP1 Trp84 and Phe85 (Booe, Walker et al., 2015). CLR and RAMP1 binding pocket residues are summarised in Table **1.5**.

Table 1.5 – Amino acid residues in CGRP receptor binding pocket

Protein	Binding Pocket Residues
CLR	Asp70, Gly71, Trp72, Phe92, Phe95, Trp121, Thr122, Tyr124
RAMP1	Trp74, Trp84, Pro85

Despite there being very limited sequence homology between RAMP1 and RAMP2, the CLR-RAMP2 ECD complex in the AM_1 receptor is very similar to the CLR-RAMP1 complex in the CGRP receptor (Kusano, Kukimoto-Niino et al., 2012). As with the CLR-RAMP1 ECD, there are hydrophobic and hydrophilic interactions between CLR α1 helix and RAMP2 α2 and α3 helices (Figure **1.9 A**). The hydrophobic interactions include CLR Met42 with RAMP2 Tyr93, Arg97 and Ser94, CLR Tyr46 with RAMP2 Trp86, Tyr93, His124 and Phe128, CLR Tyr49 with RAMP2 Ile120, Phe121 and His124, and CLR Met53 with RAMP2 Phe121, Gln125 and Ala129 (Kusano, Kukimoto-Niino et al., 2012) (Figure **1.9 B**) (Table **1.6**) . Hydrophilic interactions include Gln45-Tyr93 and Tyr49-Glu117 CLR-RAMP2 hydrogen bonds (Figure **1.9 C**) (Table **1.6**). Additionally, CLR Gln50 forms hydrogen bonds with the sidechains of RAMP2 His124, Phe128 and Ser132, whilst CLR Gln54 forms hydrogen bonds with RAMP2 Ala129 and Cys131 (Kusano, Kukimoto-Niino et al., 2012).

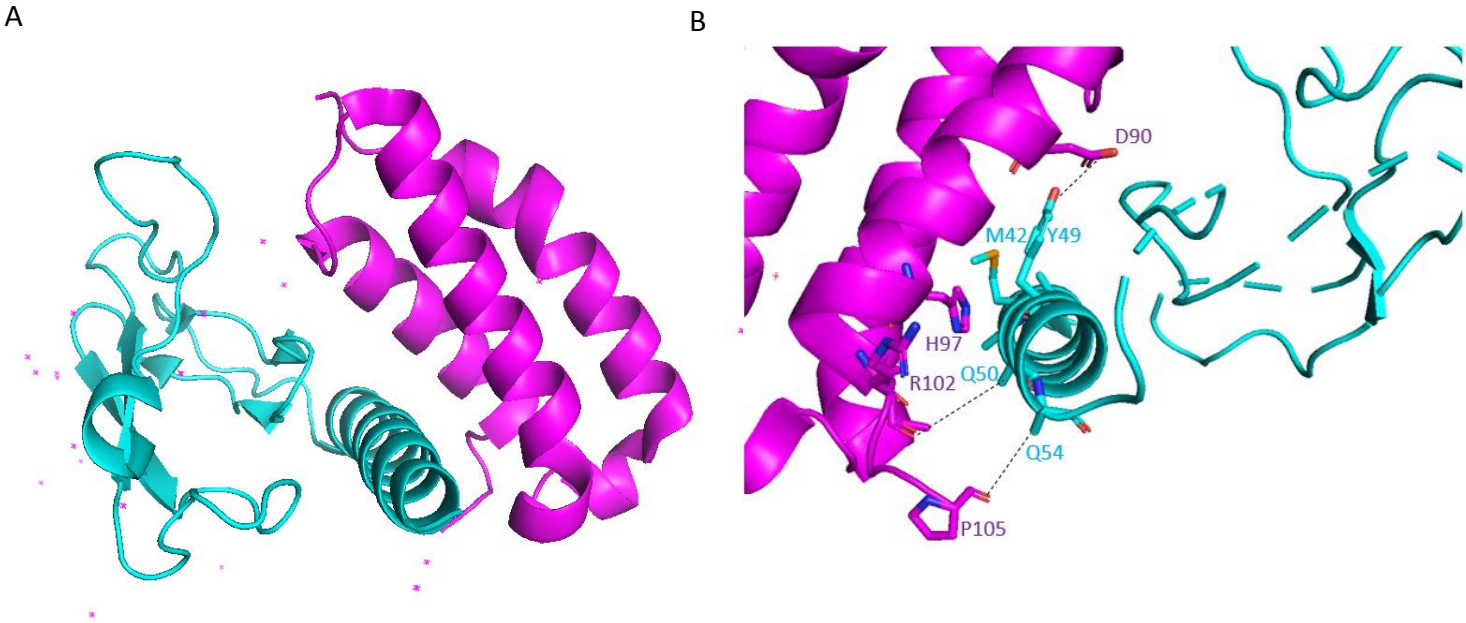

Figure 1.8 – Structure of the CGRP receptor ECD. (A) Overview of the structure of the CLR (cyan) and RAMP1 (magenta) interface (PDB: 3N7P). **(B)** Close up of the interface between CLR α-helix and RAMP1 α2 and α3 revealing hydrophilic and hydrophobic interactions between the two proteins. Hydrogen bonds are indicated by dashed lines. Image was generated using PyMol Molecular Graphics System, Version 1.7.4.5- Educational Product, Schrodinger.

Additionally, CLR Gln50 forms hydrogen bonds with the sidechains of RAMP2 His124, Phe128 and Ser132, whilst CLR Gln54 forms hydrogen bonds with RAMP2 Ala129 and Cys131 (Kusano, Kukimoto-Niino et al., 2012).

Table 1.6 – Amino acid residue interactions between CLR and RAMP2 in the AM_1 Receptor

CLR Residue	RAMP2 Residues	Interaction Type
Met42	Tyr93, Ser94, Arg97	Hydrophobic
Gln45	Tyr93	Hydrogen Bond
Tyr46	Trp86, Tyr93, His124, Phe128	Hydrophobic
Tyr49	Ile120, Phe121, His124	Hydrophobic
Tyr49	Glu117	Hydrogen Bond
Gln50	His124	Hydrogen Bond
Met53	Phe121, Gln125, Ala129	Hydrophobic
Gln54	Ala129, Cys131	Hydrogen Bond

The importance of many of the interactions between CLR and RAMP2 have been confirmed by mutagenesis (Table **1.7**). The His124Ala mutant significantly reduces cell surface expression of the AM_1 receptor, highlighting the importance of the interaction with CLR Gln50 (Kuwasako, 2008). Alanine substitution of CLR Tyr49 has also been shown to have a similar effect, whilst CLR Met42 and Gln45 substitution both lowered potency of AM (Watkins, 2014). Furthermore, deletion of RAMP2 Trp86-Pro92 also reduces cell surface expression despite not appearing to make any significant contact with RAMP2 (Kuwasako, Kitamura et al., 2001) (Kusano, Kukimoto-Niino et al., 2012), implying that these residues may be important in altering the conformation of RAMP2 so that it forms an interface with the CLR.

Table 1.7 – The effects of mutating key amino acid residues in the CLR/RAMP2 interface in the AM_1 receptor

Receptor Residue	Effect After Mutagenesis
CLR Met42	Reduced AM Potency
CLR Gln45	Reduced AM Potency
CLR Tyr49	Reduced Surface Expression
RAMP2 His124	Reduced Surface Expression
RAMP2 His127	Reduced Surface Expression
RAMP2 Trp86-Pro92	Reduced Surface Expression

The binding pocket of the AM_1 receptor is like that of the CGRP in that it contains a pocket and a hydrophobic patch separated by the Trp72 shelf. The patch and pocket contain the same CLR residues except the RAMP2 residues R97, E101, E105 and P112 (Booe, Walker et al., 2015) (Table **1.8**). There are also differences in the shape of the CGRP and AM_1 binding pockets. RAMP2 in AM_1 is shifted relative to RAMP1 in CGRP, with α2 closer to CLR α1 and α3 being further away from CLR α1 (Kusano, Kukimoto-Niino et al., 2012). As a result, the ligand binding pocket of AM_1 is shorter than that of CGRP, with RAMP2 residues Arg97, Glu101, Leu109, Phe111 and Pro112 closer to the surface (Figure **1.10**). Another key feature of the AM_1 receptor is the occlusion of the binding pocket by the large Arg97 sidechain. The equivalent residue in the CGRP receptor is RAMP1 Ala70, which is much smaller and hence this occlusion is not observed (Figure **1.10**). RAMP2 Arg97 additionally forms an intramolecular salt bridge with RAMP2 Glu101, which cannot be observed between equivalent RAMP1 residues Ala70 and Trp74 (Kusano, Kukimoto-Niino et al., 2012).

Another key difference between the ligand free CGRP and AM_1 binding pockets are the positioning of CLR residues. A notable example is Arg119 on CLR loop 4. The sidechain of this residue points away from the binding pocket in AM_1, whereas in CGRP this residue is positioned towards the binding pocket, pointing towards CLR Trp72 (Figure **1.10**). Additionally the position of Trp72 also differs between the two binding pockets, with the sidechain of this residue orientated further towards the binding pocket in CGRP than in AM_1. These differences imply that the presence of a different RAMP in the two receptors may allosterically alter the conformation of the CLR, which could be a factor in ligand selectivity between the CGRP and AM_1 receptors (Booe, Warner et al., 2018).

Table 1.8 – Amino acid residues in the AM_1 binding pocket

AM_1 Receptor Component	Residues in Binding Pocket
CLR	Pocket: Asp70, Gly71, Trp72, Trp121, Thr122, Tyr124 Patch: Phe92, Phe95, Tyr124
RAMP2	Arg97, Glu101, Glu105, Pro112

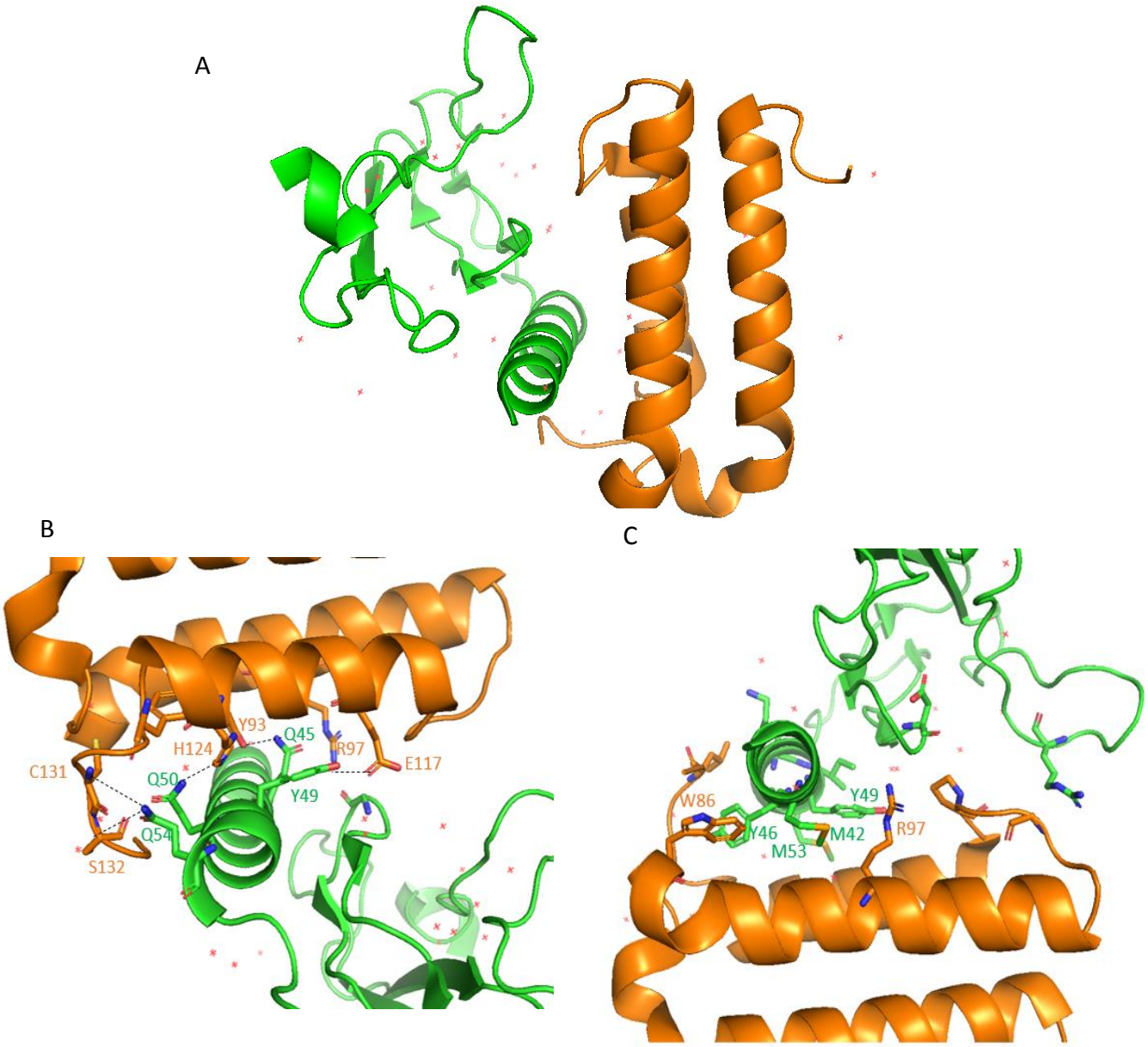

Figure 1.9 – Structure of the AM_1 receptor ECD. (A) Overview of the structure of CLR (green) and RAMP2 (orange) interface (PDB: 3AQF). (**B)** Close up of the CLR-RAMP2 interface depicting hydrophilic interactions between the CLR and RAMP2. Hydrogen bonds are indicated by dashed lines. **(C)** Close up of the CLR-RAMP2 interface depicting hydrophobic interactions between CLR and RAMP2. Image was generated using PyMol Molecular Graphics System, Version 1.7.4.5- Educational Product, Schrodinger.

A

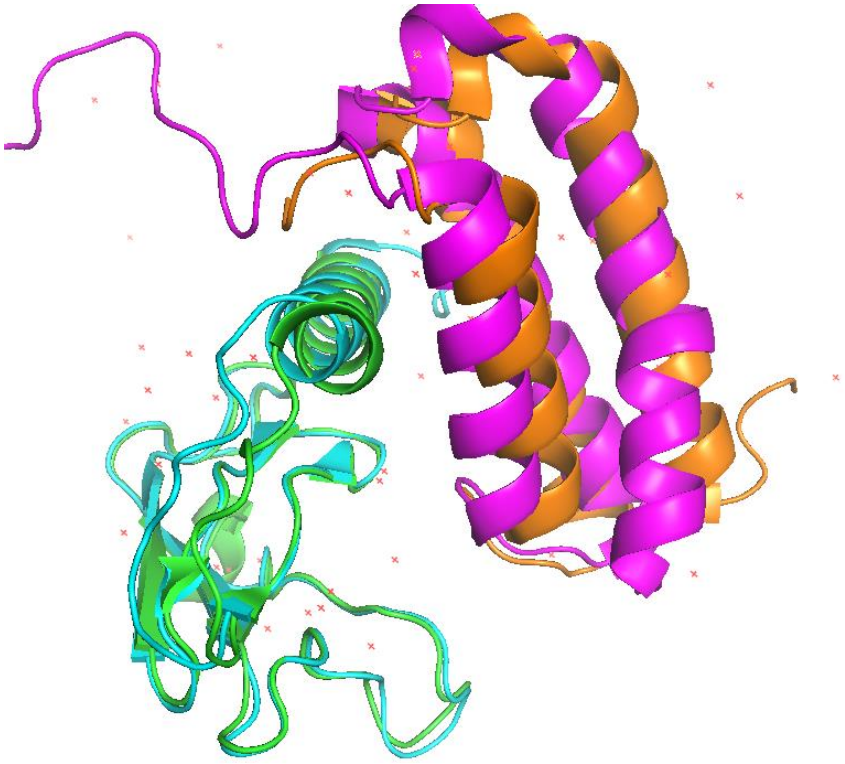

B

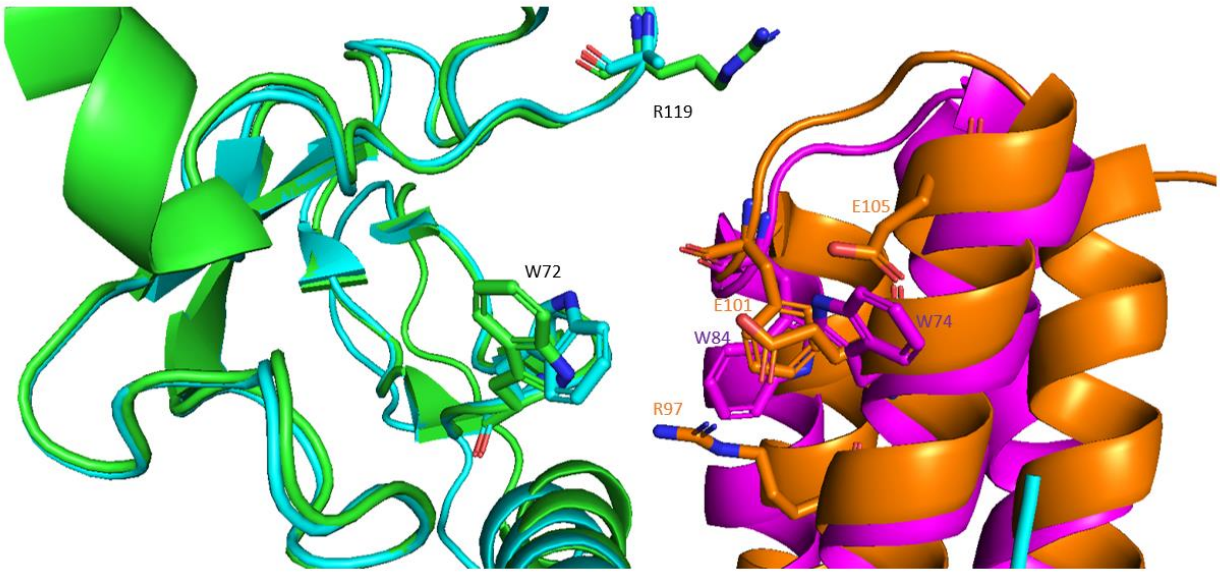

Figure 1.10 – Structure of the ligand free CGRP receptor ECD (PDB: 3N7P) superimposed onto the ligand free AM_1 receptor ECD (PDB: 3AQF). (A) Superimposition of the CGRP CLR (cyan) on AM_1 CLR (green), and RAMP1 (magenta) on RAMP2 (orange). **(B)** Close up view of the binding pocket showing RAMP residue differences and the relative positions of key CLR binding pocket residues. Key residues are labelled and highlighted. Protein structures were superimposed using PyMol Molecular Graphics System, Version 1.7.4.5- Educational Product, Schrodinger.

There is currently no resolved crystal structure of the AM_2 ECD but previous mutagenesis studies can allow predictions of some of the key interactions between CLR and RAMP3. Mutation of RAMP2 residues 86-92 have previously shown to reduce cell surface expression of the AM_1 receptor. Mutation of the equivalent residues of RAMP3, 86-92, showed a significant decrease in AM affinity at AM_2, and although it was not clear in this case if this was due to a reduction in cell surface expression, these residues are unlikely to directly contact the AM peptide (Kuwasako, Kitamura et al., 2001). Further studies have shown that mutating RAMP3 residues His97 and His110 did reduce cell surface expression of AM_2 (Kuwasako, Kitamura et al., 2008). It has been confirmed that RAMP1 His97, the equivalent residue, forms key interactions with CLR (ter Haar, Koth et al., 2010), possibly implying that these same interactions are observed in RAMP3.

1.3.5 Cryo-EM Analysis of CLR/RAMP Transmembrane Domains

The transmembrane CLR-RAMP1 interface has been resolved by Liang et al using Cryo Electron Microscopy (Cryo-EM). It was revealed that RAMP1 is positioned at an interface formed by CLR TM3, TM4 and TM5 (Figure **1.11**), with hydrophobic interactions occurring between CLR TM5 and the upper half of RAMP1 TMD, and between CLR TM3 and the base of the RAMP1 TMD (Liang, Khoshouei et al., 2018). The key interactions between the CLR and RAMP1 TMDs are hydrogen bonds between RAMP1 Glu113 and CLR ECL2 Tyr278, TM5 Thr288, and TM5 His289, with mutagenesis of these residues leading to a decrease in CGRP potency (Liang, Khoshouei et al., 2018).

A

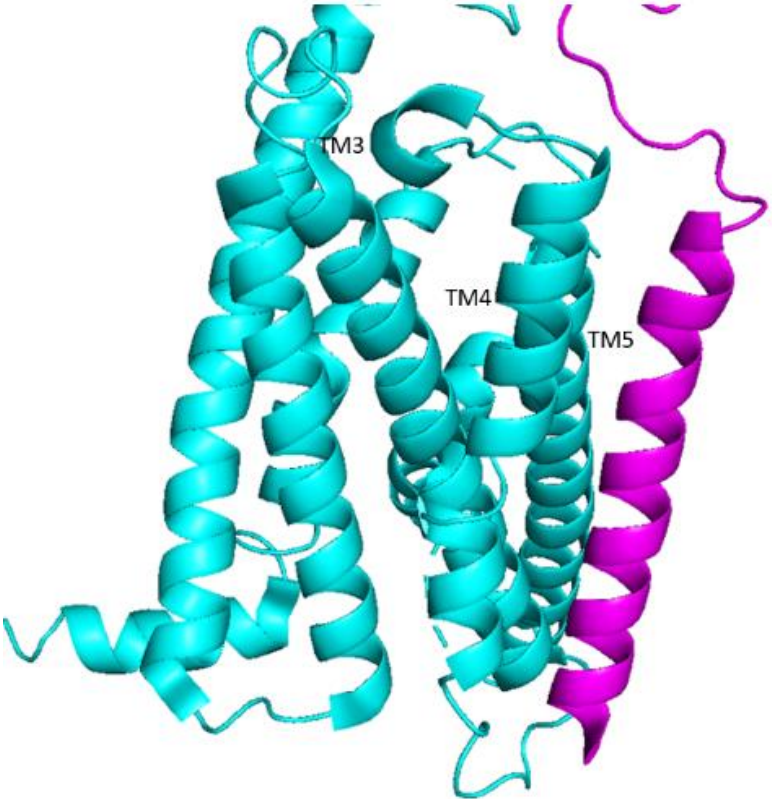

B

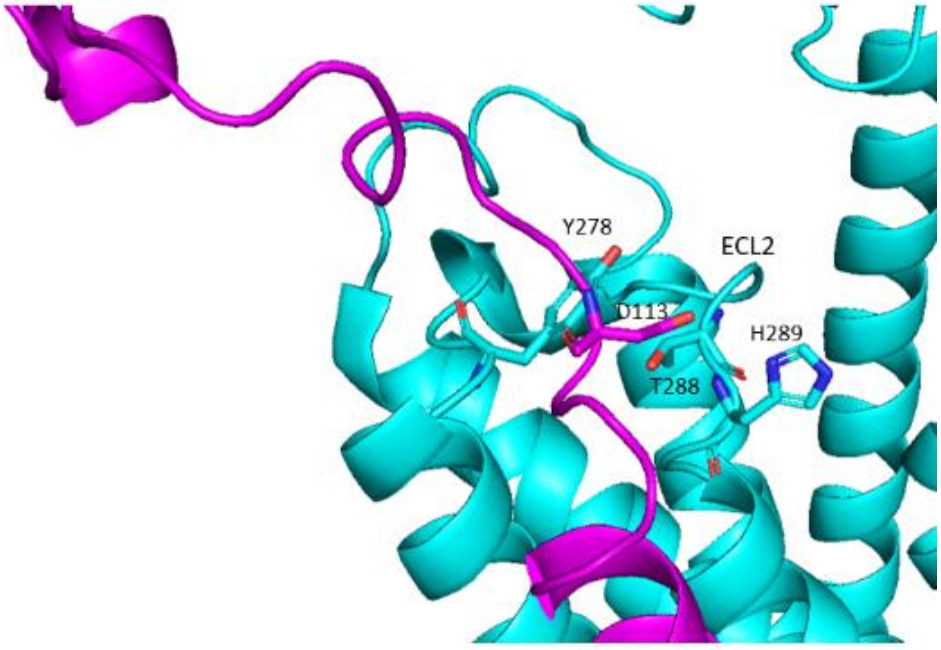

Figure 1.11 – Structure of the CLR-RAMP1 interface in the CGRP receptor TMD (PDB: 6E3Y). (A) Orientation of RAMP1 TMD in relation to the CLR TMD. **(B)** Key interaction between RAMP1 and CLR TMDs. CLR is coloured in cyan and RAMP1 is coloured in magenta. Key residues and regions are labelled. Image was generated using PyMol Molecular Graphics System, Version 1.7.4.5- Educational Product, Schrodinger.

More recently, Liang and co-workers have resolved the structures of both the AM_1 and AM_2 receptors using Cyro-EM. The CLR/RAMP interface was again studied, with focus on the interface between RAMP2 and RAMP3 and the CLR on the AM_1 and AM_2 respectively (Figure **1.12**) (Figure **1.13**). Comparisons were made with the CGRP receptor from previous work. As with RAMP1, RAMP2 and RAMP3 form an interface with TM3, TM4 and TM5 of the CLR and loop over the ECL2 of the CLR before forming a disordered linker that connects the TMD to the RAMP ECD (Liang, Belousoff et al., 2020). The key differences between the CLR/RAMP interface at the AM receptors includes RAMP3 exhibiting tighter packing with the CLR TMD when compared with RAMP2, and the interactions between the RAMP linker and the ECL2 of the CLR. RAMP3, and RAMP1, form hydrogen bonds between Asp113 of both RAMP1 and RAMP3, and both Thr288 and His289 of the ECL2 in the CLR (Figure **1.13**). This was not the case for RAMP2, but there was a potential hydrogen bond occurring between Ser139 of RAMP2 and Thr288 of the ECL2, which may limit productive engagement with ECL2 (Liang, Belousoff et al., 2020) (Figure **1.12**). Key residues involved are listed in Table **1.9**.

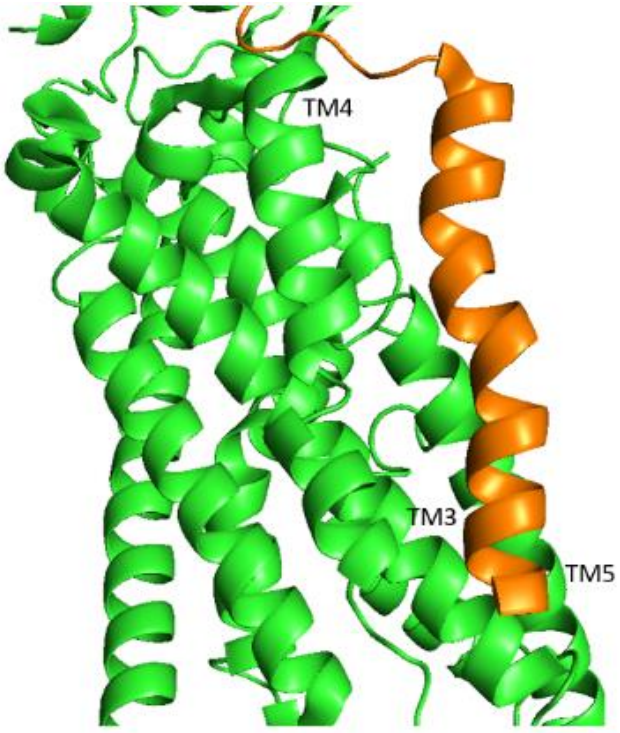

Figure 1.12 – Structure of the CLR-RAMP2 interface in the AM_1 receptor TMD (PDB: 6UUN). CLR is coloured in green and RAMP2 is coloured in orange. Key regions are labelled. Image was generated using PyMol Molecular Graphics System, Version 1.7.4.5- Educational Product, Schrodinger.

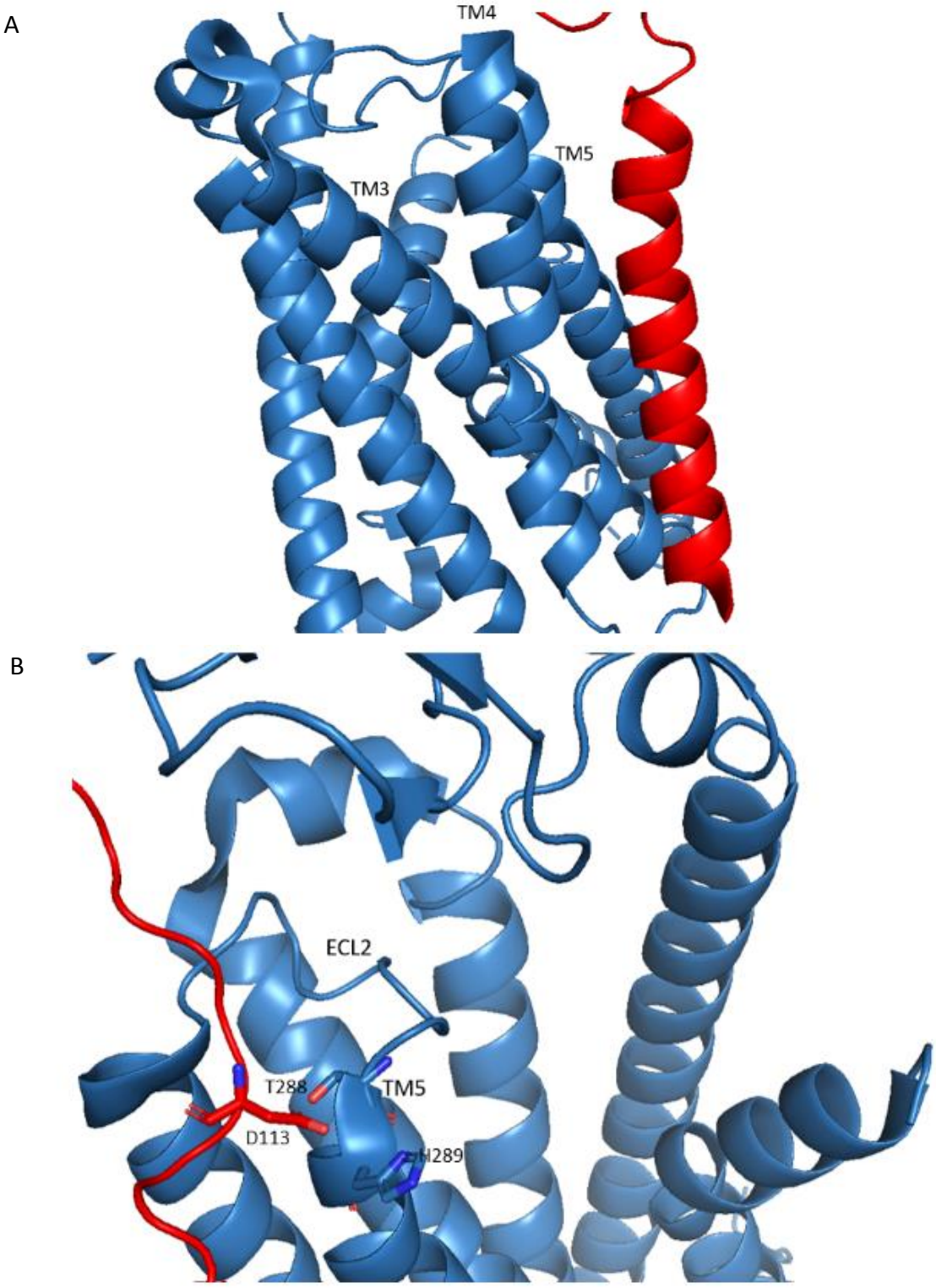

Figure 1.13 – Structure of the CLR-RAMP3 interface in the AM_2 receptor TMD. (A) Orientation of RAMP3 TMD in relation to the CLR TMD. **(B)** Key interaction between RAMP3 and CLR TMDs. CLR is coloured in blue and RAMP3 is coloured in red. Key residues and regions are labelled. Image was generated using PyMol Molecular Graphics System, Version 1.7.4.5- Educational Product, Schrodinger.

Table 1.9 – Some key residues involved in the interaction of CLR with the RAMPs at the CLR/RAMP interface of the CGRP, AM_1 and AM_2 receptors

Receptor	CLR Residues	RAMP Residues	Reference
CGRP	$Y278^{ECL2}$, $T288^{TM5/ECL2}$, $W254^{TM4}$	D113, R112	Liang, 2018
AM_1	$T288^{TM5/ECL2}$, $H289^{ECL2}$	S39	Liang, 2020
AM_2	$T288^{TM5/ECL2}$, $H289^{ECL2}$	D113	Liang, 2020

1.4 Peptide binding in CGRP, AM_1 and AM_2 Receptors

1.4.1 Mechanism of Binding

The binding of a peptide to a class B GPCR is thought to occur via a two domain model (Hoare, 2005) (Moore and Salvatore, 2012). The C-terminus of CGRP and AM firstly binds to the extracellular N-terminus of the receptor, holding the peptide in place. A peptide conformational change is then induced enabling the N-terminus to bind to the juxtamembrane of the CLR, activating the receptor (Figure **1.14**). This is demonstrated by the fact that a CGRP peptide missing its first seven amino acids can bind to the receptor but not activate it, behaving as a functional antagonist (Moore and Salvatore, 2012). Non-peptide antagonists such as small molecules can inhibit this mechanism via competitive antagonism of the receptor binding site (Bell, 2014, Hoare, 2005). This is achieved either by blocking the receptor N-terminus and preventing the peptide C-terminal region from "gripping" the receptor, or by blocking the juxtamembrane region to prevent the peptide N-terminal region from binding there, preventing receptor activation.

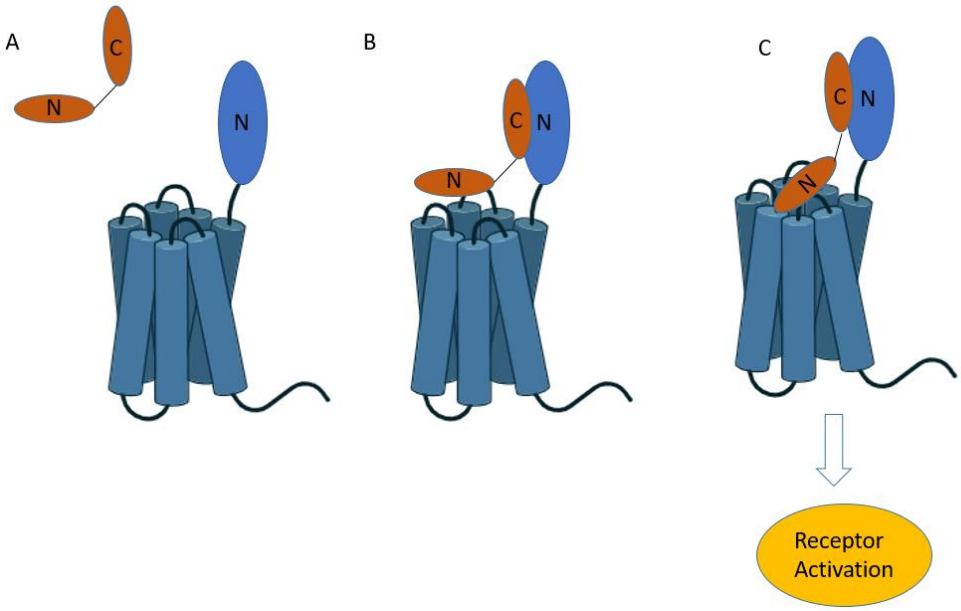

Figure 1.14 – Structure of the CLR-RAMP3 interface in the AM_2 receptor TMD. (A) Approach of peptide to GPCR. **(B)** Interaction between peptide C-terminus and receptor N-terminus. **(C)** Interaction of peptide N-terminus with receptor juxtamembrane resulting in activation of the receptor. Image was generated using Biorender.

1.4.2 CGRP Binding to CGRP Receptor

There have been many attempts made to understand binding of CGRP and AM to their respective receptors by resolving the structure of CGRP and AM bound receptors. The Crystal structure of the C-terminus of CGRP to the CLR-RAMP1 ECD complex has been resolved by Booe et al, with the binding of the C-terminus of the peptide to the N-terminal ECD of the receptor suggesting that the peptide follows the two-domain binding model mentioned above. The crystal structures of the ECDs of the CGRP and AM_1 receptors have revealed that CGRP and AM both occupy positions near CLR loops 2,3 and 4 (Booe, Walker et al., 2015) (Figure **1.15**). CGRP primarily contacts the CLR, but key RAMP contacts are also formed, despite only the C-termini of the peptides being in close proximity to the RAMPs. CGRP is completely devoid of secondary structure when bound to the receptor, and Gly33-A36 on CGRP forms a type two β-turn. The peptide β-turn is important as it allows the contact to the CLR loop via hydrogen bonds between the main chain of the turn and CLR Ser117, Arg119 and Trp121 side chains (Booe, Walker et al., 2015). The β-turn also allows the peptide C-termini to occupy to respective pockets.

The CGRP peptide extends along the CLR patch and pocket and makes key contacts with CLR loop 3 Trp72, Phe92, Asp94, and Phe95, and CLR loop 4 His114, Arg119, Trp121, Thr122 and Tyr124 (Figure **1.15**). Mutations of all of these residues reduces CGRP potency at the full length receptor by >20 fold, highlighting the significance of the interactions between CGRP and these residues (Booe, Walker et al., 2015). It is the peptide β-turn that allows helps position the CGRP C-terminal amide groups to hydrogen bond to CLR Thr122, whilst also allowing the CGRP C-terminal residues to stack against Gln71, Trp72, and RAMP1 Trp84. CGRP Thr30 forms further main chain and side chain hydrogen bonds with CLR Glu94, whilst an additional interaction is formed between CGRP Val32 and CLR Trp72. RAMP1 W84 is the only RAMP1 residue which makes contact with CGRP, forming a hydrophobic interaction with CGRP Phe37. Mutation of this residue has also shown to reduce CGRP potency (Moore, Gingell et al., 2010). Mutagenesis studies on the CGRP peptide are also in agreement with the crystal structure, with Thr30, Val32 and Phe37 mutations resulting in complete losses of CGRP binding affinity (Moad and Pioszak, 2013) Key CLR and RAMP1 residues for CGRP peptide binding are summarised in Table **1.10**.

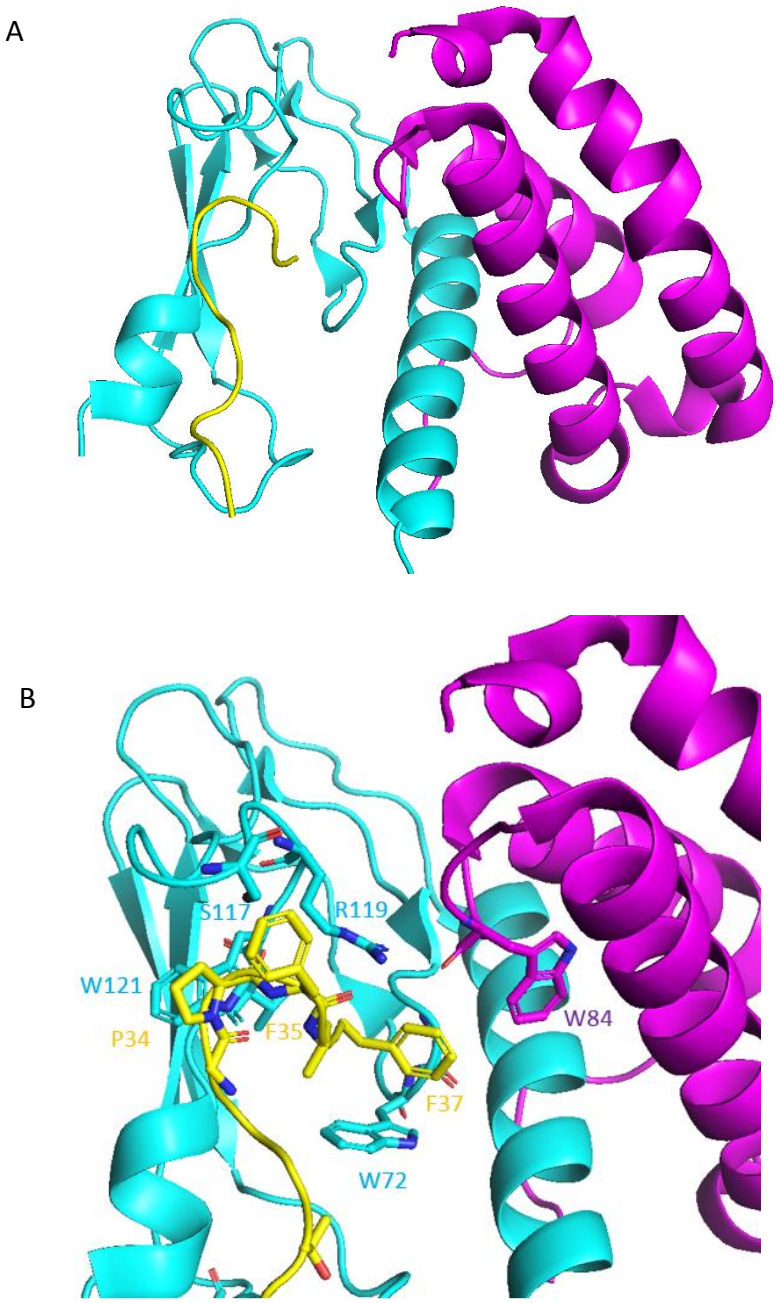

Figure 1.15 – Binding of CGRP peptide C-terminus to the CGRP receptor ECD. (A) Ribbon representation of CGRP peptide (yellow) binding to the CGRP receptor (PDB: 4RWG). CLR is coloured cyan and RAMP1 is coloured magenta. Image was generated using PyMol Molecular Graphics System, Version 1.7.4.5- Educational Product, Schrodinger. **(B)** Outline of contacts between the C-terminus of the CGRP peptide and the CLR and RAMP1 ECDs. Image was generated using PyMol Molecular Graphics System, Version 1.7.4.5- Educational Product, Schrodinger.

Cyro-EM studies on the CGRP receptor TMD have further provided an insight into how the native peptide binding occurs between the peptide N-terminus and the CLR-RAMP1 TMD complex. (Figure **1.16**) Analysis of the receptor bound CGRP structure confirmed that the C-terminus is the only point of direct contact between the peptide and RAMP1, and that the CGRP N-terminal peptide loop is buried deeply and extends into amphiphatic α-helix, forming several Van der Waals interactions with the CLR (Y. L. Liang et al., 2018). There are also a small number of hydrogen bonds formed between the peptide N-terminus and the CLR core, including between Tyr292 and CGRP Asp3, His295 and CGRP Thr6 and Ser286 and CGRP His10. There are extensive interactions between CGRP and TM3, TM5 and ECL2 of the CLR, whilst there are very limited interactions with ECL2 or ECL3. Below His295, a series of amino acids including Ile298, Leu302, Met223 and Tyr227 forms the bottom of the peptide-binding pocket (Liang, Belousoff et al., 2020).

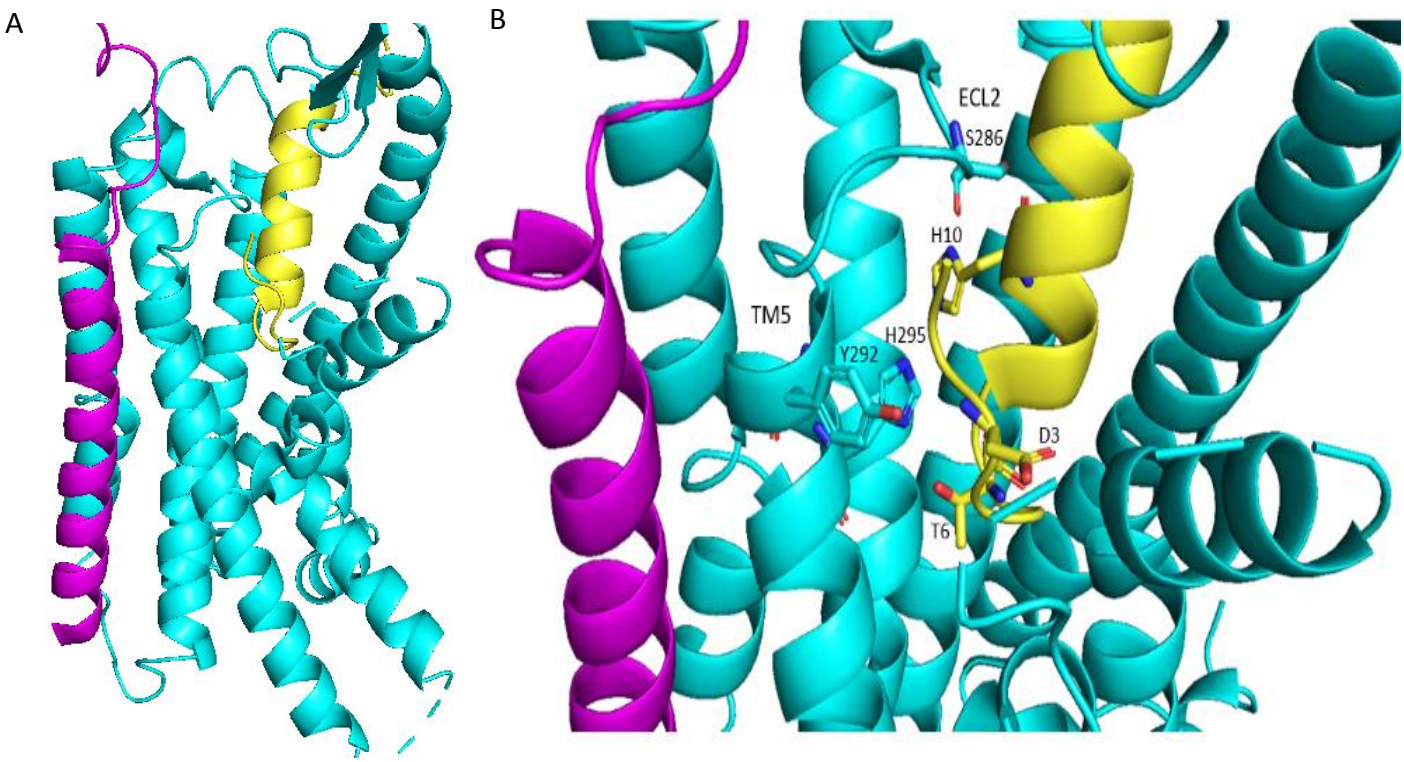

Figure 1.16 – Binding of CGRP N-terminus to the CGRP receptor TMD. (A) Overview of CGRP N-terminus bound in CLR-RAMP1 TMD **(B)** Focus on interactions between CGRP far N-terminus and CLR TM5 and ECL2. CLR is coloured in cyan, RAMP1 is coloured in magenta and the CGRP peptide is coloured in yellow. Key residues and regions are labelled. Image was generated using PyMol Molecular Graphics System, Version 1.7.4.5-Educational Product, Schrodinger.

1.4.3 AM Binding to AM_1 Receptor

As with CGRP to the CGRP receptor, AM binding to the AM_1 receptor follows the two-domain model. The crystal structure of the C-terminal end of AM bound to the CLR-RAMP2 ECD has also been resolved by Booe et al. Similar to CGRP, receptor-bound AM is also devoid of secondary structure. The β-turn in the peptide, this time from AM residues Ser48-Gly51 allows hydrogen bonds with CLR loop 4 Ser117, Arg119 and Trp121, as well as allowing the C-termini to occupy their respective positions in the pocket (Booe, Walker et al., 2015).

The AM peptide extends along the AM_1 pocket in a similar way to way to CGRP at the CGRP receptor, forming contacts with the same residues as stated above (Booe, Walker et al., 2015) (Figure **1.17**). However, despite mutation of CLR residues Trp72, Phe92, Phe95, Trp121 and Tyr124 reducing AM potency by >40-fold, CLR Asp94, His114, Arg119 and Thr122 only exhibited a 4-fold to 9-fold reduction in AM potency. This is in contrast to the CGRP receptor, in which deletion of all these residues resulted in a dramatic drop in CGRP potency, particularly with the Asp94 mutation (Booe, Walker et al., 2015).

There are also more contacts with RAMP2 for the AM bound AM_1 receptor than for RAMP1 in the CGRP bound CGRP receptor. The points of contact were between RAMP2 Arg97, Glu101 and Glu105 and AM Lys46 and Tyr52, enabled by the peptide β-turn (Figure **1.17**). Mutagenesis data has shown a dramatic decrease in AM potency with deletion of RAMP2 Glu101 and Phe111 (Watkins, Walker et al., 2014) (Booe, Walker et al., 2015) (Moore, Gingell et al., 2010), whilst interestingly deletion of Arg97 and Glu105 had no effect on AM potency, implying that contacts with these residues are not as crucial. Mutations of AM Lys46 and Tyr52 abrogates AM binding, confirming the importance of these AM residues. AM Tyr52 also contacts the Trp72 shelf, which is enabled by interaction of AM Lys46 with the Trp72 shelf via a helical turn in this region. This further enables AM Ala42 and Phe43 to contact the hydrophobic patch. Key CLR and RAMP2 residues for AM peptide binding to AM_1 are summarised in Table **1.10**.

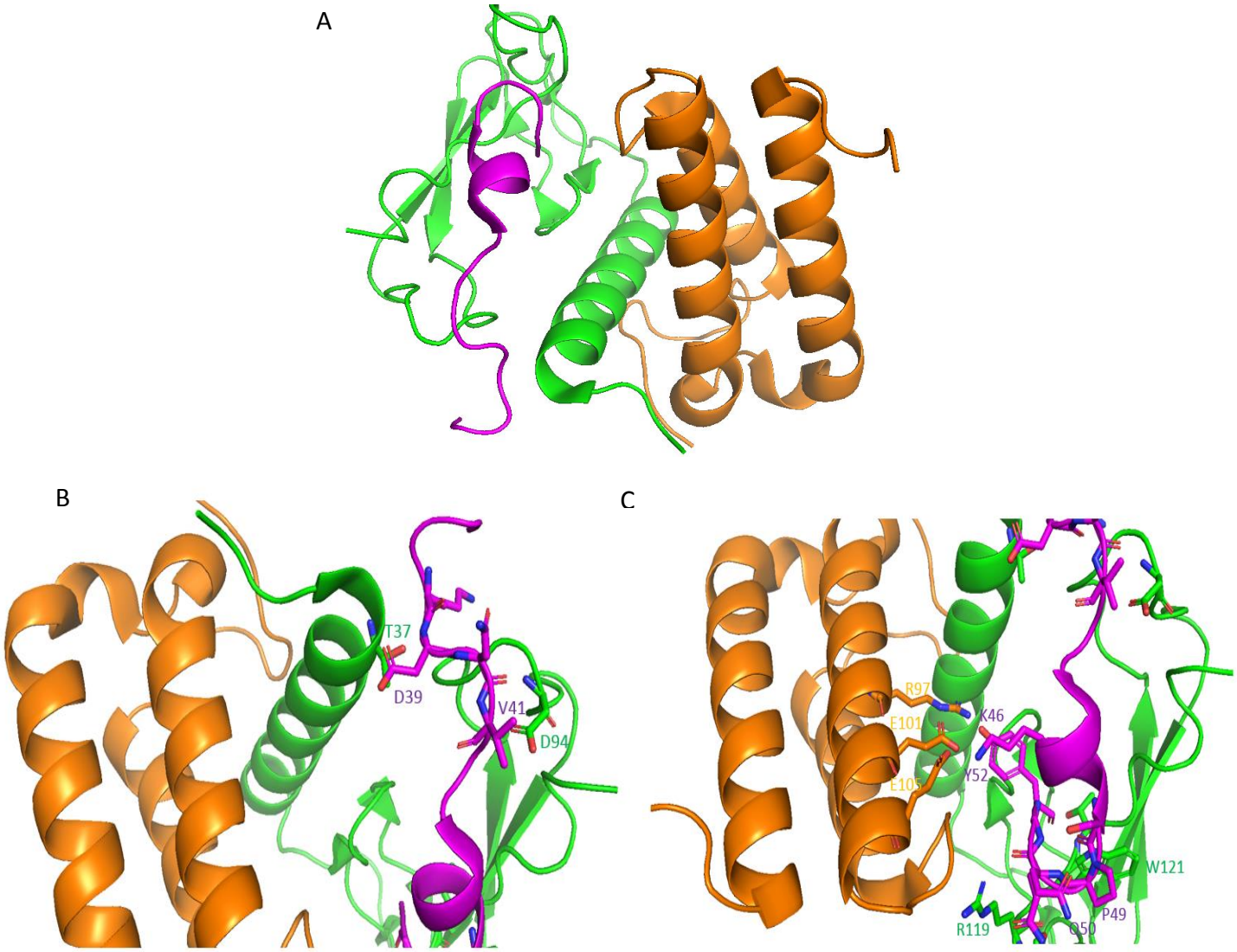

Figure 1.17 – Binding of AM C-terminus to the AM_1 receptor ECD. (A) Ribbon representation of the AM peptide (magenta) binding to the AM_1 receptor (PDB: 4RWF). The CLR is coloured in green and RAMP2 is coloured in orange. Key residues are highlighted and labelled. Image was generated using PyMol Molecular Graphics System, Version 1.7.4.5- Educational Product, Schrodinger. **(B)** Interactions of AM (Asp39-Val41) with CLR amino acid residues. Key residues are highlighted and labelled. Image was generated using PyMol Molecular Graphics System, Version 1.7.4.5- Educational Product, Schrodinger. **(C)** Interactions of AM Lys46-Tyr52 with CLR and RAMP2 amino acid residues. Key residues are highlighted and labelled. Image was generated using PyMol Molecular Graphics System, Version 1.7.4.5- Educational Product, Schrodinger.

Cyro-EM studies have also provided an insight into how the AM N-terminal region binds to AM_1 and AM_2 receptors (Liang, Belousoff et al., 2020). As observed with CGRP, there are no direct interactions between the peptide N-termini and the RAMPs for AM bound to either receptor. AM adopted a conformation that consisted of an N-terminal loop formed by a disulfide bridge, followed by a short amphipathic α-helix (Figure **1.18**). The deepest AM residue in the receptor core is Gly19 (Figure **1.18**). AM binds into an open cavity that is splayed by the outward movement of TM6/TM7/ECL3, and there are limited interactions between the peptides and these receptor segments. AM forms extensive interactions with CLR TM3, TM5 and ECL2, as well as additional interactions with TM1 and the top of TM2. This included interactions commonly observed with other class B GPCRs, including CLR His295, which likely forms hydrogen bonds to Thr20 in AM (Figure **1.18**). It has also been indicated that the His295 residue plays a key role in driving G protein coupling. The interactions between AM and the AM_1 ECL2 seem to be more selective at the distal segment, whilst the interactions are more selective with the middle region of ECL2 in the AM_2 receptor.

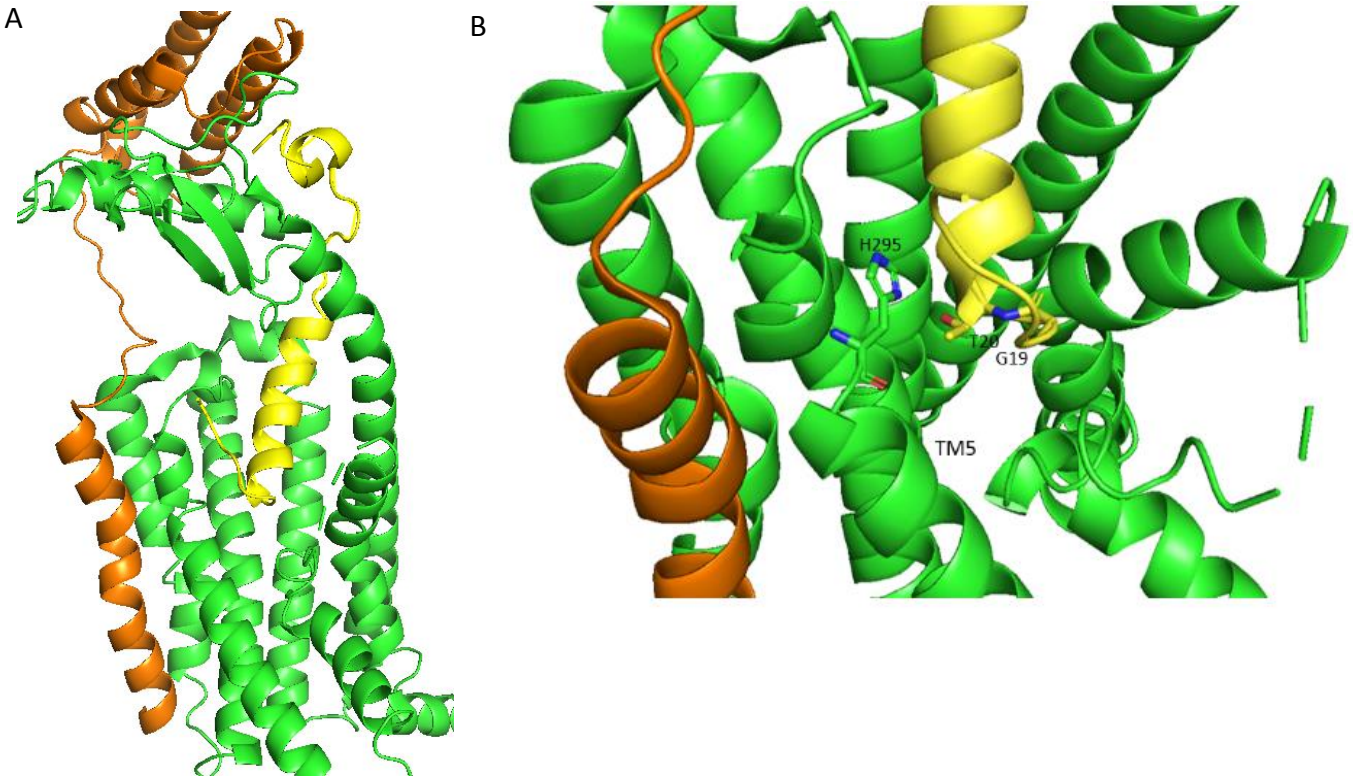

Figure 1.18 – Binding of AM N-terminus to the AM_1 receptor TMD. (A) Overview of AM N-terminus bound in CLR-RAMP1 TMD **(B)** Focus on interaction between CLR His295 and AM Thr20 and on Gly19, the deepest residue in the receptor core. CLR is coloured in green, RAMP2 is coloured in orange and the AM peptide is coloured in yellow. Key residues and regions are labelled. Image was generated using PyMol Molecular Graphics System, Version 1.7.4.5- Educational Product, Schrodinger.

1.4.4 Differences Between Ligand-bound and Ligand-free Receptors

CGRP-bound CLR-RAMP1 reveals a clamp-like movement of CLR loops 3 and 4 has taken place compared to ligand-free CLR-RAMP1 (Figure **1.19**). This is likely due the interaction between CGRP Thr30 and CLR Asp94, as well as the β-turn contacts between CLR loop 4, including CGRP Phe35 and CLR Ser117 (Booe, Walker et al., 2015). Additionally, there is a slight shift in Arg119 residue in the ligand-bound structure, which helps accommodate the peptide, whilst RAMP1 Phe83 also rotates away from CLR loop 4 (Figure **1.19**).

There are only minor conformational changes in the ligand-bound AM_1 receptor compared with the ligand-free receptor (Figure **1.20**). The AM Thr37-CLR contact moves the N-terminal region of α1 towards AM, whilst there is no movement of CLR loops 3 and 4 and no significant side chain conformational differences (Booe, Walker et al., 2015). Interestingly, RAMP2 His102 appears to rotate 180 ^{o} in the AM bound structure compared to the unbound structure (Figure **1.20**), although mutation of this residue does not decrease AM potency or AM_1 cell surface expression (Kusano, Kukimoto-Niino et al., 2012) (Booe, Walker et al., 2015), so it is unclear why this happens.

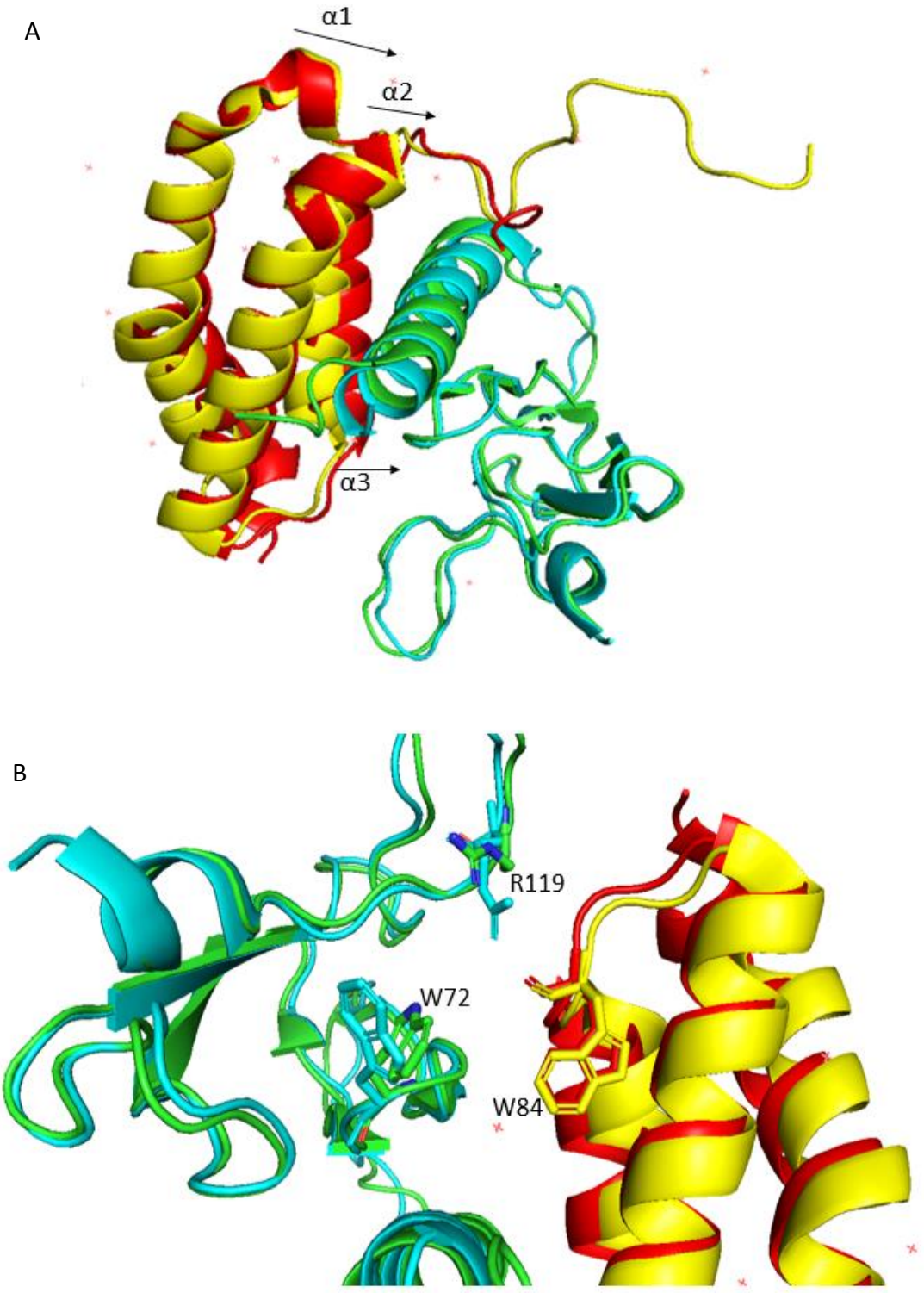

Figure 1.19 – Superimposition of ligand bound and ligand unbound CGRP receptor. (A) Ribbon representation of alignment of CGRP bound (PDB: 4RWG) and unbound (PDB: 3N7P) CGRP receptors. Arrows indicate a shift in the helices after the peptide has bound. **(B)** The differences in residue positions for amino acids in the CGRP receptor binding site between ligand bound and ligand unbound structures. Structures aligned using PyMOL Molecular Graphics System, Version 1.7.4.5- Educational Product, Schrodinger, LLC.

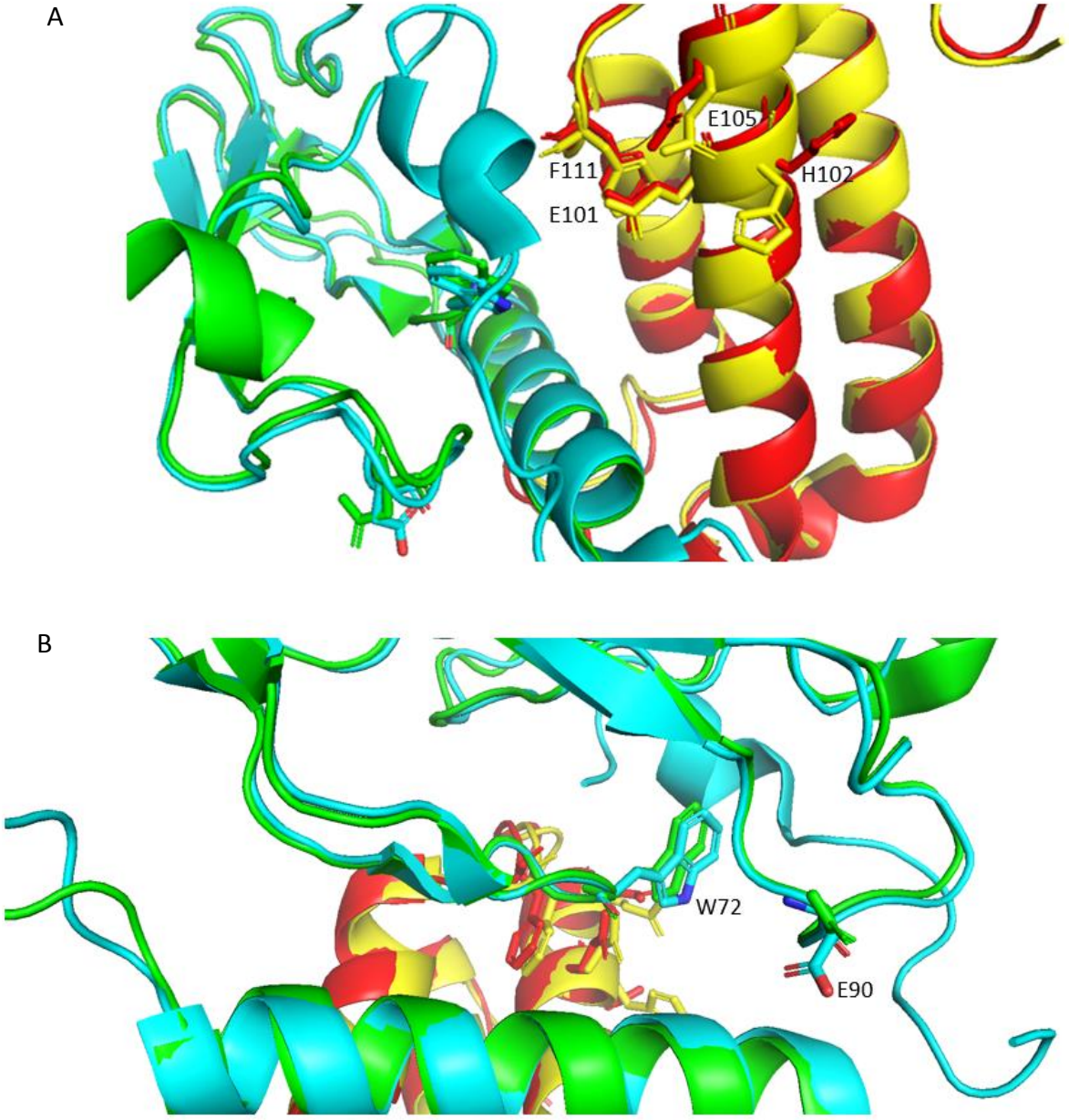

Figure 1.20 – Superimposition of ligand bound and unbound AM_1 receptor. (A) Differences between binding pocket RAMP2 amino acid residue positions in ligand bound and ligand unbound AM_1 receptor ECDs. **(B)** Differences between binding pocket CLR residue positions in ligand bound and ligand unbound AM_1 receptor. Structures aligned using PyMol Molecular Graphics System, Version 1.7.4.5 – Educational Product, Schrodinger, LLC

1.4.5 Peptide Selectivity Determinants

One of the determinants of peptide selectivity between CLR-RAMP receptors is thought to be due to the differences in RAMP residues in the peptide binding pocket. CGRP Phe32 forms a hydrophobic interaction with CLR Trp84 in the CGRP receptor binding pocket. The equivalent RAMP2 residue in the same position is Phe111, which cannot contact CGRP Phe32. Additionally, in RAMP2 Glu101 forms hydrogen bonds with AM Lys46 and Tyr52, whilst the equivalent RAMP1 residue cannot form this interaction (Booe, Walker et al., 2015) (Booe, Warner et al., 2018).

Despite the RAMP residue differences in the binding pockets of the CGRP and AM_1 receptors, the limited peptide contacts with the RAMPs imply that this is not the only determinant of peptide selectivity at these receptors. Another reason for this is due to the way RAMPs allosterically modulate CLR conformation. Differences between CLR protein when coupled to RAMP1 or RAMP2 include different conformation of CLR Arg119, an unwound N-terminus of CLR α1, and a small, subtle shift in in CLR β1-β2 loop. Booe et al investigated the effect of the β1-β2 shift by monitoring the binding affinity of a AM Lys46Leu mutant, which in theory would push AM Tyr52 to adopt a similar position to CGRP Phe37, sterically disfavouring CLR-RAMP2 binding due to a clash with Gly71 on CLR β1-β2 loop. All AM Lys46Leu mutants saw a decrease in AM_1 binding affinity and an enhancement in CGRP receptor binding affinity, thus confirming the importance of this allosteric effect (Booe, Warner et al., 2018).

Peptide interactions with the CGRP, AM_1 and AM_2 receptors at the transmembrane level are also very similar, further suggesting that allosteric effects of the RAMPs on CLR conformation play a key role in peptide binding. From the Cryo-EM maps, the biggest difference between each receptor is the location of the ECD relative to the receptor core, suggesting that conformational dynamics may be the key determinant of receptor phenotype (Liang, Belousoff et al., 2020). This is highlighted by the fact that CGRP ECD location is much more distinct compared to the AM receptors. The lower resolution of the AM_1 ECD compared to AM_2 ECD suggests that there is greater dynamic motion of this region in AM_1, with this observation being backed up by molecular dynamics simulations. This is consistent with tighter packing interactions by RAMP3 to CLR in AM_2 compared with RAMP2

to CLR in AM_1, and stronger interactions between the proximal linker and ECD in AM_2 (Liang, Belousoff et al., 2020).

1.4.6 AM Bound to AM_2 Receptor

AM bound to the full length AM_2 receptor has been visualised by Cryo-EM studies (Liang, Belousoff et al., 2020). As with the CLR-RAMP interface, the resolution on the receptor ECD was poor, meaning the specifics of the C-terminal end of the peptide binding to the ECD is unclear. However, the AM peptide appeared to bind to a similar position in the binding pocket to AM_1, so speculations can be made about the possible protein-ligand interactions.

RAMP3 Glu74 is predicted to be the equivalent residue to RAMP2 Glu101. This implies that there could be a possible hydrogen bond between RAMP3 Glu74 and AM Tyr52, similar to that seen between Tyr52 RAMP2 Glu101 in AM_1. Mutating this residue has previously seen a decrease in AM potency at AM_2, providing further evidence for this (Qi and Hay, 2010). Additionally, RAMP3 Trp84 is equivalent to RAMP1 Trp84, meaning that this residue could stack against AM Tyr52 and make contact with CGRP Phe37. Mutating this residue has led to a reduction of both CGRP and AM potency at this receptor (Watkins, Walker et al., 2014), which could explain why CGRP peptide has a higher affinity for AM_2 than for AM_1.

Binding of the AM N-terminal region to the AM_2 receptor has been elucidated using Cryo-EM. There were several similarities observed compared with AM binding at AM, including the fact that there were no direct interaction with RAMP3 and that most interactions of the peptide occur with CLR TM3, TM5 and ECL2 (Liang, Belousoff et al., 2020) (Figure **1.21**). The conformation of bound AM in the TM region of AM_2 is also very similar, mirroring the N-terminal loop and short, aliphatic α-helix observed when bound to AM_1. The interactions between AM and the AM_1 ECL2 seem to be more selective at the distal segment, whilst the interactions are more selective with the middle region of ECL2 in the AM_2 receptor.

A

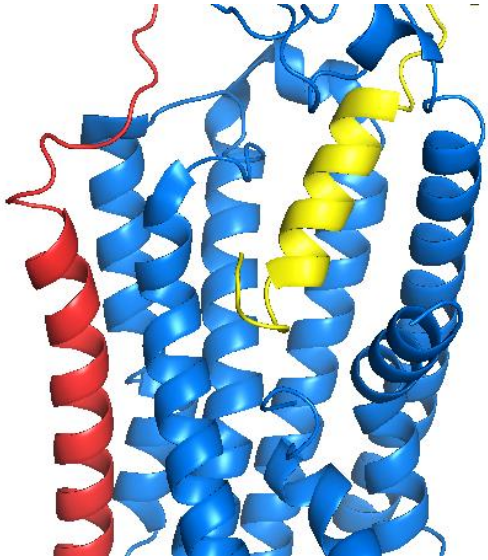

B

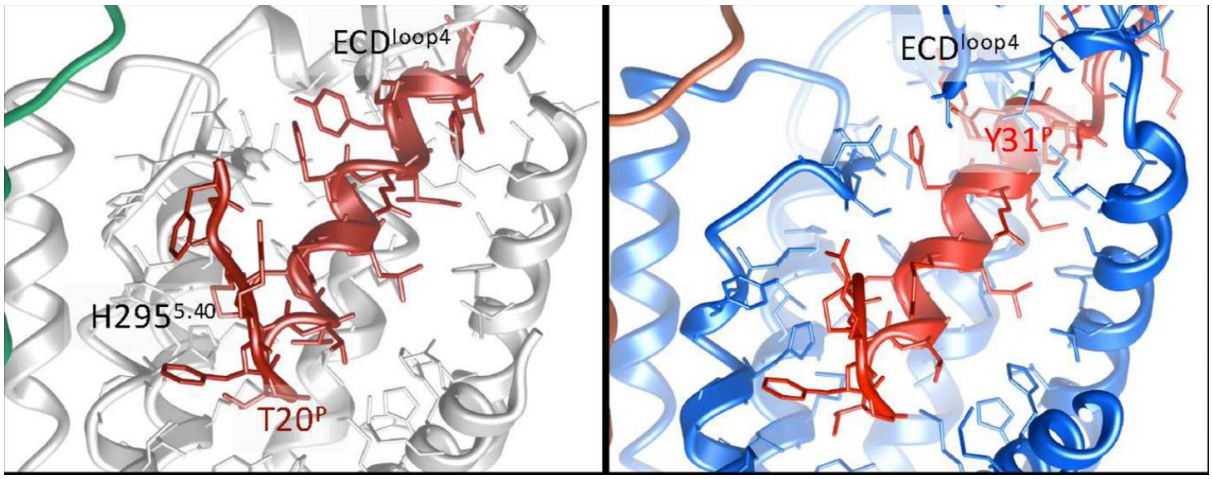

Figure 1.21 - Structure of AM N-terminal domain bound to AM_2 TMD. (A) General structure of AM N-terminus bound to CLR-RAMP3 TMD. CLR is coloured in yellow, RAMP3 is coloured in red and AM peptide is coloured in yellow. Image was generated using PyMol Molecular Graphics System, Version 1.7.4.5- Educational Product, Schrodinger. **(B)** Comparison of interactions between AM and AM_1 TMD (left panel) and AM and AM_2 TMD (right panel). For AM_1 the CLR is coloured in grey and for AM_2 the CLR is coloured in blue. AM peptide is coloured in red in both cases. Image taken form Liang et al, 2020.

Table 1.10 – Key CLR and RAMP residues involved in peptide binding at CGRP, AM_1 and AM_2 receptors

Receptor	CLR Residues	RAMP Residues	References
CGRP	W72, F92, D94, F95, H114, R119 W121, Y124	W84	(Booe, Walker et al., 2015) (Barwell et al., 2010)
AM_1	W72, F92, F95, W121, Y124	E101, F111	(Booe, Walker et al., 2015) (Watkins, Walker et al., 2014)
AM_2	No data	E74, W84	(Watkins, Walker et al., 2014)

1.5 Development of Small molecule Antagonists for CGRP and AM_2 Receptors

1.5.1 Olcegepant and Telcagepant

Olcegepant (BIBN4096BS) (Figure **1.22**) was the first small molecule developed as an antagonist for the CGRP receptor. The compound was discovered by Boehringer Ingelheim Pharmaceuticals from high throughput screening lead **1** (Figure **1.23**), containing an L-lys-D-di-Br-Tyr dipeptide-like structure. This core structure is maintained in Olcegepant, with the SAR mainly focusing on the evolution of the terminal, piperidyl-linked dihydroquinazolinone in compound **2**, eventually leading to Olcegepant (Figure **1.23**). *In vitro* binding studies have revealed a greater affinity towards the CGRP receptor (K_i = 14.4 pM) than CGRP itself (K_i = 31.7 pM) (Doods, 2000). Kinetic studies, however, have showed that equilibration of Olcegepant to the receptor was achieved at 120 minutes at 1 µM, with a k_{off} value of 0.0018 min^{-1}, demonstrating slow binding kinetics (Schindler and Doods, 2002).

The structure of Olcegepant bound to the CLR/RAMP1 complex was resolved by ter Haar et al (Figure **1.24**) Olcegepant stretches across the interface of RAMP1 and deep into a hydrophobic binding pocket. There is a hydrogen bond formed between the quinazoline

moiety and the backbone NH and carbonyl of CLR residue Thr122, whilst the piperidine ring stacks on the Trp shelf of the receptor (Figure **1.24**). A branch formed by an amide linkage contains a dibromotyrosyl group, in which the hydroxyl group interacts via a water mediated hydrogen bond with CLR αC1 and RAMP1 αR2. There is also a hydrogen bond between the carbonyl group on the second amide linkage and the indole NH of CLR Trp72. A salt bridge is formed between side chain carboxyl group of RAMP1 and Asp72 and lysine of Olcegepant, and finally there is a stacking interaction between the terminal pyridyl group and the aromatic ring of CLR Phe92, with the pyridyl group also forming a hydrogen bond with the CLR side chain Asp94 carbonyl group (ter Haar et al., 2010). Key CLR and RAMP1 residues involved for Olcegepant binding to the CGRP receptor are highlighted in (Table **1.11**)

Olcegepant previously underwent clinical trials as a potential migrane treatment. The drug was found to be very effective at reducing migrane symptoms in the double blind trial compared with the placebo, and also exhibited very few adverse side effects in the patients (Olsen, 2004). However, due to the fact that the compound was a high molecular weight, polar, peptide-like compound containing more than 10 hydrogen bonding groups, the drugs oral bioavailability was very poor. This meant that the only real feasible method of administration was intravenous administration (Rudolph, 2005), (Doods, 2000). Therefore it's applications as a drug molecule for the treatment of migrane was limited.

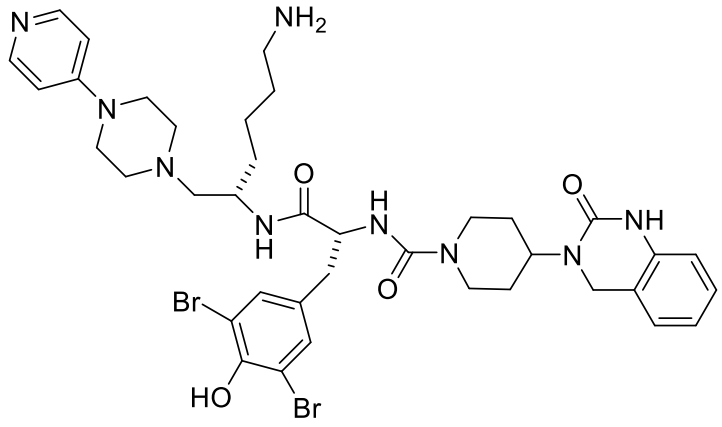

Olcegepant

Figure 1.22 – Chemical structure of Olcegepant

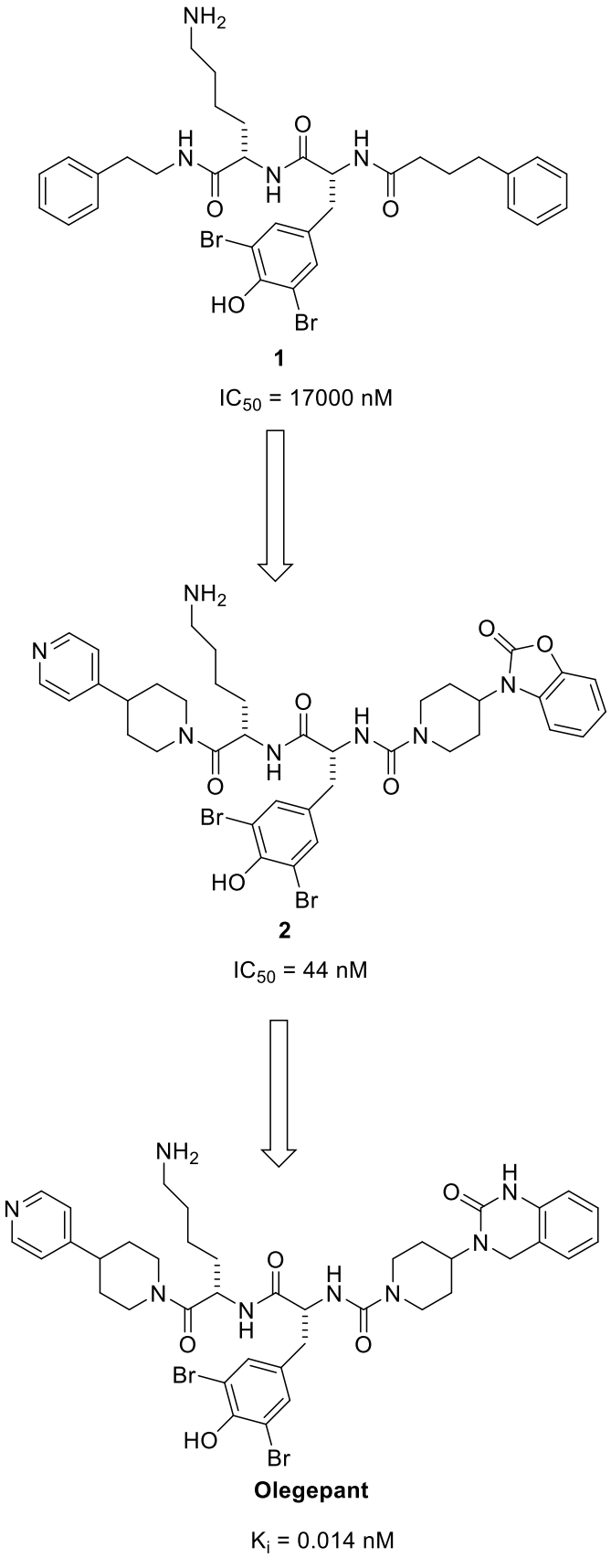

Figure 1.23 – Evolution of Boehringer Ingelheim lead compound 1 to Olcegepant. K_i and IC50 values are for CGRP

A

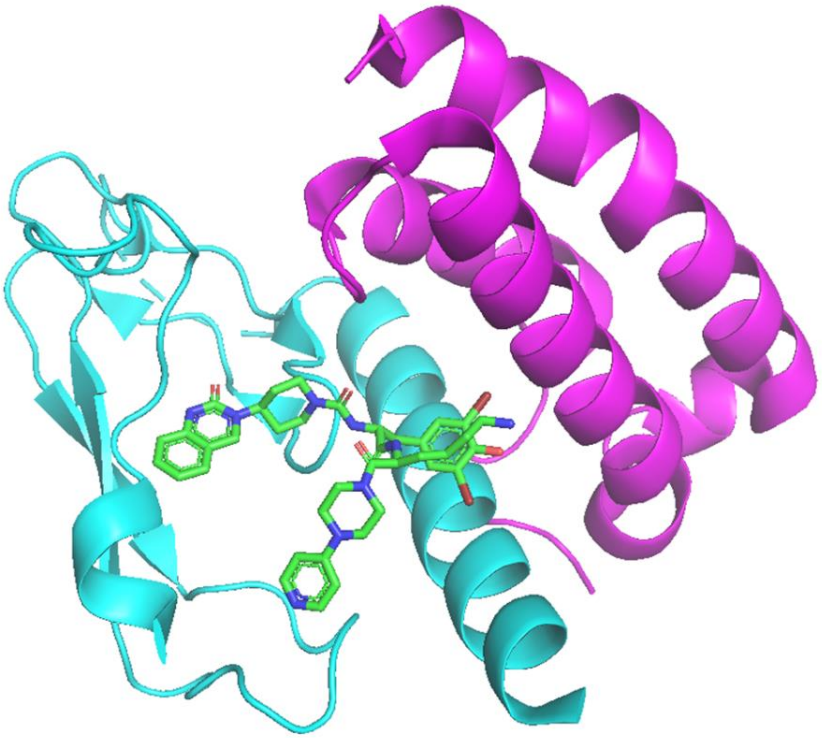

B

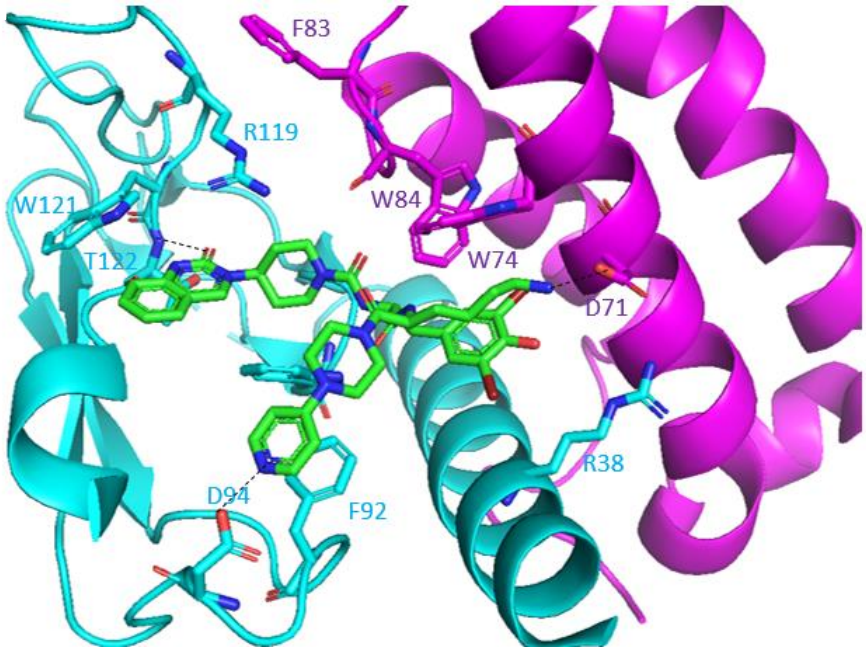

Figure 1.24 – Olcegepant bound to the CLR/RAMP1 complex. (A) Overview of Olcegepant binding to CLR (cyan) and RAMP2 (magenta) ECD. **(B)** Close up view of olcegepant binding to the CGRP receptor ECD. Key CLR and RAMP2 amino acid residues are outlined. Hydrogen bonds are indicated with dashed lines. Image was recreated from Ter Haar et al, 2010 and generated using PyMol Molecular Graphics System, Version 1.7.4.5-Educational Product, Schrodinger.

Encouraged by the potency of olcegepant, companies such as Merck set out to find a potent CGRP antagonist with good oral bioavailability. This led to the discovery of Telcagepant (Figure **1.25**) from screening lead **3** (Figure **1.26**). Initial SAR studies showed that replacing the spirohydantoin moiety with a piperidyl dihydroquinoline dramatically improved CGRP affinity (Williams, Stump et al., 2006). This group was later replaced with an azabenzimidazalone fragment seen in compound **5**, as compound **4** was prone to benzylic oxidation (Burgey, Stump et al., 2006). The benzodiazepinone ring was also investigated, with simplification to the caprolactam in Compound **6** greatly improving oral bioavailability (Shaw,2007), whilst the (3R,6S) stereochemistry of the 6-aryl ring proved to be optimal for binding affinity (Panone, 2007) (Figure **1.26**). Optimization of the substituents on the caprolactam ring eventually led to Telcagepant (Panone, 2007).

Although Telcagepant's potency towards the CGRP receptor (K_i = 0.78 nM) was lower than that of olcegepant, it's lower molecular weight meant the oral bioavailability was much improved and was therefore more clinically applicable (Salvatore, 2008). Telcagepant also displayed fast binding kinetics, with association rate constant k_{on} of 1.01 x 10^{-9} M^{-1} min^{-1} and a k_{off} of 0.51 min^{-1} (Moore, Burgey et al., 2009)

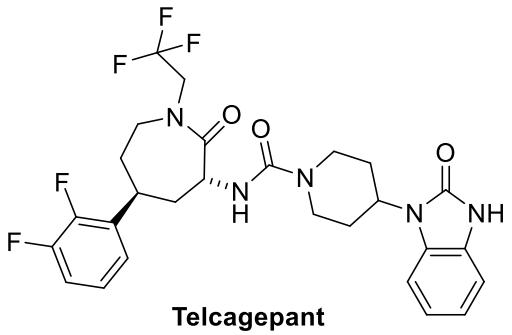

Telcagepant

Figure 1.25 – Chemical structure of telcagepant

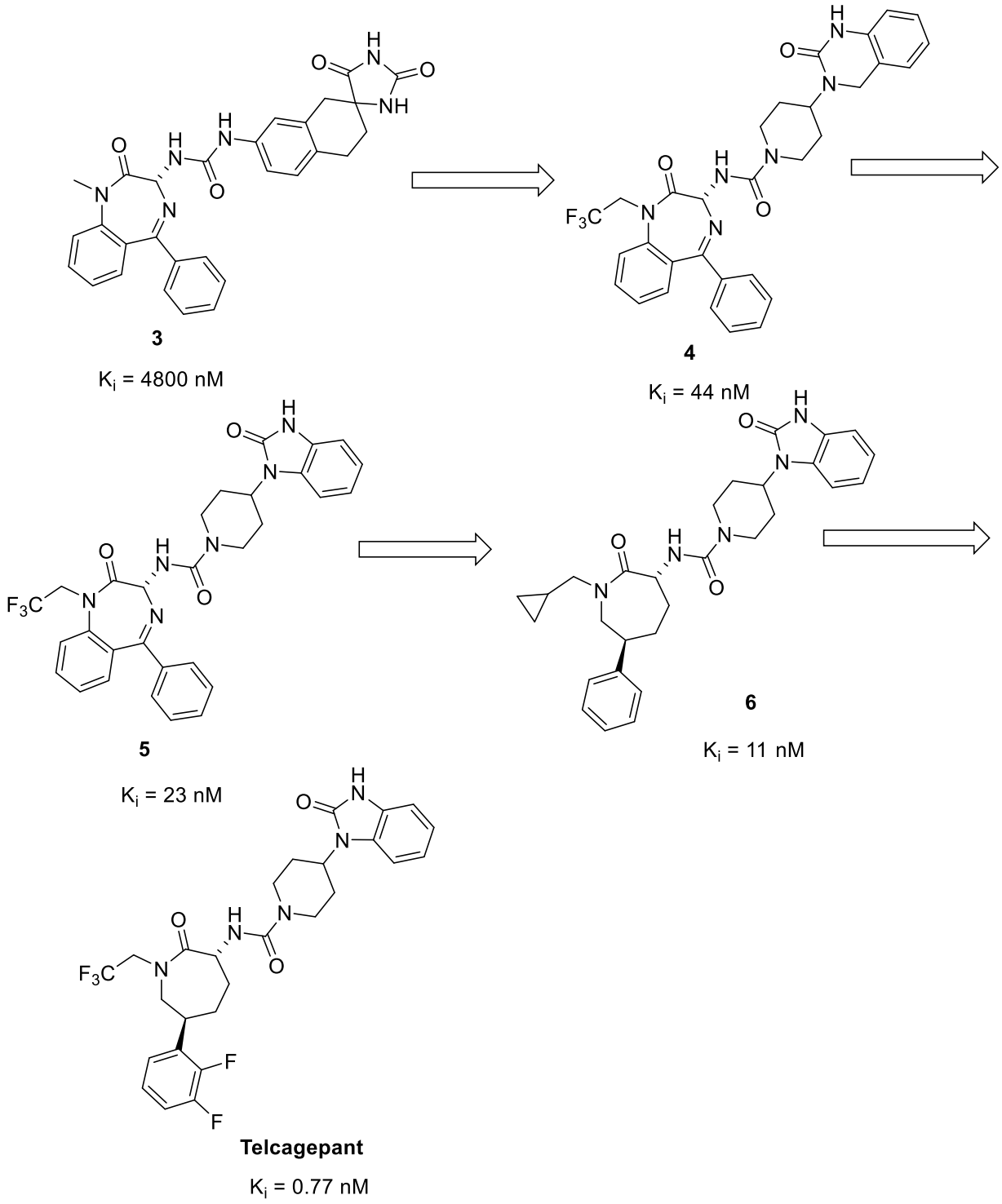

Figure 1.26 – Evolution of Merck lead compound 3 to Telcagepant. K_i values are for CGRP

Telcegapant contains subtle differences in structure but maintains similar binding topology to Olcegepant (ter Haar, Koth et al., 2010) (Figure **1.27**). As with Olcegepant, the piperidyl moiety forms stacking interactions with CLR Trp72, whilst the carbonyl group of the amide, this time on a seven-membered caprolactam ring forms hydrogen bonds with indole NH of

the Trp72 residue. However, there is slightly different topology at the hydrogen bond donor-acceptor site on CLR to hydrophobic pocket on RAMP1. The azabenzimidazole ring system of Telcegapant forms additional hydrogen bonds at backbone carbonyl of CLR Thr122 (Figure **1.27**). The binding of the difluorophenyl group appears hydrophobic, and additional contacts arise between ligand trifluoroethyl group and side chain of CLR Ile41 (ter Haar, Koth et al., 2010). Key CLR and RAMP1 residues involved in Telcagepant binding are summarised in Table **1.11**)

As Telcagepant is significantly smaller and more lipophilic than Olcegepant, the pharmacokinetic properties of this compound were significantly improved. Telcagepant showed good oral bioavailability in rats (F = 22%) and dogs (F = 35%) (Roller, 2009). Oral bioavailability in monkeys, however, was lower (F = 6%) and not dose-proportional, indicative of intestinal first-pass metabolism (Roller, 2009). Telcagepant is also highly protein bound compared to Olcegepant. As a result of good bioavailability, affinity and potency, Telcagepant became the first CGRP antagonist to reach clinical trials (Roller, 2009). Despite promising results in phase II and phase III trials, however, there were several reports of patients experiencing elevated liver transaminase, resulting in a hepatoxicity risk. This resulted in the drug being discontinued in 2011 .

The resolved crystal structures of Olcegepant and Telcagepant bound to the CGRP receptor provided explanations for the observed SAR properties during the development of the two antagonists. The SAR studies during development of Olcegepant (Rudolf et al., 2005) showed that the piperidyl amide group is crucial to antagonist binding to the CGRP receptor, as this forms extensive hydrogen bonds with CLR Thr122. In addition this unit can form a stacking interaction with CLR Trp72. In telcagepant, there is a tight SAR around the stereochemistry of the seven-membered caprolactam ring (Paone et al., 2007). The 6-phenyl caprolactam is more active than the 7-phenyl caprolactam as the latter cannot access the hydrophobic pocket. Furthermore, the stereochemistry at this benzylic position is also important, with the 3S compound resulting in a highly strained caprolactam ring that is unable to adopt the confirmation required for the phenyl to enter the hydrophobic pocket.

The binding modes of olcegepant and telcagepant are also consistent with previous mutagenesis studies. Data from ^{125}I-CGRP radioligand binding assays on human and rat CGRP receptors indicated that both olcegepant and telcagepant were more potent on the

human CGRP receptor (Mallee, Salvatore et al., 2002). The key residue was shown to be the 74 position on RAMP1, which forms the stacking interaction with the difluoroethyl group. The corresponding residue in rodent CGRP is a lysine unit, displaying the implications RAMP1 has on the binding of CGRP antagonists. Additionally, mutagenesis has also revealed a drop in potency when the CLR Met42 residue is substituted for an aniline (Miller, Barwell et al., 2010). This residue contacts the difluorophenyl group of telcagepant via hydrophobic interactions according to the published crystal structure.

Table 1.11 – Key residues involved in binding of Olcegepant and Telcagapent to CGRP Receptor

Compound	CLR Residues	RAMP Residues	Reference
Olcegepant	R38, M42, W72, F92, D94, T122	D72, W74	(ter Haar, Koth et al., 2010) (Miller et al., 2010)
Telcagepant	I41, M42, W72, T122	W74, W84	(ter Haar, Koth et al., 2010) (Miller, Barwell et al., 2010)

A

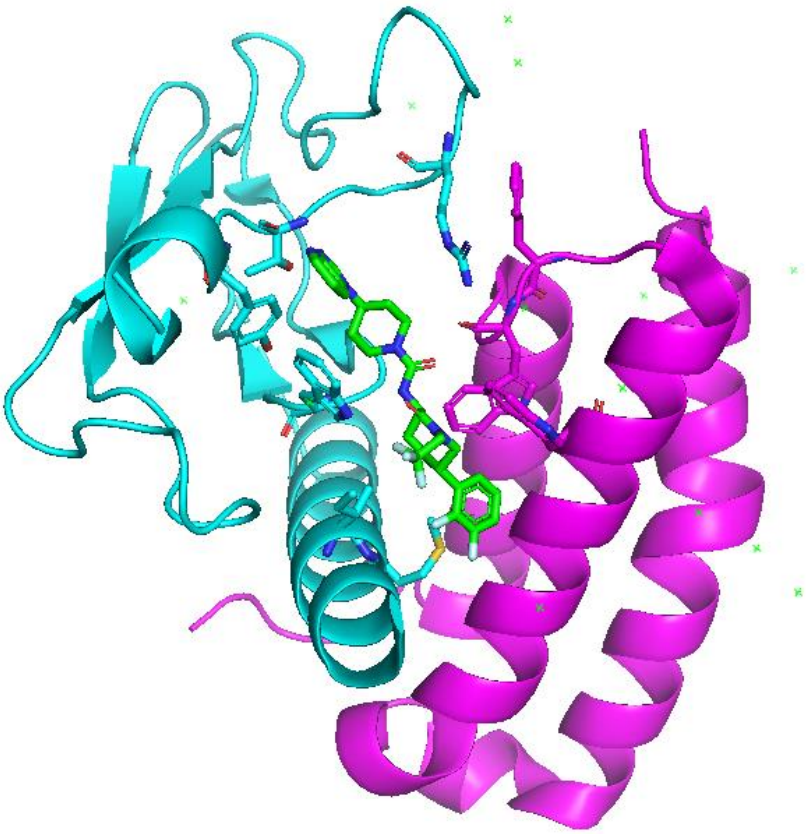

B

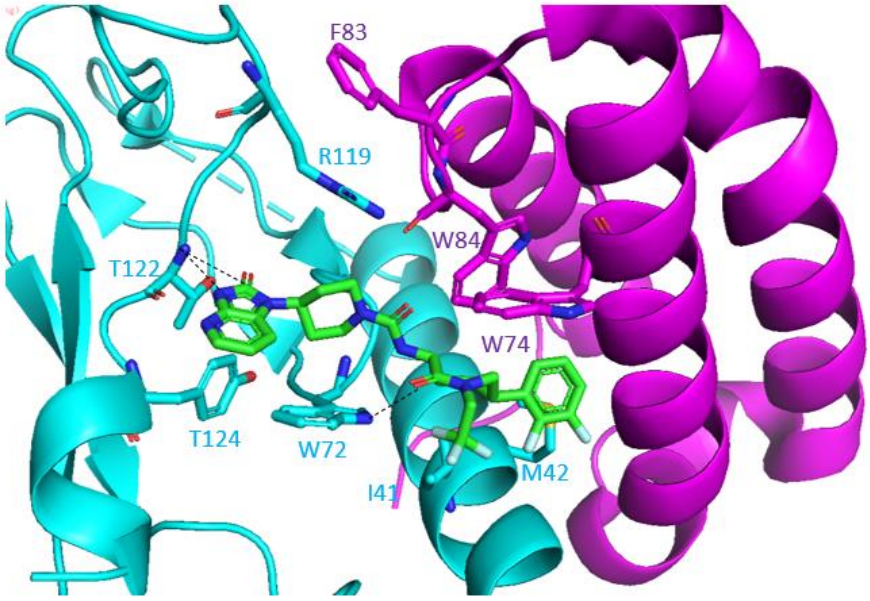

Figure 1.27 – Telcagepant bound to CLR/RAMP1 interface. (A) Overview of Telcagepant binding to CLR (cyan) and RAMP1 (magenta) ECD complex. **(B)** Close up view of Telcagepant binding to the CGRP receptor ECD. Key amino acid residues are outlined. Hydrogen bonds are indicated with dashed lines. Image was recreated from Ter Haar et al, 2010 and was generated using PyMol Molecular Graphics System, Version 1.7.4.5- Educational Product, Schrodinger.

1.5.2 Further CGRP Receptor Antagonists

Further development of Telcagepant by Merck led to the discovery of MK-2918 (Figure **1.28**). The aim was to improve the bioavailability and the pharmacokinetic properties of this compound. The idea was to fuse a triazole ring to the caprolactam group of Telcagepant in order to improve the aqueous solubility of the compound and reduce plasma protein binding (Paone, Nguyen et al., 2011). Compound **7** showed similar in vitro affinity (K_i = 1 nM) and potency (IC50 = 1.6 nM), and improved aqueous solubility, but displayed poor pharmacokinetics (F = 2%) which was thought to be due to low membrane permeability (Panone, 2011). Changing the triazole ring to an imidazole ring led to compound **8**, with

significantly improved membrane permeability and therefore improved bioavailability (F = 35%) whilst maintaining affinity and potency (K_i = 0.14 nM, IC50 = 0.37 nM) (Paone, Nguyen et al., 2011) (Figure **1.28**). Further optimization by varying substituents on the imidazole ring **8**led to the discovery of

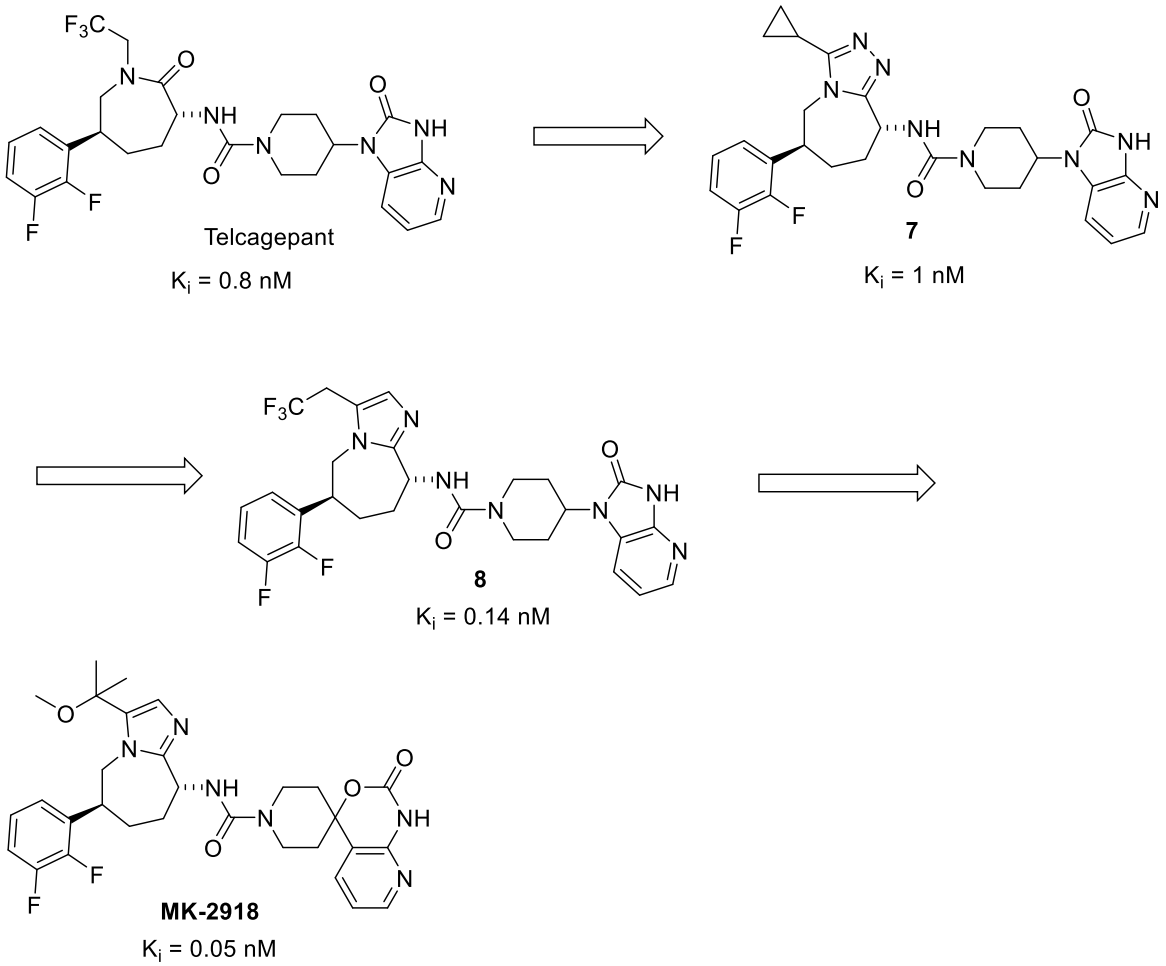

Figure 1.28 – SAR studies on Telcagepant leading to the discovery of MK-291. K_i values are for CGRP.

MK-2918, with much improved affinity and potency for the CGRP receptor (K_i = 0.05 nM, IC50 = 0.24 nM) (Paone, Nguyen et al., 2011) (Figure **1.28**).

As well as Telcagepant and subsequently MK-2918, a 2nd generation of CGRP antagonists was developed by Merck from compound **9** (Figure **1.29**). Replacement of the benzodiazepinone group with a benzimidazolinone group led to the discovery of compound **10** (K_i = 21 nM, IC50 = 78 nM) (Bell, Bednar et al., 2006) (Figure **1.29**). It was also noted that the stereochemistry of the spirohydantoin group was important for activity, with the (*R*)-enantiomer proving to be significantly more active than the (*S*)-enantiomer. Further modification of the spirohydantoin group to azaoxindole to improve receptor binding, as well as the benzodiazepinone group led to the tricyclic compound **11**, with significantly improved affinity and potency on CGRP (K_i = 0.23 nM, IC50 = 0.88 nM) (Stump, Bell et al., 2009) (Figure **1.29**).

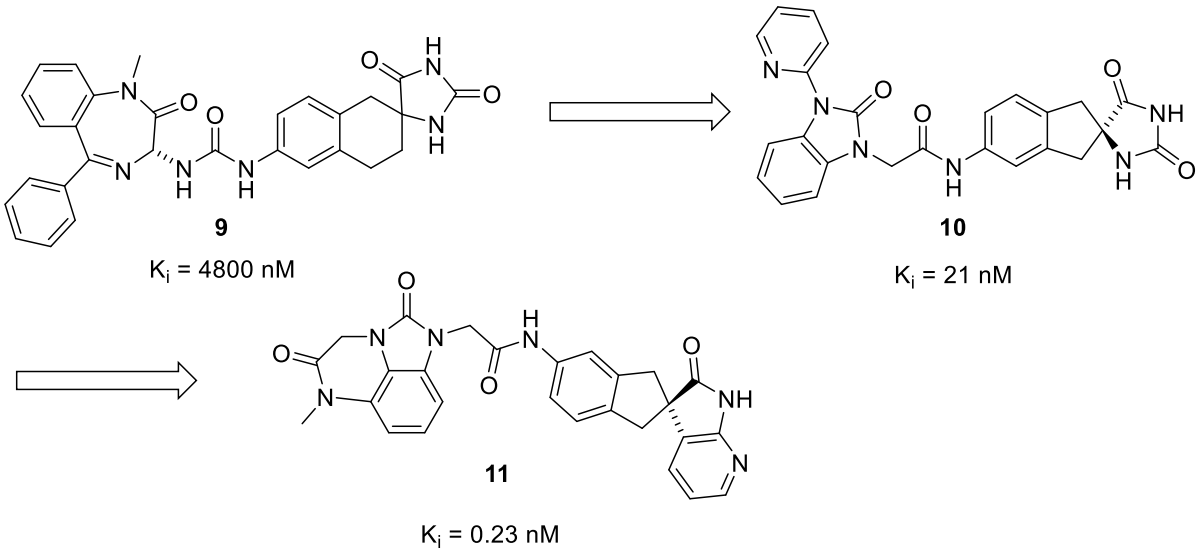

Figure 1.29 – **SAR Studies on compound 9 leading to the discovery of Compound 11.** K_i values are for CGRP

Despite the sub-nanomolar potency on the CGRP receptor, compound **11** exhibited poor bioavailability (F < 1%). This was thought to be due to the high polar surface area (PSA) of the compound, which subsequently leads to poor membrane permeability (Bell, Bednar et

al., 2009). Decreasing PSA by amide rigidification and simplification of structure led to compound **12** with good affinity for CGRP (K_i = 1.9 nM) (Wood, Schirripa et al., 2009) (Figure **1.30**). Interestingly for this compound, the stereochemistry of the spirohydantin group was (*S*) instead of (*R*). Compound **12**, however, also exhibited sub micromolar affinity for the AM_2 receptor (K_i (AM_2) = 710 nM), which meant further SAR studies were required to improve CGRP selectivity. Modification of the benzyl group to a 3,5-difluoro benzyl group led to significantly improved CGRP selectivity over AM_2, whilst subsequent reduction of flexibility by incorporation of the six-membered lactam led to compound **13** with subnanomolar CGRP affinity (K_i = 0.035 nM) (Figure **1.30**). The drawback of compound **13** was that it displayed low bioavailability in monkeys, which was thought to be due to poor aqueous solubility and a susceptibility to oxidative metabolism of the valerolactam. As a result, increasing polarity of the molecule by incorporating(Dubowchik, Conway et al., 2020) a heteroatom into the lactam ring led to the discovery of MK-3207, a compound with sub-nanomolar affinity and potency for CGRP (K_i = 0.021 nM, IC50 = 0.12 nM) and improved bioavailability and pharmacokinetic profile (Bell, Gallicchio et al., 2010) (Figure **1.30**). MK-3207 was taken further to clinical trials.

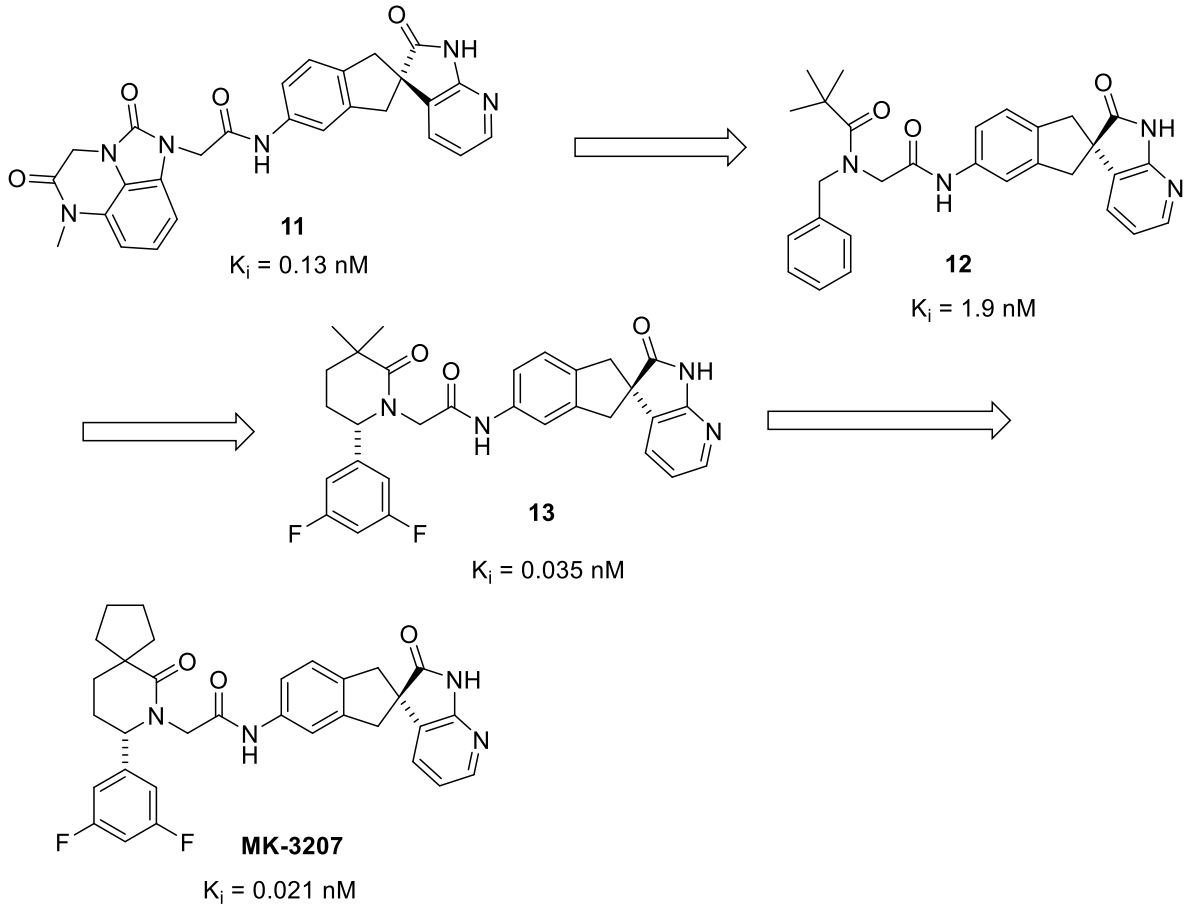

Figure 1.30 – SAR studies on Compound 11 leading to the discovery of MK-3207. K_i values are for CGRP

Despite the initial success of Telcagepant and MK-3207, there were reports during clinical trials that telcagepant was leading to hepatotoxicity in patients, leading to the drug not being approved for the commercial market. Merck research laboratories later confirmed that they thought that this just due to the chemical properties of the compound rather than non-specific binding in liver cells. Further work by Merck led to the discovery of atogepant and ubrogepant (Figure **1.31**), the first commercially available oral CGRP antagonist for the treatment of migrane. Ubrogepant and atogepant are structurally similar to telcagepant and differ only by their terminal benzene rings, with atogepant containing a trifluorophenyl group compared to the phenyl ring in ubrogepant. Atogepant is slightly more potent at the CGRP receptor, with a K_i of 0.015 nM compared to 0.067 nM for ubrogepant, suggesting that the trifluorophenyl group leads to greater CGRP potency (Dubowchik, Conway et al., 2020).

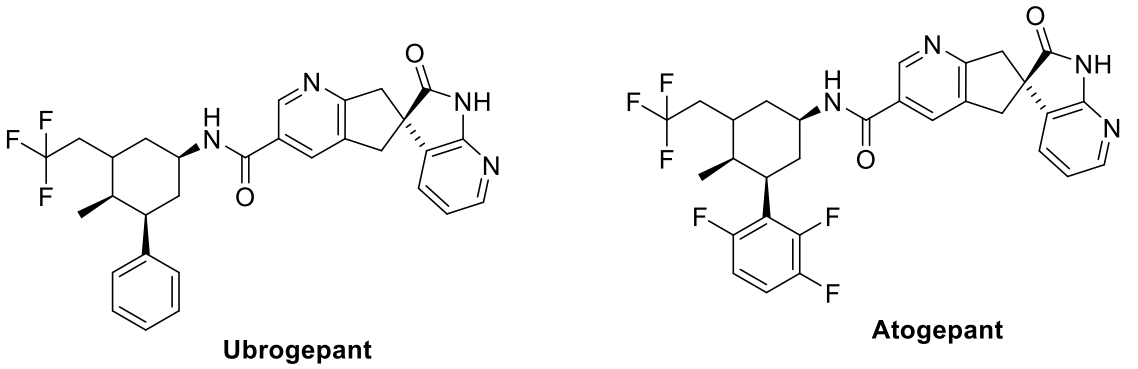

Figure 1.31 – Chemical structures of Ubrogepant and Atogepant

1.5.3 Selectivity of CGRP Antagonists

Olcagepant and telcagepant are very selective for the CGRP receptor over the AM receptors. Data has revealed, however, that despite this high selectivity the CGRP antagonists shown above do show some affinity to the AM receptors. One of the key reasons for the selectivity of CGRP antagonists is the differences in the amino acid residues between RAMP1 and RAMPs 2 and 3. In RAMP2, for example, the key W74 residue for RAMP1 in the binding pocket is non-conservatory replaced by an acidic glutamate residue (also observed at the 101 position). RAMP2 additionally contains a salt bridge between Arg97 and Glu101 in both peptide bound and unligated AM_1. The RAMP3 ECD has not yet been fully resolved, but, on the basis of a homology model, it is believed that the W74 residue is also replaced with a glutamate residue. It is also thought that the RAMP residues in the antagonist binding site in which the small molecule antagonists interact could be very different in the AM receptors compared to the CGRP receptor.

The CLR/RAMP pocket will differ the most between the binding sites of CGRP receptor and the AM receptors. Therefore, it will be the blue, aromatic pharmacophore of the antagonists at the RAMP binding end that will modulate the selectivity of the antagonists. The W74 residue in RAMP1 is replaced by a negatively charged, acidic E101 residue in RAMP2. Although the W84 residue is also not conserved, this is replaced by the aromatic residue Phe111. This is also the case for RAMP3, suggesting that retaining the aromatic group but introducing some basic centres to target the glutamate residues might be the best way forward to developing antagonists that are more selective for the AM receptors (see later).

1.5.4 AM_2 Antagonists

Potent AM_2 antagonists have recently been discovered by Avgoustou *et al* as a potential anticancer drug (Avgoustou, Jailani et al., 2020) (Figure **1.32**). The structure of this compound was based off of the general structure of previous CGRP antagonists, with the strategy to identify key differences in binding pocket residues between RAMP1 and RAMP3 and modify the RAMP binding end of the molecule accordingly. The key target was RAMP3 Glu74 residue, with the equivalent position in RAMP1 being Trp74. Therefore AM_2 antagonists were designed by using CLR binding fragments previously established in CGRP antagonists whilst introducing basic centres into the RAMP end with the aim of forming an ionic interaction with RAMP3 E74 (Zirimwabagabo, Jailani et al., 2021). Using compound **12** as a starting point, a highly potent AM_2 antagonist compound **14** was discovered (cAMP IC_{50} = 0.63 nM), whilst displaying over 1000-fold selectivity for AM_1 and 6-fold selectivity for CGRP.

The anticancer properties of compound **14** was shown *in vitro*, with a 3 µM concentration decreasing cancer cell viability over 9 days. Compound **14** was also effective *in vivo*, with daily administration demonstrating 56% tumour growth inhibition in mice. The ADME properties of compound **14** also make it promising for drug development. The compound was shown to be moderately lipophilic (Log $D_{7.4}$ = 1.58) and showed moderate binding to plasma proteins, with unbound fractions of 22.9% in humans. Additionally compound **14** displayed moderate inhibition of P450 enzymes, and displayed low inhibition of hERG potassium channels (IC50 > 30 µM), indicating low risk of cardiac arrhythmia (Avgoustou, Jailani et al., 2020).

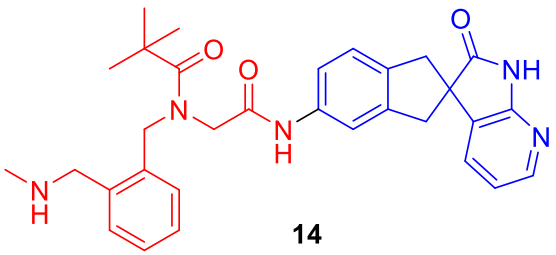

14

Figure 1.32 – Chemical structure of lead small molecule antagonist for the AM_2 receptor. CLR binding section of the molecule is highlighted in blue, and the RAMP binding section is highlighted in red.

Despite the relatively modest selectivity for the AM_2 receptor over the CGRP receptor for compound **9**, the 10-fold selectivity is still significant. The compound was synthesised by an efficient synthetic route, with all 10 steps producing high to excellent yields, making the compound accessible in reasonable quantities (Zirimwabagabo, 2021). Compounds such as these can provide a starting point for further potent, and more selective, small molecule antagonists for the AM_2 receptor as well as help us to further understand how AM is involved in the growth of tumours.

1.6 Aims and Objectives

Our group is currently devoted to finding small molecule antagonists for CLR/RAMP receptors. Developing antagonists such as these can aid in further understanding of how RAMPs allosterically alter the pharmacology of the CLR, and by extension GPCRs. Previous CLR/RAMP antagonist have been shown to treat against various diseases. Work by Merck among others have led to highly potent and selective CGRP receptor (CLR/RAMP1) small molecule antagonists which have been applied to the treatment of migraine. Two such antagonists are now commercially available. Previous work in house has led to the discovery of highly potent AM_2 (CLR/RAMP3) receptor antagonists with high selectivity over the AM_1 receptor. Whilst not commercially available, these molecules have shown to be very promising anticancer drugs, with *in vitro* studies showing the inhibition of growth of a pancreatic cancer cell line. They have also been shown to inhibit pancreatic cell growth *in vivo.* Furthermore, the compounds have shown promising potential for development into drug-like compounds.

This is focused on the development of potent and selective small molecule antagonist for the AM_1 receptor (CLR/RAMP2). This is currently an underdeveloped area; no small molecule AM_1 antagonists have been reported in the literature. It is theorized that these compounds could have medical applications, particularly in Septic Shock. AM concentrations increase 40 fold during the onset of sepsis and it is thought that, due to the peptide being a potent vasodilator, that AM plays a key role in the dramatic blood pressure drop observed during septic shock. As AM signalling through the AM_1 receptor is thought to be the cause of AMs vasodilator actions, we theorize that compounds blocking this receptor will reverse the

blood pressure drop seen in Septic Shock patients, to then allow treatment with antibiotics to cure the initial infection. We will use classic medicinal chemistry strategies to design potential AM_1 antagonists. Our starting points for this will be to design structurally similar molecules to previous AM_2 antagonists with focus on targeting RAMP2 residues, and to use the results of a high throughput screening from a European Lead Factory to generate candidate compounds.

Hypothesis:

1. Designing small molecules based on the AM_2 antagonists but tweaking the RAMP binding motifs to target RAMP2 residues will lead to potent and selective small molecule AM_1 antagonists.
2. Designing molecules based on the structures of the active compounds from the results of a high throughput screening from the European Lead Factory will lead to potent AM_1 antagonists

Objectives

- Use previous AM_2 antagonists and active compounds from the ELF high throughput screening to design novel small molecule antagonists for the AM_1 receptor
- Use the Schrodinger software Maestro to dock candidate compounds into the extracellular domain of the AM_1 receptor to study their interactions with the CLR and RAMP2 proteins
- Carry out the efficient chemical synthesis of candidate compounds using well known synthetic organic chemistry techniques
- Carry out the *in vitro* biological testing of the synthesised compounds by measuring their ability to inhibit the AM induced production of the secondary messenger cAMP on CHO-k1 cells overexpressing the AM_1 receptor. Potent compounds will be counter-screened against CGRP and AM_2

Chapter 2 – Design of AM1 Antagonists Using Structures of Previous CGRP and AM2 Antagonists

Chapter 2: Design of AM_1 Antagonists Using Structures of Previous CGRP and AM_2 Antagonists

2.1 Design of AM_1 Antagonists from CGRP and AM_2 antagonists

2.1.1 Structural Analysis of CGRP Antagonists

The chemical structures of the CGRP antagonists Olcegepant, Telcagepant, MK-2198 and MK-3207 can be divided into three different fragments or binding motifs based on the regions of the CGRP binding pocket they associate with: the CLR binding region, the CLR/RAMP interface and the RAMP/CLR interacting region (Figure **2.1**). The CLR binding fragment refers to the region of the molecule that binds exclusively to the CLR end of the receptor, whilst the CLR/RAMP interface fragment is designed mainly to target the CLR Trp72 residue. Finally, fragments targeting the RAMP/CLR interacting region are designed to target variable residues on the RAMP1 protein.

During the discovery of Olcegepant (Figure **2.1 A**), large increases in potency were observed when a hydroquinazolinone group was introduced into the molecule (Rudolph, 2005). This structure contains a hydrogen bond donor acceptor pair. The crystal structure of Olcegepant bound the CGRP receptor revealed that this group forms hydrogen bonds with the amide backbone of the CLR Thr122 residue (Figure **2.2**), indicating that this motif is key to Olcegepant binding with the CLR end of the receptor (ter Haar, Koth et al., 2010) (Figure **2.1**). The structure of Telcagepant contains a very similar CLR binding motif, with the crystal structure of this compound bound to the CGRP receptor also confirming the interactions with the Thr122 residue (Figure **2.2**). Although the crystal structures of the additional Merck CGRP antagonists hasn't been solved, all structures contain similar groups with the hydrogen bond donor acceptor pair, indicating that these compounds also form similar interactions with Thr122.

The structures of Olcegepant and Telcagepant also show that the dipeptide unit in Olegepant and the heteroatoms in the caprolactam group of Telcagepant interact with the

same residues, W72 of CLR and W74 and W84 of RAMP1, at the CLR/RAMP1 interface (Archbold, Flanagan et al., 2011). The Lys moiety of Olegepant and the trifluoro ethyl group of Telcagepant also occupy similar positions, with the pyridyl chain of Olegepant extending further away from this site. Replacements for the seven-membered caprolactam group on Telcagepant have included the imidazoazepane group on MK-2918 (Figure **2.1**), whilst the substituted imidazole group on this compound serves as a replacement for the caprolactam carbonyl group (Paone, Nguyen et al., 2011). For MK-3207, the spiropentane piperazinone core corresponds to the caprolactam group.

The receptor structure of Telcagepant shows that the halogen containing aromatic ring accesses the rear of the hydrophobic binding pocket formed by the CLR/RAMP1 interface. It is thought that the corresponding groups in MK-3207 and MK2918 do likewise (Figure **2.1**). SAR studies show that the stereochemical orientation of this group is important, as the R configuration here instead of the S configuration leads to a significant decrease in potency (Paone, Nguyen et al., 2011).

A

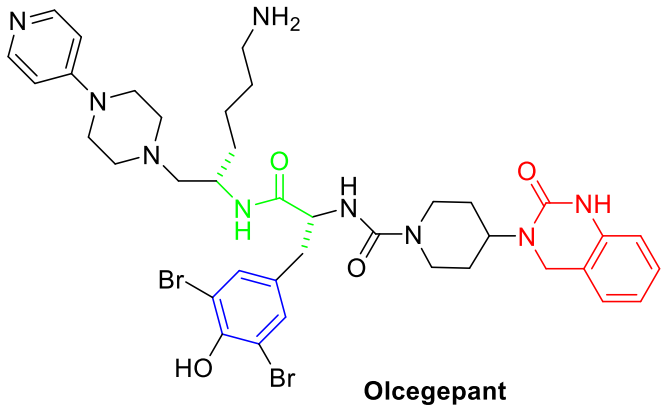

Olcegepant

B

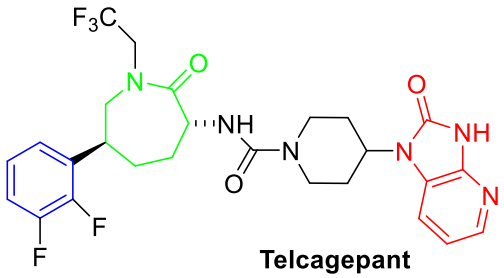

Telcagepant

C

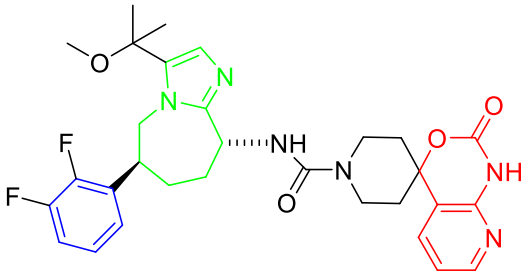

MK-2918

D

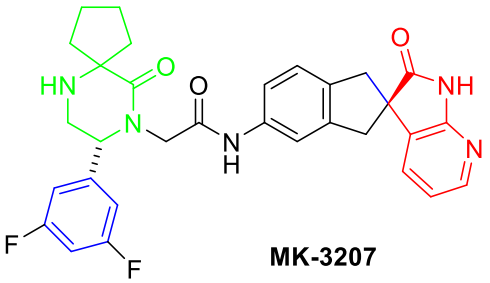

MK-3207

Figure 2.1 – Comparison of the chemical structures of CGRP antagonists Olcegepant (A), Telcagepant (B), MK-2918 (C) and MK-3207 (D), highlighting the key binding fragments. The CLR binding regions are highlighted in red, the CLR/RAMP interface binding regions are highlighted in green, and the RAMP/CLR interacting region is highlighted in blue.

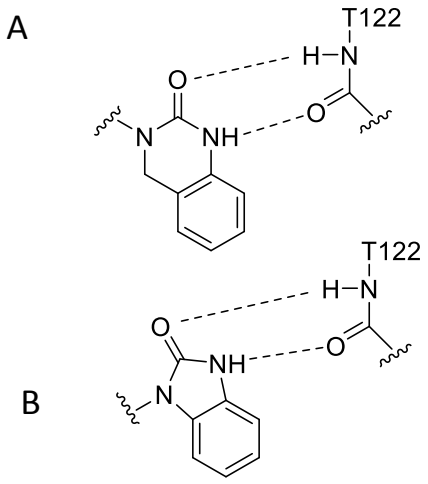

Figure 2.2 – CLR binding motifs of Olcegepant (A) and Telcagepant (B) interacting with CLR Thr122 amide backbone. Hydrogen bonds are indicated by dashed lines

2.1.2 Structural Analysis of AM_2 Antagonists

The structures of current lead compounds for AM_2 inhibitors are largely based on the structures of the CGRP antagonists (see Chapter 1). As stated previously, the key differences in RAMP3 residues compared with RAMP1 residues in the receptor binding pocket were exploited, whilst interactions with the CLR end of the binding pocket were maintained (Zirimwabagabo, Jailani et al., 2021). The key target was the RAMP3 Glu74 residue, with the corresponding RAMP1 residue being a Trp residue. With no available crystal structure, a homology model of the AM_2 binding pocket was subsequently constructed by transposing the Glu105 side chain of RAMP2 into the RAMP1 Trp74 position in the CGRP binding pocket (Figure **2.3**). Subsequent docking studies led to the use of compound **15** as a starting point (Figure **2.4**) (Zirimwabagabo, Jailani et al., 2021).

During the process of the discovery of AM_2 lead compound **14** from compound **15**, there was minimal optimisation of the CLR binding group of the molecule, with only a small selection of CLR binding fragments investigated. The optimal CLR binding group for the AM_2 antagonists was the indene group also seen in MK-3207 (Zirimwabagabo, Jailani et al., 2021). The RAMP end of the molecule required significantly more attention during optimisation, with key focus on varying the type and position of the substituent on the

benzyl group of the RAMP fragment. It was found that adding a benzylic amine group to the 2-position of the benzyl ring significantly increased AM_2 potency, thus confirming the hypothesis that adding basic groups to the RAMP binding fragment would increase AM_2 potency (Figure **2.4**).

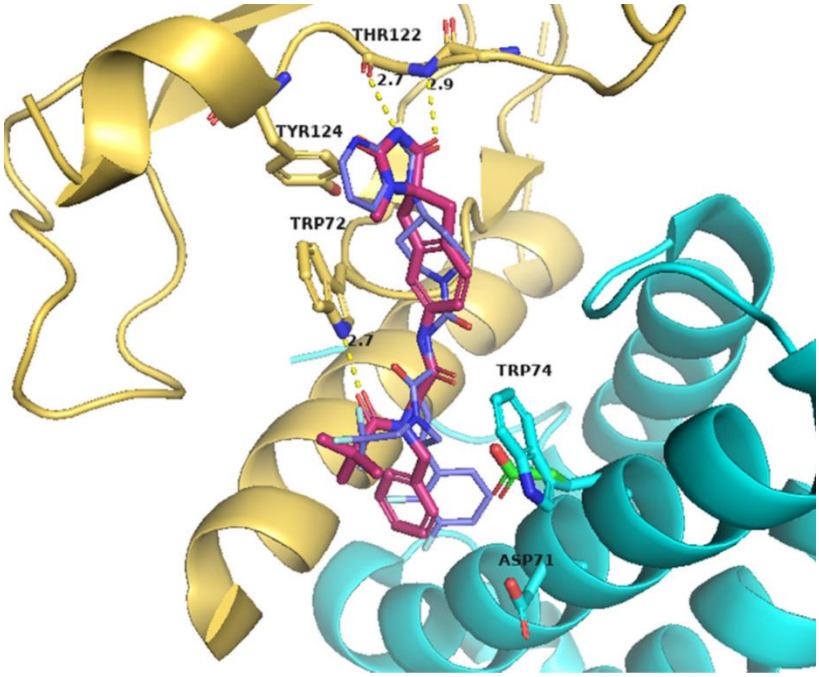

Figure 2.3 – Docking poses of Telcagepant (Magenta) and Compound 1 (Purple) in the homology model of the AM_2 receptor ECD. The CLR is coloured in yellow and RAMP3 is coloured in cyan. Hydrogen bonds are displayed as dashed yellow lines. Key CLR and RAMP3 residues are outlined.. Image from Zirimwabagabo, 2021.

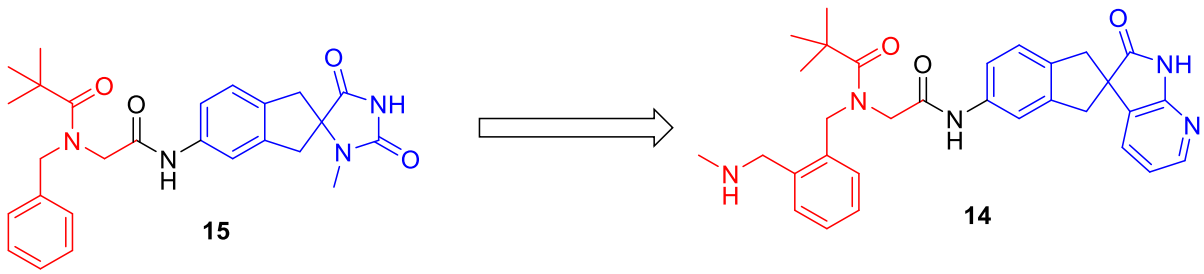

IC50 = 1300 nM

IC50 = 0.6 nM

Figure 2.4 – Discovery of AM_2 lead 2 from Merck compound 1. CLR binding fragments are highlighted in blue, whilst RAMP binding are highlighted in red. IC50 values are displayed for comparison

Although there is no crystal structure available for the binding of these compounds to the AM_2 receptor, analysis of the structures of lead AM_2 antagonist compound **14**, and comparison to the structures of CGRP antagonists, can lead to predictions of the key binding groups of these compounds. Previous evidence suggests that the lactam of the CLR binding group will form hydrogen bonds with the backbone amide of the CLR Thr122 residue, due to the retention of the hydrogen bond donor acceptor pair from CGRP antagonist CLR binding group. Evidence also suggests that the pivalamide group is the CLR/RAMP interface binding fragment, in which the carbonyl of this group can form a hydrogen bond with the CLR Trp72 residue. Indeed, the dock of compound **1** into the homology model suggests that this interaction, as well as the Thr122 hydrogen bond with the CLR binding fragment, is present (Zirimwabagabo, Jailani et al., 2021). Finally, it is likely that the benzyl group of the molecule reaches into the rear of the binding pocket and interacts with RAMP3 residues. As the benzylic amine would be ionised at physiological pH, it can be assumed that this will form a salt bridge with the RAMP3 Glu74 residue. As this residue is not conserved in RAMP1 or RAMP2, it is likely that this interaction contributes to selectivity over the CGRP and AM_1 receptors (Figure **2.3**).

2.1.3 Design of Potential AM_1 Antagonists and Hypothesis

As with the CGRP and the AM_2 receptor, the AM_1 receptor is a heterodimer consisting of the CLR and a RAMP. The key difference between the three receptors is the RAMP part, with RAMP2 being present in AM_1 rather than RAMP1 or RAMP3 in CGRP and AM_2 respectively. The RAMPs just 30 % sequence homology, and the RAMP2 residues in the AM_1 binding pocket have been shown to be very different when compared to those in the CGRP binding pocket (Booe, Walker et al., 2015). On the other hand, the CGRP, AM_1 and AM_2 residues share the same CLR unit, with the CLR binding pocket residues remaining consistent across the CGRP and AM_1 receptor.

It is therefore hypothesised that development of potent AM_1 antagonists can be achieved modifying the structure of previous CGRP and AM_2 antagonists to target binding to RAMP2 binding pocket residues. To that end the aim was to use the optimized CLR end from the AM_2 antagonists, designated SHF355 (Figure **2.5**), and couple this fragment to various potential RAMP2 ends to perform a screening of potential AM_1 antagonists (Figure **2.6**). Furthermore, examining the key RAMP residues in the CGRP, AM_1 and AM_2 antagonists

(Table **2.1**), the biggest difference in RAMP2 was the serine residue at position 9, with the equivalent residues being Arg67 in RAMP1 and Glu67 in RAMP3. Therefore it was hypothesised that RAMP binding motifs containing hydrogen bond donors or acceptors would provide antagonists with greater potency at the AM_1 receptor.

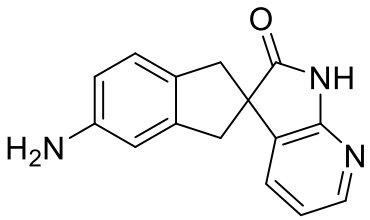

SHF355

Figure 2.5 – Chemical Structure of SHF355

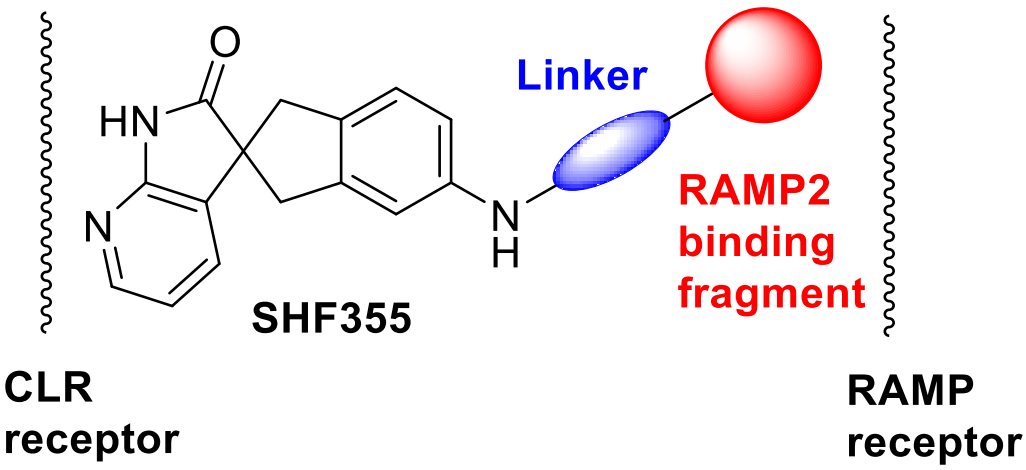

Figure 2.6 – Outline of the design strategy for AM_1 antagonists using a known CLR binding fragment, CLR B, linked to potential RAMP2 binding fragments

Table 2.1 – Significant RAMP residue differences in the CLR/RAMP receptor binding pocket identified during the discovery of AM_2 antagonist. RAMP2 residues displayed are in the equivalent positions to that of RAMP1 and RAMP3

Protein Residue Number	RAMP1	RAMP2	RAMP3
67	Arg	Ser94	Glu
70	Ala	Arg97	Thr
71	Asp	Asp98	Asn
74	Trp	Glu101	Glu

2.2 Synthesis of SHF355 Based AM_1 Antagonists

2.2.1 Synthesis of SHF355

The synthesis of the SHF355 based antagonists began with the synthesis of racemic CLR B. This was carried out using a route previously utilised in house (Scheme **2.1**). The synthesis began with the trimethylsilylethoxymethyl (SEM) protection of the indole nitrogen of 7-azaindole (Compound **16**) using SEM-Cl and sodium hydride to form compound **17**. Compound **17** was then oxidised and brominated using pyridinium tribromide to form the α-dibromo ketone, before debromination using zinc and ammonium chloride led to the formation of compound **19**.

The next stage of the synthesis was to form compound **24**, the alkylating agent for the formation of the spirocycle. Dicarboxylic acid **22** was firstly reduced to the corresponding dialcohol **23** using borane dimethyl sulfide complex, before double bromination using phosphorus tribromide successfully yielded the desired dibromo compound **24**.

With both compounds **19** and **24** in hand, the next step was the formation of the spirocyclic compound **20.** Using caesium carbonate as the base led to the successful formation of compound **20**, albeit at a moderate yield (45%). The lower yield for this step was likely due to the instability of the dibromo compound **24.** Compound **20** then underwent subsequent nitro reduction to the corresponding aniline using zinc and ammonium chloride, before

finally deprotecting the SEM group using hydrochloric acid in methanol led to the successful formation of SHF355.

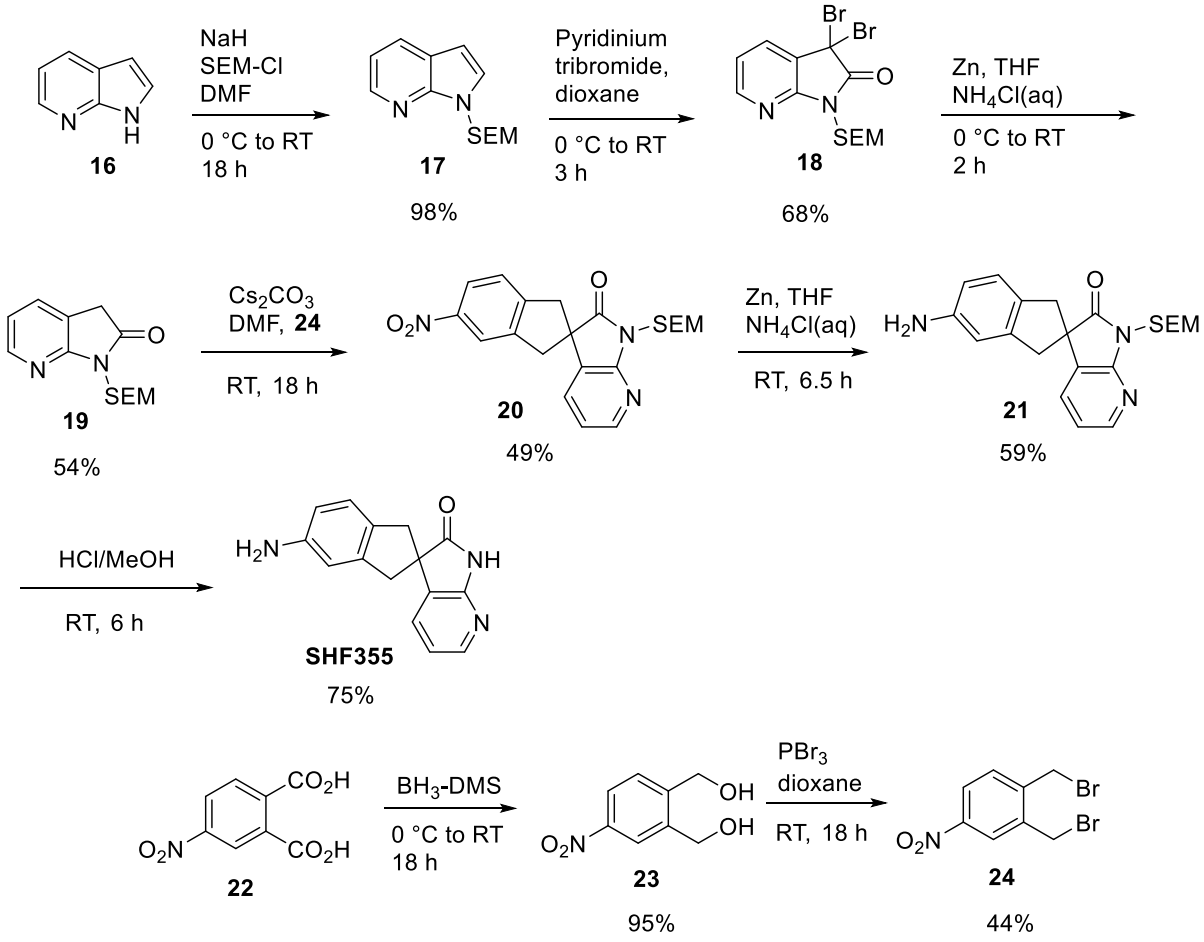

Scheme 2.1 – Synthetic route towards racemic SHF355

2.2.2 Coupling of SHF355 to RAMP ends

SHF355 was next coupled to various fragments acting as potential RAMP binding motifs. A variety of readily available carboxylic acids were linked to SHF355 via amide coupling using hexafluorophosphate azabenzotriazole tetramethyl uronium (HATU) as the coupling reagent and N-methylmorpholine (NMM) as the base (Scheme **2.2**). This method had previously been used in the synthesis of AM_2 antagonists (Zirimwabagabo, 2021). The reactions were carried out at a 10 mg scale before purification by high performance liquid chromatography (HPLC). A range of aromatic carboxylic acids were used in the coupling, including those bearing fluoro, bromo, nitro, trifluoromethyl and aniline substituents.

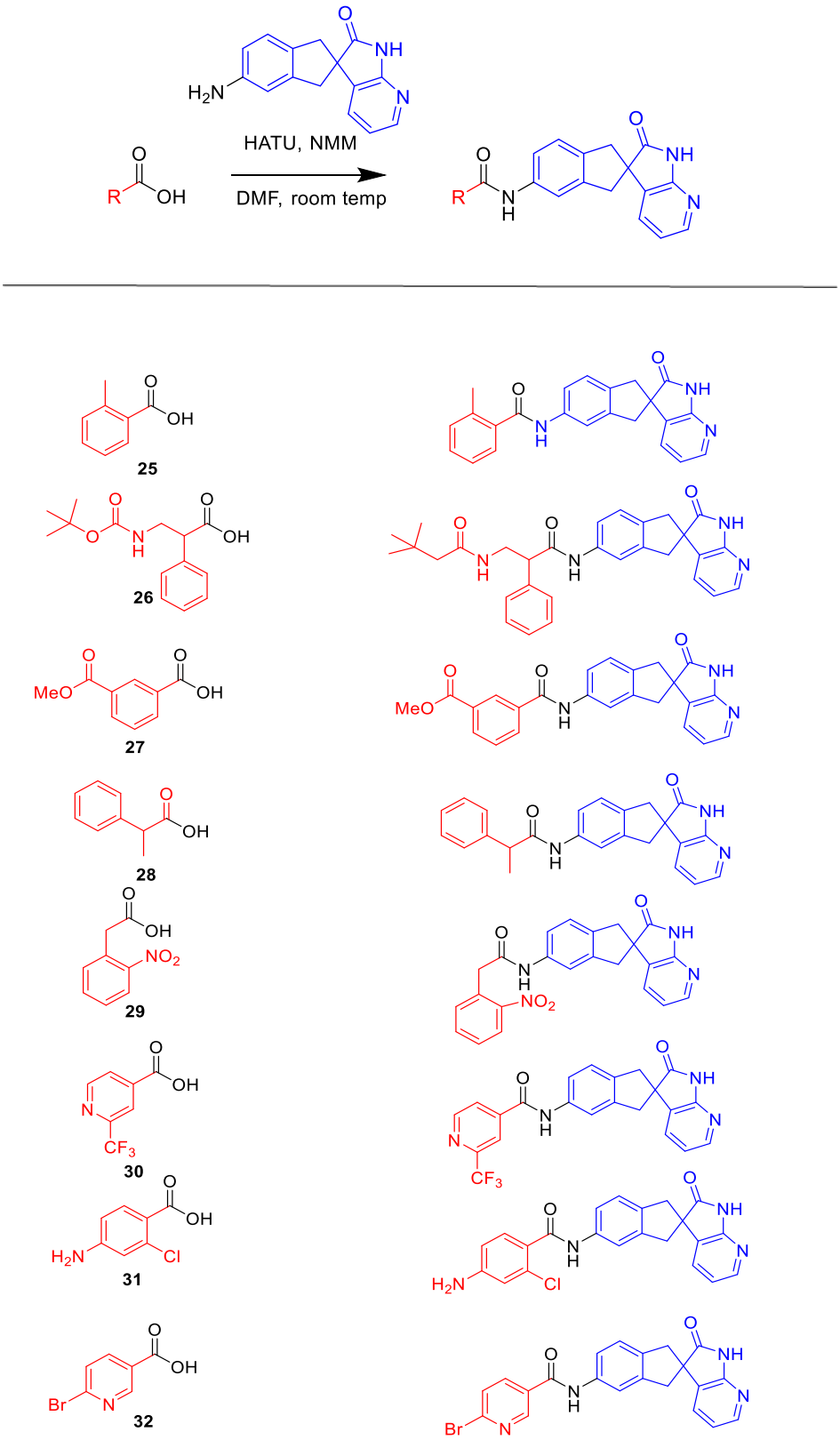

Scheme 2.2 – Coupling of potential RAMP (red) binding motifs to SHF355 (blue) by formation of an amide bond.

A small range of available esters were also subjected to coupling to SHF355 via ester hydrolysis to the corresponding carboxylic acid using lithium hydroxide, followed by subsequent HATU coupling to SHF355 using the method described above (Scheme **2.3**). Compounds produced by this method included RAMP ends with imidazole pyridine and Boc protected piperidine. Compounds containing groups suitable for hydrogen bonding were also coupled to CLR B (Scheme **2.4**). Compound **35** was coupled to SHF355 at the acid chloride, resulting in the formation of the SHF355 coupled ester compound. The ethyl ester was additionally hydrolysed to the corresponding carboxylic acid. Both the ester and the carboxylic acid were submitted for testing.

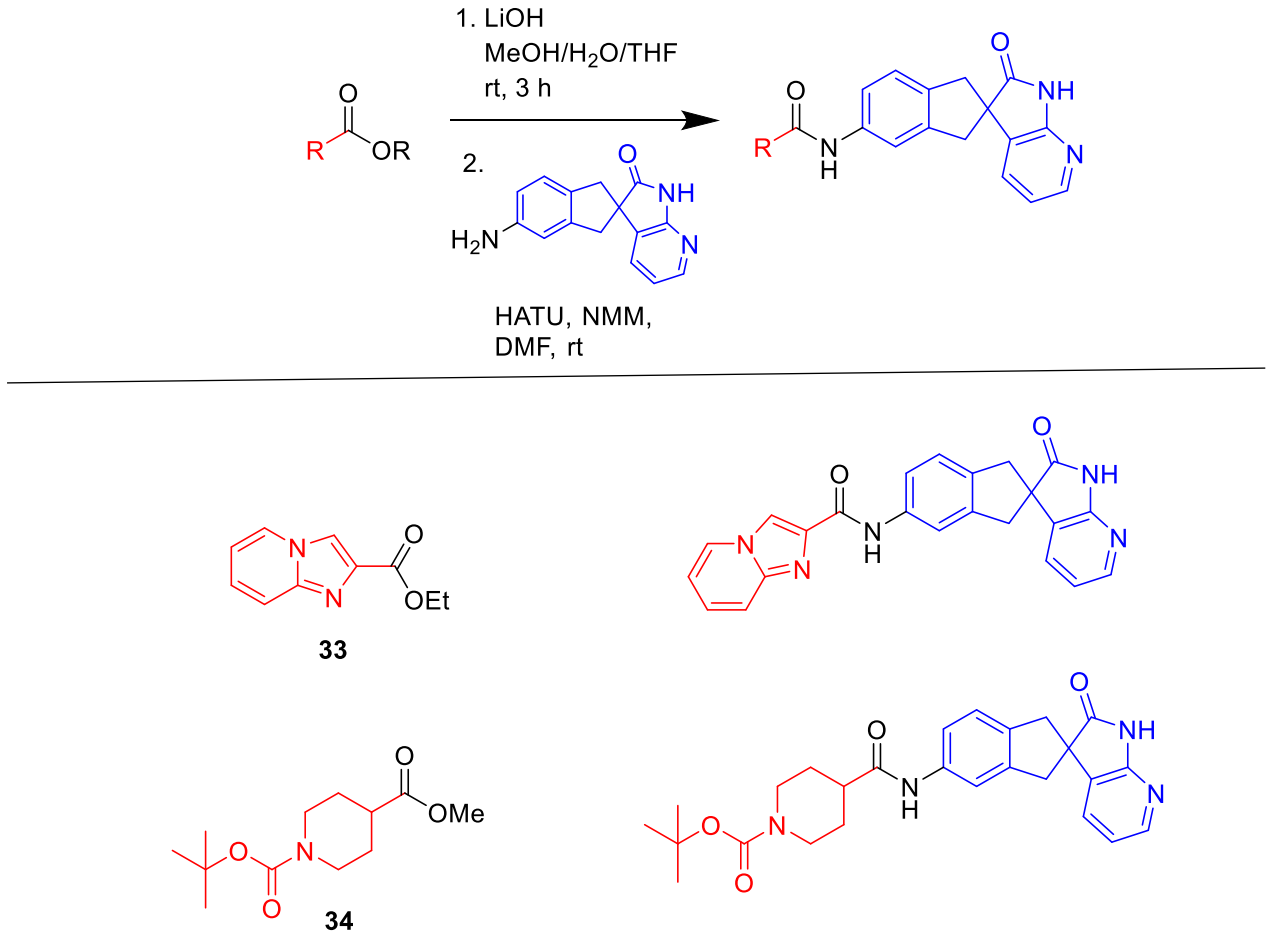

Scheme 2.3 – Coupling of potential RAMP binding motifs (red) to SHF355 (blue) by formation of an amide bond from the corresponding esters

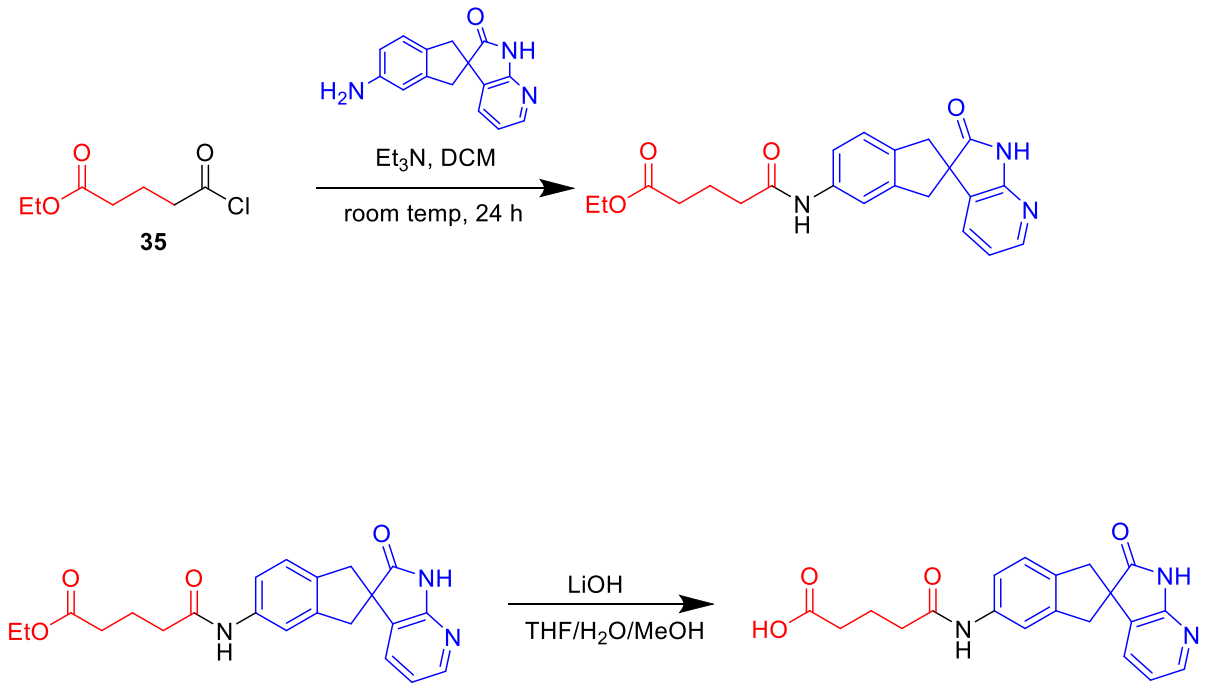

Scheme 2.4 – Formation of SHF355 based AM_1 antagonists from compound 22. CLR binding motif is highlighted in blue and RAMP binding motifs are highlighted in red.

Other SHF355 based compounds were formed using available amines as RAMP ends (Scheme **2.5**). This was achieved by linking the two fragments together by the formation of a urea link. The urea bridge was formed by firstly using the amine RAMP fragment and triphosgene to form the corresponding isocyanate, followed by treatment of the isocyanate with SHF355 and trimethylamine to form the urea linker. Amines used in this coupling included those with benzyl and alkene groups. There were also compounds containing RAMP ends with the potential to hydrogen bond to Ser94, including methoxy ether (compound **22**) and alcohol groups (compound **23**).

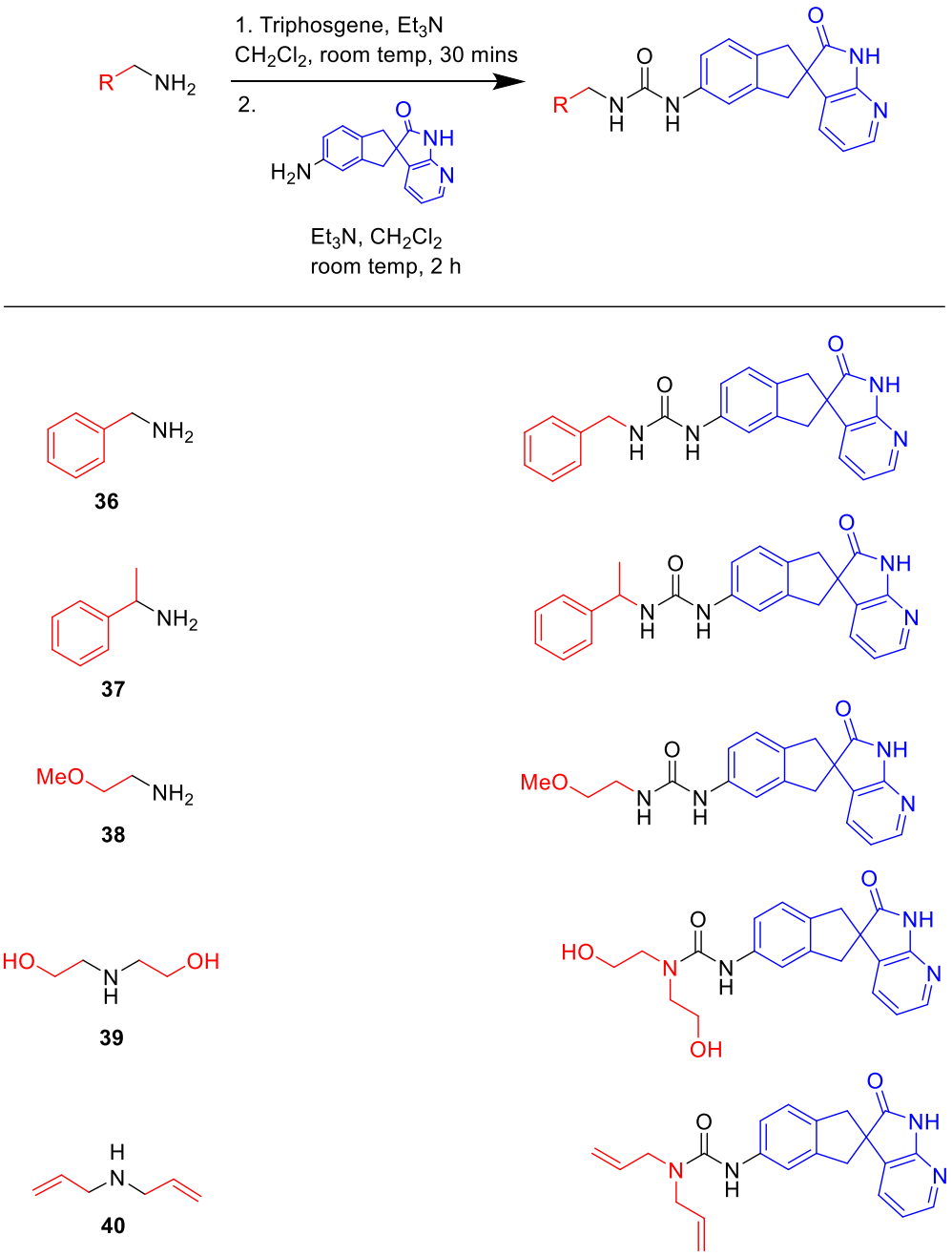

Scheme 2.5 Coupling of potential RAMP binding motifs (red) to SHF355 (blue) via urea bridge formation.

2.3 *In Vitro* Testing of CLR B Based AM_1 Antagonists

2.3.1 cAMP Assay Principles

The *in vitro* testing method for compounds produced during the AM_1 screening is based on the detection of cAMP. cAMP is a secondary messenger released as a result of the activation of GPCRs, therefore the inhibition of a GPCR will result in the inhibition of cAMP in cells expressing the desired receptor. The assay is a cell-based assay and is based upon the detection of receptor inhibition by time-resolved fluorescence resonance energy transfer (TR-FRET). In the absence of free cAMP a europium-labelled cAMP tracer binds to a cAMP specific antibody labelled with Ulight dye. When the europium (the FRET donor) is bound to the Ulight (the FRET acceptor), light at 340 nm excites the europium and results in an energy transfer to the Ulight. The Ulight will them emit light at 665 nm, which is the TR-FRET emission (Figure **2.7**). In the presence of cAMP from activation of the GPCR, the Ulight antibody will bind to the free cAMP, which will result in a reduced TR-FRET emission at 665 nm upon excitation of the europium (Figure **2.7**). In other words, %TR-FRET emission corresponds to %inhibition. Following normalisation of the data using a blank control with no agonist or antagonist (100% TR-FRET emission) and a control with no antagonist (0% TR-FRET emission), a graph of %FRET signal vs antagonist concentration can be plotted to determine the half maximum inhibitory concentration (IC50). Further details of the procedure of this assay can be found in the Materials and Methods section (see Chapter 7)

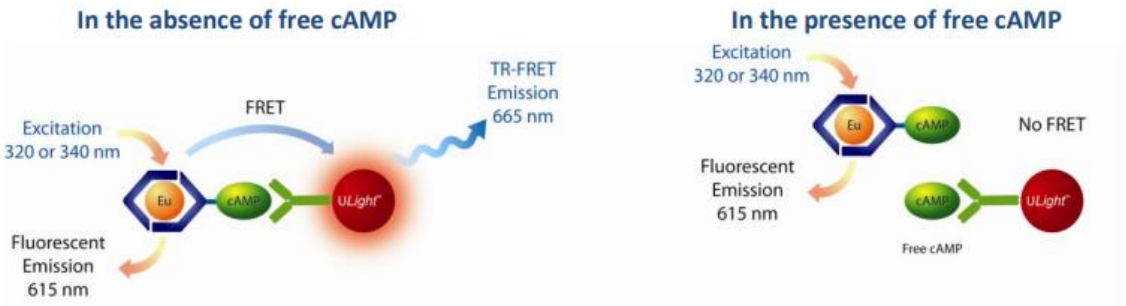

Figure 2.7 – Principles of the TR-FRET detection system in the cAMP assay. The Eu-labelled cAMP tracer binds to the Ulight antibody in the absence of cAMP and releases a TR-FRET signal at 665 nm **(A)**. In the presence of cAMP, the Ulight antibody binds to the free cAMP instead, resulting in no TR-FRET signal **(B)**.

2.3.2 AM_1 Potency of SHF355 Based Compounds

In order to determine how effective an antagonist the SHF355 based compounds are at the AM_1 receptor, the compounds were subjected to the cAMP assay described above to determine potency at blocking receptor activation. Firstly, the compounds formed with an

amide link between the CLR and RAMP ends were tested for AM_1 potency (Figure **2.8**), with the results of this screening displayed in Figure **2.9** and Figure **2.10**.

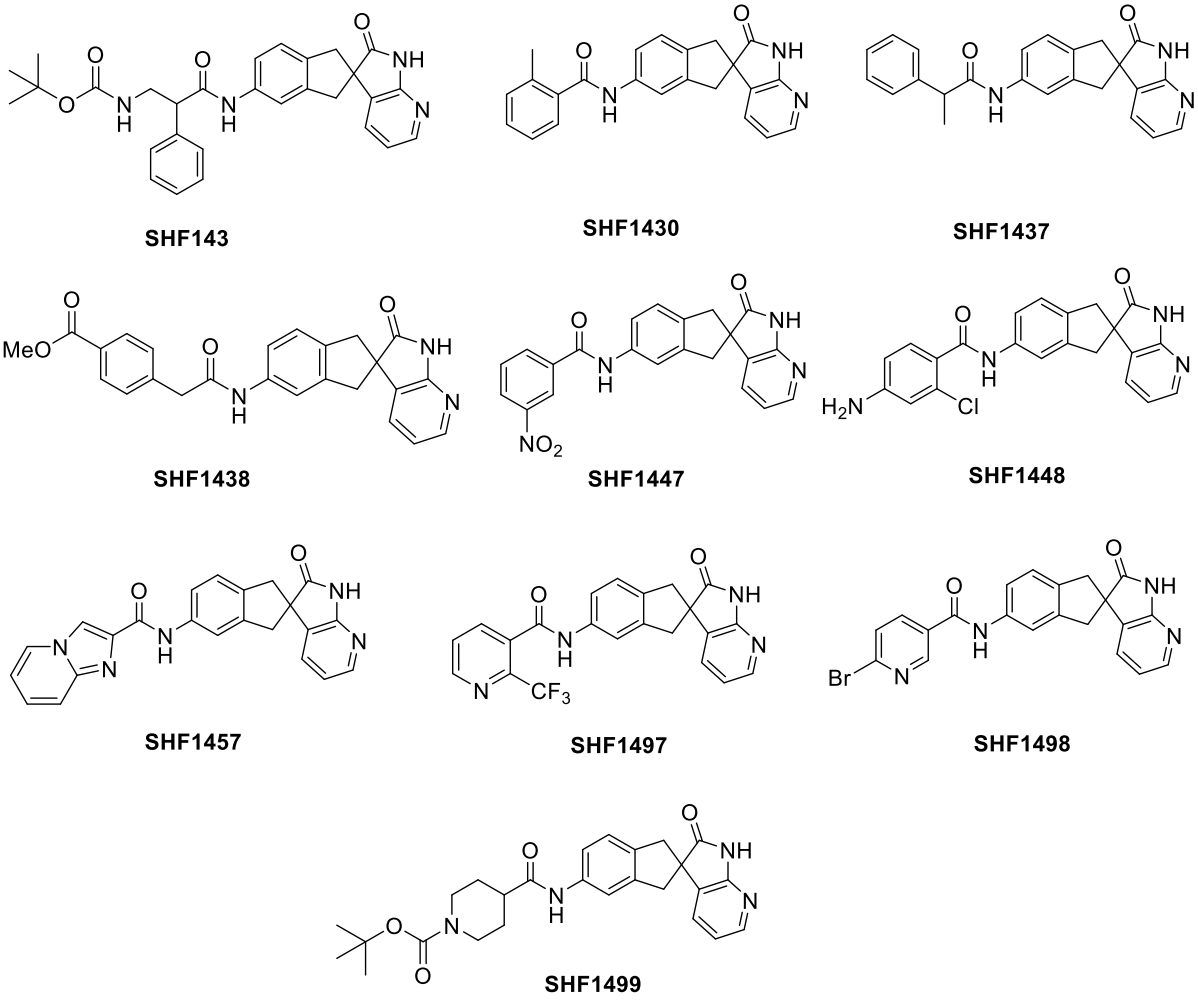

Figure 2.8 – Structures of amide linked SHF355 based antagonists investigated in compound screening and their corresponding SHF ID numbers

Despite the presence of the well known CLR binding motif, none of the compounds displayed any potency towards the AM_1 receptor (Figure **2.9**) (Figure **2.10**). The presence of various substituents on the RAMP end of the molecules did nothing to gain any potency, including aromatic methyl, halo, nitro and trifluoromethyl groups. Changing the phenyl groups to pyridine or a fused imidazole pyridine structure also did nothing to gain potency. Furthermore, compounds containing potential hydrogen bonding groups such as Boc protected amine (SHF143), methyl ester (SHF1438) or aniline (SHF1448) also displayed no potency towards the AM_1 receptor.

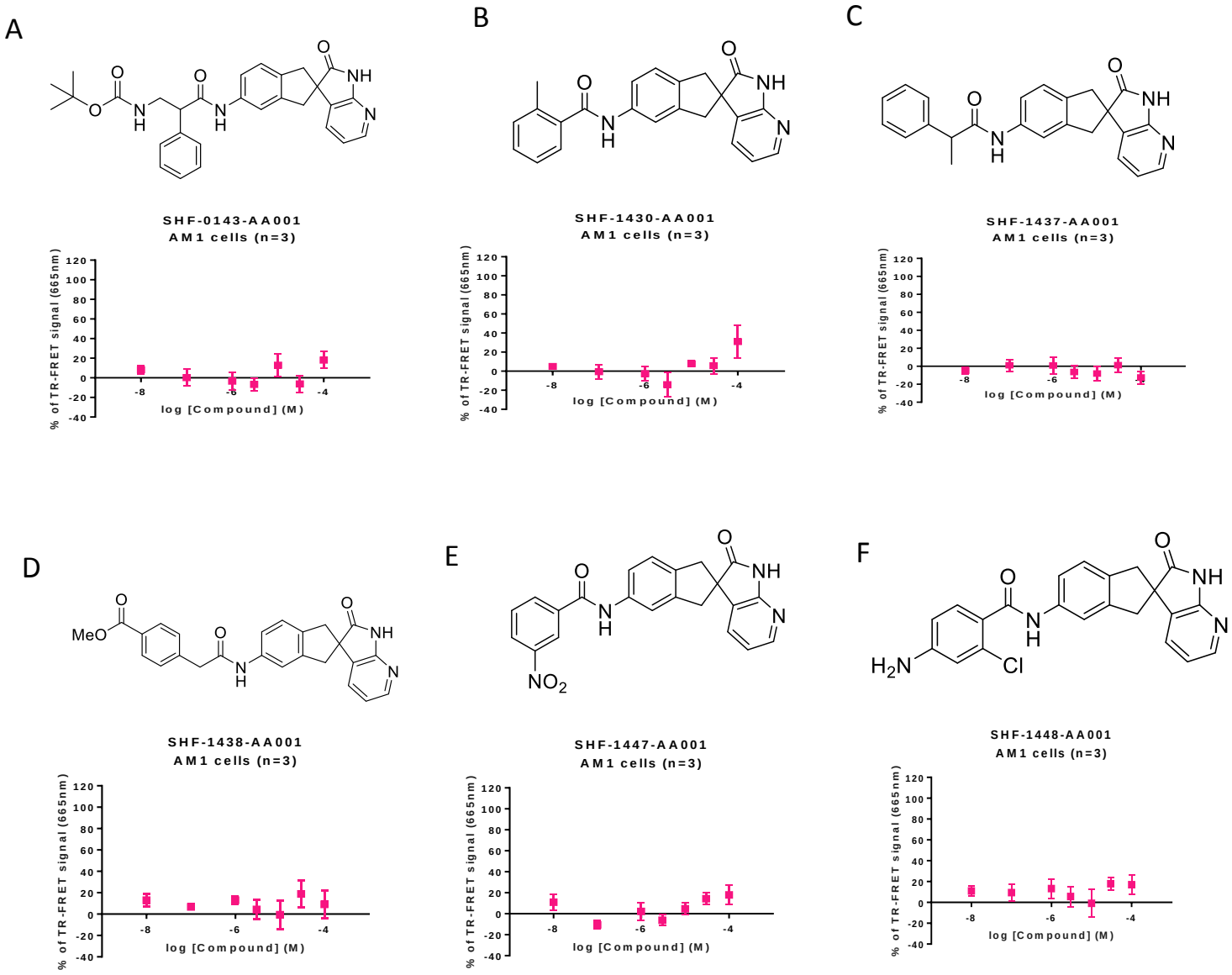

Figure 2.9 – Concentration-response plots of SHF143 (A), SHF1430 (B), SHF1437 (C), SHF1438 (D), SHF1447 (E) and SHF1448 (F) generated from the cAMP assay. The Compounds were tested on CLR/RAMP2 overexpressing cells which were subsequently stimulated by the EC50 concentration of AM (1 nM). Data was plotted using GraphPad Prism 9.0.

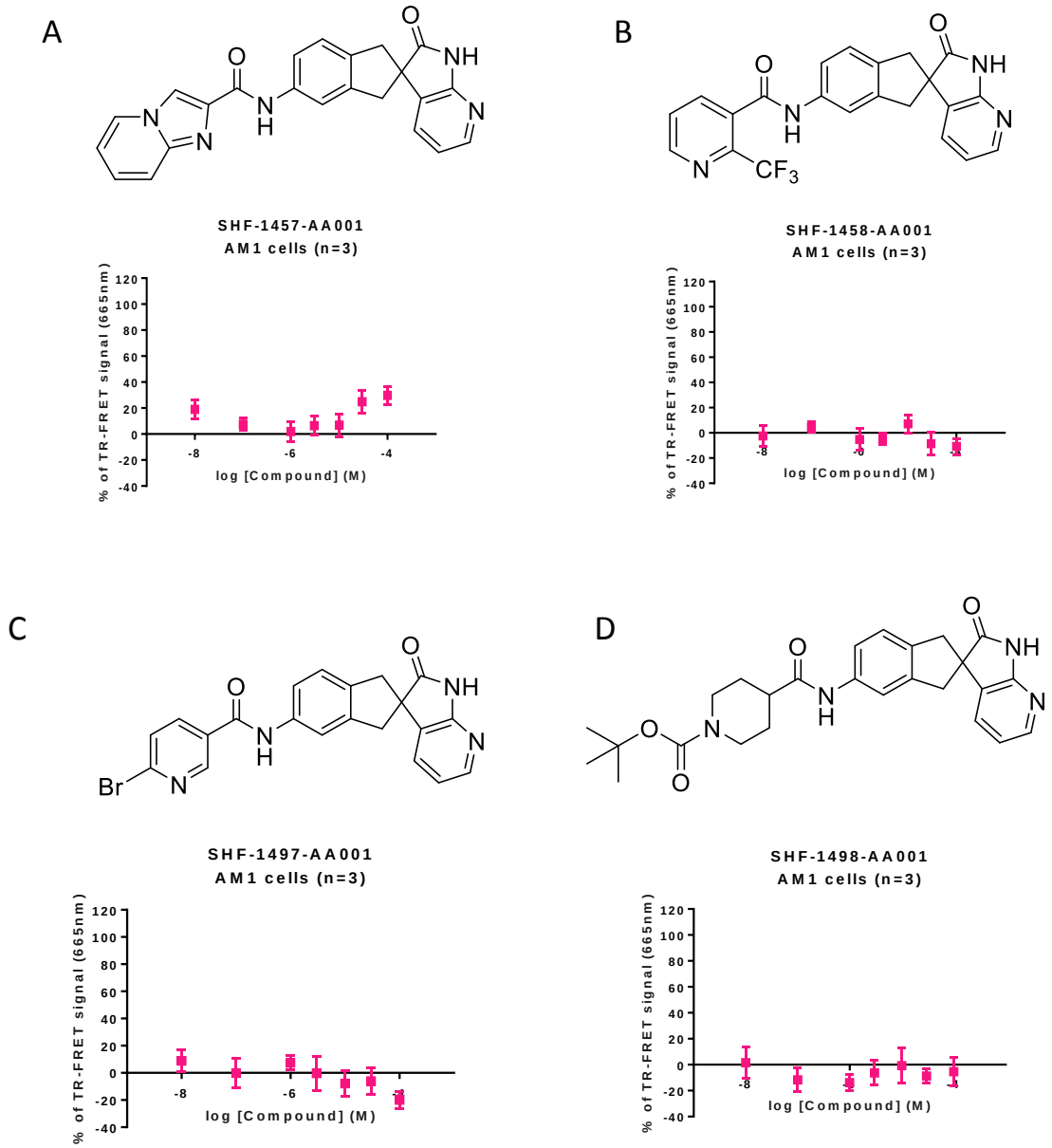

Figure 2.10 – Concentration-response plots of SHF1457 (A), SHF1458 (B), SHF1497 (C) and SHF1498 (D) generated from the cAMP assay. The Compound was tested on CLR/RAMP2 overexpressing cells which were subsequently stimulated by the EC50 concentration of AM (1 nM). Data was plotted using GraphPad Prism 9.0.

The SHF355 based compounds made from acid chloride **22** (Figure **2.11**) were also tested for AM_1 potency (Figure **2.12**). These compounds were especially interesting as the RAMP motif contained ester (SHF1458) and carboxylic acid (SHF1501) groups with the potential to form

hydrogen bonds with RAMP2 Ser94. Neither compound, however, showed any potency towards the AM_1 receptor, suggesting that these interactions do not occur in this case.

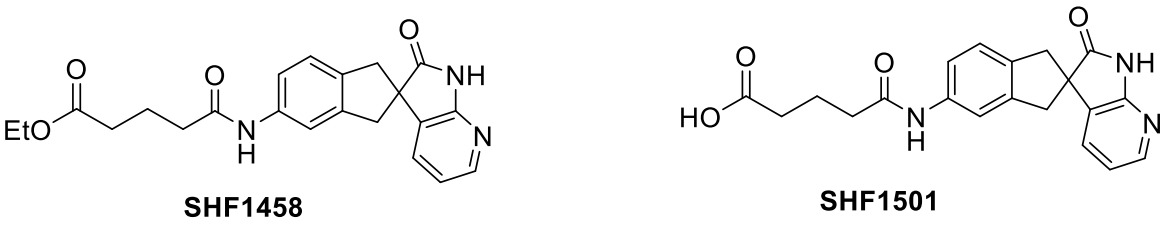

Figure 2.11 – Chemical structures of SHF355 based compounds SHF1458 and SHF1501

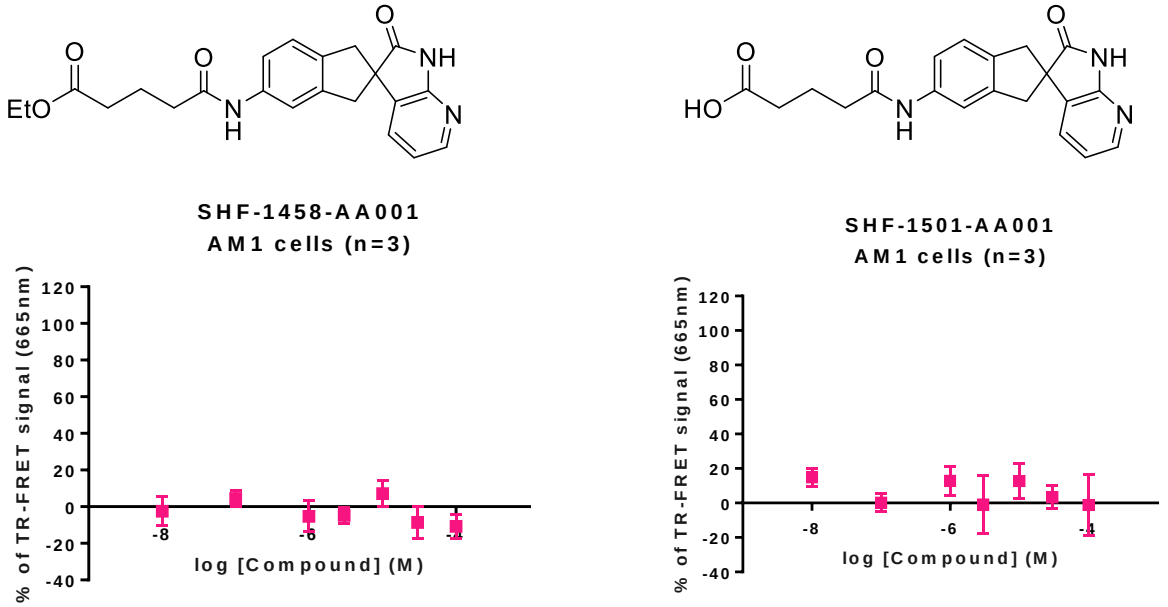

Figure 2.12 – Concentration-response plots of SHF1458 (A) and SHF1501 (B) generated from the cAMP assay. The Compound was tested on CLR/RAMP2 overexpressing cells which were subsequently stimulated by the EC50 concentration of AM (1 nM). Data was plotted using GraphPad Prism 9.0.

The compounds formed by linking the CLR and RAMP motifs by a urea bridge (Figure **2.13**) were additionally tested for AM_1 activity (Figure **2.14**). A small variety of urea bridged compounds were tested but, as with the compounds above, these compounds showed minimal potency at AM_1. This included RAMP motifs such as methyl benzyl and alkenyl groups. Potential RAMP hydrogen bonding groups such as methoxy ether (SHF1468) and alcohol groups (SHF1500) also did little to improve potency.

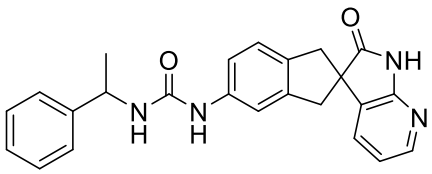

SHF1462

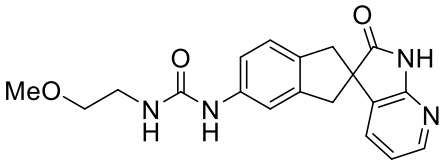

SHF1468

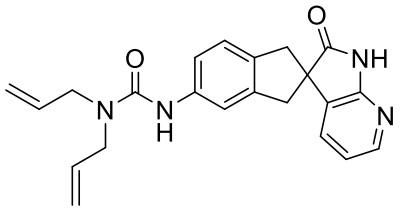

SHF1496

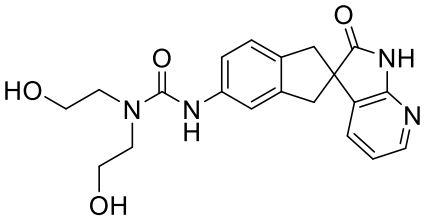

SHF1500

Figure 2.13 – Chemical structures of urea linked SHF355 based compounds investigated in compound screening and their corresponding SHF ID numbers.

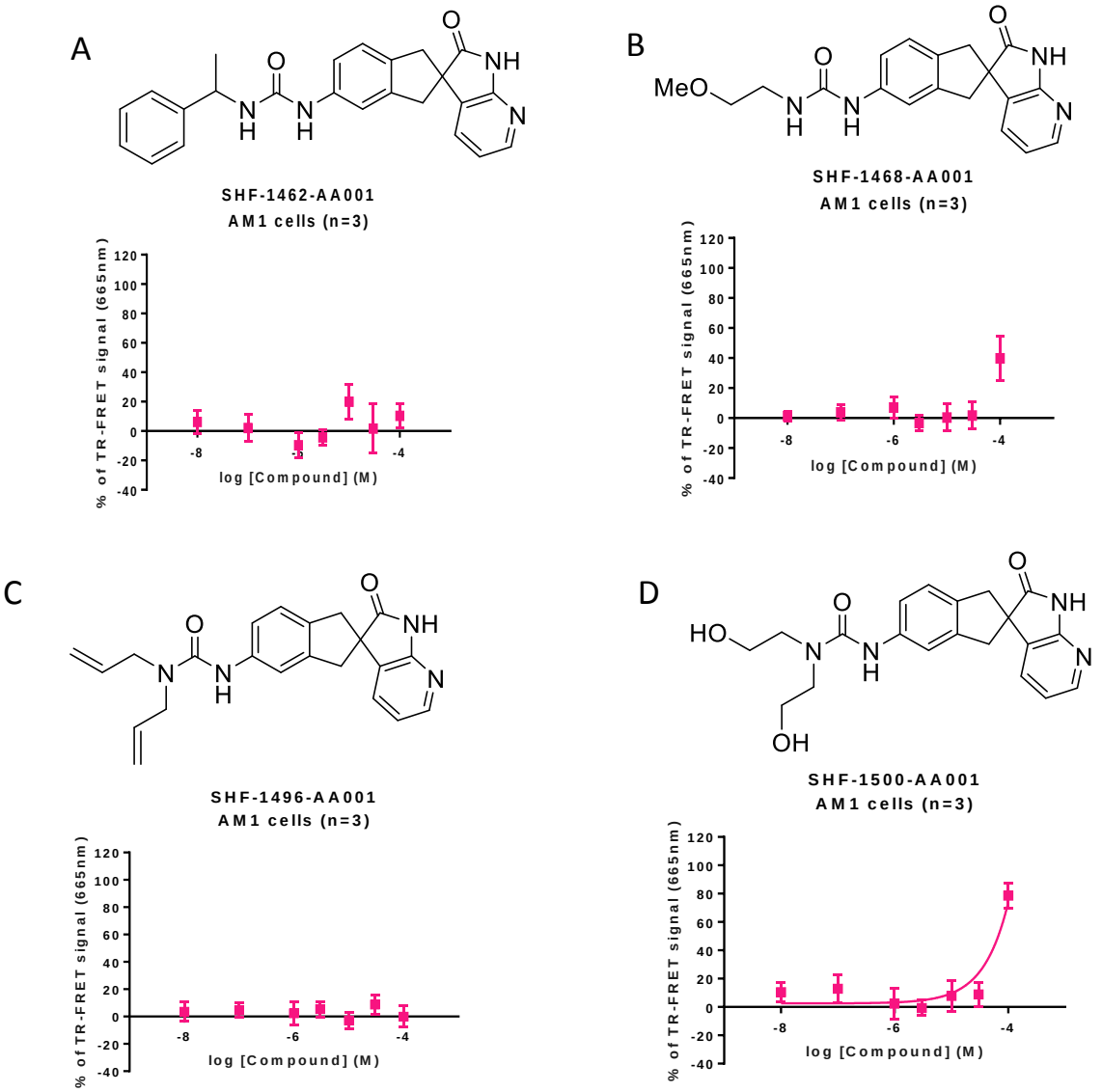

Figure 2.14 – Concentration-response plots of SHF1462 (A), SHF1468 (B), SHF1496 (C) and SHF1500 (D) generated from the cAMP assay. The Compound was tested on CLR/RAMP2 overexpressing cells which were subsequently stimulated by the EC50 concentration of AM (1 nM). Data was plotted using GraphPad Prism 9.0.

2.4 Docking of CLR B Based Analogues in AM_1

In order to rationalise why the SHF355 based analogues were not displaying potency at the AM_1 receptor, the compounds were docked into the AM_1 receptor ECD using Schrodinger (Maestro 13.2). For docking studies on the AM_1 receptor, the ligand free crystal structure of the AM_1 ECD published by Kusano et al was used (PDB: 3AQF). Other models of the AM_1 receptor available on the Protein Data Bank include the AM-bound AM_1 receptor ECD (PDB:

4RWF), and the Cryo-EM structure of the full length AM_1 receptor (PDB: 6UUN). 6UUN was not selected for docking studies due to the poorly resolved ECD on this structure, whilst 3AQF was chosen over 4RWF as the ligand-free structure more closely resembled the conditions of the assay, in which the compounds were allowed to equilibrate with the receptor before addition of AM.

Each compound generally docked in one of two poses in the AM_1 ECD. In the first pose, the carbonyl and nitrogen in the spirocyclic lactam ring forms hydrogen bonds with the backbone of CLR Thr122, whilst the benzene ring in the SHF355 end in the molecule stacks against CLR Trp72 (Figure **2.15A**). As predicted, in this pose the designated RAMP end would point towards RAMP2, with any interactions observed at this end between Arg97 or Glu101. This pose is consistent with that observed from the crystal structure of Olcegepant and Telcagepant binding to the CGRP receptor (ter Haar, Koth et al., 2010).

The alternative docking pose of these compounds shows them binding exclusively to the CLR protein, away from RAMP2 (Figure **2.15B**). Generally the pi stacking interaction between the SHF355 benzene ring and CLR Trp72 is retained, but the hydrogen bonding between CLR Thr122 backbone and the spirocyclic lactam is lost, with some compounds displaying alternative interactions with Thr120 or Tyr124 in this portion of the molecule. In many compounds, the amide nitrogen in the linker displays a hydrogen bond interaction with CLR Asp70.

In the first docking pose, despite the RAMP end of the molecules pointing towards RAMP2 as predicted, the presence of the large Arg97 residue appears to block this part of the binding pocket (ter Haar, Koth et al., 2010). This is evident given the number of unfavourable interactions observed between this residue and the RAMP end of the compounds. The presence of the salt bridge between Arg97 and Glu101 also means that antagonist binding here is unfavourable. Additionally, the Ser94 residue appears to be shielded by Arg97, making it very difficult for the compound to contact this residue. It is therefore likely that these compounds are too large to fit into the binding pocket in this way. The alternative docking pose is more likely to occur as this avoids the steric clash with RAMP2 Arg97. However, in this pose many of the optimal interactions between the CLR end of the compounds and the CLR protein are lost. Both of these points may explain why these CLR B based compounds display minimal potency at the AM_1 receptor.

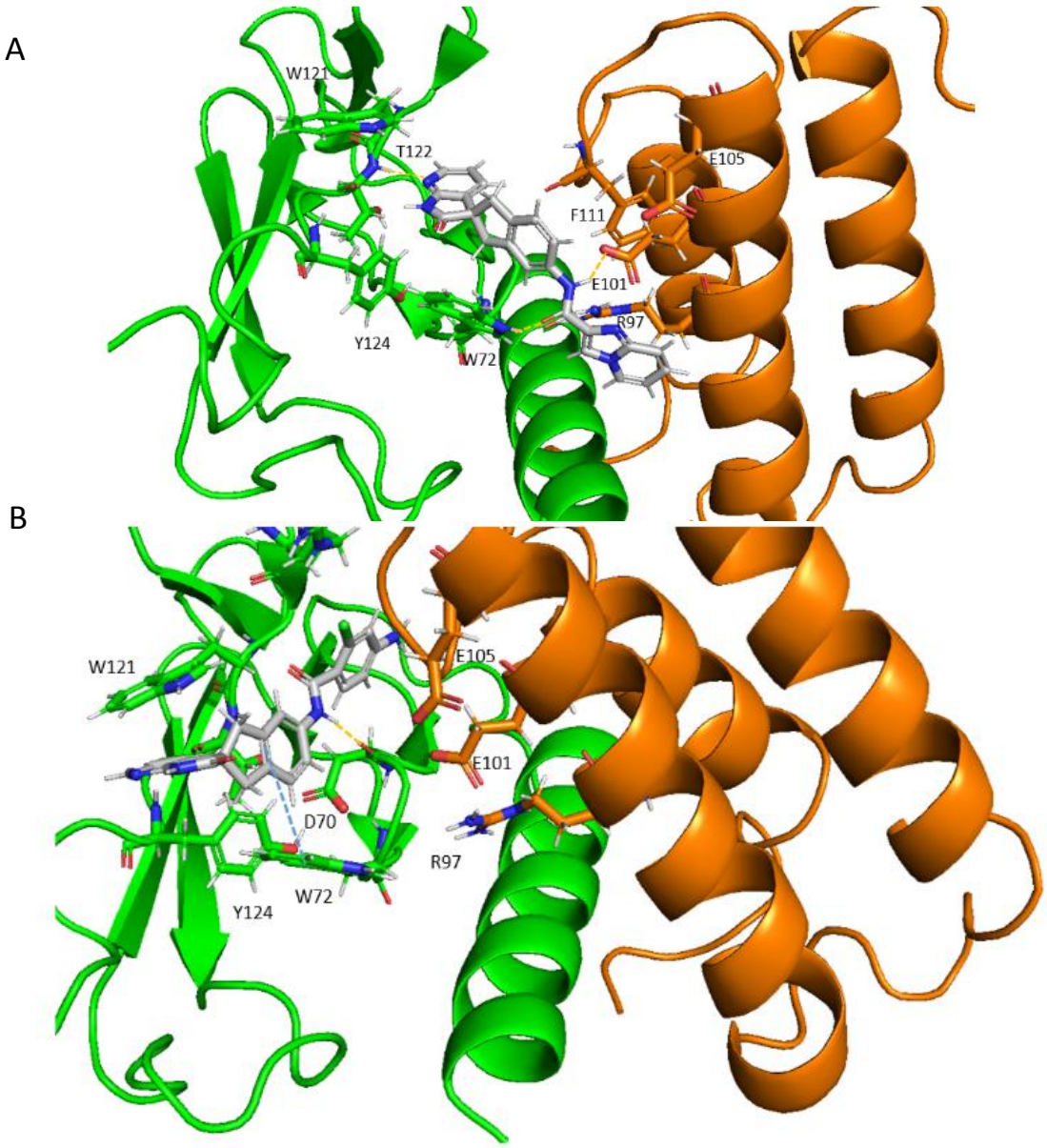

Figure 2.15 – Docking poses of compounds SHF1457 (A) and SHF1448 (B) in the AM_1 receptor ECD (PDB: 3AQF). (A) Demonstrates the docking pose in which the RAMP binding motif reaches out towards RAMP2, whilst (B) demonstrates the pose in which the compound binds across the CLR. The CLR is coloured in green and RAMP2 is coloured in orange. Hydrogen bonds are indicated by yellow dashed lines and pi-pi interactions are indicated by blue dashed lines. Key residues in the binding pocket are shown and labelled. Docking was carried out using Schrodinger (Maestro 13.2) and the image was generated using PyMol Molecular Graphics System, Version 1.7.4.5- Educational Product, Schrodinger.

2.5 Conclusion

To summarise, the SHF355 based compounds formed in this work displayed no antagonistic potency towards the AM_1 receptor, with a variety of different structures, including those with hydrogen bond donor/acceptor groups, as RAMP2 binding fragments trialled. This is despite the fact that compounds with the CLR binding fragment have displayed activity on both the CGRP and AM_2 receptors. This is likely due to the compounds being too large to bind to the AM_1 binding pocket in the same way CGRP and AM_2 antagonists do at their respective receptors, with the large RAMP2 Arg97 effectively occluding the AM_1 pocket and blocking access to other RAMP2 residues such as Ser94.

Chapter 3 – Discovery of a Lead Antagonist Against the AM_1 Receptor

Chapter 3: Discovery of a Lead Antagonist Against the AM_1 Receptor

3.1 High Throughput Screening

High throughput screening has become a very popular tool in the process of drug discovery. They allow the screening of thousands of compounds or biological modulators against selective and specific biological targets, and are often performed in 1536-well microplates in order to achieve this (Kasibhatla, 2004). The overall goal of a high throughput screening is to generate one or several lead compounds over a short period of time and effectively accelerate the drug discovery process (Martis, 2011). The number of compounds screened in a high throughput screening can range between 10^3-10^6 compounds.

To develop a successful high throughput screen, several aspects need to be taken into account. The first is the development of the bioassay. When a target is identified, a simple, quick and relevant *in vitro* test is needed to analyse the biological activity of compounds on the desired target (Aldewachi, Al-Zidan et al., 2021). This test will be different depending on the protein of interest. For GPCRs, cell-based assays are generally based on the detection of secondary messengers released as a result of receptor activation. For example, there are extensive methods available to detect cAMP release from $G_{\alpha\text{-}s}$ activation, including fluorescence polarization (Prystay, Gagne et al., 2001), enzyme fragment complementation (Golla, 2002) and TR-FRET (Norskov-Lauritsen, Thomsen et al., 2014), which is our in house method (see Chapter 2). Other assays include the detection of Ca^{2+} ions using photoproteins, the detection of β-arrestin recruitment using bioluminescence resonance energy transfer (BRET) (Michelini, Cevenini et al., 2010) and the use of reporter genes, firefly luciferase for example, to monitor the activation or transcription of a gene (Yasi, Kruyer et al., 2020). For other proteins, *in vitro* biochemical assays may be more suitable but are less suited to GPCRs due to the low stability of purified recombinant GPCRs.

A bioassay for a HTS also needs to be of good quality and produce reliable data. To test this, an initial study exclusively using positive and negative controls is carried out. From this, the assay Z-factor can be determined, which is defined as the separation band between the positive and negative controls (Zhang, 1999). Z-factor value is between 0-1 and can be

calculated from the equation below. A value of 0.5-1 generally indicates an excellent quality assay.

$$Z = 1 - \frac{3(SD)p + 3(SD)n}{Mean(p) - Mean(n)}$$

SD = Standard Deviation, p = Positive Control, n = Negative Control

Another important aspect of a high throughput screening is the synthesis of compounds. If the process is to be quick and efficient, alternative methods to traditional synthetic techniques need to be used (Szymanski, Markowicz et al., 2012). Examples of this include parallel and combinatorial synthesis. Parallel synthesis is the process in which a reaction is carried out in a series of wells such that each well contains a single different product. The general idea is that a single reaction can be carried out with different substrates in different wells at the same time, resulting in the formation of several compounds at once. This process is possible using miniaturized equipment, which allows the small scale synthesis and purification of several compounds in a mini-synthetic laboratory. Combinatorial synthesis is an alternative method in which mixtures of compounds are produced in each reaction vessel. The compounds in each well are not separated and purified, but are tested for biological activity as a whole. If biological activity is observed, then one or more compounds in the mixture may be active. This process allows chemists to synthesize thousands of compounds in a short space of time (Liu, Li et al., 2017).

High throughput screenings can generate hits from thousands of candidates. Despite this, however, there are still several tests the hit needs to pass to make it to the market as a drug, and the compounds are usually modified extensively to improve efficacy and pharmacokinetic properties. Nevertheless, hits generated from high throughput screenings are often useful starting points for generating a lead compound.

3.2 European Lead Factory High Throughput Screening: Hypothesis and Aims

European Lead Factory (ELF) is a company that provide high quality HTSs from a large compound library with the aim of boosting drug discovery programmes by providing high quality hits. There are approximately 500,000 compounds in the library, including 300,000

compounds from the ESCulab Compound Collection and 190,000 compounds from the Public Compound Collection.

One of our strategies to develop a lead AM_1 receptor antagonist was to utilise the process of high throughput screening. A grant was submitted to a European Lead Factory to carry out a screening of their library of compounds on AM_1 overexpressing cells. It was therefore hypothesised that the ELF high-throughput screening would generate some hit AM_1 antagonists, which we could subsequently modify and optimise to find a lead compound with excellent potency on AM_1.

3.3 European Lead Factory High Throughput Screening

From the results of the ELF high throughput screening, a series of hit compounds were identified with promising activity from their tests. The chemical structures of the most potent compounds outlined in Figure **3.1**

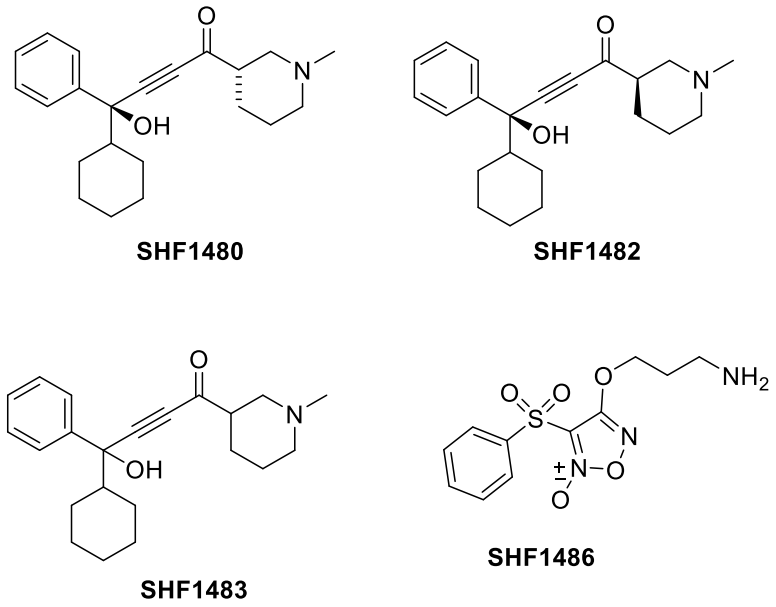

Figure 3.1 – Chemical structures of hit compounds from European Lead Factory High Throughput Screening

3.3.1 European Lead Factory AM_1 Potency on In House cAMP Assay

Encouraged by the generation of hit compounds from the European Lead Factory, the compounds were tested on AM_1 overexpressing cells using the in house cAMP assay (see Chapter 2). pIC50 values for potent compounds are displayed in Table **3.1**

Table 3.1 – IC50 and best fit data for European Lead Factory Compounds on AM_1 cells

	Compound			
Parameter	**SHF1480**	**SHF1482**	**SHF1483**	**SHF1486**
pIC50	6.10	6.05	6.00	6.56
Std Error	0.165	0.132	0.183	0.180
R Square	0.7912	0.8505	0.7421	0.8139
Best Fit Top	104.0	97.45	100.6	79.18
Best Fit Bottom	-2.81	-8.69	-0.9880	-6.144

Among the most potent compounds in the European Lead Factory series were SHF 1483 and it's diastereomers, SHF 1480 (*S*,*S*) and SHF1482 (*S*,*R*), with all three compounds displaying a pIC50 value of 6.1 (0.79 µM). The most potent compound was SHF1486, displaying a pIC50 value of 6.6 (0.28 µM). To our knowledge these are the first compounds to display sub micromolar potency towards the AM_1 receptor (Table **3.1**) (Figure **3.2**).

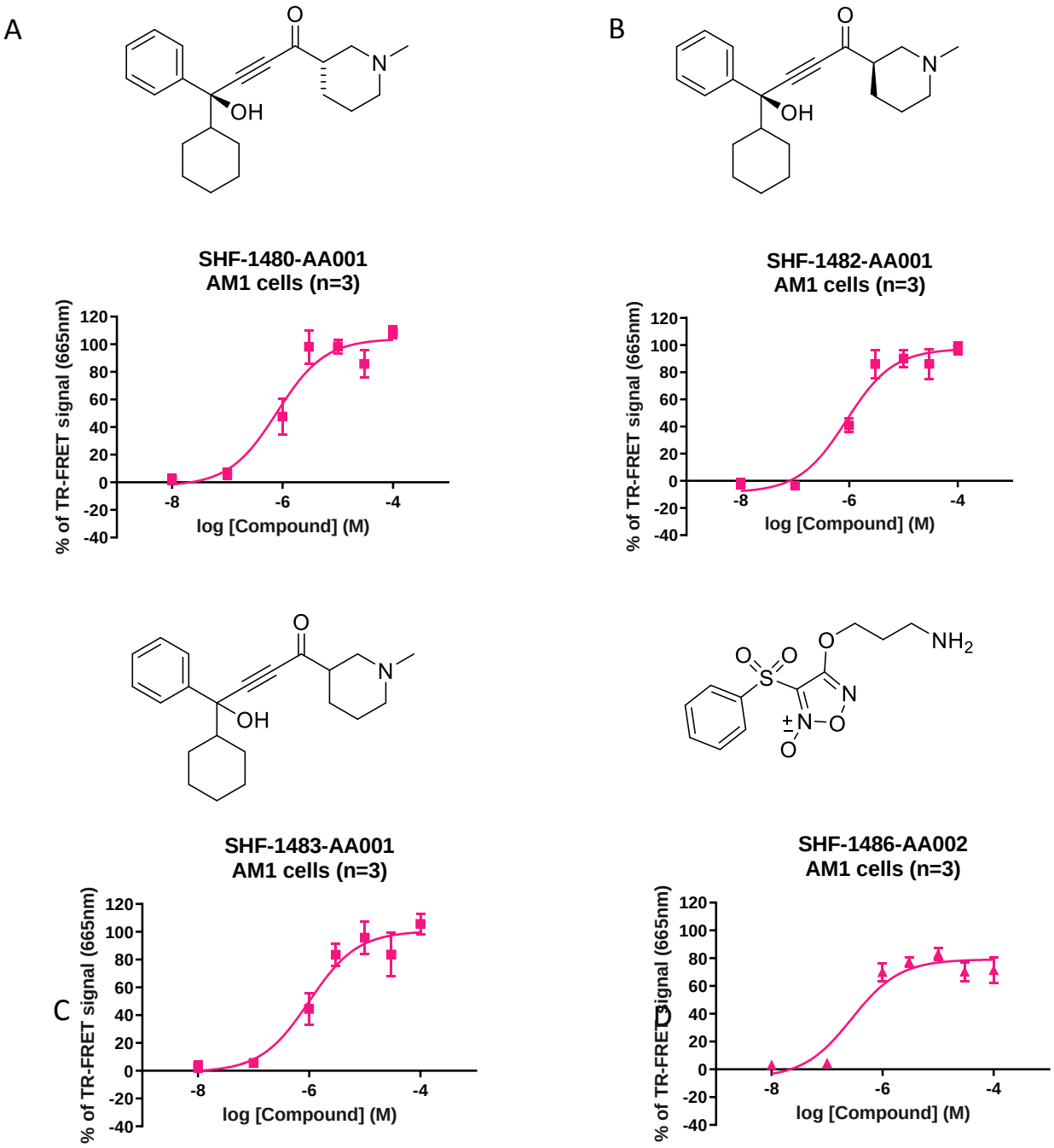

Figure 3.2 – Concentration-response plots of SHF1580 (A), SHF1582 (B), SHF1583 (C) and SHF1586 (D) generated from the cAMP assay. Compounds were tested on CLR/RAMP2 overexpressing cells which were subsequently stimulated by the EC50 concentration of AM (1 nM). Data was plotted using GraphPad Prism 9.0.2 and the IC50 was determined using a non-linear 3-parameter inhibition curve.

3.3.2 Counter Screening of ELF Compounds on CGRP and AM_2

The European Lead Factory compounds were also screened against CGRP and AM_2 in order to determine selectivity for AM_1 (Table **3.2**). For AM_2 and CGRP screening, the compounds were tested at concentrations ranging between 10 µM and 1 pM. SHF1480, SHF1482 and SHF1483 all showed incomplete inhibition curves at this concentration range, meaning an exact pIC50 couldn't be determined (Figure **3.3**). This data implies that these compounds all display very good selectivity for AM_1 over CGRP and AM_2. SHF1486 presented more modest selectivity for AM_1, being 14-fold more selective for CGRP (pIC50 = 5.43) and 4-fold more selective for AM_2 (pIC50 = 6.02).

Table 3.2 – IC50 data for European Lead Factory Compounds on CGRP and AM_2

Compound	pIC50 (AM_1)	pIC50 (CGRP)	pIC50 (AM_2)
SHF1480	6.10	<5	<5
SHF1482	6.05	<5	<5
SHF1483	6.00	<5	<5
SHF1486	6.56	5.43	6.02

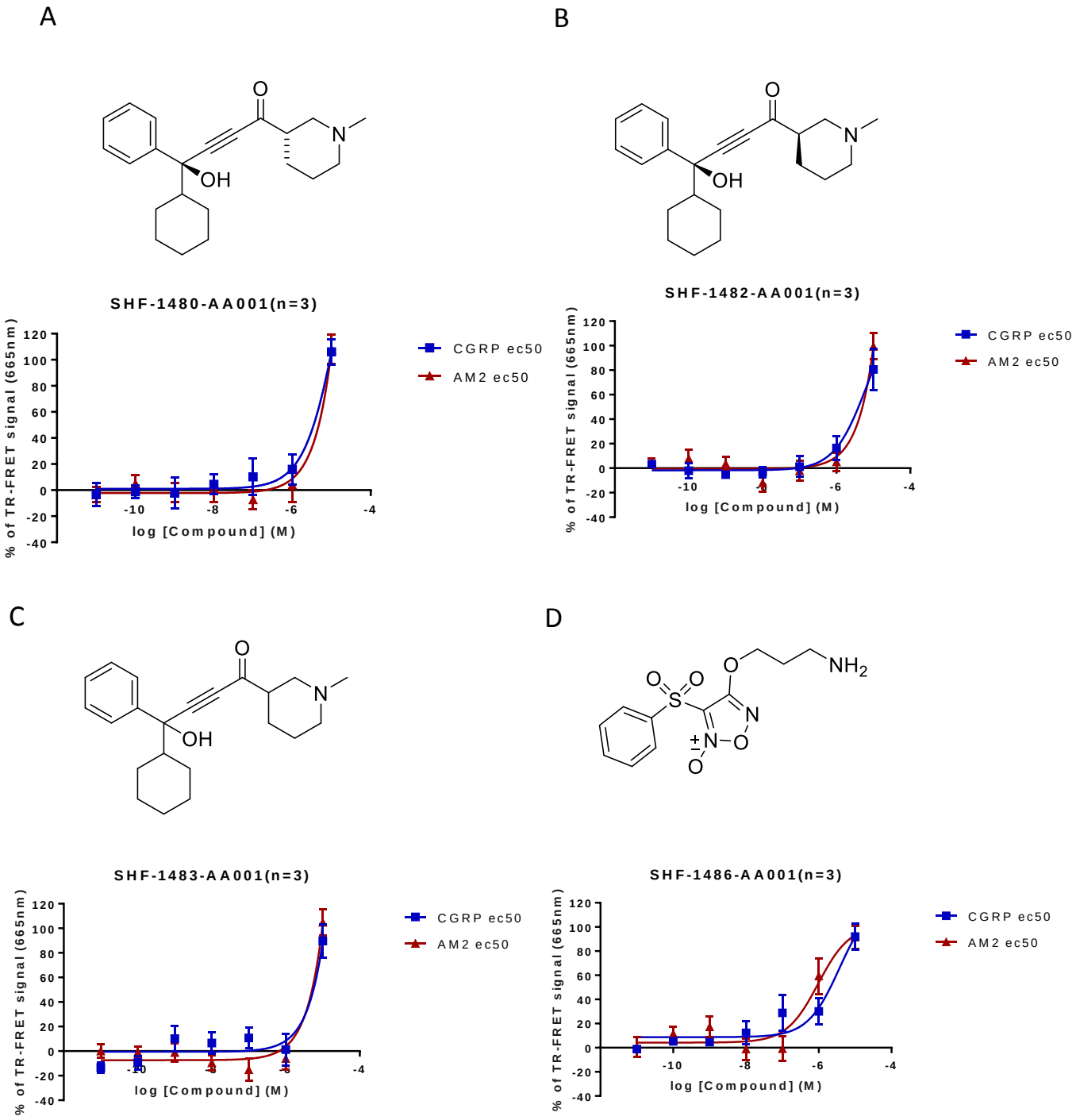

Figure 3.3 – Concentration-response plots of SHF1580 (A), SHF1582 (B), SHF1583 (C) and SHF1586 (D) generated from the cAMP assay. Compounds were tested on CLR/RAMP1 and CLR/RAMP3 overexpressing cells which were subsequently stimulated by the EC50 concentration of CGRP (0.8 nM) and AM (2 nM) respectively. Data was plotted using GraphPad Prism 9.0.2 and the IC50 was determined using a non-linear 3-parameter inhibition curve. CGRP curve is displayed in blue and the AM_2 curve is displayed in brown,

3.3.3 Docking of European Lead Compounds in Maestro

In order to gain an insight into where the European Lead Factory compounds could be binding in the AM_1 binding pocket and which functional groups in the compounds could be key to potency, the compounds were docked into the AM_1 receptor ECD in Maestro (PDB: 3AQF)(Figure **3.4**) (Figure **3.5**).

The active diastereomers of SHF1483 fit reasonably well into the AM_1 receptor binding pocket, giving docking scores of -6.1 kcal mol^{-1} and – 5.8 kcal mol^{-1} for SHF1480 (*S*,*S*) and SHF1482 (*S*,*R*) respectively (Table **3.3**), matching the trend shown in the experimental data. In both cases, the left hand side of the molecule binds to the CLR end of the receptor. The alcohol group on this side makes key interactions with protein for both diastereomers, with the SHF1480 alcohol forming a hydrogen bond with the carbonyl backbone of CLR Asp70 and SHF1482 alcohol forming a hydrogen bond with the carbonyl backbone of CLR Thr120 (Figure **3.4**). The cyclic tertiary amine on the right hand side of the molecule appears to interact with the RAMP2 protein, with SHF1480 forming a salt bridge with Glu101. The corresponding piperidine in SHF1482 instead forms a pi-cation interaction with CLR Trp72.

SHF1486 displays the most negative docking score of all the active European Lead Factory compounds (-6.9 kcal mol^{-1}) (Table **3.3**) The sulfone end of the molecule is predicted to interact with the CLR end of the receptor, with the key interaction being a hydrogen bond between one of the oxygen atoms of the sulfone and the CLR Thr122 NH amide backbone (Figure **3.5**). The N-O group on the five membered heterocycle is predicted to form a salt bridge with CLR Asp70, as well as a pi-cation interaction with CLR Trp72. The amine on the other end of the molecule, meanwhile, is predicted to interact with RAMP2, forming a hydrogen and an ionic interaction with RAMP2 Glu101 and Glu105.

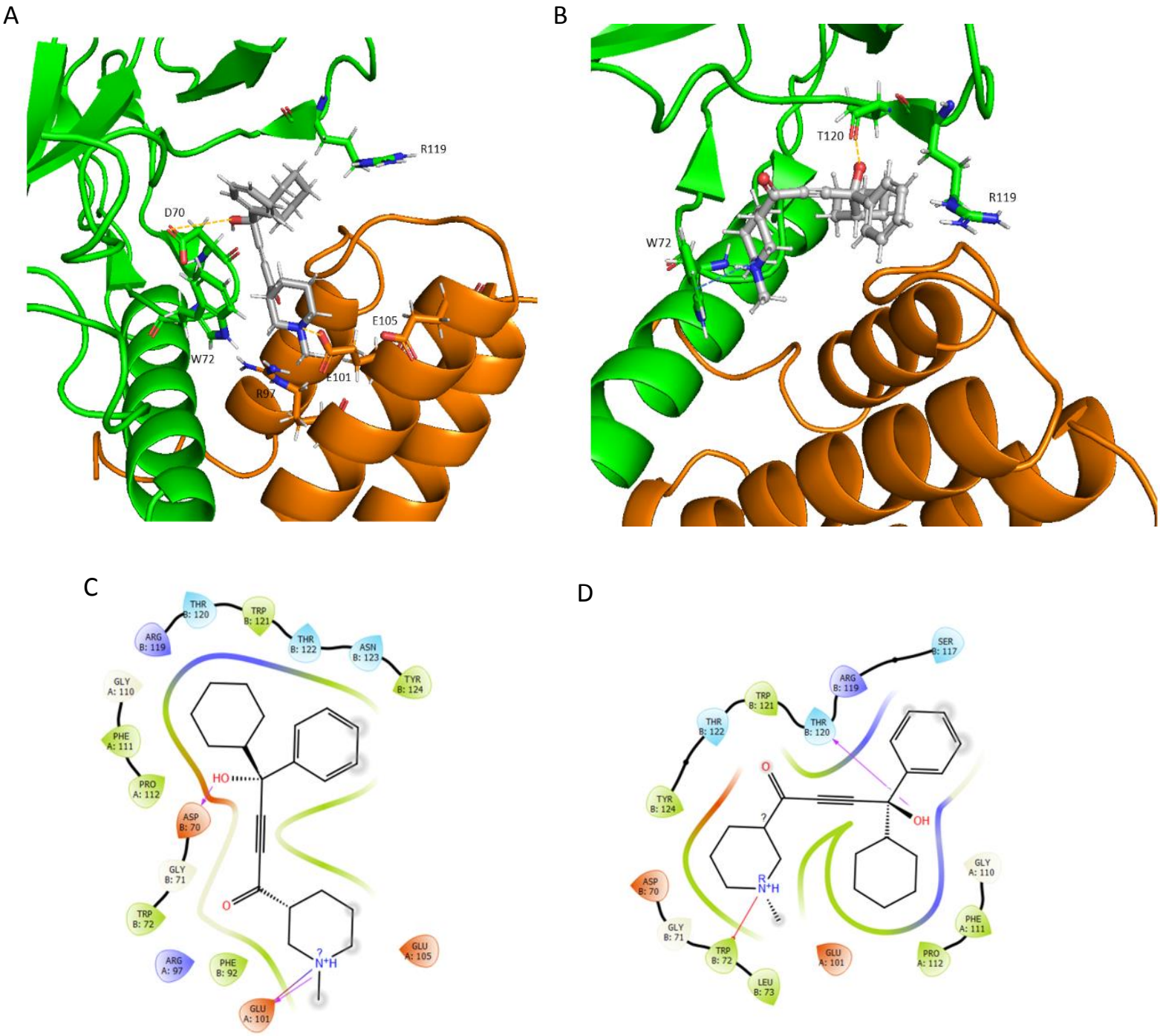

Figure 3.4 - Lowest energy docking pose of European Lead Factory compounds SHF1580, (A) and (C), and SHF1582, (B) and (D) bound to the AM_1 receptor (PDB: 3AQF). (A) and (B) show the 3D images of the compound docked into the AM_1 receptor ECD. The CLR is coloured in green and RAMP2 is coloured in orange. Hydrogen bonds are indicated by yellow dashed lines and pi-pi interactions are indicated by blue dashed lines. Key residues in the binding pocket are shown and labelled. Docking was carried out using Schrodinger (Maestro 13.2) and the image was generated using PyMol Molecular Graphics System, Version 1.7.4.5-Educational Product, Schrodinger. (C) and (D) show the corresponding 2D ligand interaction diagrams generated by Maestro 13.2. Hydrogen bonds are indicated by purple lines and ionic interactions are indicated by red lines.

A

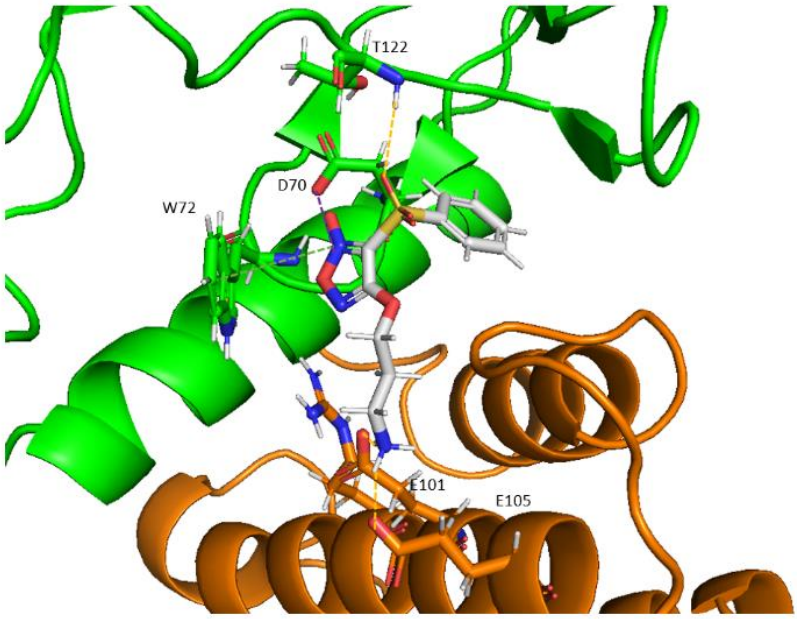

B

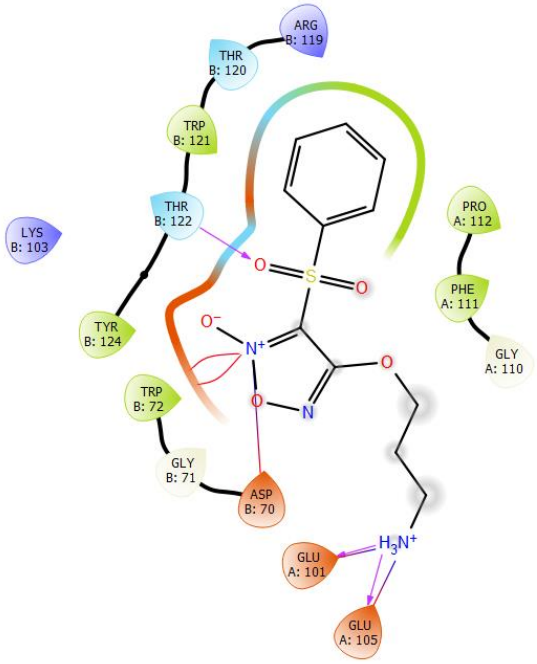

Figure 3.5 – Lowest energy docking pose of European Lead Factory compound SHF1486 bound to the AM_1 receptor (PDB: 3AQF). (A) 3D image of SHF1486 docked into the AM_1 receptor ECD. The CLR is coloured in green and RAMP2 is coloured in orange. Hydrogen bonds are indicated by yellow dashed lines and pi-cation interactions are indicated by green dashed lines. Key residues in the binding pocket are shown and labelled. Docking was carried out using Schrodinger (Maestro 13.2) and the image was generated using PyMol Molecular Graphics System, Version 1.7.4.5- Educational Product, Schrodinger. (B) 2D ligand interaction diagram generated from Maestro 13.2. Hydrogen bonds are indicated by purple lines and ionic interactions are indicated by red lines.

Table 3.3 – Docking Scores of the lead ELF compounds in the AM_1 receptor ECD (PDB: 3AQF). Docking scores generated by Schrodinger (Maestro 13.2)

Compound	Docking Score (kcal mol^{-1})
SHF1480	-6.1
SHF1482	-5.8
SHF1486	-6.9

3.4 SHF1556 and Hypothesis

3.4.1 Problems Associated with ELF Compounds

The suitability of a compound for druglikeness and oral bioavailability can often be determined by evaluating the physiochemical properties of the molecule. Lipinski's rule of 5 is frequently used as a guideline for this, and states that an orally active compound should have a molecular weight of less than 500 daltons, a partition coefficient (Log P) of less than 5, no more than 5 hydrogen bond donors and no more than 10 hydrogen bond acceptors (Lipinski, 1997). Verber's rules additionally state that the compound should have less than 10 rotatable bonds and exhibit a topological polar surface area (TPSA) of less than 140 $Å^2$ (Veber, 2002). Evaluation of the physiochemical properties of SHF1483 and SHF1486 shows that both compounds obey all of the above rules (Table **3.4**), making them promising drug candidates.

Table 3.4 – Physiochemical Properties of SHF1483 and SHF1486.

	Compound	
Property	SHF1483	SHF1486
Molecular Weight	339.5	299.3
Log P	4.1	2.0
H-bond Donors	1	2
H-bond Acceptors	3	8
Rotatable Bonds	3	6
TPSA	40.5 $Å^2$	122.4 $Å^2$

However, despite the promising potency and physiochemical properties of the ELF compounds on AM_1, there are a few problems associated with these compounds that prevent them from being suitable leads. SHF1483 and its diastereomers contain an alkyne and a ketone within their chemical structures, both of which are undesirable for drug-like compounds. The ketone is a reasonably strong electrophile, meaning it's a reactive site that could be prone to attack from nucleophilic amino acid residues from other proteins such as enzymes. Alkyne groups can also be disadvantageous in medicinal chemistry due to their ability to irreversibly inhibit cytochrome P450 enzymes in the liver, key enzymes in drug metabolism (Talele, 2020). This is largely due to the alkylation of nucleophilic amino acid residues in the enzyme active site. Whilst SHF1486 does not contain such undesirable groups, the molecule itself is difficult to synthesise whilst there are also limited options open to modify the compound to improve potency or pharmacokinetic properties.

3.4.2 SHF1556

Despite the problems with the ELF compounds, a search of the literature found a compound with structural similarities to SHF1486, designated SHF1556 (Aiyar, 2000) (Figure **3.6**). The structure of SHF1556 is similar to SHF1486 in that it contained an oxidised sulphur atom directly attached to a 5-membered nitrogen-based heterocycle and a 6-membered aromatic ring (Figure **3.7**). Specifically, the heterocycle on SHF1556 is similar the phenyl ring in SHF1486, the sulfoxide in SHF1556 is equivalent to the sulfone in SHF1486, and the nitro group in SHF1556 could be equivalent the N-O substituent on the SHF1486 heterocyclic ring.

Aiyar et al have previously identified SHF1556 to have reasonable potency towards the CGRP receptor. Using both a binding assay and a functional assay by measuring the conversion of radiolabelled ATP to cAMP by activated adenylate cyclase, affinity and potency towards the CGRP receptor was measured for SHF1556 and its enantiomers (Table **3.5**). In both assays, SHF1556, along with is (+) and (-) enantiomers (absolute stereochemistry not defined) display sub micro-molar affinity and potency towards CGRP. The (+)-enantiomer was consistently more active than the (-)-enantiomer, displaying 2-fold greater affinity in the binding assay and 5-fold greater potency in the adenylate cyclase assay (Aiyar, 2000).

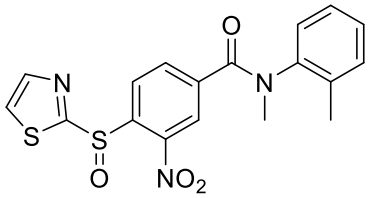

Figure 3.6 – Chemical Structure of SHF1556

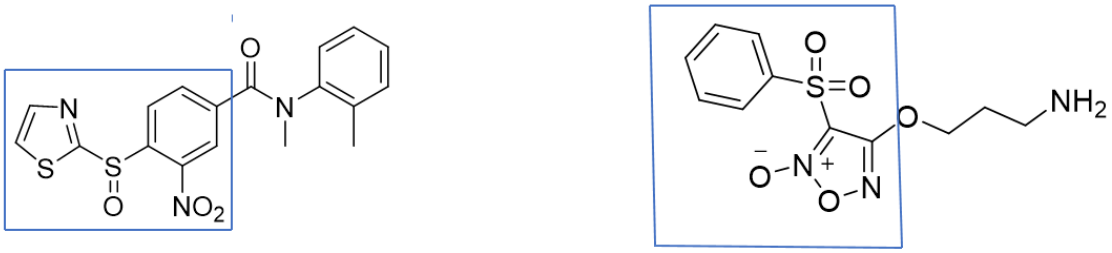

SHF1556 **SHF1486**

Figure 3.7 – Structural similarities between SHF1556 and SHF1486. Region of the structures that are similar are highlighted by a blue square

Table 3.5 – Binding and functional assay data of SHF1556 on the CGRP receptor from the literature (Aiyar, 2000)

Compound	Binding IC50 (µM)	Adenylate Cyclase IC50 (µM)
SHF1556	0.24	0.83
SHF1556 (+)	0.31	0.39
SHF1556 (-)	0.69	2.07

Evaluation of the physiochemical properties of SHF1556 also suggest that the compound shows good suitability for druglikeness (Table **3.6**). The compound has a molecular weight of less than 500 daltons, a Log P value of 3.8, no hydrogen bond donors and 7 hydrogen bond acceptors, therefore obeying all of Lipinski's rules. Verber's rules are also obeyed, with SHF1556 containing only 5 rotatable bonds and a TPSA of 93.4 $Å^2$, therefore further highlighting the suitability of this compound as a lead compound.

Table 3.6 – Physiochemical Properties of SHF1556.

Property	Value
Molecular Weight	401.5
Log P	3.8
H-bond Donors	0
H-bond Acceptors	7
Rotatable Bonds	5
TPSA	93.4 $Å^2$

Given that SHF1556 contains structural similarities to SHF1486, and due to the promising activity SHF1556 displays on the CGRP receptor, it was hypothesised that SHF1556 would show good potency towards the AM_1 receptor and prove to be a useful lead compound for the project. An additional advantage of SHF1556 over the ELF compounds was that it is a better drug-like molecule, with plenty of opportunity to modify various sites of the molecule to investigate structure activity relationships (see Chapter 4) and optimise AM_1 activity.

The aims of this work was to synthesise SHF1556 and to carry out *in vitro* testing on AM_1 overexpressing cells to determine potency, as well as on AM_2 and CGRP cells to determine selectivity. An additional goal was to resolve the two enantiomers SHF1556 and determine which enantiomer is the more potent. An X-ray crystal structure of the most potent enantiomer could then be taken to determine the absolute stereochemistry of this compound.

3.5 Docking Studies of SHF1556

Both enantiomers were docked into the ECD of the AM_1 receptor using Maestro (PDB: 3AQF). The lowest energy docking poses are displayed in Figure **3.8**. The (*S*)-enantiomer is predicted to bind exclusively to the CLR end of the receptor ECD. Key interactions between the molecule and the protein include a hydrogen bond between the sulfoxide oxygen and the NH amide backbone of CLR Thr122 residue. This interaction is conserved in SHF1486, with the sulfone oxygen interacting with the same residue. Additionally, the amide oxygen atom appears to form a hydrogen bond with CLR Arg119 side chain, whilst the thiazole ring also forms a pi cation stacking interaction with CLR Trp72.

The (*R*)-enantiomer of SHF1556 sits in a similar position to the (*S*)-enantiomer. As with (*S*)-enantiomer, the key interactions between the molecule and the receptor also take place with the CLR protein. A hydrogen bond is once again formed with the amide backbone of CLR Thr122, although in this case it is the amide oxygen on SHF1556 making this contact. The nitro group also appears to be a key group in this case, forming hydrogen bonds with the CLR Trp121 side chain as well as with Tyr124 main chain. There is additionally predicted to be a pi-pi stacking interaction between the central aromatic ring and the CLR Tyr124 side chain. Both enantiomers gave docking scores of -4.4 kcal mol^{-1} (Table **3.7**), suggesting that both would bind to the receptor with the same affinity.

Table 3.7 – Docking Scores of SHF1556 enantiomers in the AM_1 receptor ECD (PDB: 3AQF). Docking scores generated by Schrodinger (Maestro 13.2)

SHF1556 Enantiomer	Docking Score (kcal mol^{-1})
(R)	-4.4
(S)	-4.4

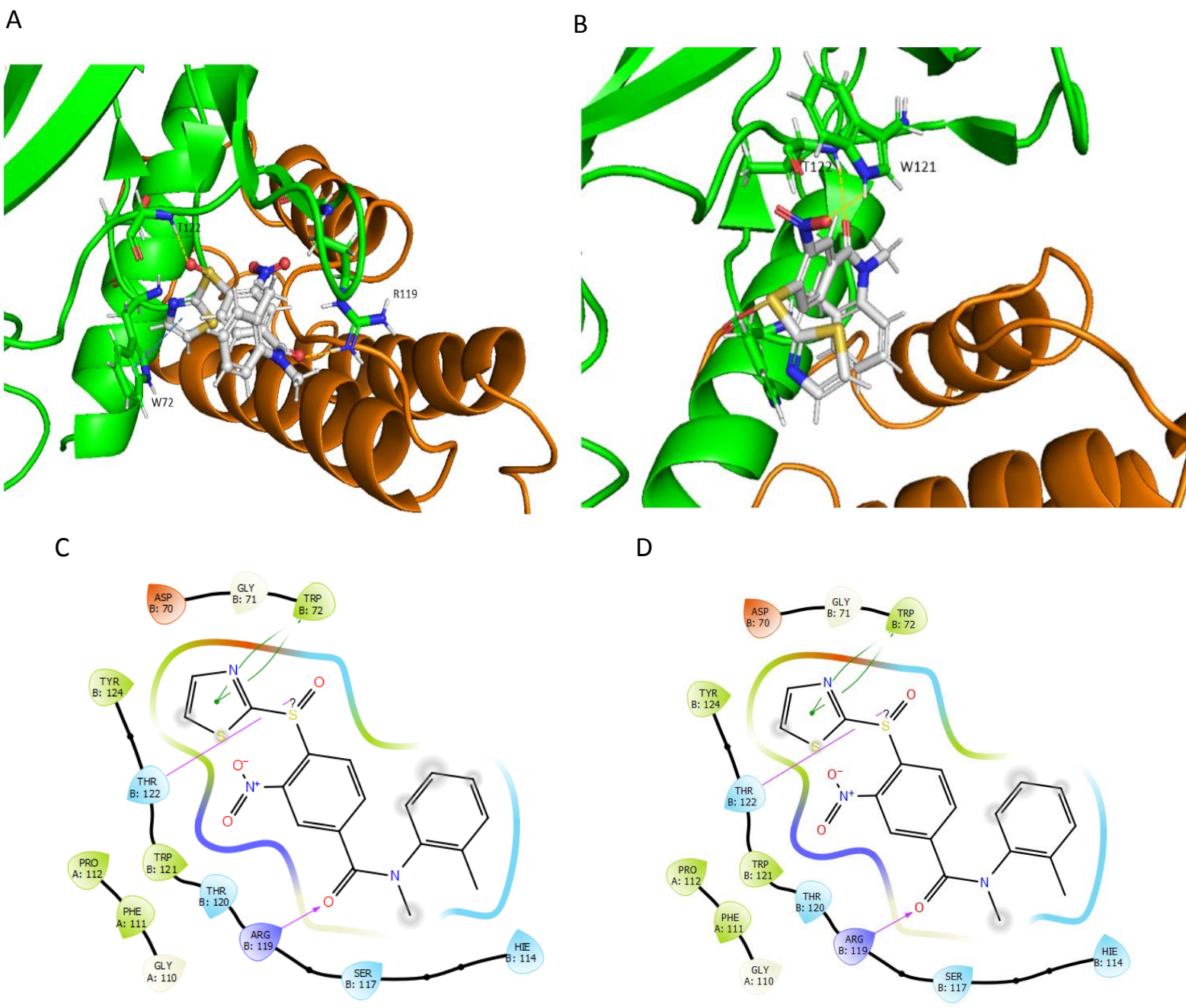

Figure 3.8 - Lowest energy docking pose of SHF1556 (*S*) enantiomer, (A) and (C), and (*R*) enantiomer, (B) and (D) bound to the AM_1 receptor (PDB: 3AQF). (A) and (B) show the 3D image of the compound docked into the AM_1 receptor ECD. The CLR is coloured in green and RAMP2 is coloured in orange. Hydrogen bonds are indicated by yellow dashed lines and pi-pi interactions are indicated by blue dashed lines. Key residues in the binding pocket are shown and labelled. Docking was carried out using Schrodinger (Maestro 13.2) and the image was generated using PyMol Molecular Graphics System, Version 1.7.4.5- Educational Product, Schrodinger. (C) and (D) show the corresponding 2D ligand interaction diagrams generated by Maestro 13.2. Hydrogen bonds are indicated by purple lines, ionic interactions are indicated by red lines and hydrophobic interactions are indicated by green lines.

3.6 Chemical Synthesis and Resolution of SHF1556

3.6.1 Synthesis of SHF1556

The chemical synthesis of SHF1556 was carried out in four steps following a procedure previously stated in the literature. 4-fluoro-3-nitrobenzoic acid was coupled with N-methyl-*o*-toluidine to form the corresponding amide by first converting the acid to the corresponding acid chloride using oxalyl chloride (Scheme **3.1**). The acid chloride was then treated with the aniline in the presence of triethylamine to give the amide product. The next step was the formation of 2-mercaptothiazole by alkylation of 2-bromothiazole using thiourea, followed by an aqueous basic workup. It should be noted that 2-bromothiazole had to be stored under nitrogen to prevent its dimerization.

With the flouro-nitro amide and the thiazole in hand, the two fragments could be coupled together using a nucleophilic aromatic substitution reaction to form compound **43** (Sheme **3.1**). The sulfide was then oxidised to the corresponding sulfoxide using mCPBA (1.2 eq) at 0 ^{o}C. These conditions were to prevent overoxidation to the sulfone. Under these conditions, there was a small but significant amount of sulfide still present in the crude product. Attempts to separate the sulfide from the sulfoxide using column chromatography proved fruitless due to the similar retention times of both compounds. However, trituration of the crude in diethyl ether successfully removed the sulfide from the mixture, giving a clean sample of SHF1556.

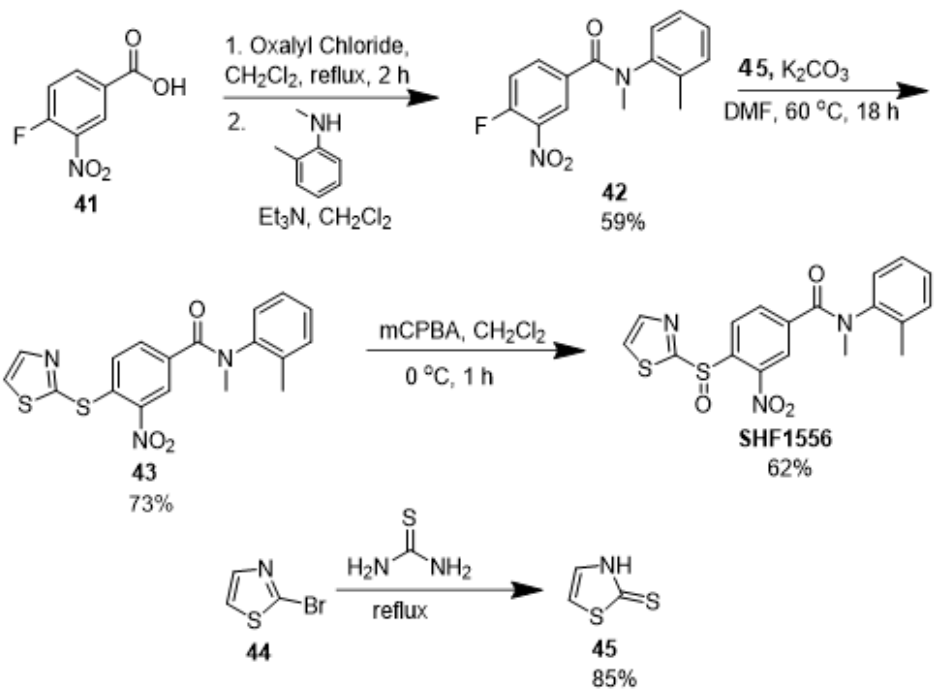

Scheme 3.1 – Synthesis of SHF1556

3.6.2 Resolution of SHF1556 Enantiomers

3.6.2.1 Synthesis of Compound 46

To separate the enantiomers of SHF1556, a classical resolution method was used (Scheme **3.2**). This involved taking the corresponding carboxylic acid and mixing it in solution with a single enantiomer of α-methyl benzylamine. This would form the corresponding salt, which would be a mixture of two diasteroemers. The two diastereomers could then, in principle, be separated by recrystallisation. Subsequent acidification of the diastereomers would form the corresponding enantiomers of the acid, both of which could then be coupled to N-methyl-*o*-toluidine to form the corresponding SHF1556 enantiomers.

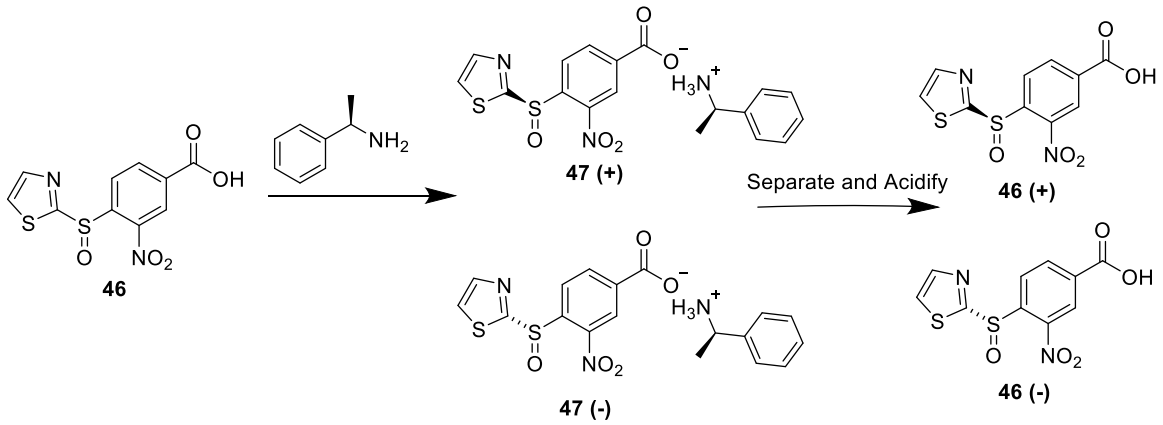

Scheme 3.2 – General idea of the resolution of the enantiomers of compound 6

The first challenge of the resolution was to synthesise the carboxylic acid, compound **46**. The initial strategy involved forming compound **45** as stated above, before coupling to 4-fluoro-3-nitrobenzoic acid by means of the S_NAr reaction and then oxidation of the sulfide with mCPBA. Attempts at the S_NAr with 4-fluoro-3-nitrobenzoic acid, however, resulted in a poor yield of the corresponding sulfide.

An alternative synthetic route was then devised starting from 4-fluoro-3-nitrobenzonitrile (Scheme **3.3**). S_NAr with compound **45** afforded compound **49** in a 72% yield, showing that the S_NAr conditions were more suited the nitrile substrate. Oxidation of compound **49** with mCPBA using the conditions stated above gave compound **50**. As with the original synthesis of SHF1556, the sulfoxide was able to be separated from any unreacted with sulfide by trituration with diethyl ether. Compound **46** was finally formed by hydrolysis of the nitrile under acidic conditions to form the desired carboxylic acid.

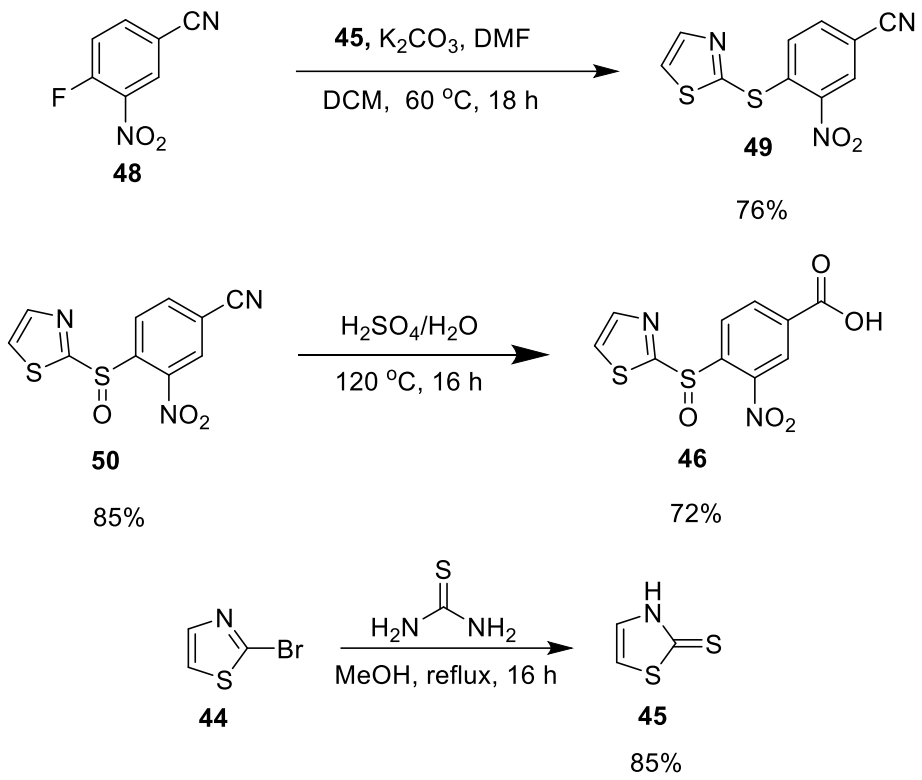

Scheme 3.3 – Synthesis of compound 46

3.6.2.2 Formation and Separation of Compound 6 Enantiomers

The next step was to take compound **46** and the (*S*)-enantiomer of α-methyl benzylamine and form the corresponding salt. This initially proved challenging due to the poor solubility of compound **46** in common organic solvents such as dichloromethane, diethyl ether and ethyl acetate. Fortunately, compound **46** was partially soluble in acetonitrile at room temperature, whilst heating to 60 °C allowed the compound to fully dissolve in the acetonitrile. As a result, the compound **46**-α-methyl benzylamine salt (Compound **47**) was formed by dissolving 1 equivalent of compound **6** and (*S*)-α-methyl benzylamine in acetonitrile at 60 °C. After stirring for 3 hours the solvent was removed to yield the desired salt (Scheme **3.4**).

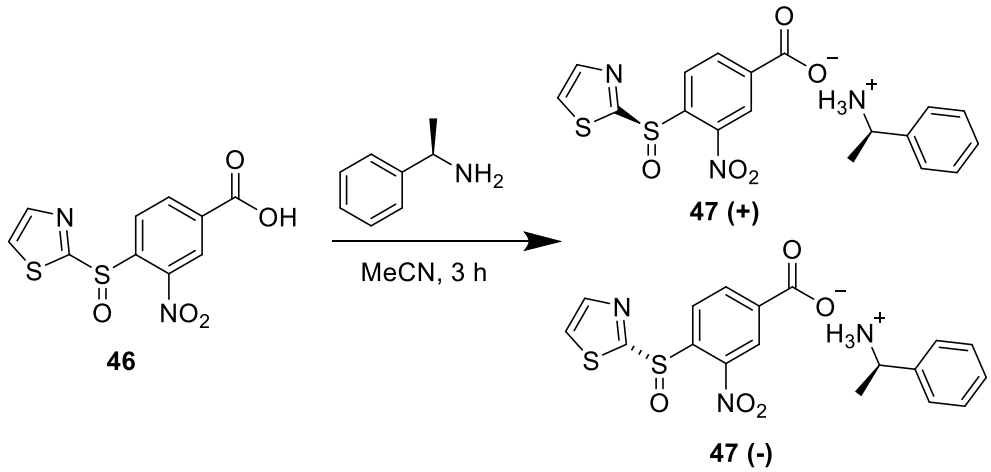

Scheme 3.4 – Formation of the compound 47 diastereomers

Attention was then turned to the separation of the diastereomers of the salt via recrystallisation. The idea was to chose a solvent in which one diastereomer of the salt would be soluble in, whilst the other diastereomer would precipitate out. The diastereomers could then be separated by vacuum filtration, with the subsequent solid containing exclusively one diastereomer and the filtrate containing the other.

Attempted recrystallisation using diethyl ether or dichloromethane proved unsuccessful due to poor solubility of the salt in these solvents. Use of ethyl acetate as the solvent successfully separated the two diastereomers of the salt. Analysis of the recrystallised solid and the filtrate by ^{1}H NMR gave two identical spectra, likely due to the fact that there are no protons in close proximity to the sulfoxide. Determination of the optical rotation of the corresponding acids of the two samples was therefore the best way to determine whether the recrystallization was successful (see later).

With the separated diastereomers of the salt in hand, the next step was to acidify the individual samples back to the carboxylic acid. This would provide the corresponding enantiomers of compound **46**. This was achieved by mixing the individual diastereomers with 1M hydrochloric acid and extracting with ethyl acetate (Scheme **3.5**). As with the salt, both enantiomers of compound **46** displayed identical ^{1}H NMRs, therefore the optical rotation of both samples were measured using a polarimeter (Table **3.8**).

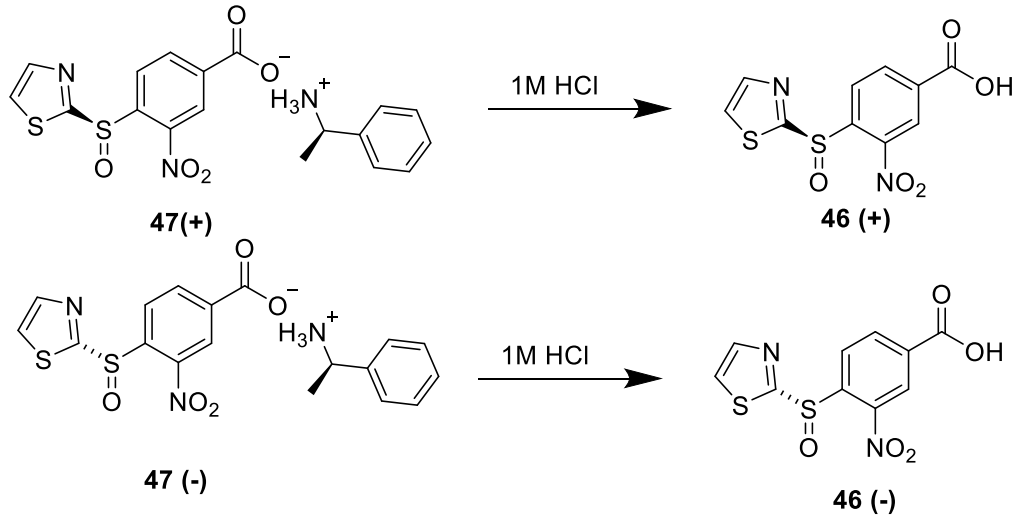

Scheme 3.5 – Acidification of the two salt diastereomers

Polarimetry is a method used to determine the optical rotation of chiral compounds. Two opposite enantiomers will rotate the plane of polarised light in different directions. One enantiomer will rotate the light in the positive direction, giving a (+) angle of rotation value,

whilst the other enantiomer will rotate the light in the negative direction, giving a (-) angle of rotation value. Therefore if the above recrystallization has been successful, then one acid sample will give a positive optical rotation value, and the other will give a negative value. Table **3.8** shows the optical rotation results for the recrystallized sample and the sample from the filtrate. Pleasingly, the samples rotated the plane of polarised light in the opposite directions, with the recrystallized sample being the (+) enantiomer, and the filtrate the (-) enantiomer. This data shows that the recrystallization was successful and the enantiomers of compound **46** were successfully separated.

Table 3.8 – Optical rotation values of the two compound 46 samples

Sample	Optical Rotation
Recrystallized Solid	+257
Filtrate	-213

The final task was the subsequent coupling of the individual enantiomers of compound **46** with compound **46** to form the enantiopure samples of SHF1556. Amide coupling was initially attempted using the same method as in the synthesis of racemic SHF1556, via the corresponding acid chloride. However, no SHF1556 was detected in the product of this reaction, with several unidentified products seen instead (Scheme **3.5**). It was reasoned that the sulfoxide in compound **46** was attacking the oxalyl chloride in the reaction mixture, resulting in a Swern-type reaction which was interfering with the formation of the acid chloride.

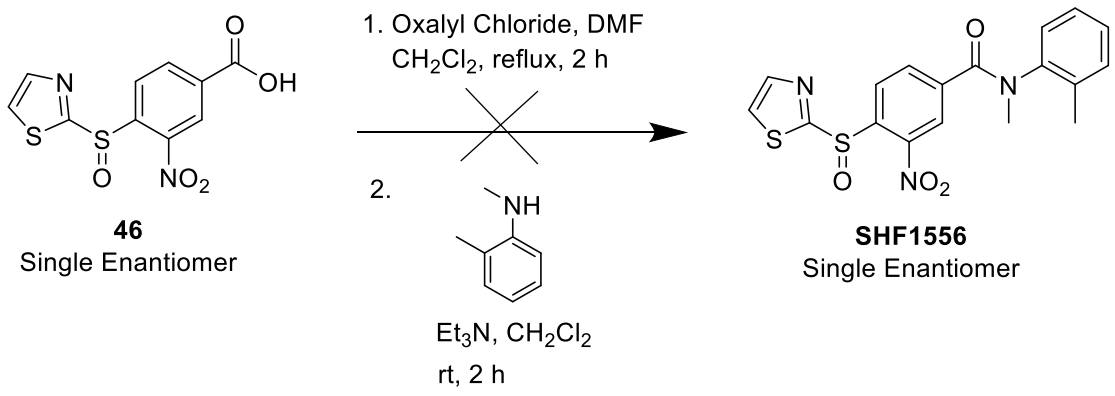

Scheme 3.6 – Attempted amide coupling of compound 6 via conversion to the acid chloride

Consequently, an alternative amide coupling method was carried out. Coupling of both enantiomers with compound 46 using N,N-dicyclohexylcarboiimide (DCC) and 4-dimethylaminopyridine (DMAP) successfully gave the (+) and (-) enantiomers of SHF1556. (Scheme **3.7**).

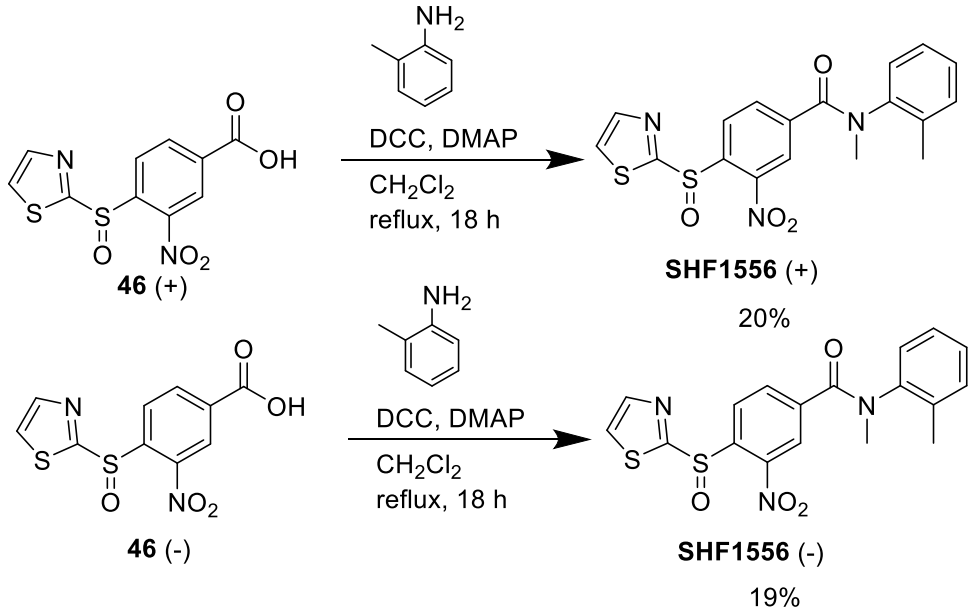

Scheme 3.7 – Amide coupling of both enantiomers of compound 6 using DCC

Both enantiomers were subjected to chiral HPLC to determine the enantiopurity of the samples. Analysis of the racemic SHF1556 by chiral HPLC revealed that, using a solvent system of 20% isopropanol in hexane, the peaks for each individual enantiomer appeared at 64 minutes and 97 minutes. Running the (+)-enantiomer on the chiral HPLC revealed it to correspond to the peak at 97 minutes. Pleasingly, the chromatograph displayed that the enantiomeric excess (ee) of the sample was greater than 99%, indicating an extremely enantiopure compound. The (-)-enantiomer, appearing at 64 minutes, was also revealed to be very enantiopure, giving an ee value of 95%. The reduced ee value for this sample makes sense due to the fact that this enantiomer came from the filtrate of the recrystallisation, meaning it is less likely to be as clean as the recrystallised solid. Regardless, the very high ee values of both samples showed that the resolution of the enantiomers had been a success. The enantiomers were subsequently subjected to *in vitro* testing.

3.7 *In Vitro* Testing of SHF1556

3.7.1 Potency of Racemic SHF1556

The racemic sample of SHF1556 was first tested on AM_1 overexpressing cells using the cAMP assay (see Chapter 2 for theory, Chapter 7 for method details). Pleasingly, the racemic sample gave a pIC50 value of 7.03 +/- 0.202 (Figure **3.9**), which is equivalent to approximately 93 nM. SHF1556 is therefore the most potent compound on the AM_1 receptor to date, and the first compound with an AM_1 IC50 of below 100 nM.

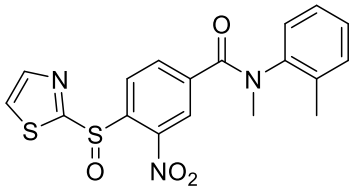

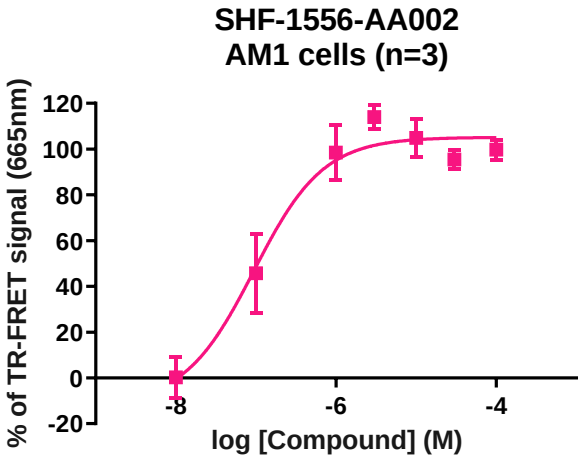

Parameter	Value
pIC50	7.03
Standard Error	0.202
R Square	0.671
Best Fit Top	105.2
Best Fit Bottom	-11.62

Figure 3.9 – Concentration-response plot of SHF1556 generated from the cAMP assay and the curve best fit data. Compound was tested on CLR/RAMP2 overexpressing cells which were subsequently stimulated by the EC50 concentration of AM (1 nM). Data was plotted using GraphPad Prism 9.0.2 and the IC50 was determined using a non-linear 3-parameter inhibition curve.

SHF1556 was next counter screened against cells overexpressing the CGRP receptor and cells overexpressing the AM_2 receptor, in order to determine selectivity for AM_1 over the closely related receptors (Figure **3.10**). SHF1556 displayed only modest selectivity over CGRP and AM_2. The pIC50 value of SHF1556 for CGRP was 6.39 +/- 0.179, equating to 407 nM. This

displays around a 4-fold selectivity for AM_1 over CGRP, hence showing reasonable selectivity. The IC50 value of 407 nM is similar to that observed in the functional adenylate cyclase assay in the literature (830 nM), with the discrepancies likely caused by the differences between the two assays. SHF1556 is slightly more potent on AM_2 than CGRP, giving a pIC50 value of 6.77 (169 nM). The compound is therefore less than 2-fold more selective for AM_1 over AM_2, although this difference is not considered to be statistically significant (P = 0.1996).

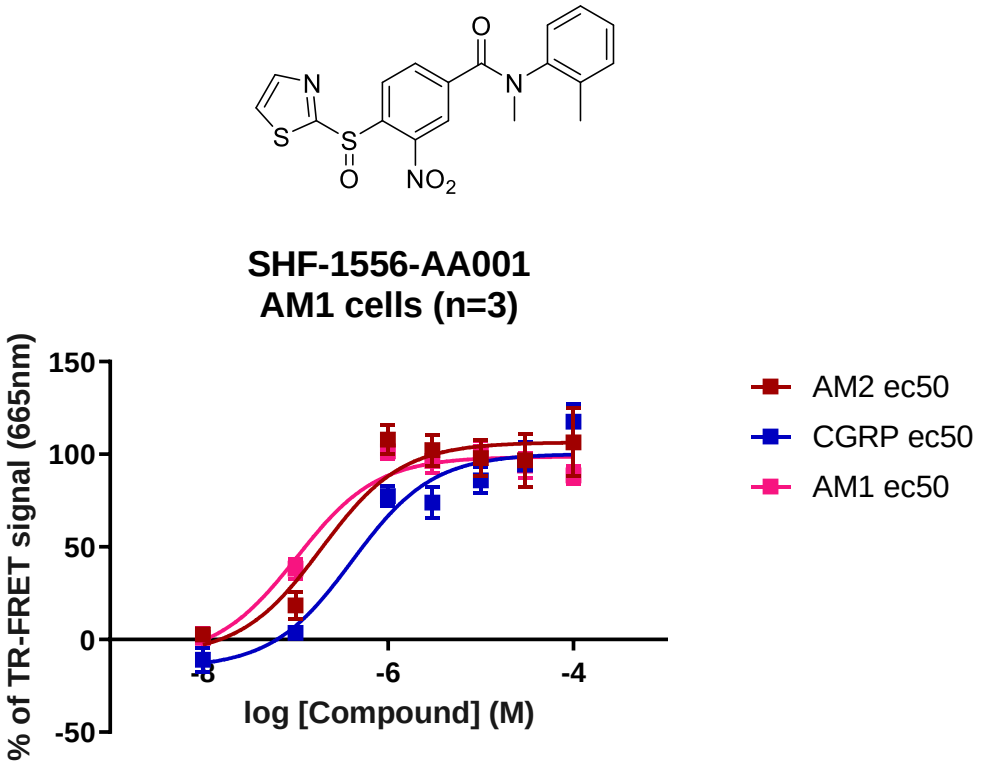

Figure 3.10 – Concentration-response plots of SHF1556 on AM_1, AM_2 and CGRP generated from the cAMP assay. Compounds were tested on CLR/RAMP1, which were stimulated by the EC50 concentration of CGRP (0.8 nM), CLR/RAMP2 cells and CLR/RAMP3 overexpressing cells which were subsequently stimulated by the EC50 concentration of AM (1 nM and 2 nM respectively. Data was plotted using GraphPad Prism 9.0.2 and the IC50 was determined using a non-linear 3-parameter inhibition curve. AM_1 curve is displayed in pink, CGRP curve is displayed in blue and the AM_2 curve is displayed in brown.

Table 3.9 – pIC50 values of racemic SHF1556 on CGRP, AM_1 and AM_2

	Receptor		
Parameter	**AM_1**	**AM_2**	**CGRP**
pIC50	7.03	6.72	6.39
Std Error	0.202	0.242	0.179
R Square	0.671	0.781	0.867
Best Fit Top	105.2	106.5	100.3
Best Fit Bottom	-11.62	-6.722	-15.46
P Value	-	0.1996	0.0058

3.7.2 Potency of SHF1556 Enantiomers

The resolved enantiomers of SHF1556 were then screened against the AM_1 receptor to determine which enantiomer was the more potent (Figure **3.11**) (Table **3.10**). The (+)-enantiomer was the most potent of the two, displaying a pIC50 value of 6.27 +/- 0.098. The (-)-enantiomer displayed a pIC50 value of 5.55 +/- 0.080, failing to display sub micro-molar potency. As a result, the (+)-enantiomer was 5-fold more potent than the (-)-enantiomer ($P < 0.0001$). The enantiomers were directly tested alongside racemic SHF1556 for comparison, with this compound in this test displaying a pIC50 of 6.38, which was statistically similar to the (+)-enantiomer ($P = 0.3117$) and was significantly more potent than the (-) enantiomer ($P < 0.0001$).

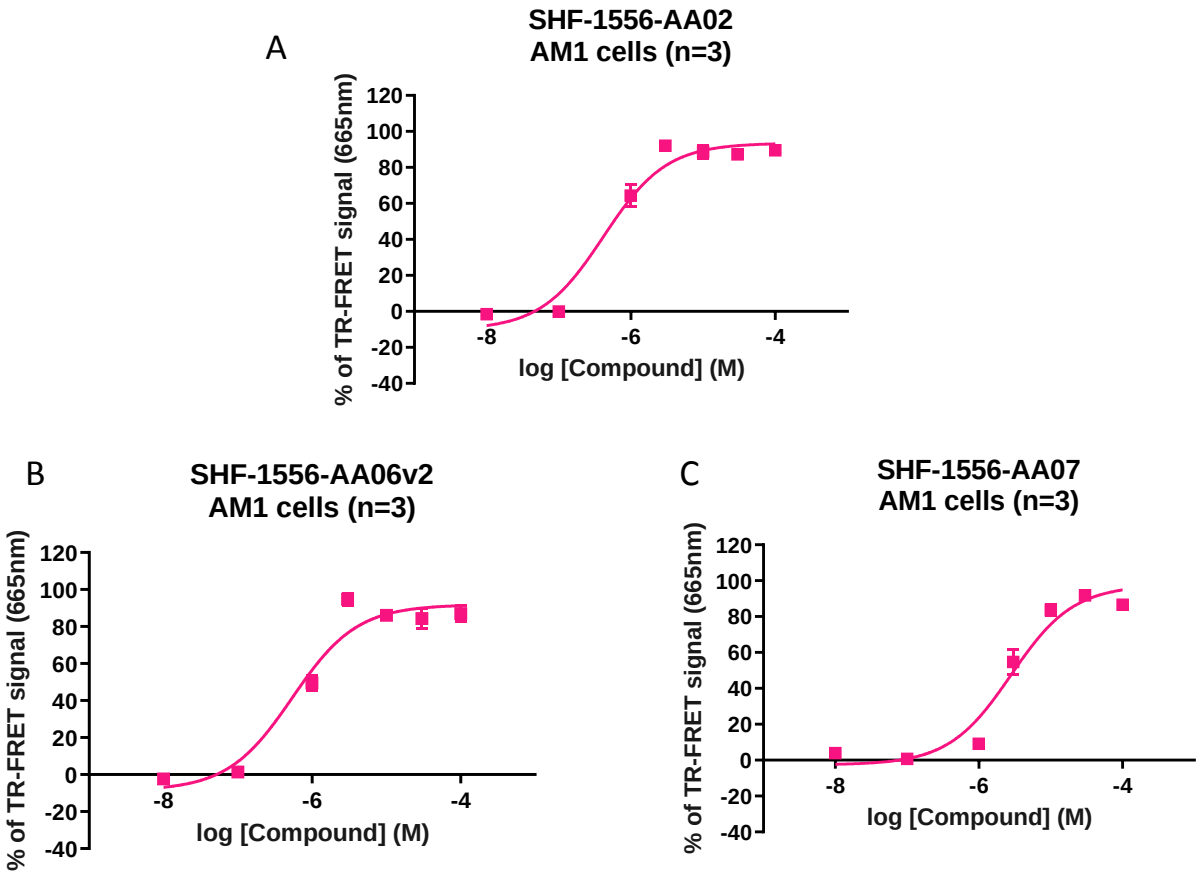

Figure 3.11 – Concentration-response plot of racemic SHF1556 (A), (+) SHF1556 (B) and (-) SHF1556 (C) generated from the cAMP assay and the curve best fit data. Compound was tested on CLR/RAMP2 overexpressing cells which were subsequently stimulated by the EC50 concentration of AM (1 nM). Data was plotted using GraphPad Prism 9.0.2 and the IC50 was determined using a non-linear 3-parameter inhibition curve.

Table 3.10 – pIC50 and best fit values for racemic, (+), and (-) SHF1556

	Compound		
Parameter	**SHF1556 (±)**	**SHF1556 (+)**	**SHF1556 (-)**
pIC50	6.38	6.27	5.55
Std Error	0.088	0.098	0.080
R Square	0.9267	0.9017	0.9107
Best Fit Top	93.53	91.79	97.56
Best Fit Bottom	-10.29	-8.695	-2.645
P Value	-	0.3117	<0.0001

3.8 Stereochemistry of SHF1556 (+) Enantiomer

Having determined the (+) enantiomer to be the more potent enantiomer of SHF1556, the next step was to determine the absolute stereochemistry of this enantiomer, thereby determining whether the sulfoxide is in the (*R*) or (*S*) configuration. Samples of the (+) enantiomer of compound **6** and SHF1556 were submitted for X-ray diffraction studies (Figure **3.12**)

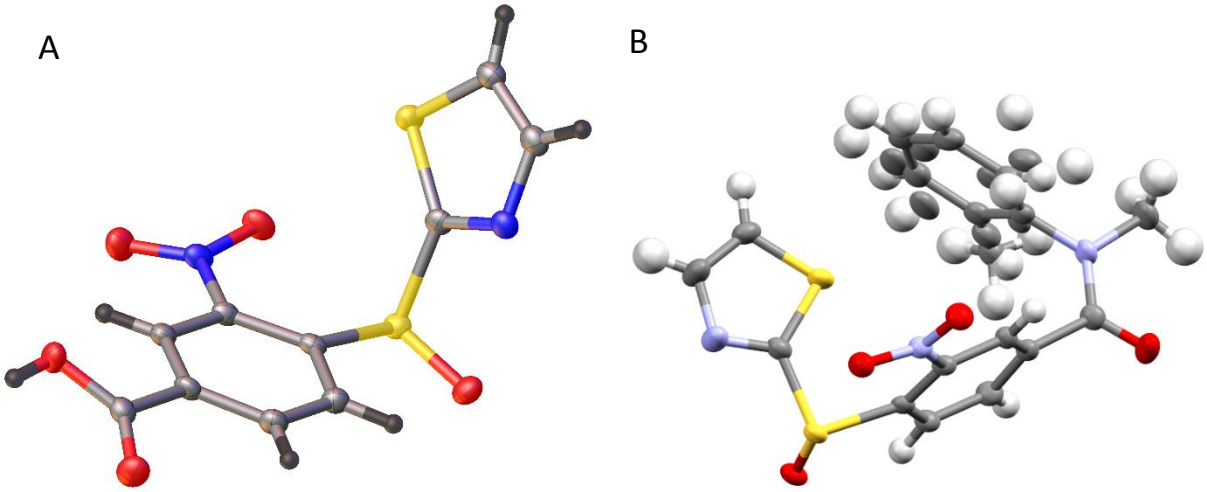

Figure 3.12 – X-ray crystal structures of Compound 6 and SHF1556. Absolute configuration of both compounds was determined to be (*S*) from the analysis

In terms of priority assignment, for both compounds the sulfoxide oxygen is priority 1, the thiazole is priority 2 and the nitro-phenyl group is priority 3. Both X-ray structures show an anticlockwise orientation of these substituents, therefore showing the absolute stereochemistry of the sulfoxide to be (*S*) for this enantiomer.

3.9 Counter Screening of SHF1556 Enantiomers on AM_2 and CGRP

The SHF1556 enantiomers were also counter screened against AM_2 and CGRP (Figure **3.13**) (Table **3.11**) (Figure **3.14**) (Table **3.12**). The potency of both enantiomers on CGRP cells were similar to that of AM_1 cells. As with AM_1 the (*S*) enantiomer (pIC50 = 6.32 +/-0.196) was more potent on CGRP cells than the (*R*) enantiomer (pIC50 = 5.42 +/-0.174)), displaying a 8-fold increase in potency. On AM_2 cells, however, the stereochemical effect on potency was reversed, with the (-) enantiomer (pIC50 = 5.91 +/-0.215) displaying greater potency than the

(+)-enantiomer (pIC50 = 5.6), albeit with a modest 2-fold selectivity. The (*S*)-enantiomer additionally displayed the lowest potency on AM_2, showing a 5-fold decrease in potency compared to AM_1 (P = 0.0038) whilst the (*R*) enantiomer displayed the highest potency on AM_2, a 2.5 fold increase compared to AM_1 and CGRP although this was not considered statistically significant (P = 0.0566).

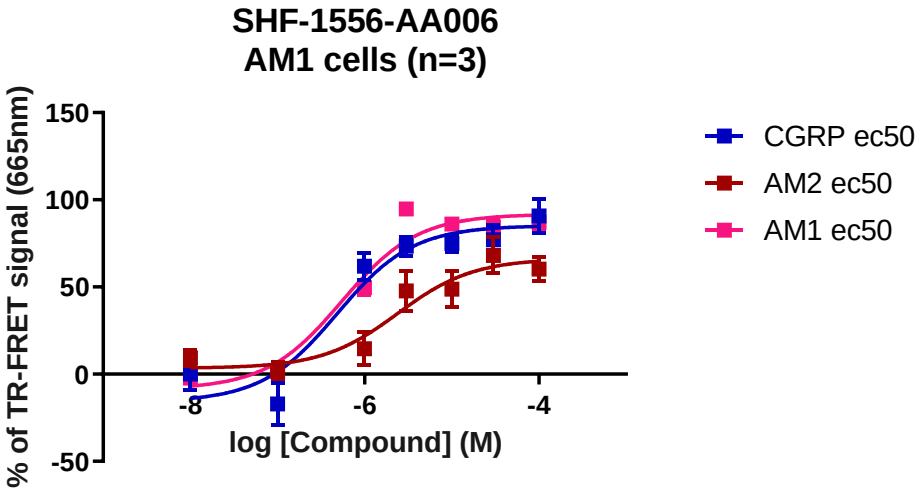

Figure 3.13 – Concentration-response plots of SHF1556 (+) on AM_1, AM_2 and CGRP generated from the cAMP assay. Compounds were tested on CLR/RAMP1, which were stimulated by the EC50 concentration of CGRP (0.8 nM), CLR/RAMP2 cells and CLR/RAMP3 overexpressing cells which were subsequently stimulated by the EC50 concentration of AM (1 nM and 2 nM respectively. Data was plotted using GraphPad Prism 9.0.2 and the IC50 was determined using a non-linear 3-parameter inhibition curve. AM_1 curve is displayed in pink, CGRP curve is displayed in blue and the AM_2 curve is displayed in brown.

Table 3.11 – pIC50 and best fit data for (+) SHF1556 on CGRP, AM_1 and AM_2.

	Receptor		
Parameter	**AM_1**	**AM_2**	**CGRP**
pIC50	6.27	5.62	6.32
Std Error	0.098	0.251	0.196
R Square	0.9017	0.5302	0.7006
Best Fit Top	91.79	66.26	85.23
Best Fit Bottom	-8.695	3.371	-15.96
P Value	-	0.0038	0.7775

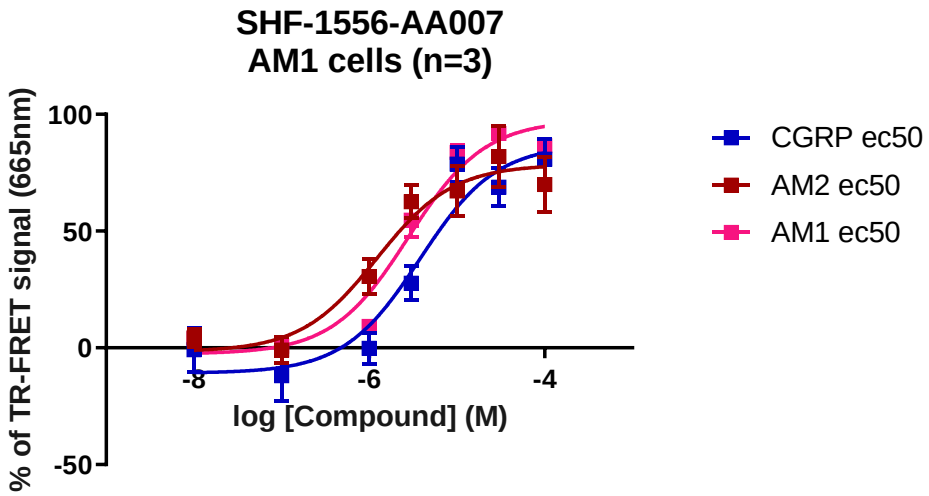

Figure 3.14 - Concentration-response plots of SHF1556 (-) on AM_1, AM_2 and CGRP generated from the cAMP assay. Compounds were tested on CLR/RAMP1, which were stimulated by the EC50 concentration of CGRP (0.8 nM), CLR/RAMP2 cells and CLR/RAMP3 overexpressing cells which were subsequently stimulated by the EC50 concentration of AM (1 nM and 2 nM respectively. Data was plotted using GraphPad Prism 9.0.2 and the IC50 was determined using a non-linear 3-parameter inhibition curve. AM_1 curve is displayed in pink, CGRP curve is displayed in blue and the AM_2 curve is displayed in brown.

Table 3.12 - pIC50 and best fit data for (-) SHF1556 on CGRP, AM_1 and AM_2

	Receptor		
Parameter	**AM_1**	**AM_2**	**CGRP**
pIC50	5.55	5.91	5.42
Std Error	0.080	0.215	0.174
R Square	0.9107	0.6056	0.6899
Best Fit Top	97.56	78.51	87.10
Best Fit Bottom	-2.645	-1.694	-10.86
P Value	-	0.0566	0.4127

3.10 Docking of SHF1556 to CGRP and AM_2

In order to elucidate the potential binding mode of SHF1556 on CGRP and AM_2, and to potentially rationalise AM_1 selectivity, both enantiomers of the compound were docked into the CGRP ECD (PDB: 3N7R) (Figure **3.15**) and the AM_2 ECD (6UUS) (Figure **3.16**). For docking studies on the CGRP receptor, the Telcagepant-bound crystal structure of the CGRP ECD (PDB: 3N7R), published by Ter Haar et al, was used. Alternative CGRP receptor models available on the Protein Data Bank include the ligand free CGRP ECD (PDB: 3N7P), the CGRP-bound CGRP receptor ECD (PDB: 4RWG) and the Cryo-EM structure of the full length CGRP receptor (PDB: 6E3Y). 3N7R was chosen for docking as this ECD structure most closely resembles the antagonist-bound conformation of the receptor. Additionally, viability of docking procedure can be confirmed by re-docking Telcagepant into the structure.

The binding mode of SHF1556 in CGRP was predicted to be different to that of AM_1, with the compound docking outwards from the CLR and forming interactions with RAMP1. The (*R*) enantiomer of SHF1556 saw the thiazole ring of the molecule form a pi stacking interaction with RAMP1 Trp74, whilst the nitro group formed pi-cation interactions with RAMP1 Trp74 and RAMP1 Trp84 (Figure **3.15**). The amide end of the molecule is close to the CLR, although no significant interactions on this side were predicted. The (*S*) enantiomer, on the other hand, exhibited a docking pose in which the amide group instead pointed towards RAMP1, with the

phenyl group at this end interacting with CLR Arg38. The thiazole, meanwhile, pointed towards the CLR end, forming pi-stacking interactions with CLR Trp72 (Figure **3.15**).

Docking of SHF1556 in AM_2 was carried out using the ECD of the Cryo-EM model of the full length AM_2 receptor. Although the resolution of the ECD is low in this model, it is the only model of the AM_2 ECD of the AM_2 ECD available on the Protein Data Bank and therefore could still provide a useful prediction as to how compounds could bind to the AM_2 ECD.

As with CGRP, the predicted docking pose of SHF1556 in the AM_2 ECD saw the compound dock outwards from CLR towards RAMP3. The (*R*) enantiomer this time had the thiazole pointing towards the CLR and the amide phenyl group pointing towards RAMP3. Predicted interactions were primarily with CLR Trp72, with the nitro group forming a pi-cation interaction and the central phenyl group forming a pi stacking interaction (Figure **3.16**). The (*S*) enantiomer saw the thiazole end of the compound towards RAMP3, with interactions including an ionic interaction between the nitro group and RAMP3 Glu74 and a pi-cation interaction between the nitro group and RAMP3 Trp84. The amide phenyl group, meanwhile, pointed towards CLR, forming a stacking interaction with CLR Tyr124 (Figure **3.16**).

Docking scores for both enantiomers are similar to each other at both CGRP and AM_2 receptors, with the (*R*) enantiomer displaying the highest docking score at both receptors (Table **3.13**). This is in line with the experimental data seen for AM_2 but not for CGRP.

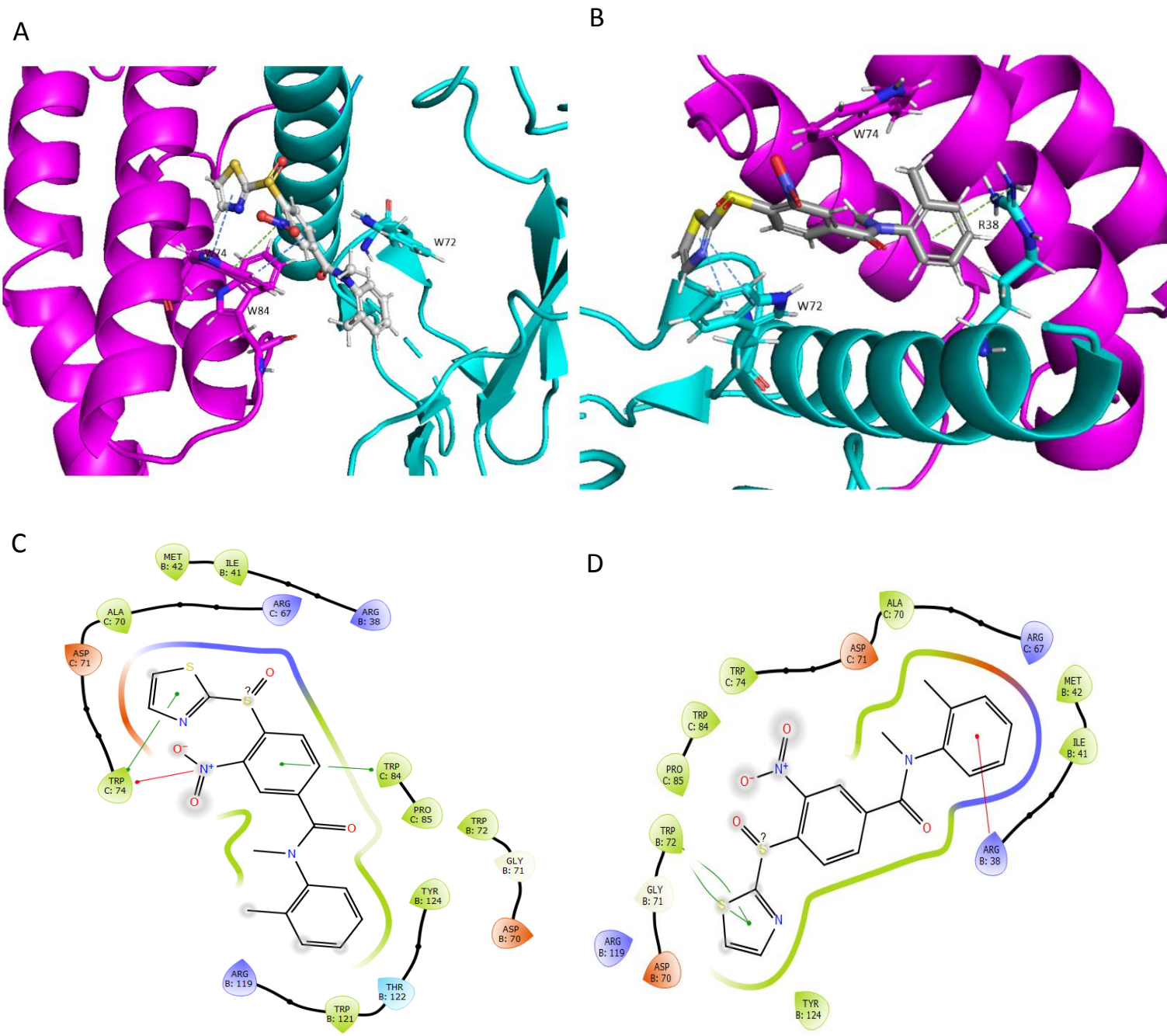

Figure 3.15 - Lowest energy docking pose of SHF1556 (*R*) enantiomer, (A) and (C), and (*S*) enantiomer, (B) and (D), bound to the CGRP receptor (PDB: 3N7R). (A) and (B) show the 3D image of the compound docked into the CGRP receptor ECD. The CLR is coloured in cyan and RAMP1 is coloured in magenta. Pi-pi interactions are indicated by blue dashed lines and pi-cation interactions are indicated by green dashed lines. Key residues in the binding pocket are shown and labelled. Docking was carried out using Schrodinger (Maestro 13.2) and the image was generated using PyMol Molecular Graphics System, Version 1.7.4.5- Educational Product, Schrodinger. (C) and (D) show the corresponding 2D ligand interaction diagrams generated by Maestro 13.2. Hydrogen bonds are indicated by purple lines, ionic interactions are indicated by red lines and hydrophobic interactions are indicated by green lines.

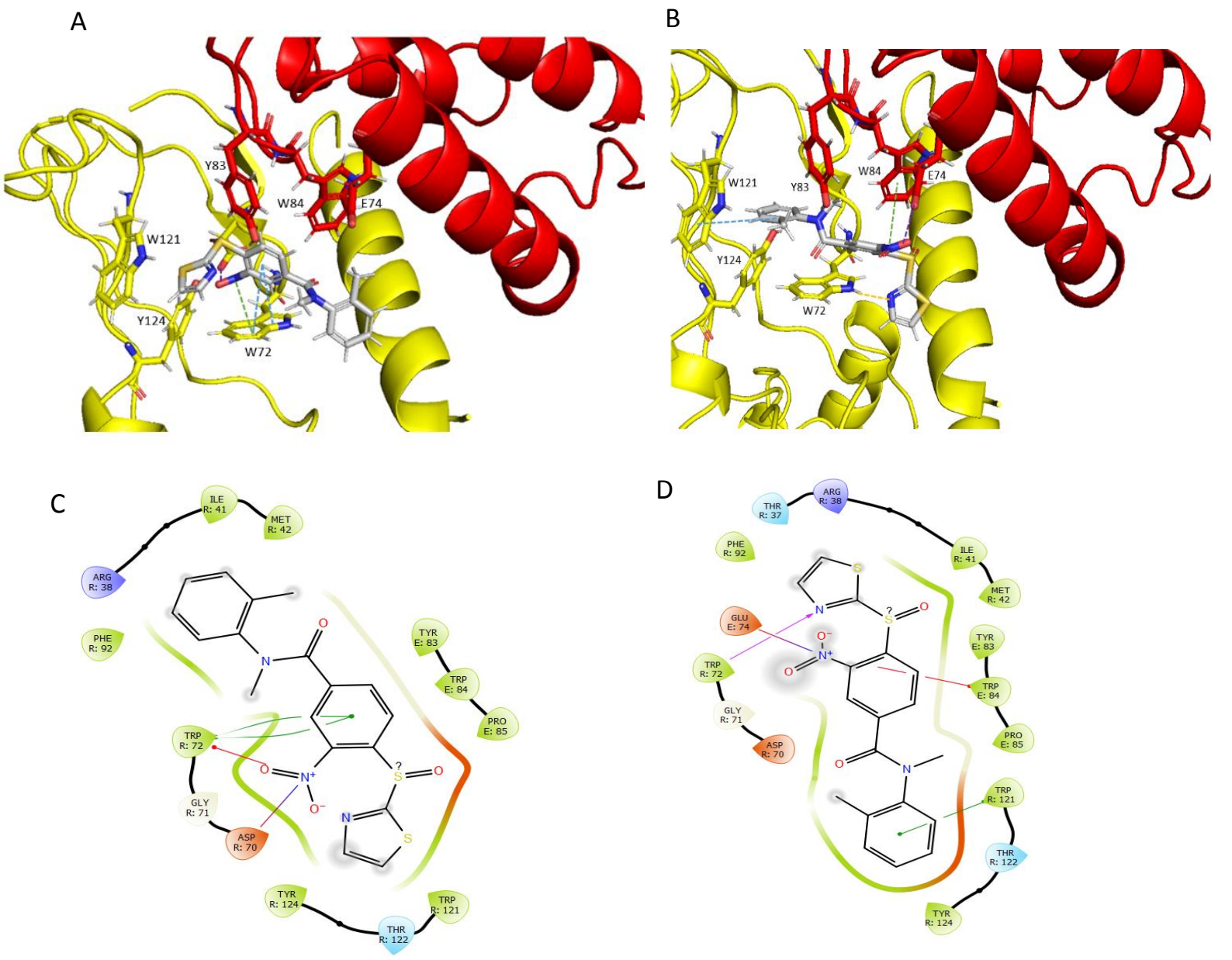

Figure 3.16 - Lowest energy docking pose of SHF1556 (*R*) enantiomer, (A) and (C), and (*S*) enantiomer, (B) and (D), bound to the AM_2 receptor (PDB: 6UUS). The CLR is coloured in yellow and RAMP3 is coloured in red. Hydrogen bonds are indicated by yellow dashed lines, pi-pi interactions are indicated by blue dashed lines and pi-cation interactions are indicated by green dashed lines. Key residues in the binding pocket are shown and labelled. Docking was carried out using Schrodinger (Maestro 13.2) and the image was generated using PyMol Molecular Graphics System, Version 1.7.4.5- Educational Product, Schrodinger. (C) and (D) show the corresponding 2D ligand interaction diagrams generated by Maestro 13.2. Hydrogen bonds are indicated by purple lines, ionic interactions are indicated by red lines and hydrophobic interactions are indicated by green lines.

Table 3.13 – Docking Scores of SHF1556 in the CGRP receptor ECD (PDB: 3N7R) and AM_2 ECD (6UUS). Docking scores generated by Schrodinger (Maestro 13.2)

SHF1556 Enantiomer	Docking Score (CGRP) (kcal mol^{-1})	Docking Score (AM_2) (kcal mol^{-1})
(R)	-6.6	-4.7
(S)	-6.1	-3.9

3.11 Conclusion

To summarise, SHF1556 was discovered as a potent small molecule AM_1 antagonist. Chosen due to structural similarities with SHF1486, one of our European Lead Factory hits, the compound displays AM_1 potency at approximately 100 nM, therefore making it the most active compound at this receptor to date. The enantiomers of this compound have also been resolved and separated, with the stereochemistry of the most active enantiomer determined to be (*S*). SHF1556 has additionally been found to exhibit modest selectivity over the CGRP receptor, although no significant selectivity over the AM_2 receptor was observed.

Chapter 4 – Investigation of the Structure Activity Relationships of SHF1556

Chapter 4: Investigation of the Structure Activity Relationships of SHF1556

4.1 Introduction to SAR

Structure Activity Relationships (SAR) describe the correlation between compound structure and its biological activity. SAR is generally studied by modifying a small section of a parent molecule, for example by removing or changing a functional group, before testing the modified compound *in vitro* to determine the effect the modification has had on the affinity or the potency of the compound towards the target protein. This method can therefore help the medicinal chemist to identify which functional groups of the molecule are crucial for biological activity. The information gained from SAR studies can also be used in lead optimisation, providing a good indication as to where biological activity can be improved in the compound series.

Examples of SAR studies in drug discovery that are particularly relevant in this thesis include that of CLR/RAMP receptors. For example, CGRP antagonist Olcegepant was developed from a high throughput screening lead. SAR studies primarily focused on the modification of the terminal aryl groups, particularly on the right hand side of the molecule, with a piperidyl amide linked to a quinazolinone structure proving optimal for CGRP affinity and potency (Figure **4.1**) (Rudolph, 2005). The major SAR developments in the discovery of Telcagepant was on the caprolactam ring. Specifically, the phenyl substituent on the 6-position of the caprolactam ring was much more active at CGRP than with the corresponding 5 or 7-substituted compounds (Figure **4.1**). Futhermore the stereochemistry of the phenyl-substituted caprolactam with also crucial, with a (3*R*,6*S*) stereochemistry proving to be optimal (Panone, 2007). Through these studies, the structural features crucial for biological activity were identified.

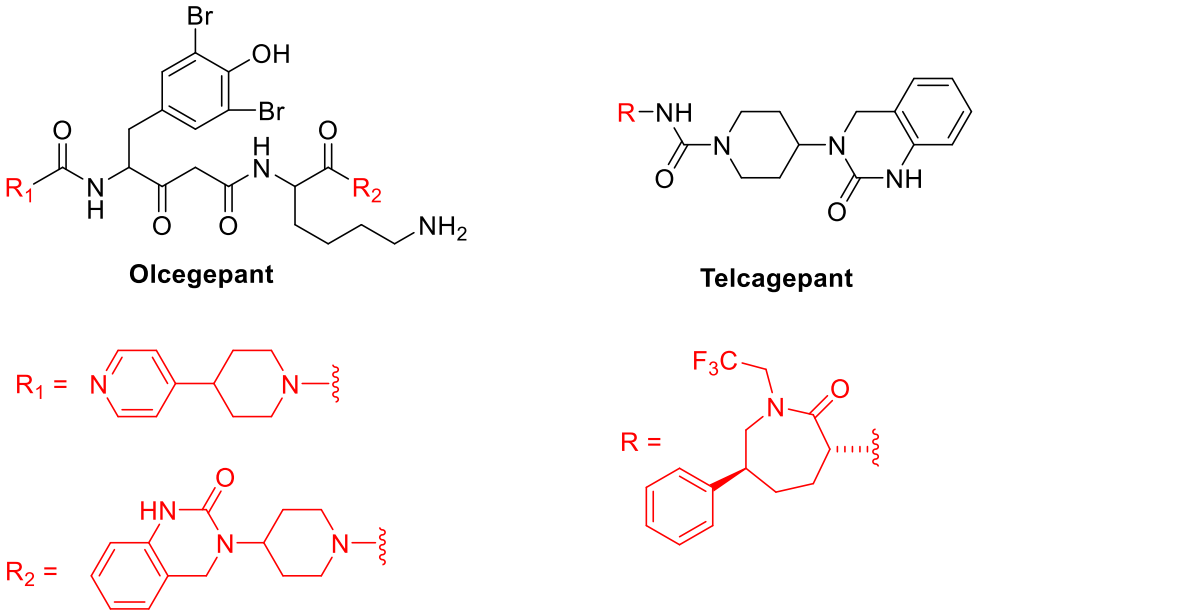

Figure 4.1 – SAR Development of Olcegepant and Telcagepant. The fragments of the molecule in which major SAR has been studied is highlighted in red.

4.1.1 Hypothesis SAR of AM_1 Antagonist SHF1556

As described previously (see Chapter 3), a lead compound, SHF1556, has been identified for AM_1 receptor antagonism. Although it is known that this compound displays good potency on AM_1, it is not known which parts of the structure are key for activity. Docking studies have indicated that the sulfoxide and nitro groups are potentially key binding groups, with the sulfoxide potentially forming a hydrogen bond with CLR Thr122 amide backbone and the nitro group potentially forming a salt bridge with CLR Trp121 (see Chapter 3), providing a useful clue to the importance of these groups. However, as SHF1556 has not been co-crystallised in the AM_1 receptor, it is uncertain as to which sections of the compound bind to the protein. The aim, therefore, was to synthesise analogues of this compound by making subtle structural modifications to investigate the SAR, with further potential to improve potency. From the docking pose of SHF1556, it can be hypothesised that the sulfoxide and nitro groups will be crucial for AM_1 potency due to the interactions predicted in the docking results.

4.2 SAR on Sulfoxide

The first structure modified in SHF1556 was the sulfoxide. Simple analogues investigated include the sulfide and the oxidised sulfone (Figure **4.2**). Determination of activity on AM_1

from these compounds would provide a useful insight into the role of the sulfoxide oxygen atom for AM_1 potency for SHF1556, as this atom is a hydrogen bond acceptor so has the potential to form hydrogen bonds with polar amino acid residues.

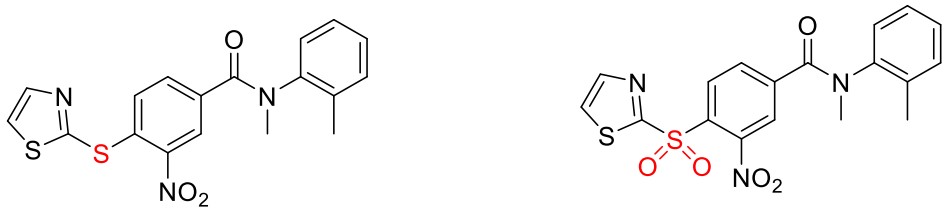

Figure 4.2 – Chemical structures of SHF1555 and SHF1558. Structural elements that differ from SHF1556 are highlighted in red

4.2.1 Docking of Sulfide and Sulfone in AM_1

The SHF1556 sulfide analogue, SHF1555, and the sulfone analogue, SHF1558, were docked into AM_1 receptor ECD (PDB: 3AQF) using Schrodinger (Maestro 13.2) (Figure **4.3**). As expected, the loss of the sulfoxide oxygen atom in SHF1555 meant that there were no interactions predicted in this region of the molecule. The only favourable drug-protein interaction observed in this docking pose was between the thiazole nitrogen and CLR Arg119, whilst many more unfavourable interactions were observed, generating a low docking score (Table **4.1**). It is therefore predicted from this model that the potency of SHF1555 at AM_1 would be significantly lower than that of SHF1556.

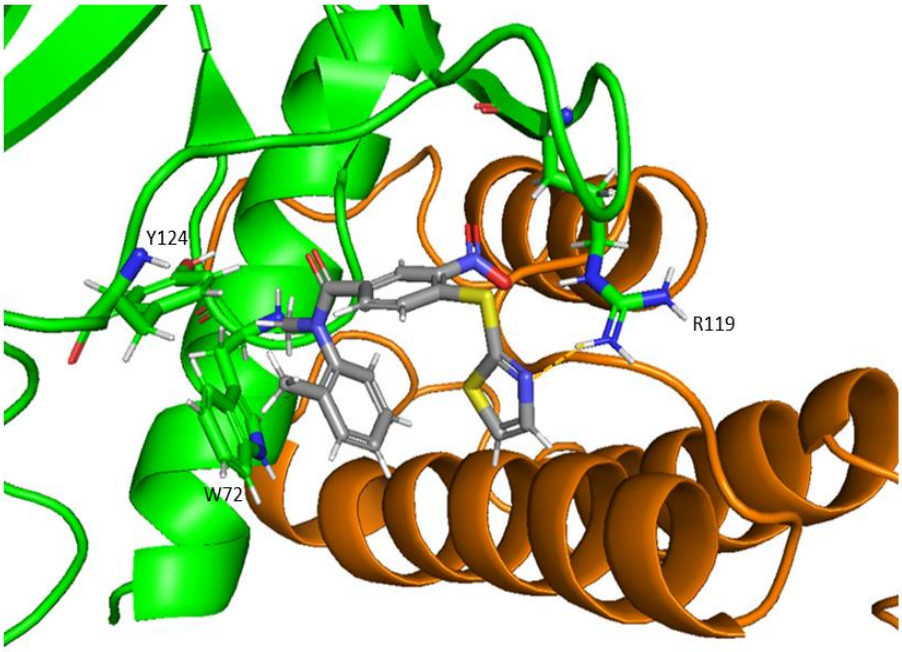

Figure 4.3 – Lowest energy docking pose of SHF1555 bound to the AM_1 receptor (PDB: 3AQF) The CLR is coloured in green and RAMP2 is coloured in orange. Hydrogen bonds are indicated by yellow dashed lines. Key residues in the binding pocket are shown and labelled. Docking was carried out using Schrodinger (Maestro 13.2) and the image was generated using PyMol Molecular Graphics System, Version 1.7.4.5- Educational Product, Schrodinger.

The docking pose for the sulfone analogue, SHF1558, predicts no interactions between the sulfone oxygen atom and the protein, contrasting with the corresponding sulfoxide (Figure **4.4**). Any interactions between the compound and the protein were exclusively towards CLR Tyr124, with the amide carbonyl predicted to form a hydrogen bond with the NH backbone, whilst the central aromatic ring was predicted to form a pi-pi stack against the side chain of this residue. A low docking score was also generated for this compound, implying that AM_1 potency will be significantly lower for this compound compared to SHF1556.

Docking scores for both SHF1555 (-3.1 kcal mol^{-1}) and SHF1558 (-3.2 kcal mol^{-1}) (Table **4.1**) are significantly lower than that seen for SHF1556, further implying that these compounds could be less active than the lead compound.

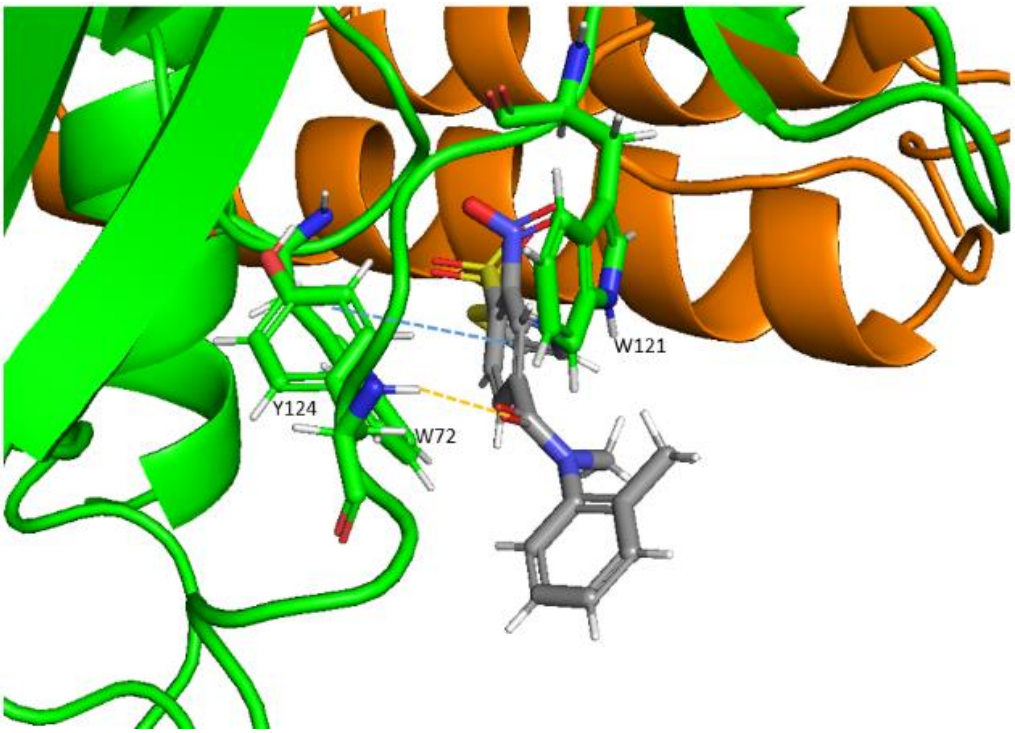

Figure 4.4 – Lowest energy docking pose of SHF1558 bound to the AM_1 receptor (PDB: 3AQF). CLR is coloured in green and RAMP2 is coloured in orange. Hydrogen bonds are indicated by yellow dashed lines and pi stacking interactions are indicated by blue dashed lines. Key residues in the binding pocket are shown and labelled. Docking was carried out using Schrodinger (Maestro 13.2) and the image was generated using PyMol Molecular Graphics System, Version 1.7.4.5- Educational Product, Schrodinger.

Table 4.1 – Docking Scores of SHF1555 and SHF1558 in the AM_1 ECD (PDB: 3AQF). Docking scores generated by Schrodinger (Maestro 13.2)

Compound	Docking Score (kcal mol^{-1})
SHF1555	-3.1
SHF1558	-3.2

4.2.2 Synthesis of Sulfide and Sulfone Analogues

The corresponding sulfide of SHF1556 is an intermediate in the synthesis of this compound (see Chapter 3). Therefore whilst proceeding on the synthetic route to SHF1556, a 3 mg sample of sulfide SHF1555 was taken for *in vitro* testing. Further oxidation of the sulfoxide in SHF1556 led to the formation of the corresponding sulfone SHF1558 (Scheme **4.1**). This compound was isolated from any remaining sulfoxide by HPLC.

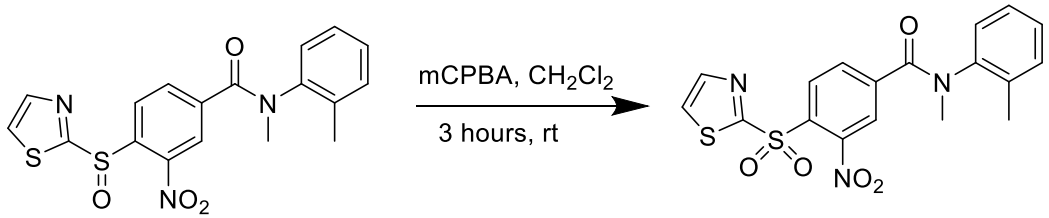

Scheme 4.1 – Synthesis of SHF1558

4.2.3 *In Vitro* Testing of Sulfide and Sulfone Analogues

SHF1556, the corresponding sulfide (SHF1555), and sulfone (SHF1558), were tested on AM_1 overexpressing cells to compare the potency of the three compounds (Figure **4.5**) (Table **4.2**). As shown previously, SHF1556 displays good potency on AM_1 (pIC50 = 7.03 +/- 0.202). Intriguingly SHF1555 containing a reduced sulfide group displayed no AM_1 activity, showing that reducing the sulfoxide to the sulfide completely removes biological activity at this receptor. The corresponding sulfone SHF1558 displayed a significant reduction of potency on AM_1 (pIC50 = 4.12 +/- 0.196) ($P < 0.0001$). These data imply that the sulfoxide group on SHF1556 is crucial for AM_1 potency, matching the observations from the docking studies. It is also worth noting that all sulfide analogues of the compounds tested in this series were inactive on AM_1, whilst all sulfones also displayed significant reductions in potency compared to their sulfoxide analogues, further confirming the generality of the sulfoxide as a key pharmacophore.

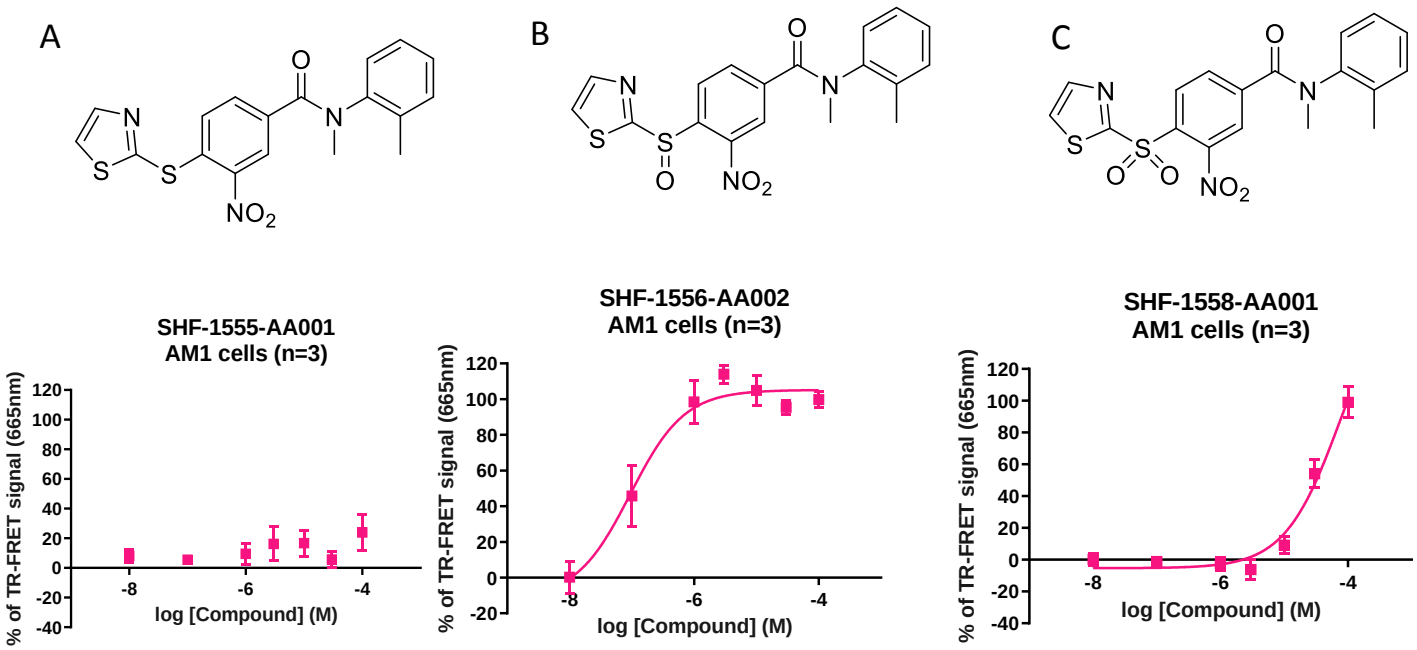

Figure 4.5 – Concentration-response plot of SHF1555 (A), SHF1556 (B) and SHF1558 (C) generated from the cAMP assay and the curve best fit data. Compound was tested on CLR/RAMP2 overexpressing cells which were subsequently stimulated by the EC50 concentration of AM (1 nM). Data was plotted using GraphPad Prism 9.0.2 and the IC50 was determined using a non-linear 3-parameter inhibition curve.

Table 4.2 – AM_1 pIC50 and best fit data for SHF1555, SHF1556 and SHF1558.

	Receptor		
Parameter	**SHF1555**	**SHF1556**	**SHF1558**
pIC50	n.d	7.03	4.12
Std Error	-	0.202	0.196
R Square	-	0.671	0.8078
Best Fit Top	-	106.5	179.9
Best Fit Bottom	-	-6.722	-5.350

4.3 Reduction of Nitro Group to Aniline

4.3.1 Docking of SHF1556 Aniline Analogue

The nitro group on SHF1556 was the next part of the molecule investigated for SAR studies. One transformation of particular interest was the reduction of the nitro group to its corresponding aniline (Figure **4.6**). This change could provide useful information about the role in the nitro group in providing AM_1 potency, as despite still containing hydrogen bond donors/acceptors, the reduced aniline loses its ability to form ionic interactions or pi-cation interactions as it is no longer charged.

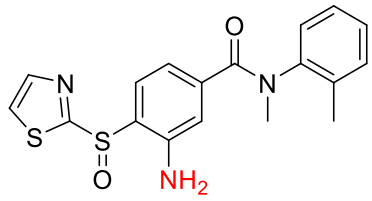

SHF1574

Figure 4.6 – Chemical Structure of SHF1574. Structural elements that differ from SHF1556 are highlighted in red

Docking of SHF1574 into the AM_1 ECD crystal structure (PDB: 3AQF), predicts this compound will adopt a similar position in the binding pocket to SHF1556 (Figure **4.7**). In both enantiomers, the sulfoxide is predicted to retain hydrogen bonding, this time to CLR Arg119, whilst the reduced aniline group is predicted to form a hydrogen bond with the main chain carbonyl of CLR Thr120. The thiazole ring in the (*S*) enantiomer is predicted to form an additional hydrogen bond to CLR Ser117. Docking scores for both enantiomers are slightly lower than that of SHF1556 (Table **4.3**), suggesting that this compound may have a small detrimental effect on AM_1 potency. Nevertheless, these docking scores, along with the predicted interactions, made this compound a potentially promising analogue of SHF1556.

Table 4.3 – Docking Scores of SHF1574 enantiomers in the AM_1 ECD (PDB: 3AQF). Docking scores generated by Schrodinger (Maestro 13.2)

SHF1574 Enantiomer	Docking Score (kcal mol^{-1})
(R)	-4.2
(S)	-3.8

A

B

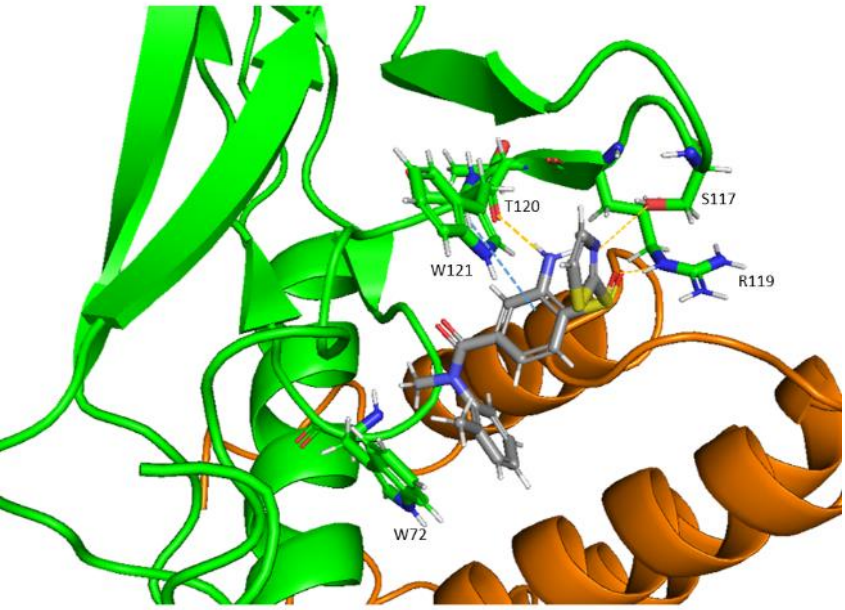

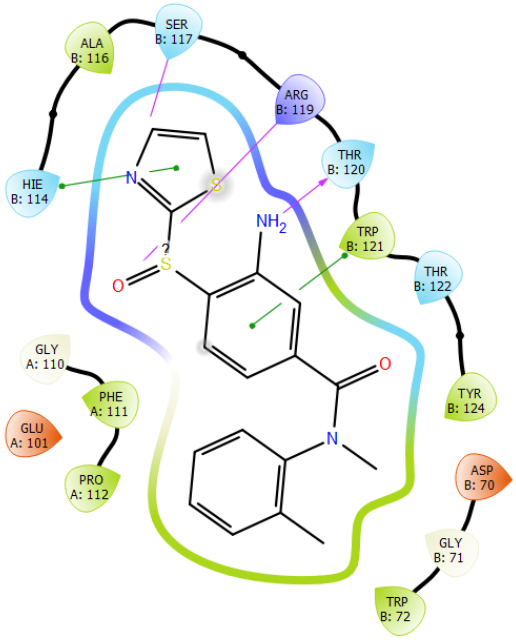

Figure 4.7 – Lowest energy docking pose of the (*S*) enantiomer of SHF1574 bound to the AM_1 receptor (PDB: 3AQF). (A) 3D image of SHF1486 docked into the AM_1 receptor ECD. CLR is coloured in green and RAMP2 is coloured in orange. Hydrogen bonds are indicated by yellow dashed lines and pi stacking interactions are indicated by blue dashed lines. Key residues in the binding pocket are shown and labelled. Docking was carried out using Schrodinger (Maestro 13.2) and the image was generated using PyMol Molecular Graphics System, Version 1.7.4.5- Educational Product, Schrodinger. (B) 2D ligand interaction diagram generated from Maestro 13.2. Hydrogen bonds are indicated by purple lines and hydrophobic interactions are indicated by green lines.

4.3.2 Synthesis of SHF1574

SHF1574 was synthesised in one step from SHF1556 (Scheme **4.2**). Reduction of the nitro group to the corresponding aniline using zinc and ammonium chloride, as described in the synthesis of CLR B (see Chapter 2) successfully yielded the desired analogue.

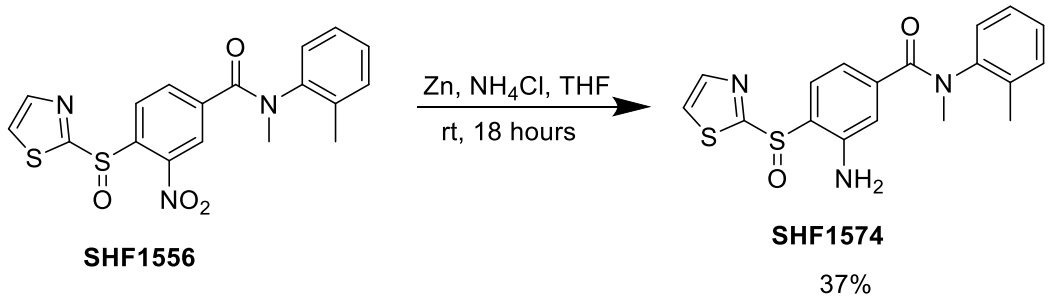

Scheme 4.2 – Synthesis of SHF1574

4.3.3 *In Vitro* Testing of SHF1574

SHF1574 was tested for AM_1 activity using the cAMP assay (Figure **4.8**). Interestingly, SHF1574 exhibited no AM_1 potency, showing that the reduction of the nitro group to the corresponding aniline completely eliminates AM_1 activity. This result was somewhat surprising, given the docking pose predicted for this compound.

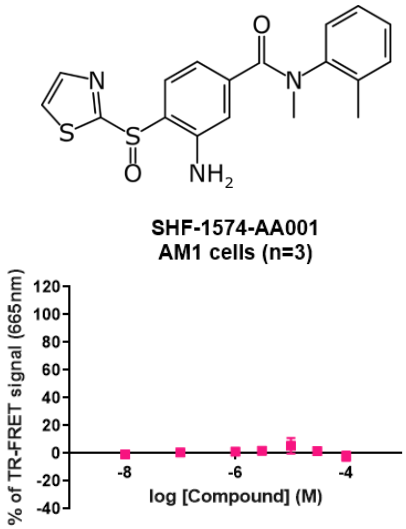

Figure 4.8 – Concentration-response plot of SHF1574 generated from the cAMP assay and the curve best fit data. Compound was tested on CLR/RAMP2 overexpressing cells which were subsequently stimulated by the EC50 concentration of AM (1 nM). Data was plotted using GraphPad Prism 9.0.2. No curve date generated due to the layout of the data points

4.4 SAR of *N*-Methyl and *o*-methyl groups

4.4.1 Docking of *N*-methyl and *o*-methyl Analogues

The next SAR investigation on SHF1556 was the modification of the *N*-methyl and *o*-methyl groups. In this series, both methyl groups were removed individually and collectively to produce new analogues of SHF1556 (SHF1568, SHF1576, SHF1582) (Figure **4.9**). In addition, the *N*-methyl group was also replaced with other alkyl groups such as ethyl and isopropyl in order to determine any effect of a bulkier substituent at this position (SHF1579, SHF1580) (Figure **4.9**).

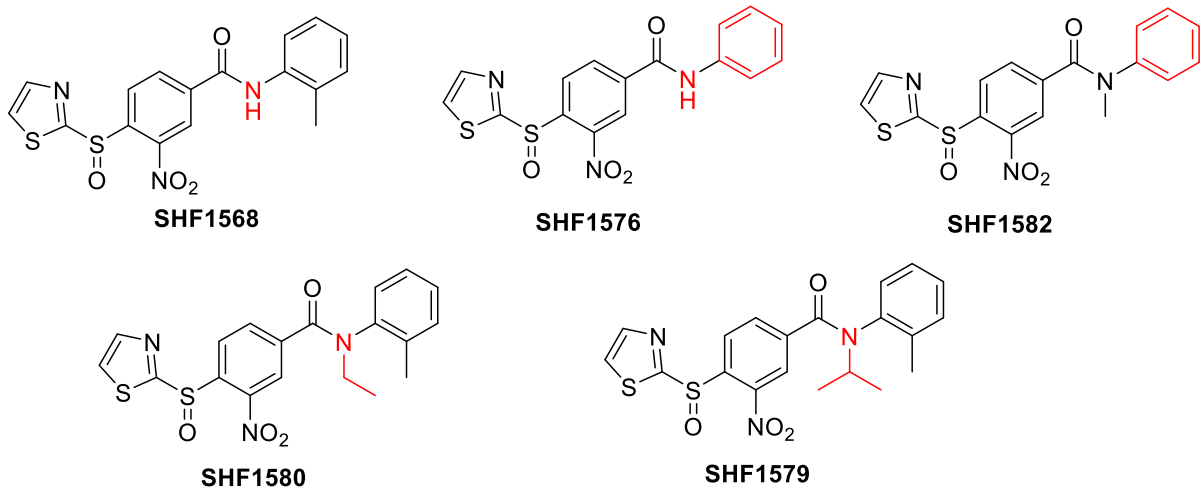

Figure 4.9 – Chemical Structures of *N*-methyl and *o*-methyl SHF1556 analogues SHF1568, SHF1576, SHF1582, SHF1580 and SHF1579. Structural elements that differ from SHF1556 are highlighted in red

The docking poses of these compounds in the AM_1 ECD (PDB: 3AQF) were predicted to be similar to that of SHF1556, with almost every compound predicted to bind at the CLR end of the receptor binding pocket. The (*R*) enantiomer of SHF1576 and SHF1582 both had the sulfoxide oxygen forming a hydrogen bond with CLR Thr122 NH backbone whilst the nitro group was predicted to form a salt bridge with CLR Asp70 and a pi cation stack with Trp72 (Figure **4.10**). The (*R*) enantiomer of SHF1568, on the other hand, sat closer to RAMP2, with the sulfoxide oxygen instead hydrogen bonding to the RAMP2 Phe111 backbone, whilst the thiazole ring formed a pi-pi stack with CLR Trp72. The (*S*) enantiomer interactions were more varied with these compounds, with only SHF1582 predicting a sulfoxide oxygen hydrogen bond, to the Tyr124 amide backbone (Figure **4.10**). In both SHF1568 and SHF1576, it was the nitro group that instead hydrogen bonded to the Thr122 amide backbone, whilst the amide carbonyl made an additional hydrogen bond to CLR Trp121 in SHF1576. Furthermore, both SHF1568 and SHF1576 formed pi-pi stacking interactions with CLR Trp72, from the thiazole and central phenyl group respectively. The thiazole of SHF1582, meanwhile, was predicted to stack against CLR Trp121. The similarity and number of interactions of these compounds compared to SHF1556 implied that they are likely to maintain similar potency to SHf1556 at the AM_1 receptor.

SHF1579 and SHF1580, the isopropyl and ethyl analogues respectively, also docked exclusively at the CLR end of the receptor. The sulfoxide oxygen on the (*R*) enantiomer of SHF1579 was again predicted to hydrogen bond to CLR Thr122, with the docking pose almost identical to those of SHF1576 and SHF1582 (Figure **4.11**). The equivalent enantiomer in SHF1580 instead had the sulfoxide oxygen hydrogen bonding to CLR Arg119, whilst stacking the thiazole against CLR Trp121 (Figure **4.11**). The sulfoxide oxygen on the (*S*) enantiomers of SHF1579 and SHF1580 is predicted to form hydrogen bonds with the backbones of CLR Arg119 and Tyr124 respectively, whilst CLR Trp121 is expected to stack against the thiazole and central phenyl ring of SHF1580 and SHF1579 respectively (Figure **4.11**). The docking poses suggest that the introduction of bulkier substituents and be accommodated reasonably well in, suggesting these compounds may exhibit similar AM_1 potency compared to SHF1556.

Average docking scores of both enantiomers of each compound in this series are all slightly lower than that of SHF1556 (Table **4.4**), suggesting a small detrimental effect on AM_1 activity, with SHF1576 and SHF1580 displaying the highest docking scores of the series.

Table 4.4 – Docking Scores of *N*-methyl and *o*-methyl analogues of SHF1556 in the AM_1 ECD (PDB: 3AQF). Docking scores generated by Schrodinger (Maestro 13.2).

Compound	Enantiomer	Docking Score (kcal mol^{-1})
SHF1568	(*R*)	-3.6
SHF1568	(*S*)	-3.0
SHF1576	(*R*)	-4.6
SHF1576	(*S*)	-3.8
SHF1582	(*R*)	-3.3
SHF1582	(*S*)	-4.2
SHF1579	(*R*)	-3.6
SHF1579	(*S*)	-2.5
SHF1580	(*R*)	-3.7
SHF1580	(*S*)	-4.6

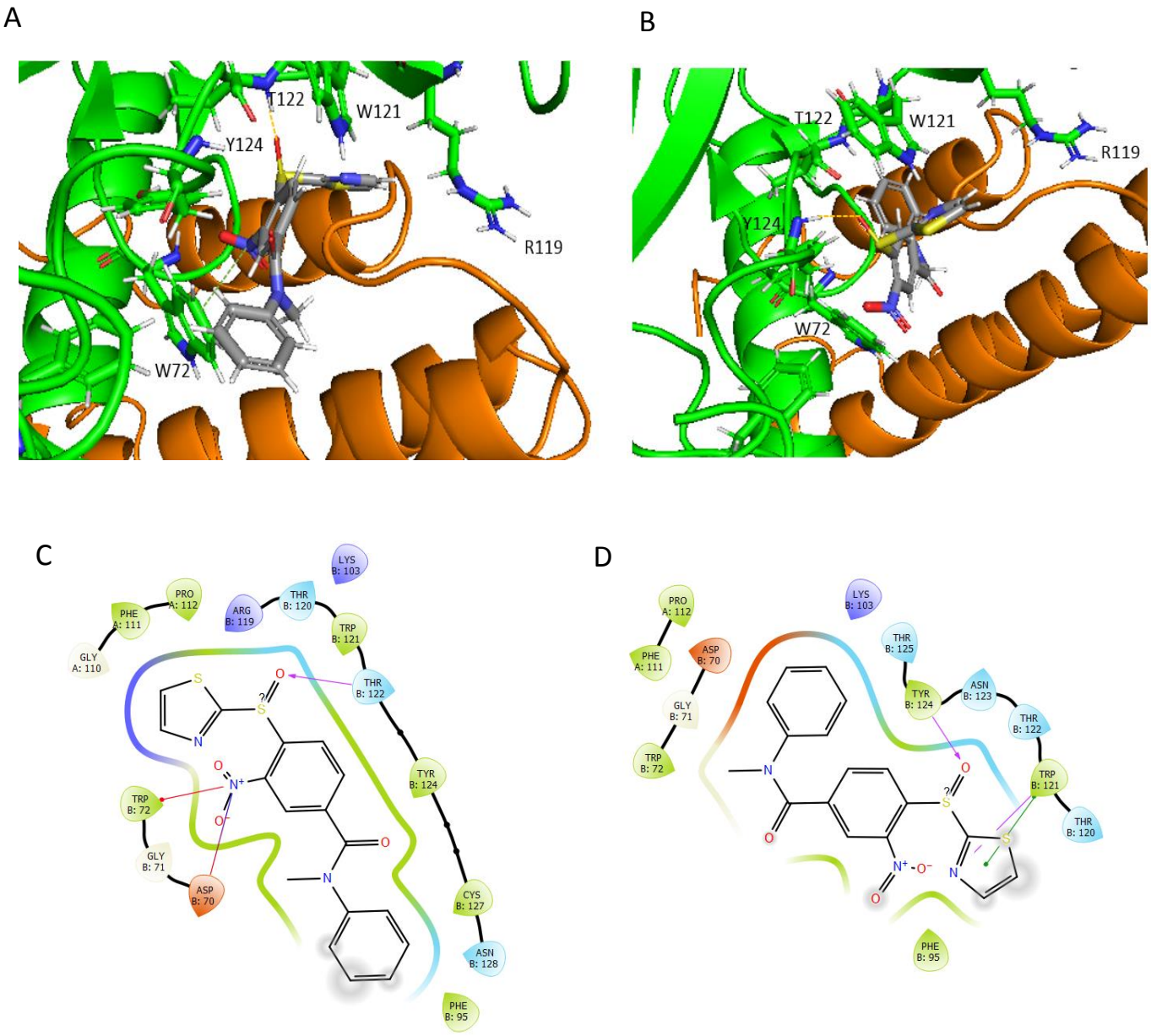

Figure 4.10 - Lowest energy docking pose of SHF1582 (*R*) enantiomer, (A) and (C), and (*S*) enantiomer, (B) and (D), bound to the AM_1 receptor (PDB: 3AQF). (A) and (B) show the 3D image of the compound docked into the AM_1 receptor ECD. The CLR is coloured in green and RAMP2 is coloured in orange. Hydrogen bonds are indicated by yellow dashed lines, pi-pi interactions are indicated by blue dashed lines and pi-cation interactions are indicated by green dashed lines. Key residues in the binding pocket are shown and labelled. Docking was carried out using Schrodinger (Maestro 13.2) and the image was generated using PyMol Molecular Graphics System, Version 1.7.4.5- Educational Product, Schrodinger. (C) and (D) show the corresponding 2D ligand interaction diagrams generated by Maestro 13.2. Hydrogen bonds are indicated by purple lines, ionic interactions are indicated by red lines and hydrophobic interactions are indicated by green lines.

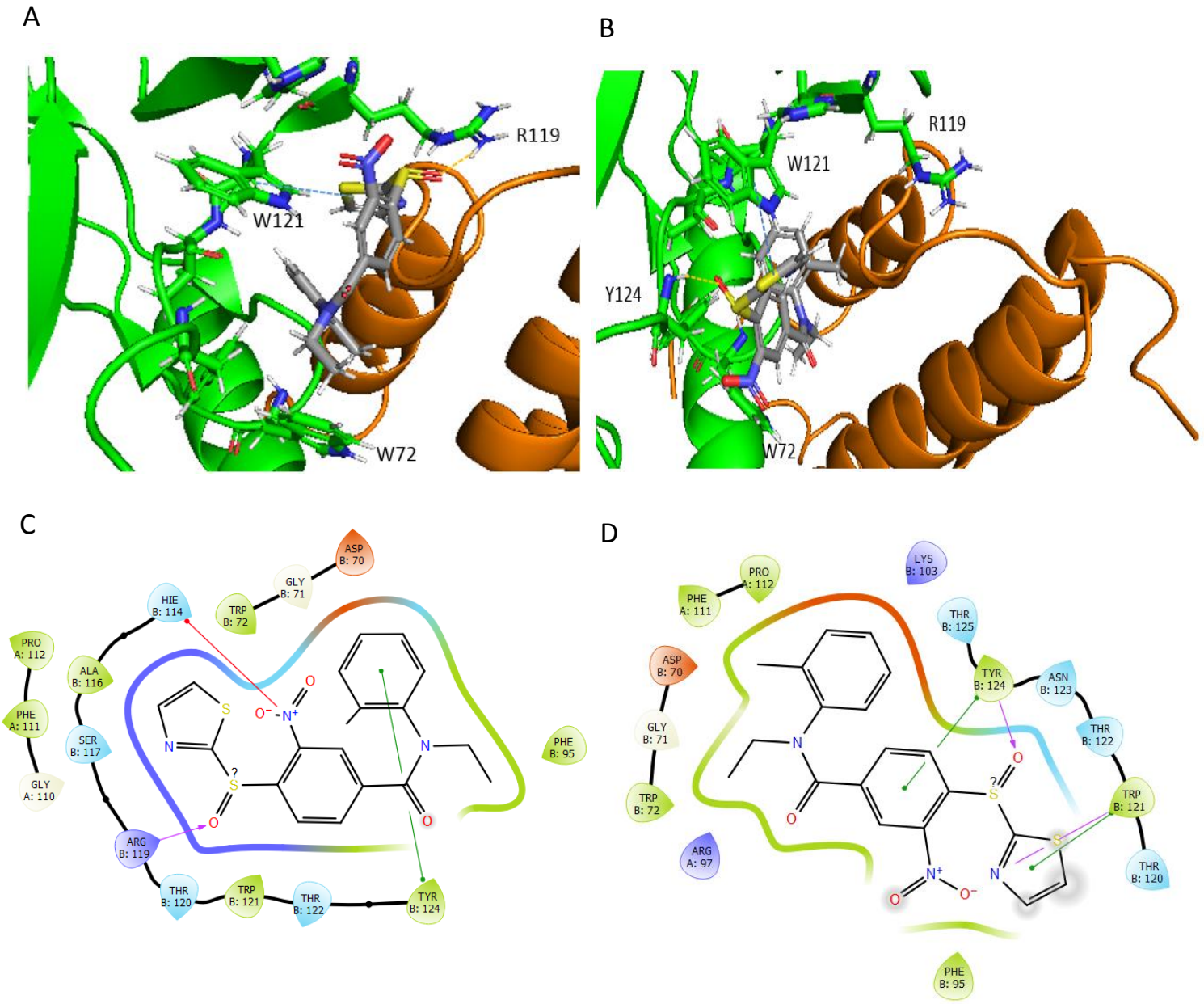

Figure 4.11 - Lowest energy docking pose of SHF1580 (*R*) enantiomer, (A) and (C), and (*S*) enantiomer, (B) and (D), bound to the AM_1 receptor (PDB: 3AQF). (A) and (B) show the 3D image of the compound docked into the AM_1 receptor ECD. The CLR is coloured in green and RAMP2 is coloured in orange. Hydrogen bonds are indicated by yellow dashed lines, pi-pi interactions are indicated by blue dashed lines and pi-cation interactions are indicated by green dashed lines. Key residues in the binding pocket are shown and labelled. Docking was carried out using Schrodinger (Maestro 13.2) and the image was generated using PyMol Molecular Graphics System, Version 1.7.4.5- Educational Product, Schrodinger. (C) and (D) show the corresponding 2D ligand interaction diagrams generated by Maestro 13.2. Hydrogen bonds are indicated by purple lines, ionic interactions are indicated by red lines and hydrophobic interactions are indicated by green lines.

4.4.2 Synthesis of *N*-methyl and *o*-methyl Analogues

The synthesis of SHF1568, SHF1582, SHF1576, SHF1580 and SHF1579 is shown in Scheme **4.3**. SHF1568 (R_1 = H, R_2 = Me), SHF1582 (R_1 = Me, R_2 = H) and SHF1576 (R_1 = H, R_2 = H) were formed from the coupling of *o*-toluidine, *N*-methyl aniline and aniline, respectively, to compound **51**, formed from the two step S_NAr coupling of compound **45** to compound **48** followed by acid catalysed hydrolysis of the nitrile **49**. The coupling was carried out using oxalyl chloride to convert the carboxylic acid to the corresponding acid chloride, before addition of the corresponding aniline and Et_3N to form the amide bond. Subsequent oxidation of the sulfide to the corresponding sulfoxide yielded the desired compounds. SHF 1580 and SHF1579 were synthesised by Mr Joe Egan and were formed by the alkylation of *o*-toluidine by reductive amination using ethanal and acetone respectively, before the two step amide coupling with compound **51** and oxidation described above to yield the desired compounds.

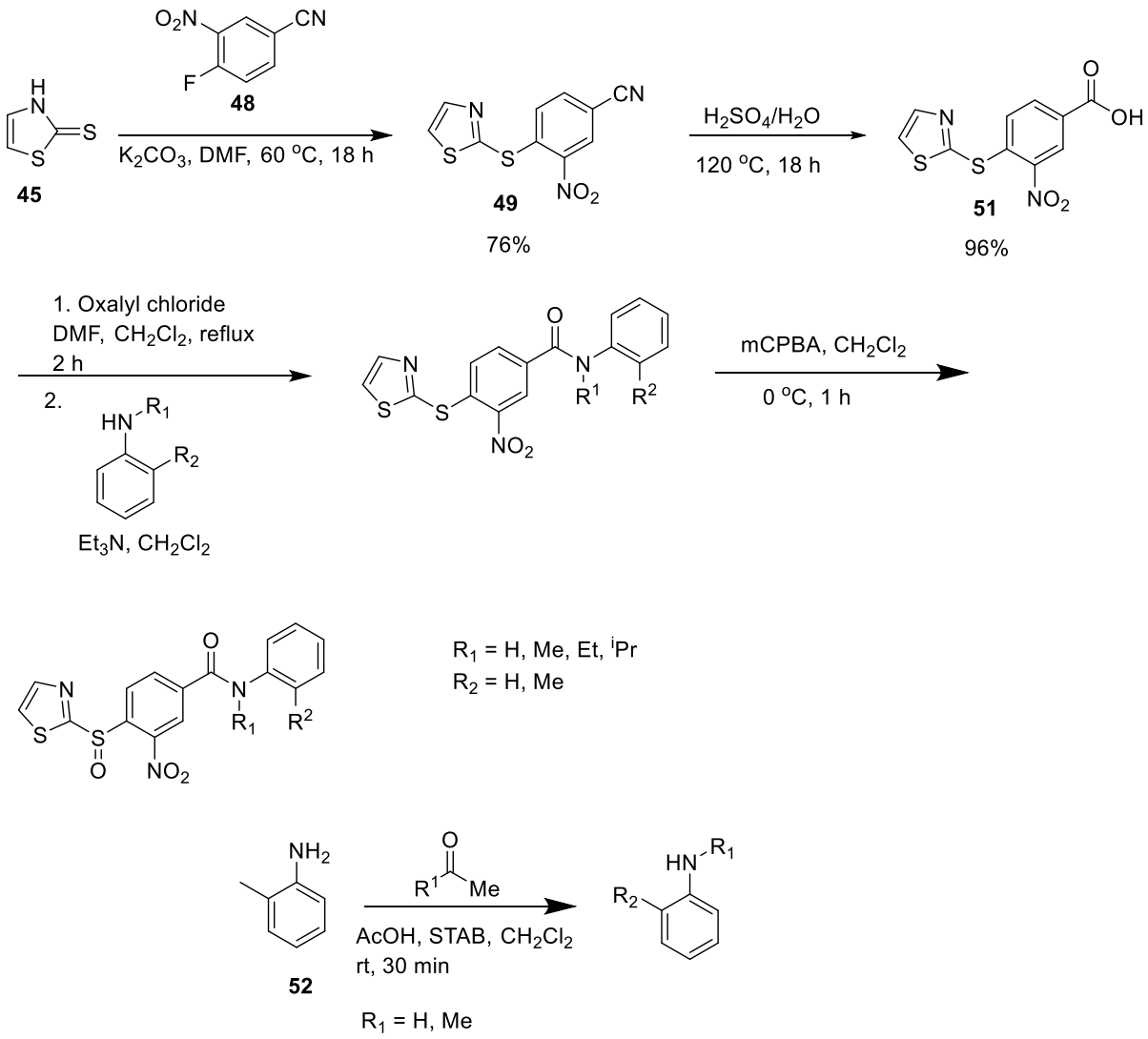

Scheme 4.3 General Synthetic Route to SHF1556 *N*-methyl and *o*-methyl analogues

4.4.3 *In Vitro* Testing of *N*-methyl and *o*-Methyl Analogues

N-Methyl and *o*-methyl groups were subsequently tested for AM_1 potency (Figure **4.12**) (Figure **4.13**) (Table **4.5**) (Table **4.6**). All compounds were tested alongside SHF1556 for a direct comparison of IC50 values. As there was some variation in pIC50 values of SHF1556 during each assay run, the % pIC50 value of each compound compared to the pIC50 value of SHF1556 was calculated in order to draw a clearer comparison between the compounds and SHF1556 (Table **4.7**).

Removing the methyl groups from both the amide nitrogen and the *ortho*-position of the phenyl ring subtly lowered AM_1 potency. Removing the *N*-methyl group to form SHF1568 (pIC50 = 5.66 +/- 0.080) showed a small decrease in AM_1, with pIC50 value being 85% of that observed with SHF1556 ($P < 0.0001$). Removing the *ortho*-methyl group on the right hand

side phenyl ring to form SHF1582 to SHF1556 also displayed a slight reduction in potency (pIC50 = 5.71 +/- 0.132), 88% of SHF1556 ($P < 0.0001$). Furthermore removing both methyl groups to form SHF1576 (pIC50 = 4.65 +/- 0.140), decreased AM_1 potency further, at 79% of the value for SHF1556 ($P < 0.0001$).

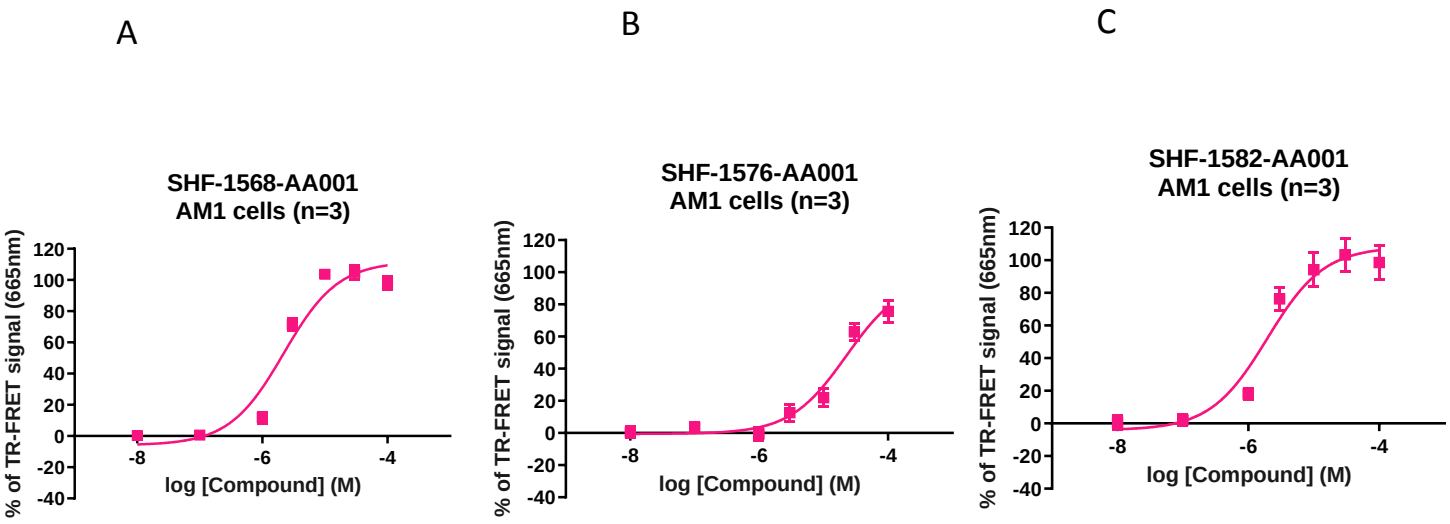

Figure 4.12 – Concentration-response plot of SHF1568 (A), SHF1576 (B) and SHF1582 (C) generated from the cAMP assay and the curve best fit data. Compound was tested on CLR/RAMP2 overexpressing cells which were subsequently stimulated by the EC50 concentration of AM (1 nM). Data was plotted using GraphPad Prism 9.0.2 and the IC50 was determined using a non-linear 3-parameter inhibition curve.

Table 4.5 – pIC50 and best fit data for SHF1568, SHF1576 and SHF1582

	Compound		
Parameter	**SHF1568**	**SHF1576**	**SHF1582**
pIC50	5.66	4.65	5.71
Std Error	0.080	0.140	0.132
R Square	0.9089	0.8100	0.7884
Best Fit Top	111.9	96.35	108.3
Best Fit Bottom	-5.927	-0.5933	-4.175

The *N*-ethyl and *N*-isopropyl analogues also showed a small reduction in potency compared to SHF1556 (Figure **4.13**) (Table **4.6**) (Table **4.7**). Replacement of the *N*-methyl group with an *N*-ethyl group to form SHF1580 (pIC50 = 5.72 +/- 0.102) only decreased AM_1 potency to 90% of SHF1556. Introduction of the *N*-isopropyl group shown in SHF1579 (pIC50 = 5.58 +/- 0.075), further reduced potency to 81% of SHF1556, implying that bulkier alkyl groups at this position are detrimental to AM_1 activity.

Table 4.6 – AM_1 pIC50 data for SHF1580 and SHF1579

Compound		
Parameter	**SHF1580**	**SHF1579**
pIC50	5.72	5.58
Std Error	0.102	0.075
R Square	0.8608	0.9199
Best Fit Top	107.5	103.0
Best Fit Bottom	-5.419	-4.370

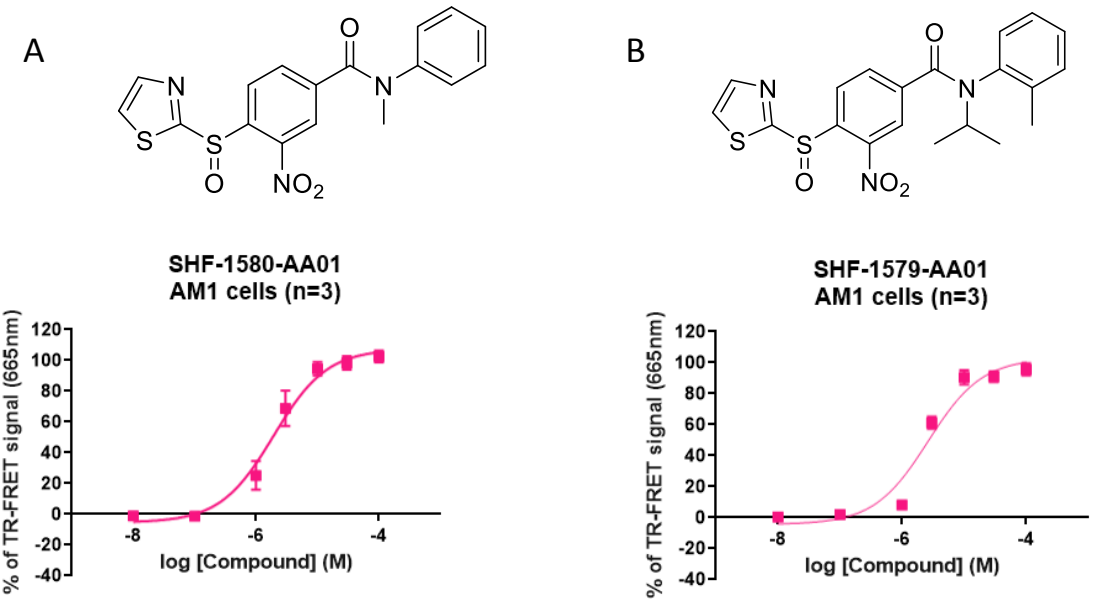

Figure 4.13 – Concentration-response plot of SHF1580 (A) and SHF1579 (B) generated from the cAMP assay and the curve best fit data. Compound was tested on CLR/RAMP2 overexpressing cells which were subsequently stimulated by the EC50 concentration of AM (1 nM). Data was plotted using GraphPad Prism 9.0.2 and the IC50 was determined using a non-linear 3-parameter inhibition curve.

Table 4.7 – AM_1 pIC50 values of SHF1556 analogues along with their standard errors. Each compound was tested alongside SHF1556 as a comparison. P values were used to statistically compare the pIC50 values with SHF1572. A P value of <0.05 was considered statistically significant

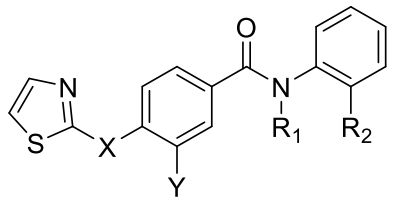

Compound	X	Y	R_1	R_2	pIC50 (+/- Std Error)	% SHF1556	P Value
SHF1555	S	NO_2	Me	Me	n.d	-	-
SHF1558	SO_2	NO_2	Me	Me	4.12 (+/- 0.196)	59	< 0.0001
SHF1568	SO	NO_2	H	Me	5.66 (+/- 0.080)	85	< 0.0001
SHF1574	SO	NH_2	Me	Me	n.d	-	-
SHF1576	SO	NO_2	H	H	4.90 (+/- 0.140)	79	< 0.0001
SHF1579	SO	NO_2	^{i}Pr	Me	5.58 (+/- 0.075)	81	< 0.0001
SHF1580	SO	NO_2	Et	Me	5.72 (+/- 0.102)	90	< 0.0001
SHF1582	SO	NO_2	Me	H	5.71 (+/- 0.132)	88	< 0.0001

4.5 SAR on 5-membered Thiazole Ring

4.5.1 Docking of Thiazole ring analogues

The next group on SHF1556 subject to investigation was the 5-membered heteroaromatic ring on the left hand side of the molecule. A small selection of modifications were made, including replacement with a six-membered benzene and pyridine ring (SHF1560, SHF1569), as well as substitution to a less polar thiophene ring (SHF1577), and more polar thiadiazole ring (SHF1571) (Figure **4.14**).

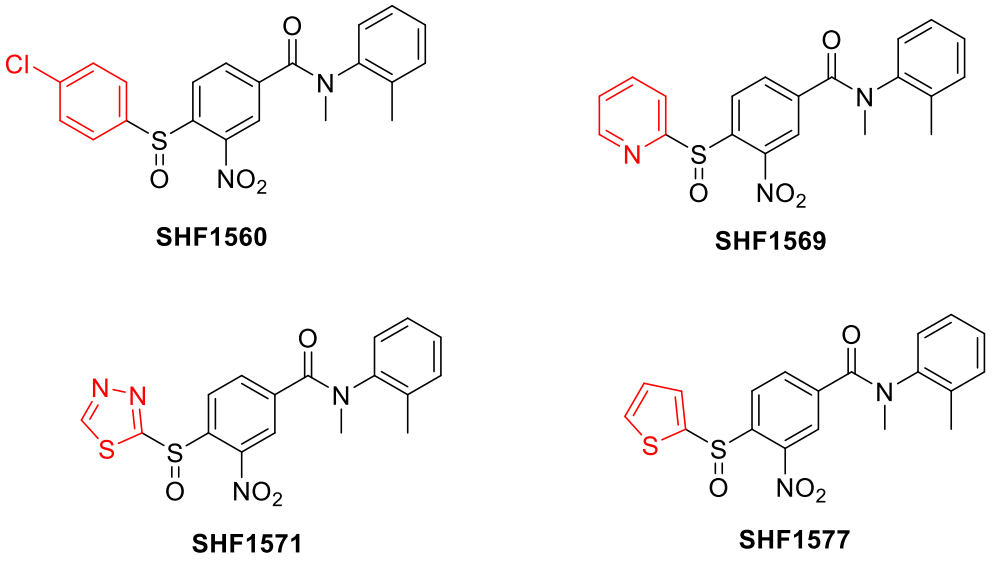

Figure 4.14 Chemical Structures of SHF1556 left hand side analogues SHf1560, SHF1569, SHF1571 and SHF1577. Structural elements that differ from SHF1556 are highlighted in red

Docking of this series of compounds to the AM_1 ECD (PDB: 3AQF) revealed similar poses to those seen in SHF1556 and previous analogues, with all compounds binding across the CLR end of the receptor. The (*R*) enantiomers of these compounds all docked in a similar manner, with the sulfoxide oxygen forming a hydrogen bond to the CLR Thr122 backbone, and the nitro group forming an ionic interaction with CLR Asp70 and a pi-cation interaction with CLR Trp72 (Figure **4.15**). The only exception was SHF1560, in which the (*R*) enantiomer sulfoxide oxygen instead hydrogen bonded to CLR Arg119, and the central phenyl ring stacked against CLR Trp121. The (*S*) enantiomer of SHF1560 formed similar interactions to the (*R*) enantiomer, with both structures aligning well. In SHF1569, only the hydrogen bond between the sulfoxide oxygen and CLR Thr122 was maintained in the (*S*) enantiomer, with no other significant interactions predicted (Figure **4.15)**. The (*S*) enantiomers of both SHF1571 and SHF1577 both only predicted a stacking interaction between the amide phenyl ring and CLR Trp72. As with the previous series of compounds, the docking scores for these compounds imply a slight detrimental effect on AM_1 potency (Table **4.8**), with SHF1569 displaying the highest docking score of this series.

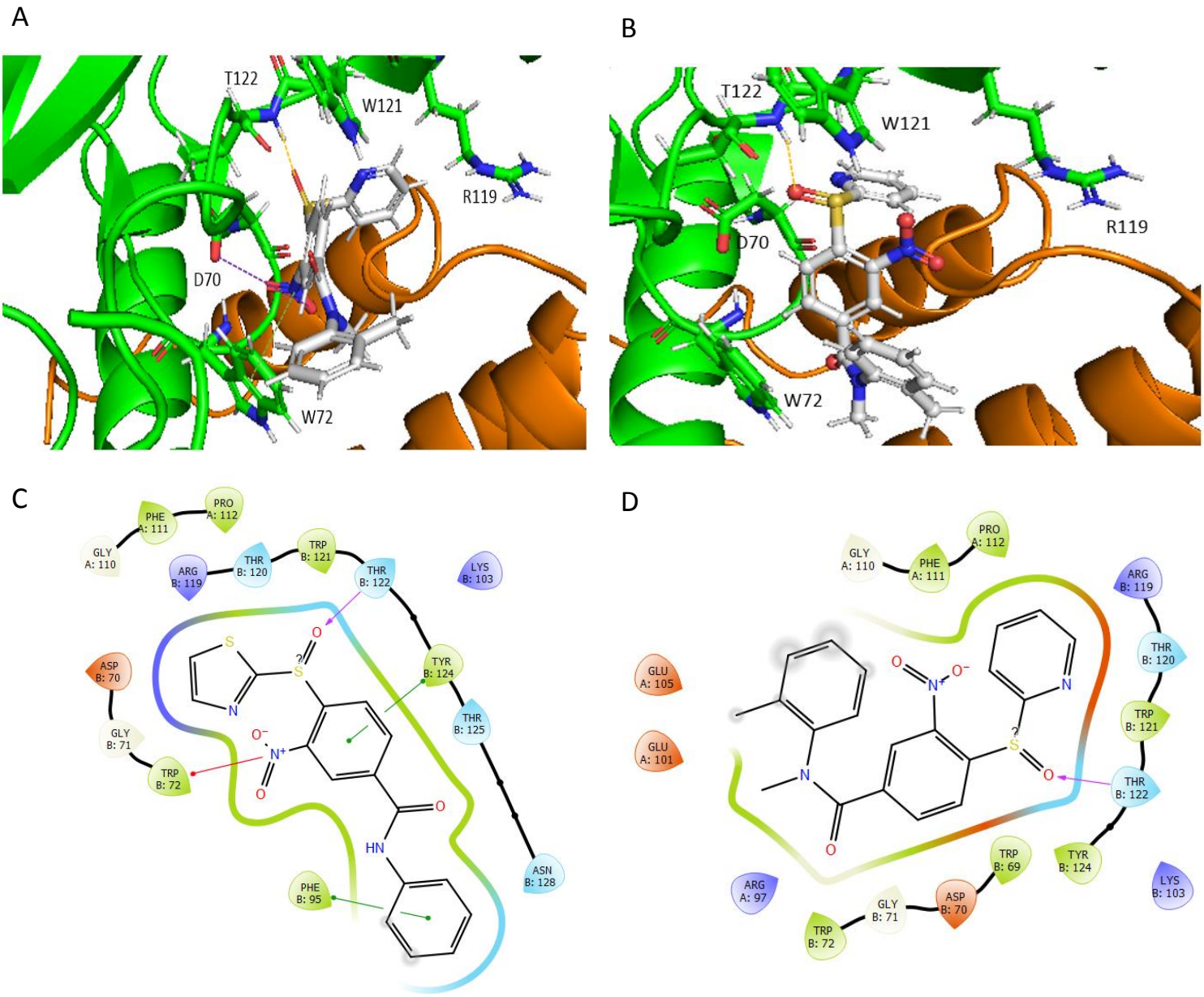

Figure 4.15 - Lowest energy docking pose of SHF1569 (*R*) enantiomer, (A) and (C), and (*S*) enantiomer, (B) and (D), bound to the AM_1 receptor (PDB: 3AQF). (A) and (B) show the 3D image of the compound docked into the AM_1 receptor ECD. The CLR is coloured in green and RAMP2 is coloured in orange. Hydrogen bonds are indicated by yellow dashed lines and ionic interactions are indicated by purple dashed lines. Key residues in the binding pocket are shown and labelled. Docking was carried out using Schrodinger (Maestro 13.2) and the image was generated using PyMol Molecular Graphics System, Version 1.7.4.5- Educational Product, Schrodinger. (C) and (D) show the corresponding 2D ligand interaction diagrams generated by Maestro 13.2. Hydrogen bonds are indicated by purple lines and ionic interactions are indicated by red lines.

Table 4.8 – Docking Scores of thiazole analogues in the AM_1 ECD (PDB: 3AQF). Docking scores generated by Schrodinger (Maestro 13.2).

Compound	Enantiomer	Docking Score (kcal mol^{-1})
SHF1560	(*R*)	-4.1
SHF1560	(*S*)	-4.0
SHF1569	(*R*)	-4.0
SHF1569	(*S*)	-4.4
SHF1571	(*R*)	-3.9
SHF1571	(*S*)	-2.7
SHF1577	(*R*)	-3.1
SHF1577	(*S*)	-3.2

4.5.2 Synthesis of SHF1556 Thiazole Analogues

The synthesis of thiazole analogues was carried out in a manner similar to the synthesis of SHF1556 (Scheme **4.4**). Compound **42** was formed in bulk from the amide coupling of 3-fluoro, 2-nitrobenzoic acid **41** and *N*-methyl-o-toluidine, before a two-step method was carried out by firstly coupling the aromatic thiol to compound **42** by nucleophilic aromatic substitution to form the sulfide, followed by oxidation to the sulfoxide to form the desired compounds (Scheme **4.4**).

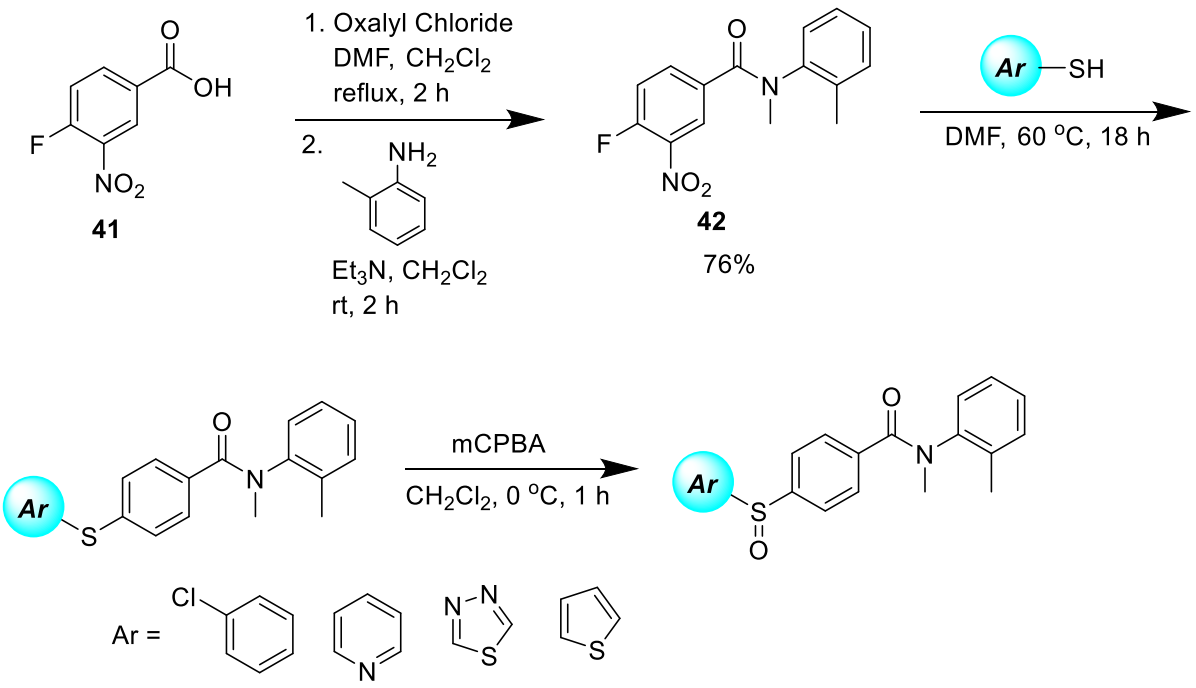

Scheme 4.4 – General synthetic route to SHF1556 left hand side analogues

4.5.3 *In Vitro* Testing of Thiazole Analogues

As with the *N*-methyl and *o*-methyl compounds, the SHF1556 thiazole analogues all saw moderate reductions in AM_1 potency compared to SHF1556 (Figure **4.16**) (Table **4.9**). The thiadiazole analogue, SHF1571, displayed the highest potency of the thiazole analogues (pIC50 = 5.84 +/- 0.114) (Figure **4.16**) (Table **4.9**) (Table **4.11**), exhibiting 94% potency of SHF1556 (P = 0,0099). Replacing the thiazole with a thiophene further decreased AM_1 potency, with SHF1577 (pIC50 = 5.83 +/- 0.205) expressing 85% of SHF1556 potency (P = 0.0045).

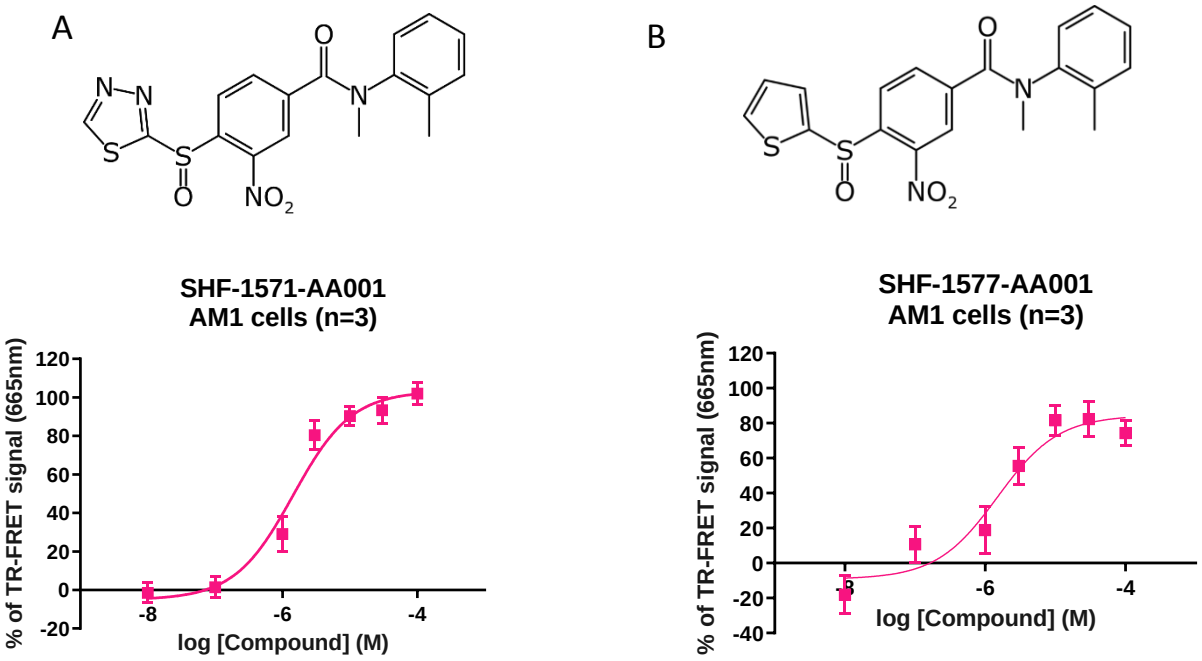

Figure 4.16 – Concentration-response plot of SHF1571 (A), SHF1577 (B) generated from the cAMP assay. Compound was tested on CLR/RAMP2 overexpressing cells which were subsequently stimulated by the EC50 concentration of AM (1 nM). Data was plotted using GraphPad Prism 9.0.2 and the IC50 was determined using a non-linear 3-parameter inhibition curve.

Table 4.9 – AM_1 pIC50 and best fit data for SHF1571 and SHF1577

	Compound	
Parameter	**SHF1571**	**SHF1577**
pIC50	5.84	5.83
Std Error	0.114	0.205
R Square	0.8353	0.6101
Best Fit Top	103.3	84.53
Best Fit Bottom	-5.133	-9.214

The six-membered ring analogues further decreased AM_1 receptor potency in comparison to SHF1556. SHF1569 (pIC50 = 5.34 +/-0.156), in which the thiazole was substituted for a pyridine ring, displayed 80% of SHF1556 potency ($P < 0.0001$), which was lower than the 5-

membered heterocycle analogues (Figure **4.17**) (Table **4.10**) (Table **4.11**). The *p*-chloro benzene analogue, SHF1560 (pIC50 = 4.62 +/- 0.162), saw a more significant drop in AM_1 potency, retaining 66% of the potency of SHF1556 ($P < 0.0001$). These data suggest that there is a slight preference for a 5-membered aromatic ring on the left hand side of the molecule compared to a 6-membered ring.

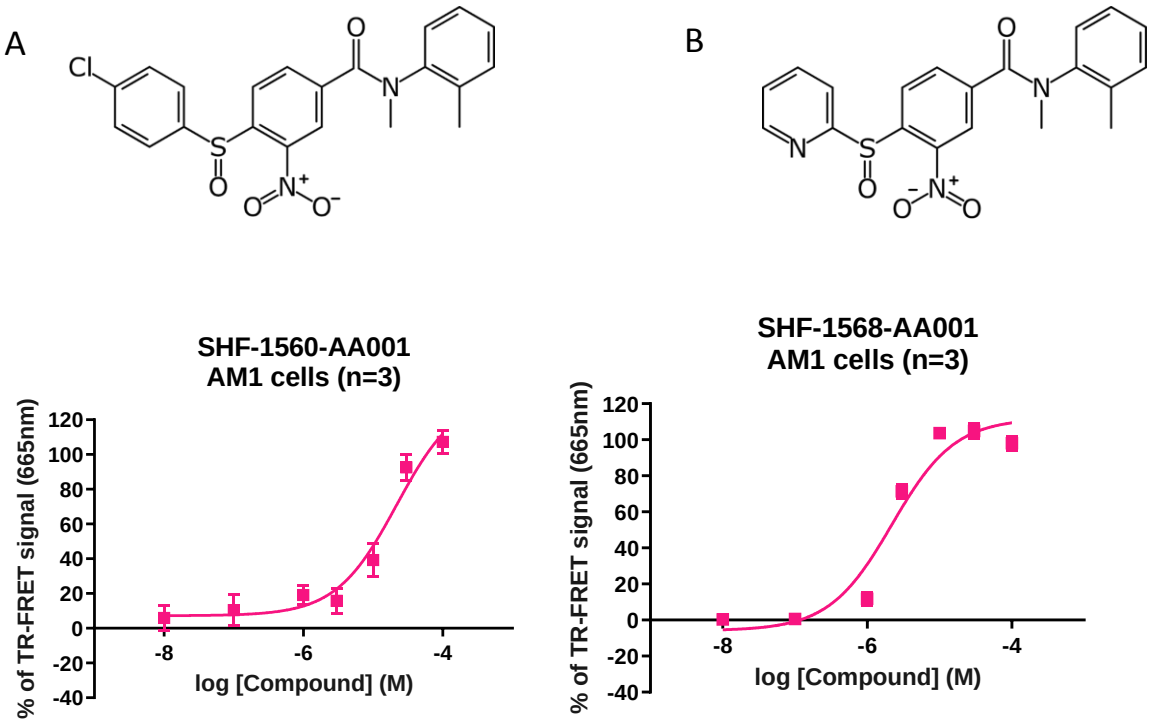

igure 4.17 – Concentration-response plot of SHF1560 (A) and SHF1569 (B) generated from the cAMP assay. Compound was tested on CLR/RAMP2 overexpressing cells which were subsequently stimulated by the EC50 concentration of AM (1 nM). Data was plotted using GraphPad Prism 9.0.2 and the IC50 was determined using a non-linear 3-parameter inhibition curve.

Table 4.10 – AM_1 pIC50 and best fit data for SHF1560 and SHF1569

	Compound	
Parameter	**SHF1560**	**SHF1569**
pIC50	4.62	5.34
Std Error	0.162	0.156
R Square	0.7595	0.7366
Best Fit Top	134.6	97.79
Best Fit Bottom	-4.662	-5.340

Table 4.11 – AM_1 pIC50 data for SHF1556 left hand side analogues and % potency compared to SHF1556. . Each compound was tested alongside SHF1556 as a comparison. P values were used to statistically compare the pIC50 values with SHF1556. A P value of <0.05 was considered statistically significant

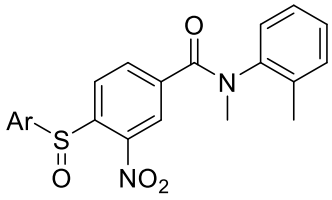

Compound	Ar	pIC50 (+/- Std Error)	% SHF1556	P Value
SHF1560	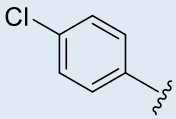	4.62 (+/- 0.162)	66	< 0.0001
SHF1569	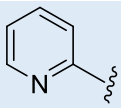	5.34 (+/- 0.156)	80	< 0.0001
SHF1571	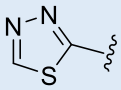	5.84 (+/- 0.114)	94	0.0099
SHF1577	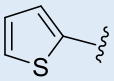	5.83 (+/- 0.205)	85	0.0045

4.6 SAR of Right Hand Side Analogues

4.6.1 Docking of Right Hand Side Analogues

Further SAR on the right hand side of SHF1556 was investigated beyond the *N*-methyl and *o*-methyl analogues discussed earlier. Accordingly, a small number of compounds were synthesised from readily available anilines containing substituents on other positions of the amide phenyl ring. This included SHF1564 and its *N*-methylated analogue, SHF1584 containing an ethoxy group in the *para*-position of the amide, and SHF1566 and its *N*-methylated analogue SHF1583, containing methoxy groups *meta* and *para* to the amide (Figure **4.18**).

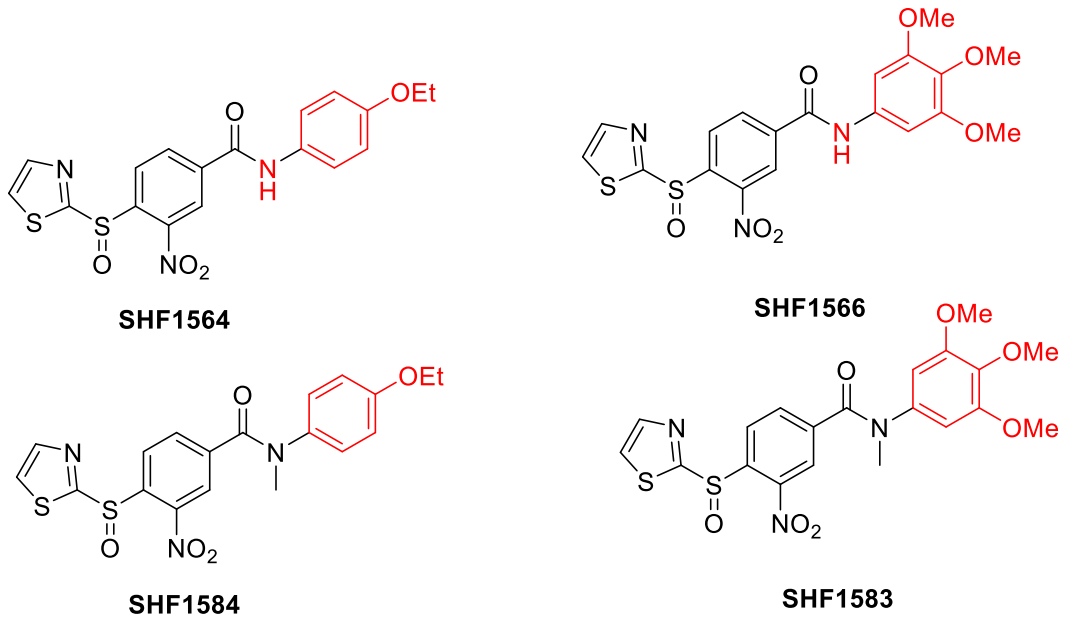

Figure 4.18 – Chemical Structures of SHF1556 Right Hand Side Analogues SHF1564, SHF1566, SHF1584 and SHF1583. Structural elements that differ from SHF1556 are highlighted in red

The docking poses of the right hand side analogues were once again consistent with those seen for previous SHF1556 analogues, docking along the CLR. The (*R*) enantiomers all generated consistent docks that were analogous to each other, with the sulfoxide and nitro groups making key interactions to CLR Thr122 and Asp70 respectively (Figure **4.19**). The interactions predicted for the (*S*) enantiomers in this series were also consistent, with the hydrogen bond between the sulfoxide oxygen and Thr122 also present, whilst the thiazole ring was predicted to stack against Trp72. Docking scores in this series are significantly lower than SHF1556 or the previous series', implying these changes will see a greater drop in AM_1 potency (Table **4.12**).

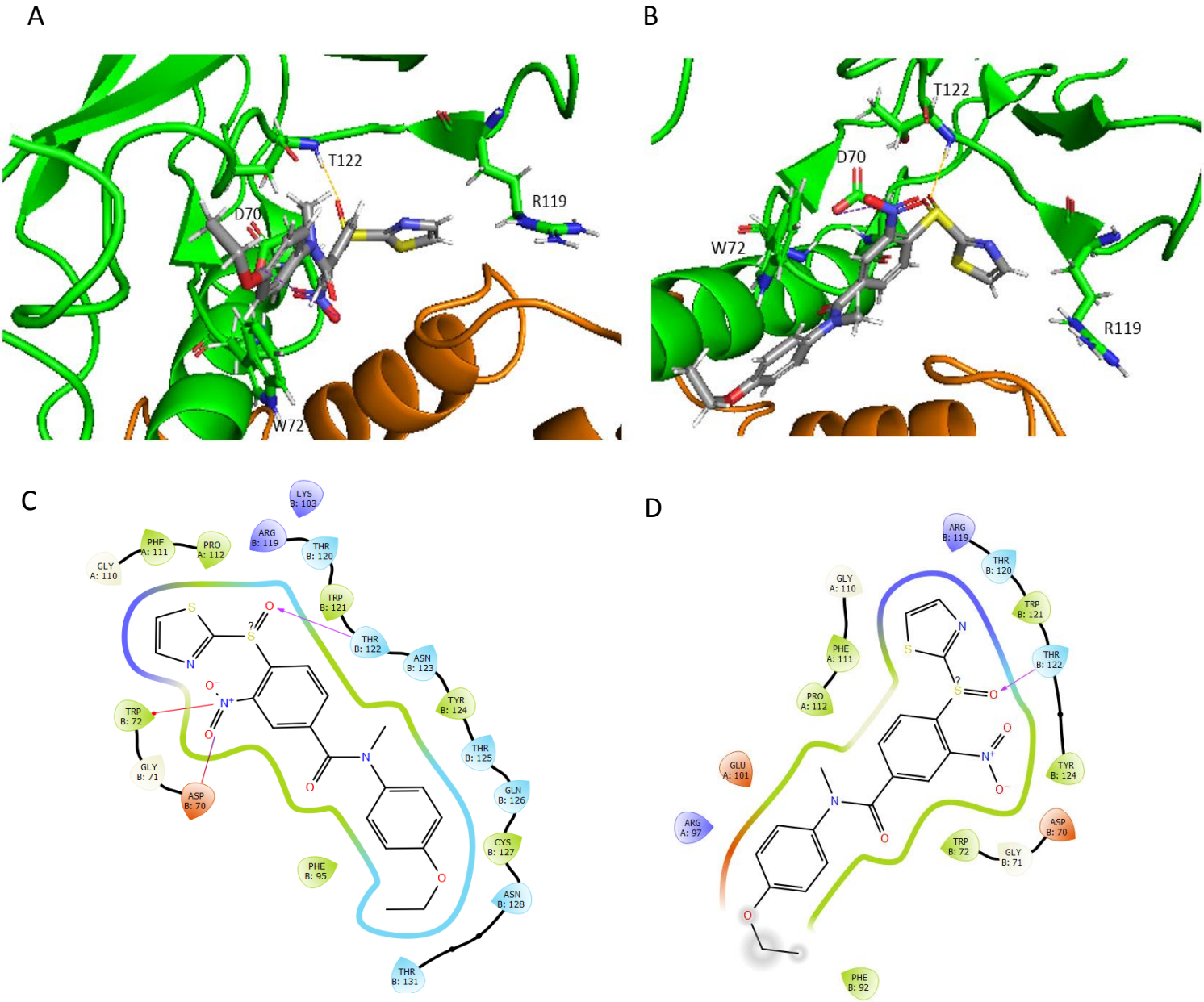

Figure 4.19 - Lowest energy docking pose of SHF1584 (*R*) enantiomer, (A) and (C), and (*S*) enantiomer, (B) and (D), bound to the AM_1 receptor (PDB: 3AQF). (A) and (B) show the 3D image of the compound docked into the AM_1 receptor ECD. The CLR is coloured in green and RAMP2 is coloured in orange. Hydrogen bonds are indicated by yellow dashed lines and ionic interactions are indicated by purple dashed lines. Key residues in the binding pocket are shown and labelled. Docking was carried out using Schrodinger (Maestro 13.2) and the image was generated using PyMol Molecular Graphics System, Version 1.7.4.5- Educational Product, Schrodinger. (C) and (D) show the corresponding 2D ligand interaction diagrams generated by Maestro 13.2. Hydrogen bonds are indicated by purple lines and ionic interactions are indicated by red lines.

Table 4.12 – Docking Scores of right hand side analogues of SHF1556 in the AM_1 ECD (PDB: 3AQF). Docking scores generated by Schrodinger (Maestro 13.2).

Compound	Enantiomer	Docking Score (kcal mol^{-1})
SHF1564	(*R*)	-4.5
SHF1564	(*S*)	-2.9
SHF1566	(*R*)	-2.6
SHF1566	(*S*)	-0.2
SHF1584	(*R*)	-3.0
SHF1584	(*S*)	-3.3
SHF1583	(*R*)	-2.3
SHF1583	(*S*)	-3.2

4.6.2 Synthesis of Right Hand Side Analogues

Right hand side analogues of SHF1556 were synthesised as shown in scheme **4.5**. Compound **49** was firstly formed in bulk by coupling thiazole **45** with 3-fluoro 2-nitrobenzonitrile **48** by nucleophilic aromatic substitution to form compound **49,** before acid catalysed hydrolysis of the nitrile to the carboxylic acid. The right hand side analogues were subsequently formed in a two-step sequence via amide coupling of compound **51** and the corresponding aniline using oxalyl chloride, followed by oxidation of the sulfide to the sulfoxide with mCPBA. SHF1564 and SHF1566 were formed using 4-ethoxyaniline and 3,4,5-trimethoxy aniline respectively, whilst for the corresponding *N*-methylated analogues SHF1584 and SHF1583, the corresponding anilines were firstly *N*-methylated using a reductive amination procedure with formaldehyde before undergoing the two step synthetic route to the final compounds.

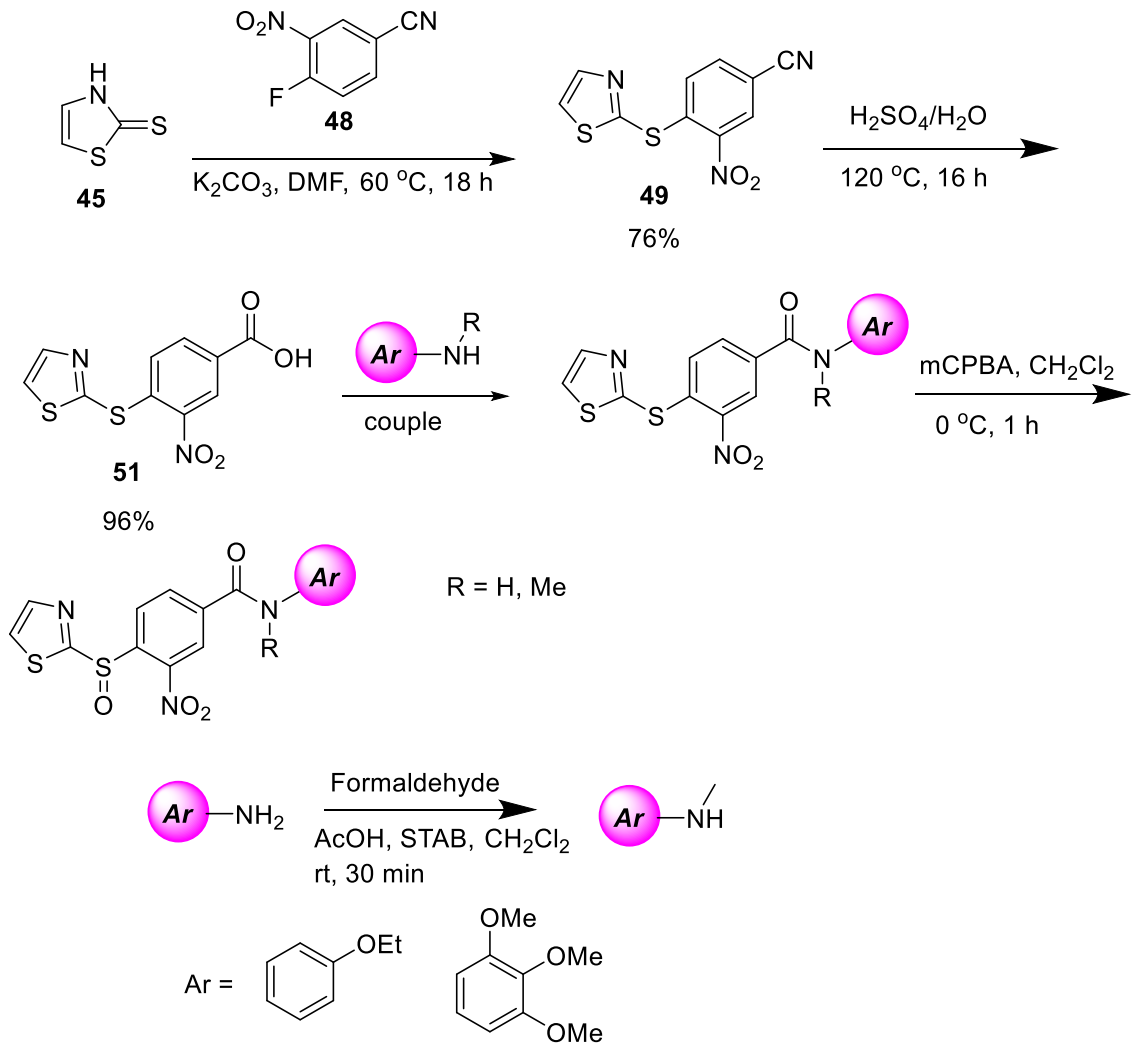

Scheme 4.5 – General synthetic route to SHF1556 right hand side analogues

4.6.3 *In Vitro* Testing of Right Hand Side Analogues

SHF1564 and SHF1566, analogues that do not contain the *N*-methyl group, saw poor retention of SHF1556 AM_1 potency (Figure **4.20**) (Table **4.13**) (Table **4.14**). Specifically, the *para*-ethoxy analogue, SHF1564, exhibited poor AM_1 potency, whilst the 3,4,5-trimethoxy analogue displayed only moderate AM_1 potency (pIC50 = 4.94 +/- 0.101), with this compound displaying 74% of SHF1556 activity ($P < 0.0001$).

As expected based on previous results, addition of the *N*-methyl groups to these analogues had the effect of improving activity (Figure **4.20**) (Table **4.13**) (Table **4.14**). SHF1583 (pIC50 =

5.06 +/- 0.123) displayed marginally improved potency over SHF1556. In contrast, the EtO series SHF1584 (pIC50 = 5.83 +/-0.097) showed a significant increase in activity as compared to its analogue SHF1564, but despite this the potency of both SHF1583 and SHF1584 was still lower than SHF1556, with the compounds displaying 78% ($P < 0.0001$) and 91% ($P < 0.0001$) of SHF1556 AM_1 potency respectively. This may be expected due to the absence of the *ortho*-methyl group on each of these compounds, which from previous SAR data has shown to moderately decrease AM_1 potency.

Table 4.13 – AM_1 pIC50 and best fit data for SHF1564, SHF1584, SHF1566 and SHF1583

	Compound			
Parameter	**SHF1564**	**SHF1584**	**SHF1566**	**SHF1583**
pIC50	-	5.83	4.94	5.06
Std Error	-	0.097	0.101	0.123
R Square	-	0.8745	0.8800	0.8289
Best Fit Top	-	99.11	108.7	104.5
Best Fit Bottom	-	-6.946	-2.402	-5.763

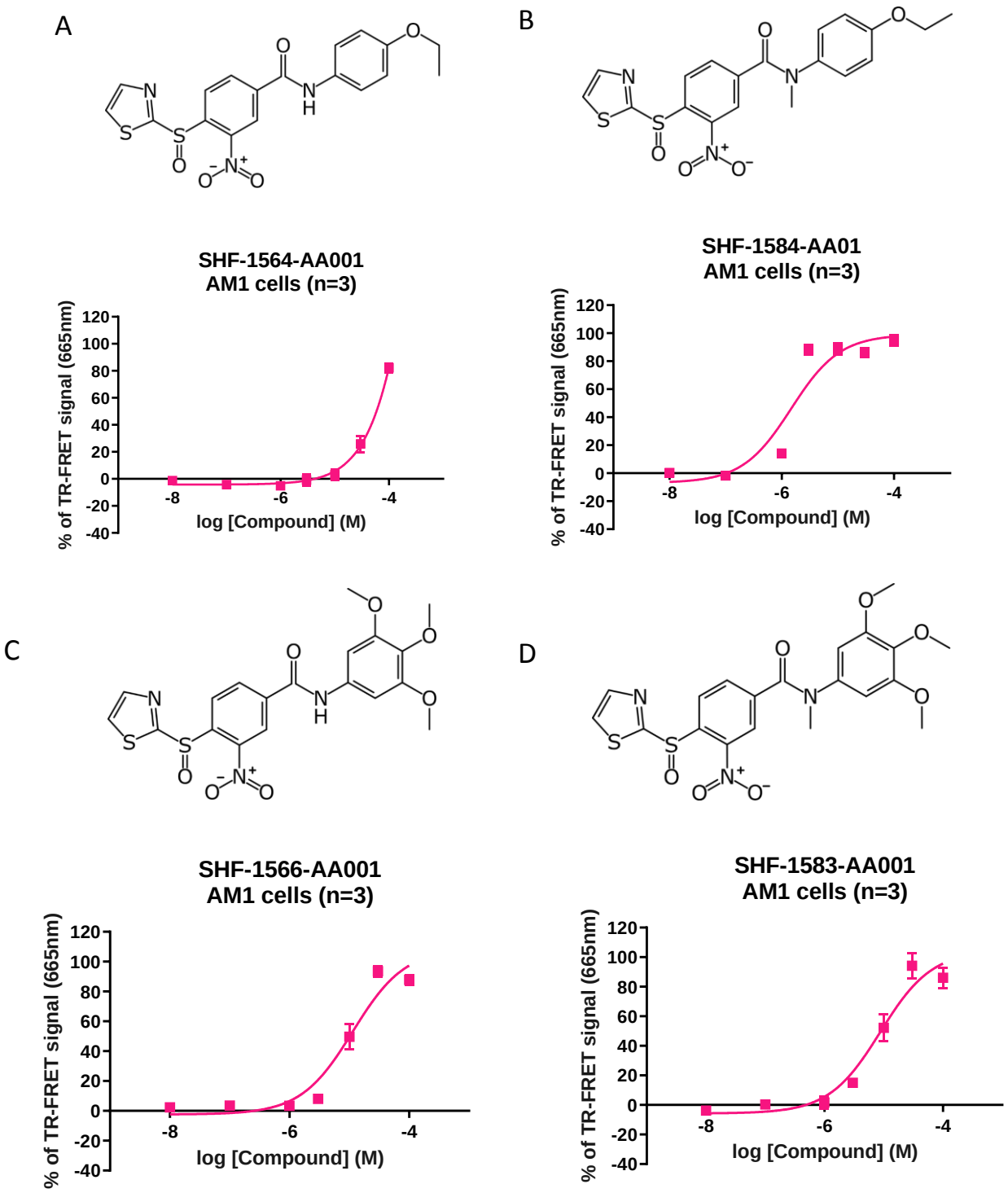

Figure 4.20 – Concentration-response plot of SHF1564 (A), SHF1584 (B), SHF1566 (C) and SHF1583 (D) generated from the cAMP assay. Compound was tested on CLR/RAMP2 overexpressing cells which were subsequently stimulated by the EC50 concentration of AM (1 nM). Data was plotted using GraphPad Prism 9.0.2 and the IC50 was determined using a non-linear 3-parameter inhibition curve.

Table 4.14 – AM_1 pIC50 values for SHF1556 right hand side analogues and % potency compared to SHF1556

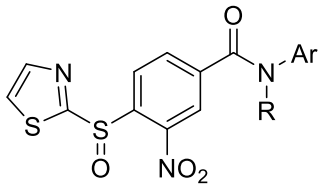

Compound	R	Ar	pIC50 (+/- Std Error)	% SHF1556	P Value
SHF1564	H	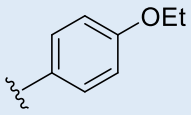	n.d	48	-
SHF1566	H	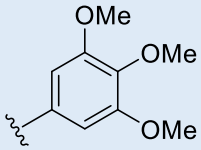	4.94 (+/- 0.101)	74	< 0.0001
SHF1583	Me	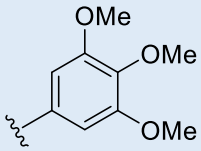	5.06 (+/- 0.123)	78	< 0.0001
SHF1584	Me	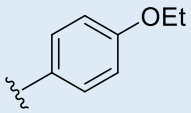	5.83 (+/- 0.097)	91	< 0.0001

4.7 CGRP and AM_2 Counter Screening of SHF1556 Analogues

4.7.1 Counter Screening of Sulfide, Sulfone and *N*-Methyl Analogues

Analogues of SHF1556, including the sulfide, sulfone, reduced nitro, *N*-methyl and *o*-methyl groups were screened against CGRP and AM_2 overexpressing cells in order to determine the selectivity of these compounds for antagonism at AM_1 over these related receptor sub-types (Table **4.15**). Interestingly, despite not exhibiting any potency on AM_1, SHF1555 displayed good potency at CGRP (pIC50 = 5.65 +/- 0.166) and AM_2 (pIC50 = 6.44 +/- 0.293) (Figure

4.21) (Table **4.16**). This data suggests that whilst the sulfoxide is crucial for AM_1 potency, this group is much less important for activity on CGRP and AM_2.

The pIC50 values for CGRP and AM_2 of the other compounds in this series appear to follow a similar trend to that of AM_1. Oxidation of the sulfoxide to the sulfone in SHF1558 significantly reduces potency on AM_2 (pIC50 = 4.43 +/- 0.398) and CGRP (pIC50 not determined) compared to AM_1, whilst reduction of the nitro group to the aniline in SHF1574 eliminates potency on these receptors, as with AM_1. pIC50 values across all three receptors for the other compounds in the series are all very similar, with data suggesting there is a preference for the AM_2 receptor over AM_1 in compounds SHF1568 (pIC50 = 6.27 +/- 0.257) (P = 0.0025), SHF1582 (pIC50 = 6.18 +/- 0.220) (P = 0.0160) and SHF1579 (pIC50 = 6.36 +/- 0.209), although not statistically significant in this case (P = 0.2939), whilst SHF1580 is modestly more selective for CGRP (P = 0.0002) .

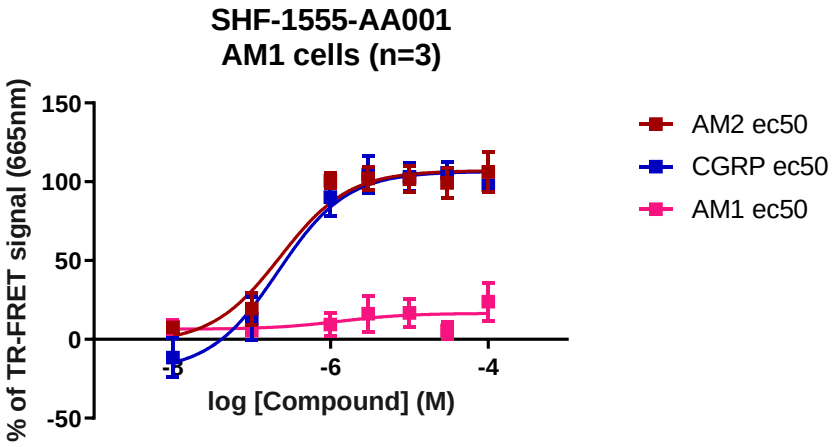

Figure 4.21 – Concentration-response plots of SHF1555 on AM_1, AM_2 and CGRP generated from the cAMP assay. Compounds were tested on CLR/RAMP1, which were stimulated by the EC50 concentration of CGRP (0.8 nM), CLR/RAMP2 cells and CLR/RAMP3 overexpressing cells which were subsequently stimulated by the EC50 concentration of AM (1 nM and 2 nM respectively. Data was plotted using GraphPad Prism 9.0.2 and the IC50 was determined using a non-linear 3-parameter inhibition curve. AM_1 curve is displayed in pink, CGRP curve is displayed in blue and the AM_2 curve is displayed in brown.

Table 4.15 – AM_1, AM_2 and CGRP pIC50 values for SHF1556 analogues

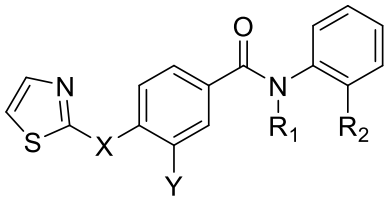

Compound	X	Y	R1	R2	pIC50 (AM1) (+/- Std Error)	pIC50 (AM_2) (+/- Std Error)	pIC50 (CGRP) (+/- Std Error)
SHF1555	S	NO_2	Me	Me	n.d	6.44 (+/= 0.293)	5.65 (+/- 0.166
SHF1556	S=O	NO_2	Me	Me	7.03 (+/-	6.77	6.39
SHF1558	SO_2	NO_2	Me	Me	4.12 (+/- 0.196)	4.43 (+/- 0.398)	n.d
SHF1574	S=O	NH_2	Me	Me	n.d	n.d	n.d
SHF1568	S=O	NO_2	H	Me	5.66 (+/- 0.080)	6.27 (+/- 0.257)	5.99 (+/- 0.292)
SHF1582	S=O	NO_2	Me	H	5.71 (+/- 0.132)	6.18 (+/- 0.220)	5.65 (+/- 0.242)
SHF1576	S=O	NO_2	H	H	4.90 (+/- 0.140)	n.d	n.d
SHF1580	S=O	NO_2	Et	Me	5.72 (+/- 102)	5.14 (+/- 0.217	6.36 (+/- 0.156)
SHF1579	S=O	NO_2	iPr	Me	5.86 (+/- 0.075)	6.36 (+/- 0.209)	5.65 (+/- 0.182)

Table 4.16 – AM_1, AM_2 and CGRP pIC50 and best fit data for SHF1555

	Receptor		
Parameter	**AM_1**	**AM_2**	**CGRP**
pIC50	n.d	6.64	6.66
Std Error	-	0.197	0.192
R Square	-	0.8494	0.8542
Best Fit Top	-	107.1	106.5
Best Fit Bottom	-	-2.452	-20.38

4.7.2 Counter Screening of Left Hand Side Thiazole Analogues

The selectivity of the left hand side analogues generated in this study for the AM_1 receptor over related receptor subtypes was also determined by counter screening against AM_2 and CGRP (Table **4.17**). The sulfide analogue, SHF1557 containing a *para*-chlorobenzene ring, showed no activity towards CGRP and AM_2 as well as AM_1. This was in stark contrast to SHF1555, which displayed potency at CGRP or AM_2 despite being completely inactive at AM_1. The other compounds in this series, all of which contained sulfoxides, all exhibited similar activity amongst all three receptors. SHF1560, also containing a *para*-chlorobenzene ring, showed moderate, sub 100 µM potency across the receptors whilst displaying modest selectivity for AM_1. SHF1569, SHF1571 and SHF1577, containing pyridine, thiadiazole and thiophene rings, respectively, displayed potency across all three receptors around the micromolar and sub-micromolar range. All three compounds showed greater, albeit modest, selectivity towards AM_2 and/or CGRP, with SHF1569 showing selectivity towards CGRP (pIC50 = 6.33 +/- 0.174) ($P < 0.0001$), and SHF1571 exhibiting selectivity towards AM_2 (pIC50 = 6.77 +/- 0.209) ($P = 0.0001$). SHF1577 was somewhat selective for AM_2 over AM_1 (pIC50 = 6.00 +/- 0.205), although there was no statistical significance in this observation ($P = 0.4950$).

With respect to the thiazole rings, increasing the polarity of the ring by adding a nitrogen atom appeared to increase potency at both CGRP and AM_2. SHF1571, containing a thiadiazole ring, is more polar than SHF1556 with a thiazole ring, which is more polar than SHF1577 with a thiophene ring. For AM_2 cells, the order of potency increases from the thiophene (pIC50 = 6.00 +/- 0.183), to the thiazole and thiadiazole (pIC50 = 6.72 +/- 0.242),

(6.77 +/- 0.209). For CGRP cells, a similar trend is observed as potency increases from the thiophene (pIC50 = 5.75 +/- 0.174) to the thiazole (pIC50 = 6.39 +/- 0.179) to the thiadiazole (pIC50 = 6.76 +/- 0.295). These data imply that adding more nitrogens to the 5-membered ring and therefore increasing the polarity of the compound, can improve potency at both AM_2 and CGRP.

Table 4.17 – AM_1, AM_2 and CGRP pIC50 values for SHF1556 left hand side analogues

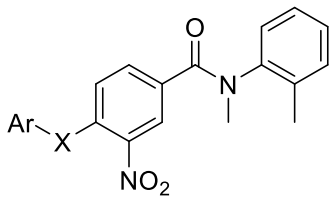

Compound	Ar	X	pIC50 (AM_1) (+/- Std Error)	pIC50 (AM_2) (+/- Std Error)	pIC50 (CGRP) (+/- Std Error)
SHF1557	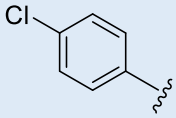	S	n.d	n.d	n.d
SHF1560	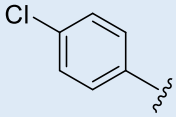	SO	4.62 (+/- 0.162)	4.45 (+/- 0.485)	4.11 (+/- 0.193)
SHF1569	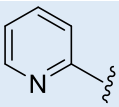	SO	5.34 (+/- 0.156)	5.99 (+/- 0.283)	6.33 (+/- 0.174)
SHF1571	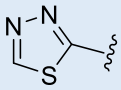	SO	5.84 (+/- 0.114)	6.77 (+/- 0.209)	6.76 (+/- 0.295)
SHF1577	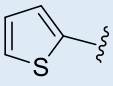	SO	5.83 (+/- 0.205)	6.00 (+/- 0.183)	5.75 (+/- 0.174)

4.7.3 Counter Screening of Right Hand Side Analogues

Right hand side analogues were also counter screened against AM_2 and CGRP (Table **4.18**). As with the left hand side analogues, all sulfides tested (SHF1563, SHF1565) were inactive at all three receptors, again contrasting with SHF1555 which is potent at both AM_2 and CGRP.

The *N*-methylated analogues were also generally more potent than the analogues missing the methyl group on the amide nitrogen. The *para*-ethoxy analogues showed comparable potencies at all three receptors, with SHF1564 exhibiting very modest potencies around the 100 µM range, whist it's *N*-methylated analogue SHF1584 showed potencies of around 1 µM across all three receptors. Both trimethoxy analogues, SHF1566 and SHF1583, afforded significantly greater selectivity towards CGRP and AM_2 over AM_1. pIC50 values for SHF1566 were 6.07 +/- 0.337 and 5.51 +/- 0.113 for AM_2 and CGRP respectively, displaying 13-fold ($P < 0.0001$) and 4-fold ($P < 0.0001$) selectivity to the corresponding receptor over AM_1 (pIC50 = 4.94 +/-0.101). *N*-Methyl analogue SHF1583 further demonstrated strong AM_2 and CGRP selectivity over AM_1. pIC50 values were 6.19 +/- 0.298 and 6.28 +/- 0.148 for AM_2 and CGRP respectively, showing 14-fold ($P < 0.0001$) and 16-fold ($P < 0.0001$) selectivity for the corresponding receptors over AM_1 (pIC50 = 5.06).

Table 4.18 – AM_1, AM_2 and CGRP pIC50 values for SHF1556 right hand side analogues

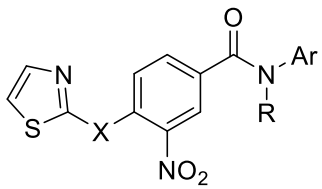

Compound	X	R	Ar	pIC50 (AM_1) (+/- Std Error)	pIC50 (AM_2) (+/- Std Error)	pIC50 (CGRP) (+/- Std Error)
SHF1563	S	H	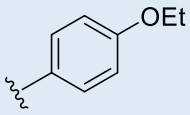	n.d	n.d	n.d
SHF1564	SO	H	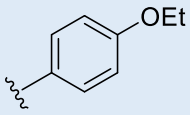	n.d	4.58 (+/- 0.375)	4.48 (+/- 0.259)
SHF1584	SO	Me	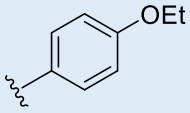	5.83 (+/- 0.097)	5.99 (=/- 0.181)	6.17 (+/- 0.111)
SHF1565	S	H	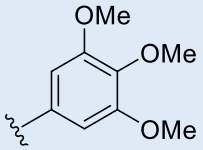	n.d	n.d	n.d
SHF1566	SO	H	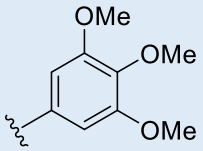	4.94 (+/- 0.101)	6.07 (+/- 0.337)	5.51 (+/- 0.113)
SHF1583	SO	Me	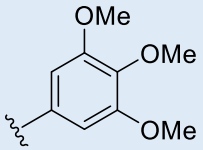	5.06 (+/- 0.123)	6.19 (+/- 0.298)	6.28 (+/- 0.148)

4.8 Docking of Selected Compounds at CGRP and AM_2

In order to predict how the SHF1556 analogues might be binding to the CGRP and AM_2 receptors, molecular docking studies were carried out. Docking of compounds to the CGRP receptor ECD was carried out using Schrodinger (Maestro 13.2), using the crystal structure of Telcagepant bound to CGRP (PDB: 3N7R). The docking poses of SHF1556 analogues into

CGRP showed binding modes that were more similar to the CGRP-bound crystal structures of Olcegepant and Telcagepant, with the compounds extending from the CLR end of the receptor out towards the RAMP1 protein. The end of the molecule which contacted the CLR or RAMP1 protein was varied, with the docking poses exploring the effectiveness of the ability of either the thiazole or the amide phenyl to point towards RAMP1.

The docking pose of SHF1555 showed the thiazole ring pointing towards the CLR, with this group forming a stacking interaction with CLR Trp72 (Figure **4.22**). Meanwhile the amide phenyl ring on the right hand side of the compound pointed towards RAMP1, forming a pi-cation interaction with CLR Arg38 whilst sitting in close proximity to RAMP1 Trp74 and Trp84. The formation of these interactions may provide an explanation as to how the sulfide can still be well tolerated in CGRP. However SHF1558, the corresponding sulfone, adopted exactly the same pose and formed identical interactions to SHF1555 despite showing significantly reduced potency at CGRP. This suggests that if this were the case, the sulfone oxygen atoms could be forming unfavourable interactions when placed at this site.

The docking pose of SHF1574 in CGRP was more like that observed with the docking of SHF1556 analogues in AM_1 (Figure **4.23**). The hydrogen bond between the sulfoxide oxygen and the CLR Thr122 backbone was again present in the (*R*) enantiomer, as was a hydrogen bond between the aniline and CLR Asp70 whilst the central phenyl ring stacked against CLR Arg119. In the docking pose of the (*S*) enantiomer, only interactions of the central phenyl ring with Trp72 and Gly71 were detected. Given the extensive interactions predicted in the docking poses of SHF1574, it is therefore somewhat surprising that this compound does not exhibit any CGRP potency in the cAMP assay.

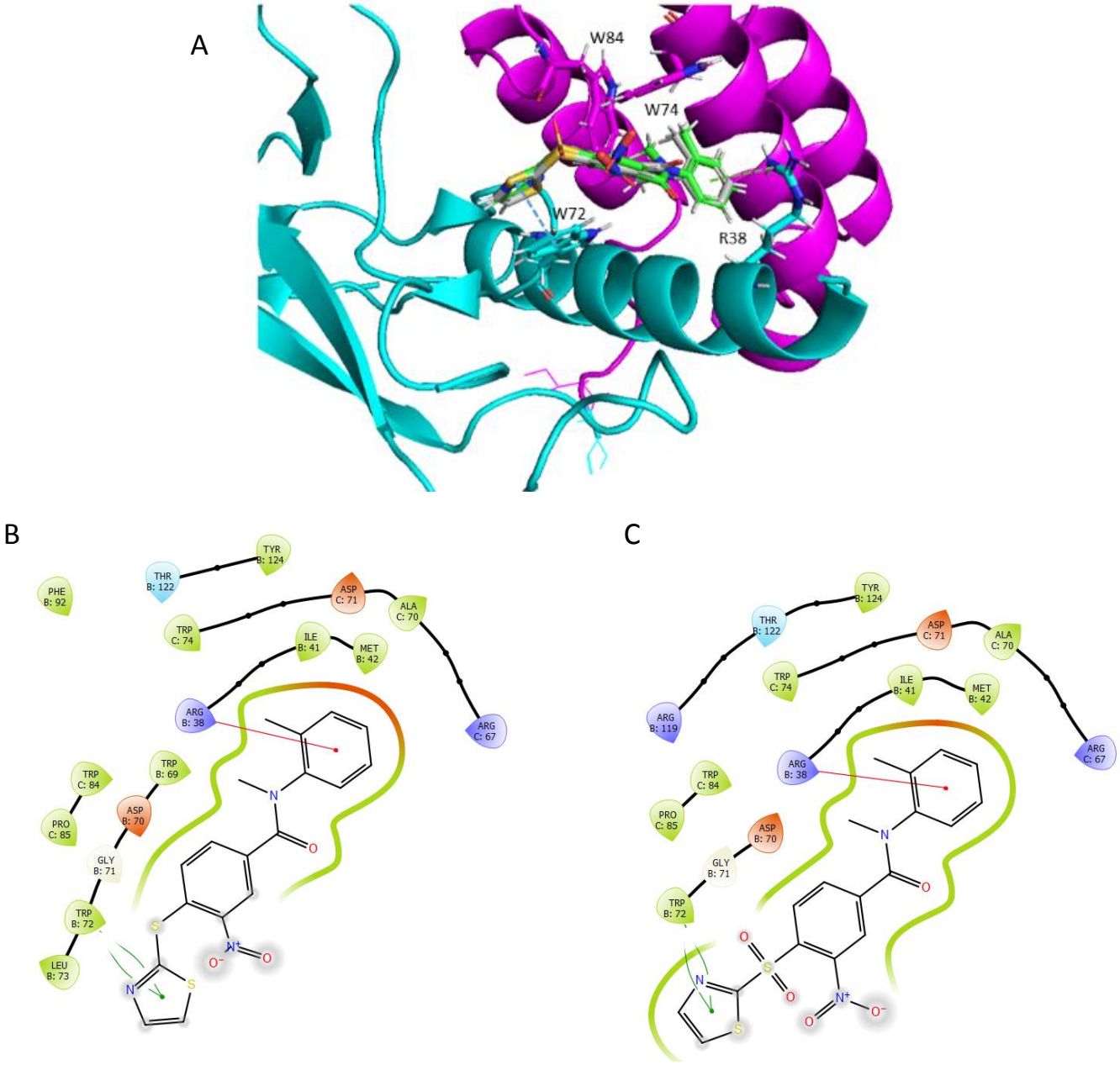

Figure 4.22 – Lowest energy docking pose of SHF1555 and SHF1558 bound to the CGRP receptor (PDB: 3N7R). (A) SHF1555 is coloured in green and SHF1558 is coloured in grey. CLR is coloured in cyan and RAMP1 is coloured in magenta. Pi stacking interactions are indicated by blue dashed lines, and pi cation interactions are indicated by green dashed lines. Key residues in the binding pocket are shown and labelled. Docking was carried out using Schrodinger (Maestro 13.2) and the image was generated using PyMol Molecular Graphics System, Version 1.7.4.5- Educational Product, Schrodinger. (B) and (C) show the corresponding 2D ligand interaction diagrams of SHF1555 and SHF1558 respectively, generated by Maestro 13.2. Hydrogen bonds are indicated by purple lines and hydrophobic interactions are indicated by green lines.

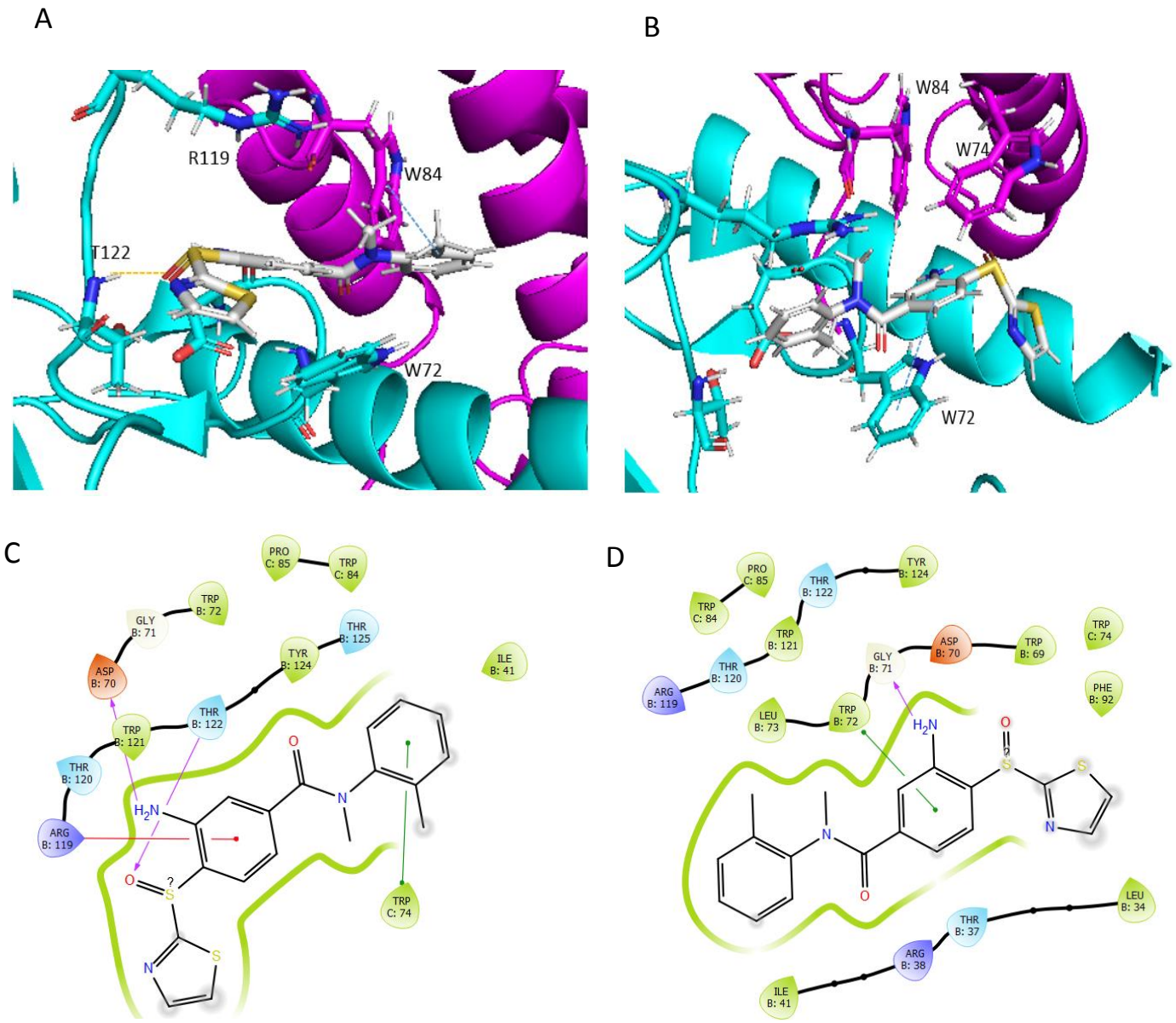

Figure 4.23 - Lowest energy docking pose of SHF1574 (*R*) enantiomer, (A) and (C), and (*S*) enantiomer, (B) and (D), bound to the CGRP receptor (PDB: 3N7R). (A) and (B) show the 3D image of the compound docked into the AM_1 receptor ECD. The CLR is coloured in cyan and RAMP1 is coloured in magenta. Hydrogen bonds are indicated by yellow dashed lines and pi-pi interactions are indicated by blue dashed lines. Key residues in the binding pocket are shown and labelled. Docking was carried out using Schrodinger (Maestro 13.2) and the image was generated using PyMol Molecular Graphics System, Version 1.7.4.5- Educational Product, Schrodinger. (C) and (D) show the corresponding 2D ligand interaction diagrams generated by Maestro 13.2. Hydrogen bonds are indicated by purple lines, ionic interactions are indicated by red lines adn hydrophobic interactions are indicated by green lines.

The other SHF1556 analogues displayed docking poses in CGRP similar to SHF1555). The first pose predicts the thiazole ring or equivalent would point towards RAMP1 and form stacking interactions with Trp74 and/or Trp84, whilst also forming a pi-cation interaction with CLR Arg38 (Figure **4.24**). In some cases the nitro group would also form a pi-cation interaction with CLR Trp74. The amide phenyl group in this pose, meanwhile, would point towards the CLR, often stacking with CLR Trp72, Arg119 and Tyr124. The alternative pose is the reverse to the first pose, and predicts the amide phenyl to point towards RAMP1 and interact with Trp74 or CLR Arg38, with the thiazole ring often stacking against CLR Trp72 (Figure **4.25**). In almost all cases, the sulfoxide oxygen points out into solvent and forms no significant interactions with the receptor.

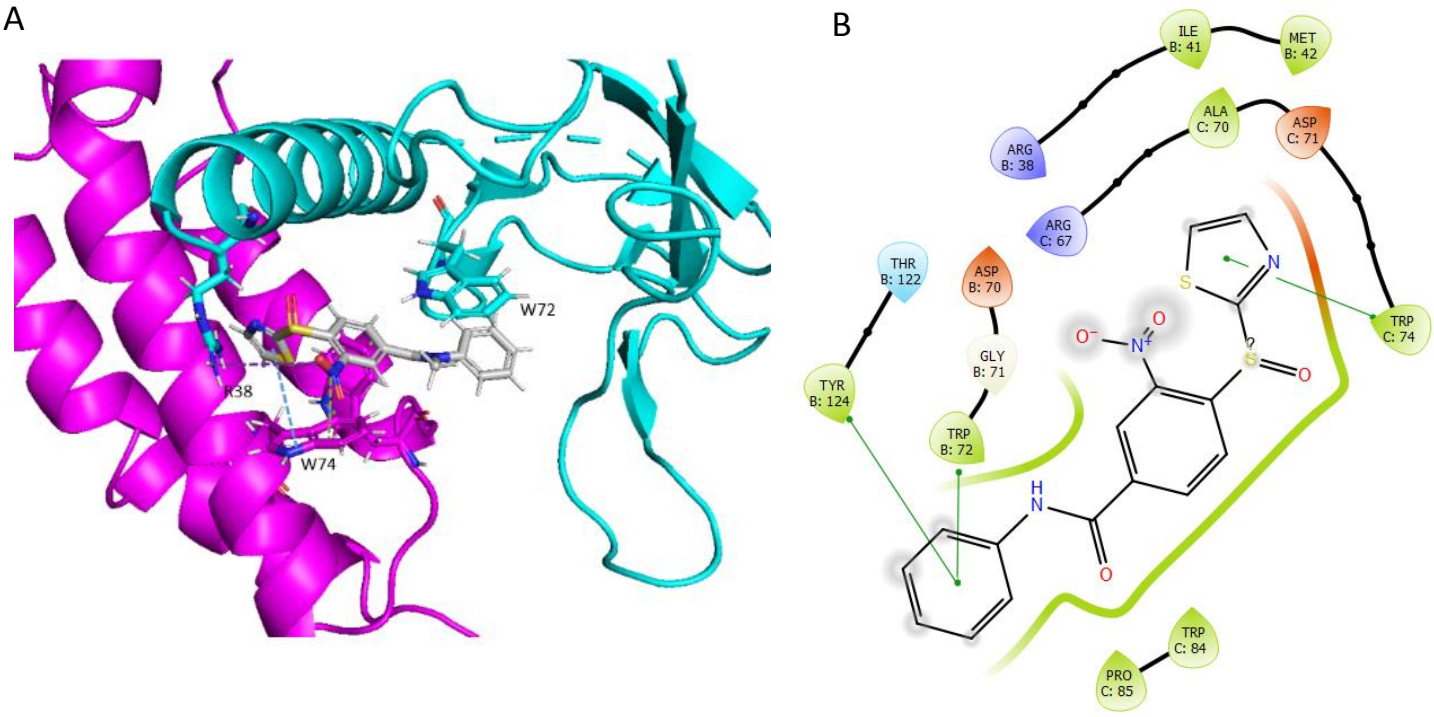

Figure 4.24 – Lowest energy docking pose of the (R) enantiomer of SHF1576 bound to the CGRP receptor (PDB: 3N7R). (A) 3D image of SHF1576 docked into the CGRP receptor ECD. The CLR is coloured in cyan and RAMP1 is coloured in magenta. Pi-Pi interactions are indicated by blue lines. Key residues in the binding pocket are shown and labelled. Docking was carried out using Schrodinger (Maestro 13.2) and the image was generated using PyMol Molecular Graphics System, Version 1.7.4.5- Educational Product, Schrodinger. (B) 2D ligand interaction diagram generated from Maestro 13.2. Hydrophobic interactions are indicated by green lines.

A

B

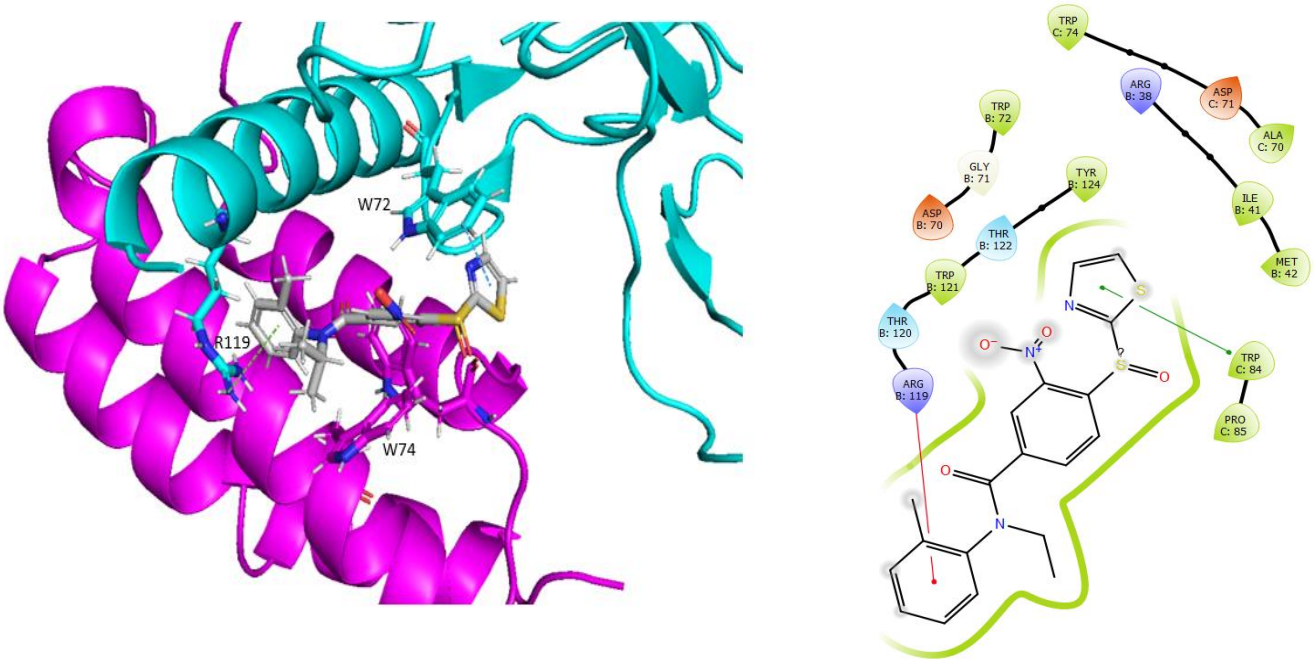

Figure 4.25 – Lowest energy docking pose of the (*R*) enantiomer of SHF1580 bound to the CGRP receptor (PDB: 3N7R). (A) 3D image of SHF1576 docked into the CGRP receptor ECD. The CLR is coloured in green and RAMP2 is coloured in orange. Pi-Pi interactions are indicated by blue lines and pi-cation interactions are indicated by green lines. Key residues in the binding pocket are shown and labelled. Docking was carried out using Schrodinger (Maestro 13.2) and the image was generated using PyMol Molecular Graphics System, Version 1.7.4.5- Educational Product, Schrodinger. (B) 2D ligand interaction diagram generated from Maestro 13.2. Pi-cation interactions are indicated by red lines and hydrophobic interactions are indicated by green lines.

4.9 Docking of Selected SHF1556 Analogues to AM_2

As with SHF1556, docking of compounds in this series was carried out using the cryo-EM structure of the full length AM_2 receptor, with the docking grid only created around the ECD. As with CGRP, the docking poses of all compounds in the AM_2 ECD predicted the compounds to sit outward from the CLR, extending towards RAMP3. Again, there was variation as to whether the thiazole or the amide end of the molecule pointed towards the RAMP end of the receptor.

The docking pose of SHF1555 (Figure **4.26**) saw the thiazole extending towards RAMP3. It was the nitro group that was predicted to make key interactions at this end, forming an ionic interaction with RAMP3 Glu74 and a pi-cation interaction with RAMP3 Trp84. The presence of these interactions could again explain why SHF1555 maintains AM_2 potency in the absence of the sulfoxide. The amide side of the molecule extended further towards the CLR end of the receptor, with a hydrogen bond predicted to stabilize the interaction between the amide carbonyl and RAMP3 Tyr83, with the amide phenyl group stacking against CLR Trp72.

The docking pose of SHF1558, on the other hand, has the thiazole pointing towards the CLR end of the receptor (Figure **4.27**). Key interactions between the compound and the receptor are predicted to be a hydrogen bond between a sulfone oxygen and CLR Trp121, with an additional pi stacking interaction between the central aromatic ring and CLR Trp72.

A

B

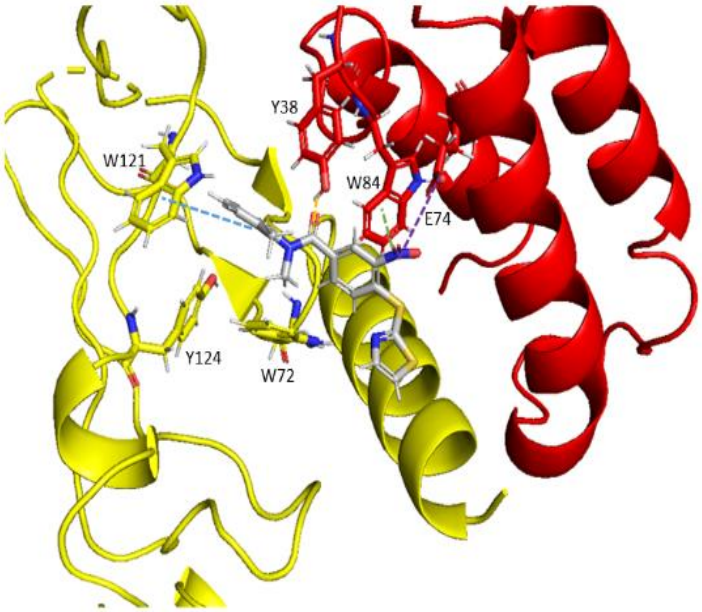

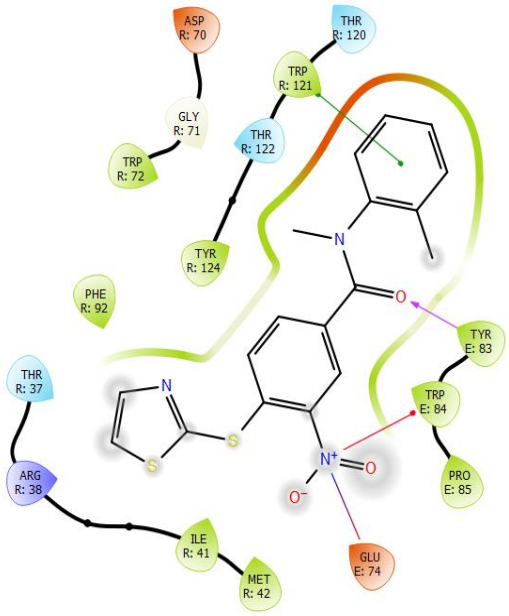

Figure 4.26 – Lowest energy docking pose of SHF1555 bound to the AM_2 receptor (PDB: 6UUS). (A) 3D image of SHF1555 docked into the AM_2 receptor ECD. The CLR is coloured in yellow and RAMP3 is coloured in red. Hydrogen bonds are indicated by yellow dashed lines, ionic interactions are indicated by purple dashed lines, pi-pi interactions are indicated by blue dashed lines and pi-cation interactions are indicated by green dashed lines. Key residues in the binding pocket are shown and labelled. Docking was carried out using Schrodinger (Maestro 13.2) and the image was generated using PyMol Molecular Graphics System, Version 1.7.4.5-Educational Product, Schrodinger. (B) 2D ligand interaction diagram generated from Maestro 13.2. Hydrogen bonds are indicated by purple lines, pi-cation interactions are indicated by red lines and hydrophobic interactions are indicated by green lines.

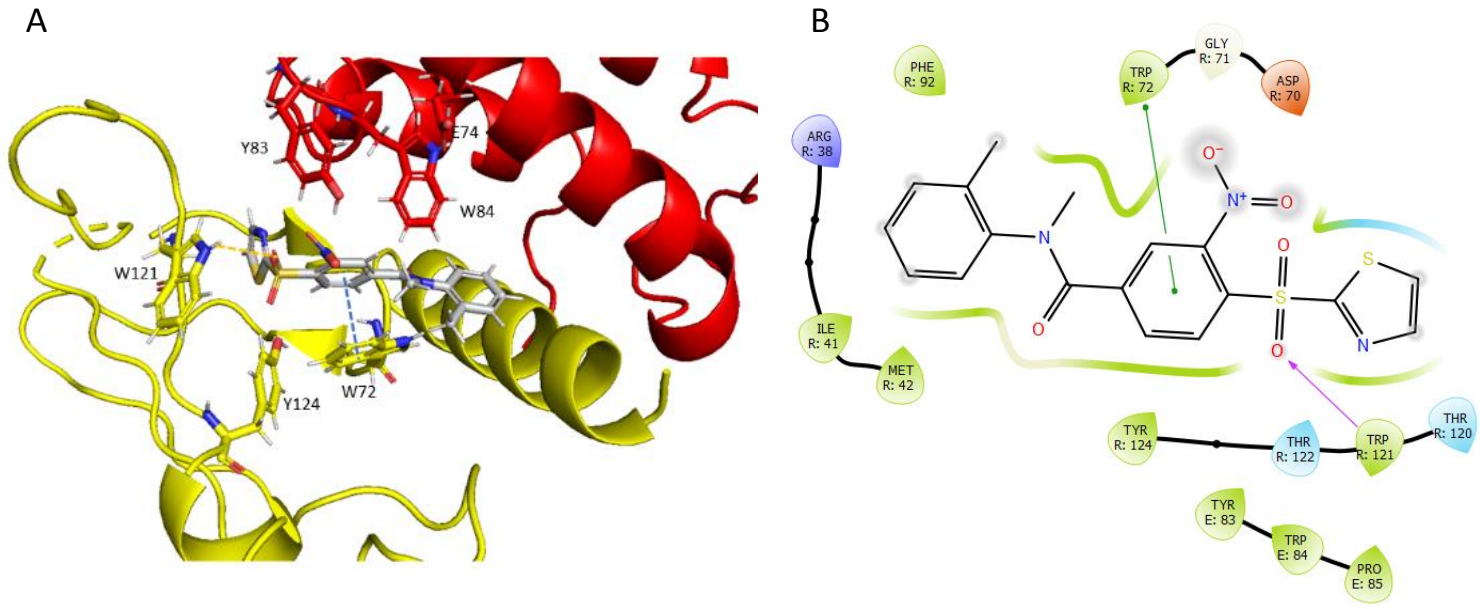

Figure 4.27 – Lowest energy docking pose of SHF1558 bound to the AM_2 receptor (PDB: 6UUS). (A) 3D image of SHF1555 docked into the AM_2 receptor ECD. The CLR is coloured in yellow and RAMP3 is coloured in red. Hydrogen bonds are indicated by yellow dashed lines and pi-cation interactions are indicated by green dashed lines. Key residues in the binding pocket are shown and labelled. Docking was carried out using Schrodinger (Maestro 13.2) and the image was generated using PyMol Molecular Graphics System, Version 1.7.4.5-Educational Product, Schrodinger. (B) 2D ligand interaction diagram generated from Maestro 13.2. Hydrogen bonds are indicated by purple lines and hydrophobic interactions are indicated by green lines.

The docking poses of both SHF1574 enantiomers overlapped well with each other (Figure **4.28**). Both enantiomers saw the thiazole pointing towards RAMP3, with the amide phenyl ring pointing towards CLR and forming pi-pi stacking interactions with CLR Trp121 and Tyr124. The aniline group was additionally predicted to form a hydrogen bond with RAMP3 Glu74, whilst the amide carbonyl formed a hydrogen bond with RAMP3 Tyr83. Once again, the potential presence of these interactions meant that the lack of potency of SHF1574 at AM_2 was surprising.

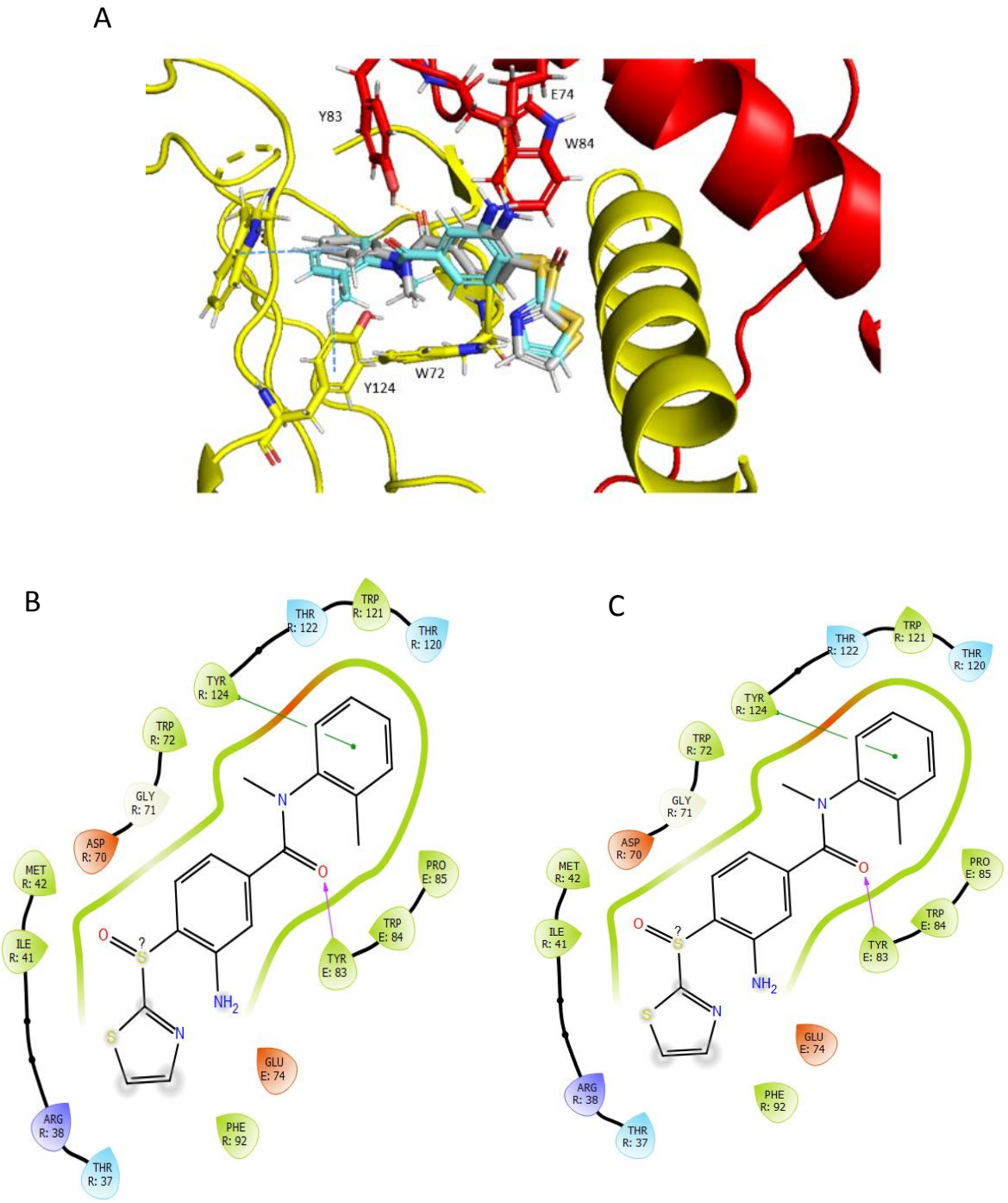

Figure 4.28 – Lowest energy docking pose of both enantiomers of SHF1574 bound to the AM_2 receptor (PDB: 6UUS). (A) (*R*) enantiomer is coloured in grey and the (*S*) enantiomer is coloured in sky blue. CLR is coloured in yellow and RAMP3 is coloured in magenta. Hydrogen bonds are indicated by yellow dashed lines and pi-pi interactions are indicated by blue dashed lines. Key residues in the binding pocket are shown and labelled. Docking was carried out using Schrodinger (Maestro 13.2) and the image was generated using PyMol Molecular Graphics System, Version 1.7.4.5- Educational Product, Schrodinger. (B) and (C) show the corresponding 2D ligand interaction diagrams of the (*R*) and (*S*) enantiomes of SHF1574 respectively, generated by Maestro 13.2. Hydrogen bonds are indicated by purple lines and hydrophobic interactions are indicated by green lines.

Other compounds in this series docked to the AM_2 receptor in one of the two poses described above. Compounds docked with the thiazole pointing towards RAMP3 principally saw interactions between the thiazole and RAMP3 Trp84 and the nitro group with RAMP3 Glu74, whilst the amide phenyl group would often interact with either with CLR Tyr124 or Trp121 (Figure **4.29**). Compounds with the thiazole pointing towards the CLR would often generate interactions between the sulfoxide oxygen and CLR Thr122 backbone, with the central phenyl ring interacting with CLR Trp72 and the carbonyl amide occasionally interacting with RAMP3 Tyr124.

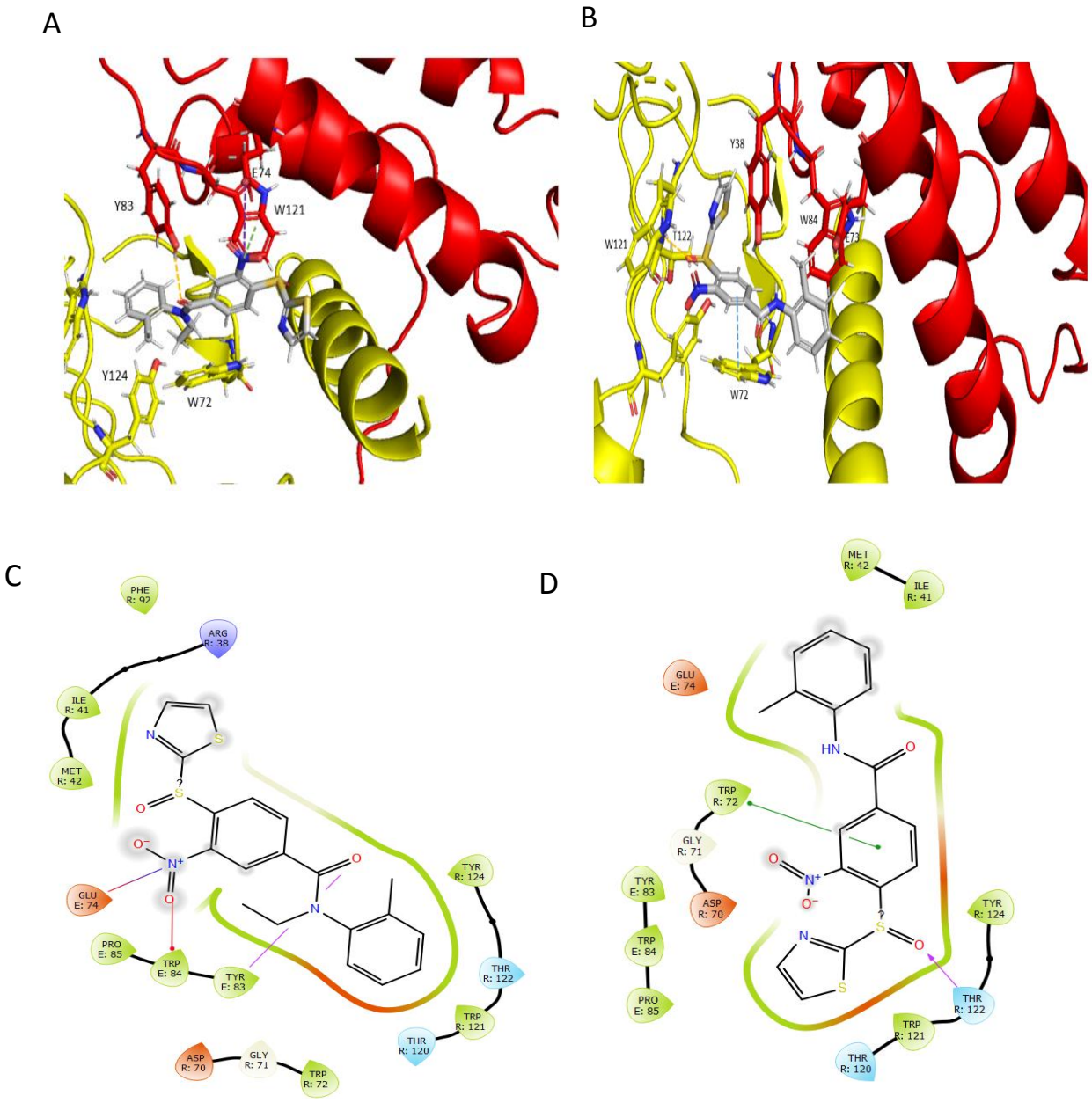

Figure 4.29 - Lowest energy docking pose of SHF1580 (*S*) enantiomer, (A) and (C), and SHF1568 (*R*) enantiomer, (B) and (D), bound to the AM_2 receptor (PDB: 6UUS). (A) and (B) show the 3D image of the compound docked into the AM_2 receptor ECD. The CLR is coloured in yellow and RAMP3 is coloured in red. Hydrogen bonds are indicated by yellow dashed lines, ionic interactions are indicated by purple dashed lines, pi-pi interactions are indicated by blue dashed lines and pi-cation interactions are indicated by green dashed lines. Key residues in the binding pocket are shown and labelled. Docking was carried out using Schrodinger (Maestro 13.2) and the image was generated using PyMol Molecular Graphics System, Version 1.7.4.5-Educational Product, Schrodinger. (C) and (D) show the corresponding 2D ligand interaction diagrams generated by Maestro 13.2. Hydrogen bonds are indicated by purple lines, ionic interactions are indicated by red lines and hydrophobic interactions are indicated by green lines.

4.10 Conclusion

To summarise, important structure activity relationship studies have been carried out on SHF1556 at the AM_1 receptor. It has been found that the sulfoxide group is essential for AM_1 potency, but not for CGRP or AM_2 potency, whilst reducing the nitro group shows a complete loss of potency on all three receptors. Other minor modifications to the structure, including the thiazole ring, the *N*-methyl group and the amide phenyl ring have so far all displayed moderate reductions in AM_1 potency compared to SHF1556, with many of these compounds showing modest selectivity for CGRP and AM_2.

Chapter 5 – Discovery of a Potent, Low Molecular Weight AM_1 Antagonist

Chapter 5: Discovery of a Potent, Low Molecular Weight AM_1 Antagonist

5.1 Discovery of SHF1572

During the SAR investigations into SHF1556, it was discovered that the sulfoxide group and the nitro group on the compound were crucial for AM_1 potency. To further explore the importance of these groups on biological activity, fragments of SHF1556 containing both of these groups can be tested to determine how much potency is retained (Figure **5.1**).

One such fragment investigated was SHF1572 (Figure **5.1**), an intermediate in the synthesis of SHF1556 analogues (see Chapter 4). This compound retains the entire left hand side of SHF1556, including the sulfoxide and nitro groups, whilst the amide group on the right hand side of the structure of SHF1556 has been deleted and replaced with a much smaller nitrile group.

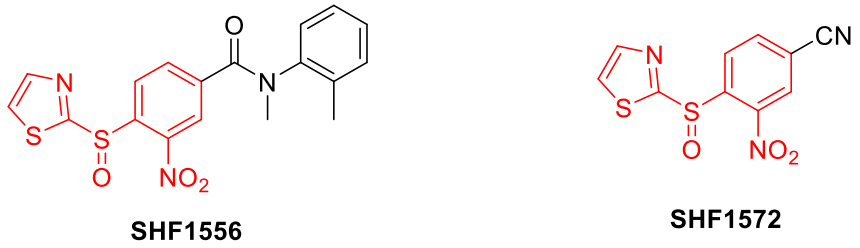

SHF1556 **SHF1572**

Figure 5.1 – Comparison of the chemical structures of SHF1556 and SHF1572. The identical structural motifs in both compounds are highlighted in red.

As with SHF1556, SHF1572 also displays suitable drug-like properties for a lead compound (Table **5.1**). All of Lipinski's rules are obeyed, with SHF1572 having a molecular weight less than 500, Log P value of 2.2, 0 hydrogen bond donors and 6 hydrogen bond acceptors. Additionally, with the compound having 3 rotatable bonds and a TPSA of 96.6 $Å^2$, Verber's parameters are also obeyed.

Table 5.1 – Physiochemical Properties of SHF1572

Property	Value
Molecular Weight	279.3
Log P	2.2
H-bond Donors	0
H-bond Acceptors	6
Rotatable Bonds	3
TPSA	96.9 $Å^2$

5.1.1 Docking of SHF1572 in AM_1 and Hypothesis

Molecular docking studies were carried out on SHF1572 to predict the binding mode of SHF1572. The docking poses of both enantiomers of SHF1572 to the AM_1 ECD (PDB: 3AQF) are in good agreement with those observed from other compounds in this series (see Chapter 4), binding across the CLR (Figure **5.2**). Both the (*R*) and (*S*) enantiomers have the sulfoxide oxygen and the nitro group making key interactions. In both cases the sulfoxide oxygen forms a hydrogen bond to CLR Thr122, whilst the nitro group on the (*R*) enantiomer forms an ionic interaction with CLR Asp70 and a pi cation interaction with CLR W72 (Figure **5.2**). The corresponding group on the (*S*) enantiomer points more towards RAMP2 and formed a hydrogen bond with the backbone of RAMP2 Phe111 (Figure **5.2**). Docking scores for both SHF1572 enantiomers are slightly lower to those seen for SHF1556 at the AM_1 receptor (Table **5.2**), further suggesting that this compound will retain most of SHF1556 potency.

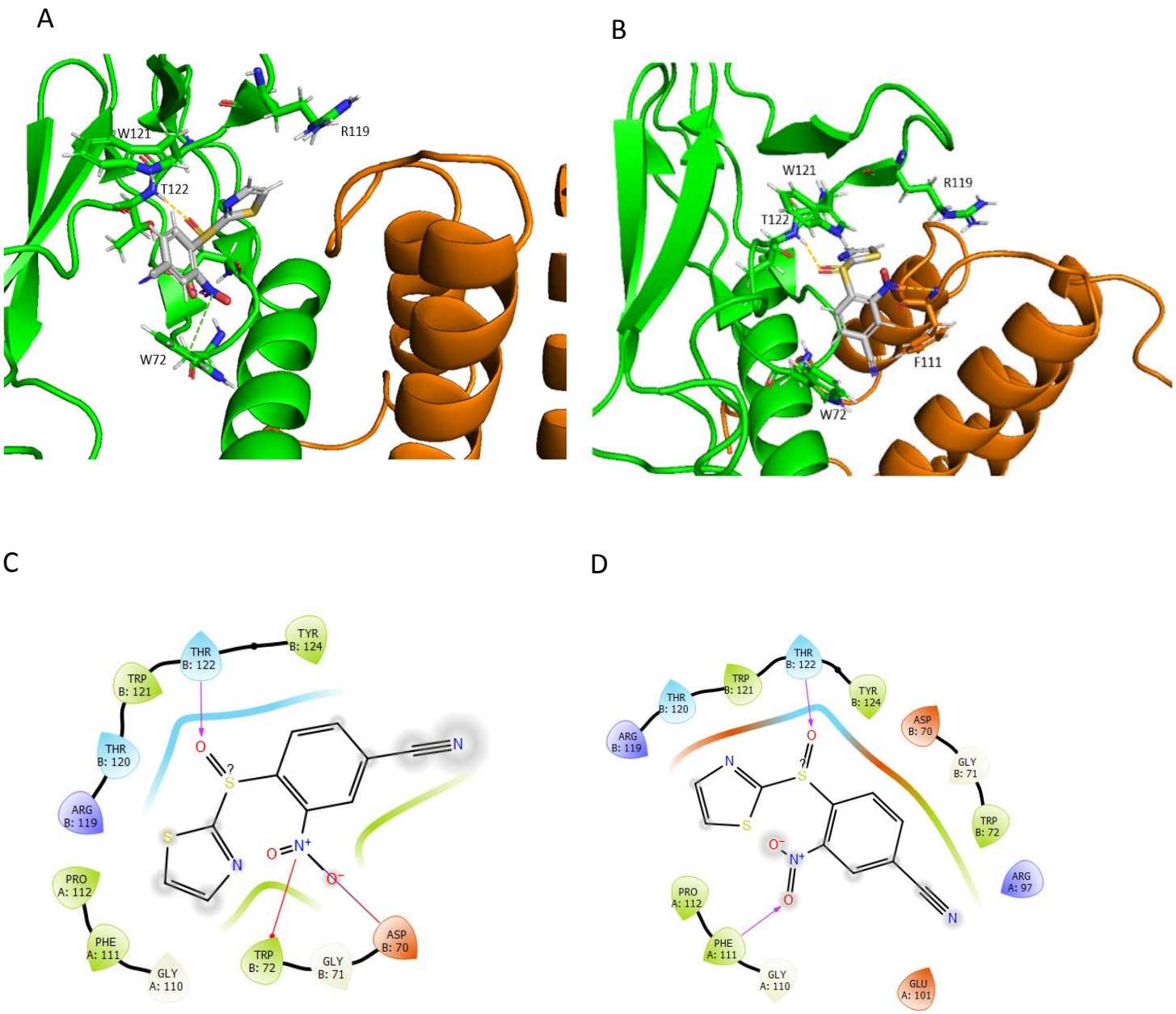

Figure 5.2 - Lowest energy docking pose of SHF1572 (*R*) enantiomer, (A) and (C), and (*S*) enantiomer, (B) and (D), bound to the AM_1 receptor (PDB: 3AQF). (A) and (B) show the compound docked into the AM_1 ECD. The CLR is coloured in green and RAMP2 is coloured in orange. Hydrogen bonds are indicated by yellow dashed lines and pi-cation interactions are indicated by green dashed lines. Key residues in the binding pocket are shown and labelled. Docking was carried out using Schrodinger (Maestro 13.2) and the image was generated using PyMol Molecular Graphics System, Version 1.7.4.5- Educational Product, Schrodinger**.** (C) and (D) show the 2D ligand interaction diagrams generated from Maestro 13.2. Hydrogen bonds are indicated by purple lines and ionic interactions are indicated by red lines.

Table 5.2 - Docking Scores of SHF1572 enantiomers in the AM_1 receptor ECD (PDB: 3AQF). Docking scores generated by Schrodinger (Maestro 13.2)

SHF1572 Enantiomer	Docking Score (kcal mol^{-1})
(R)	-4.1
(S)	-4.0

Due to the retention of the important sulfoxide and nitro groups, and the prediction of these groups interacting with the AM_1 receptor in a similar manner to SHF1556, it was therefore hypothesised that SHF1572 would display good potency on the AM_1 receptor. The aims of this work were to therefore subject SHF1572 to testing on our cAMP assay and to investigate the SAR of this compound in more detail should it retain a significant amount of the potency displayed by SHF1556.

5.1.2 *In Vitro* Testing of SHF1572 on AM_1

Being an intermediate in SHF1556 analogue synthesis, a small amount of SHF1572 was isolated and subjected to the cAMP assay on AM_1 overexpressing cells (Figure **5.3**). The compound subsequently performed very well in the assay, exhibiting sub micro molar potency (pIC50 = 6.32 +/- 0.166). SHF1572 was tested alongside SHF1556 in order to gain a direct comparison of potencies, and despite SHF1556 performing better in the assay, SHF1572 did retain 91% AM_1 potency of SHF1556 (pIC50 = 6.93 +/- 0.166), with this difference not considered statistically significant (P = 0.1479). This strong retention in potency of this fragment backs up the suggestion that most AM_1 potency comes from the left hand side of the compound, as removing the right hand amide side of SHF1556 only slightly diminishes AM_1 potency.

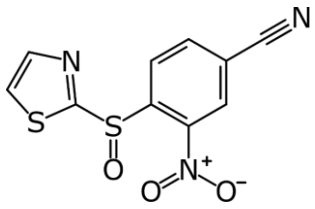

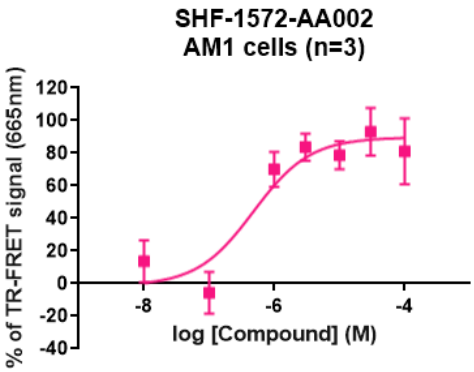

Parameter	Value
pIC50 (AM_1)	6.34
Std Error	0.166
R Square	0.7740
Best Fit Top	94.80
Best Fit Bottom	-2.566

Figure 5.3 – Concentration-response plot of SHF1572 generated from the cAMP assay and the curve best fit data. Compound was tested on CLR/RAMP2 overexpressing cells which were subsequently stimulated by the EC50 concentration of AM (1 nM). Data was plotted using GraphPad Prism 9.0.2 and the IC50 was determined using a non-linear 3-parameter inhibition curve.

The corresponding sulfide, SHF1559, was also tested against AM_1 to determine if the sulfoxide was still playing a key role in AM_1 binding (Figure **5.4**). As seen with previous compounds, the sulfide analogue of SHF1572 displayed no AM_1 potency, confirming the sulfoxide oxygen was still a key group in this compound, agreeing with the docking studies for SHF1572.

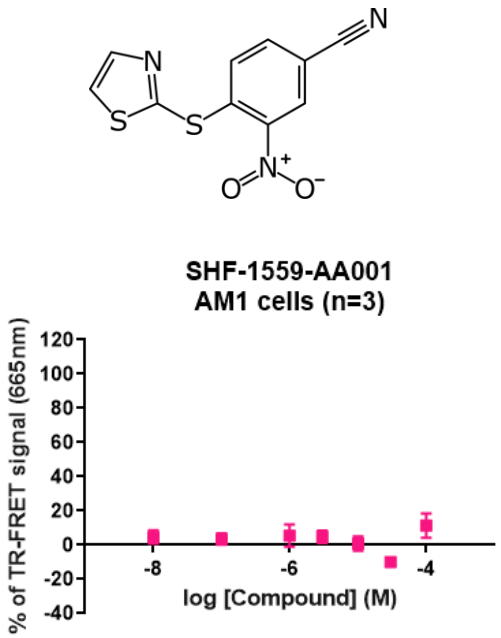

Figure 5.4 - Concentration-response plot of SHF1559 generated from the cAMP assay. The Compound was tested on CLR/RAMP2 overexpressing cells which were subsequently stimulated by the EC50 concentration of AM (1 nM). Data was plotted using GraphPad Prism 9.0. No curve data could be generated due to layout of the data points.

5.2 Modification and Removal of the Nitrile Group

Intrigued by the high retention of potency of SHF1572 compared to SHF1556, the fragment was investigated further. The effect of the nitrile group on AM_1 potency was investigated by both converting to the corresponding carboxylic acid, SHF1578 (Figure **5.5**), and removing the nitrile group form the fragment, SHF1581 (Figure **5.5**)

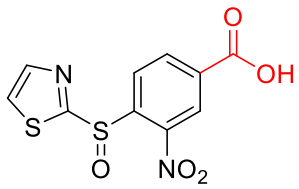

SHF1578

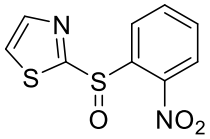

SHF1581

Figure 5.5 – Chemical Structures of SHF1578 and SHF1581. Structural differences from SHF1572 are highlighted in red

5.2.1 Docking of SHF1578 and SHF1581 in AM_1

SHF1578 docked across the CLR, with both enantiomers displaying almost identical poses (Figure **5.6**). As with SHF1572, there was a hydrogen bond between the sulfoxide oxygen and CLR Thr122 backbone, whilst the thiazole ring stacked against CLR Trp72. The nitro group in the (*R*) enantiomer was also orientated to form a hydrogen bond with CLR Trp121. Unlike the nitrile in SHF1572, however, the carboxylic acid group was predicted to form extensive interactions with CLR Arg119, forming hydrogen bonds and ionic interactions with this residue. Overall, this model implied that SHF1578 could be very potent on AM_1.

SHF1581 docked in a similar position to SHF1578, with the docking poses of both enantiomers aligning well (Figure **5.7**). The hydrogen bond between the sulfoxide oxygen and CLR Thr122 backbone is retained, whilst the nitro group on the (*R*) enantiomer forms an ionic interaction with CLR Asp70, and a pi stacking interaction with CLR Trp72. The phenyl group also points towards CLR Arg119, but the absence of the carboxylic acid group means that no interactions were predicted here, suggesting a lower potency than SHF1578.

Docking scores for both SHF1578 enantiomers were higher than those seen for SHF1556 and SHF1572 (Table **5.3**), thereby implying that this compound could bind more strongly to the AM_1 receptor. SHF1581, on the other hand, saw drop in docking score compared to the lead compounds, implying that removing the nitrile group could lead to a drop in activity.

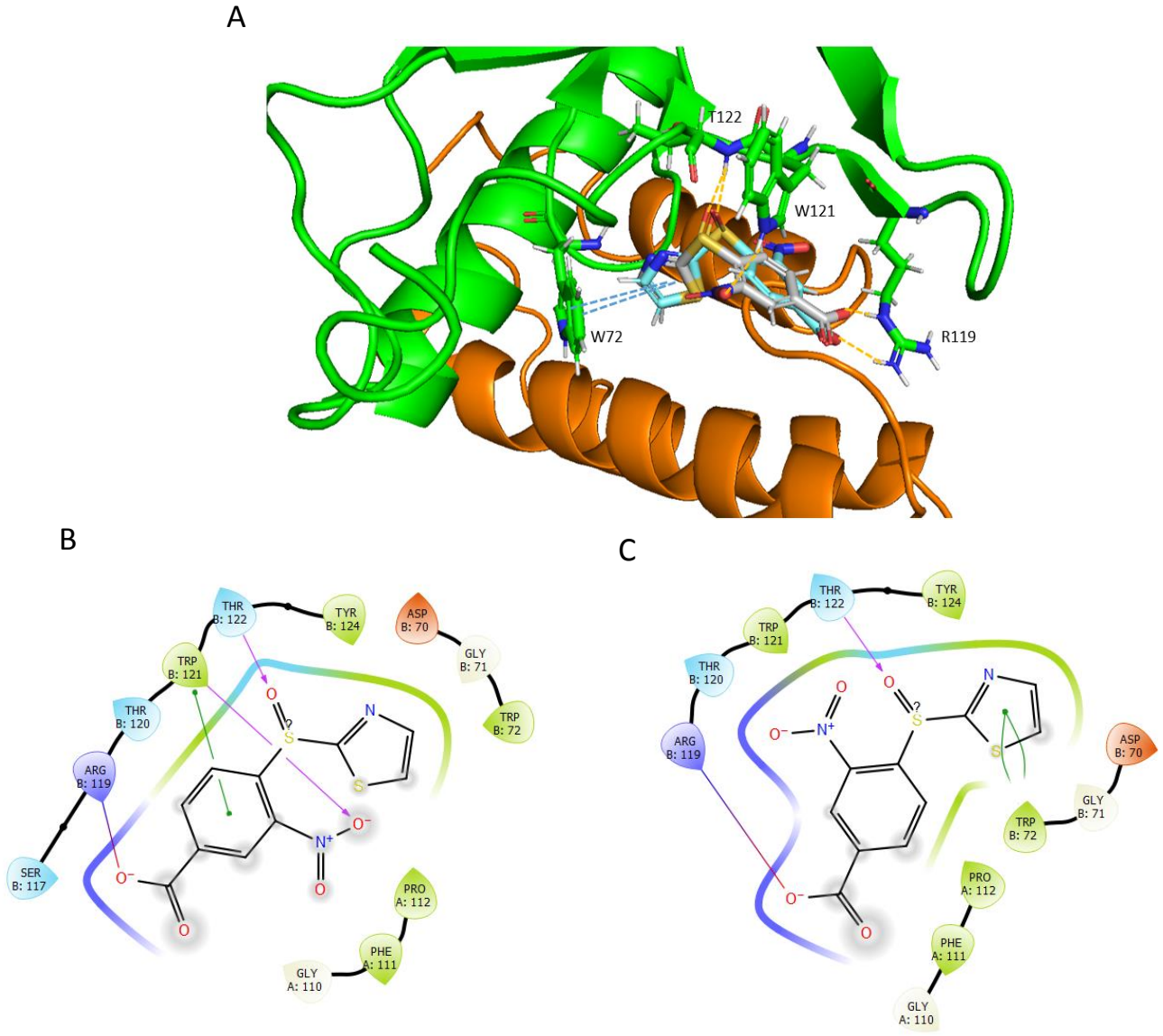

Figure 5.6 - Lowest energy docking pose of SHF1578 bound to the AM_1 receptor (PDB: 3AQF). (A) 3D image of the compound docked into the AM_1 receptor. The CLR is coloured in green and RAMP2 is coloured in orange. The (*R*) enantiomer is coloured in grey and the (*S*) enantiomer is coloured in light blue. Hydrogen bonds are indicated by yellow dashed lines and pi-pi interactions are indicated by blue dashed lines. Key residues in the binding pocket are shown and labelled. Docking was carried out using Schrodinger (Maestro 13.2) and the image was generated using PyMol Molecular Graphics System, Version 1.7.4.5- Educational Product, Schrodinger. (B) and (C) 2D ligand interaction diagrams of the (*R*) and (*S*) enantiomers of SHF1578 respectively. Hydrogen bonds are indicated by purple lines, ionic interactions are indicated by red lines and hydrophobic interactions are indicated by green lines.

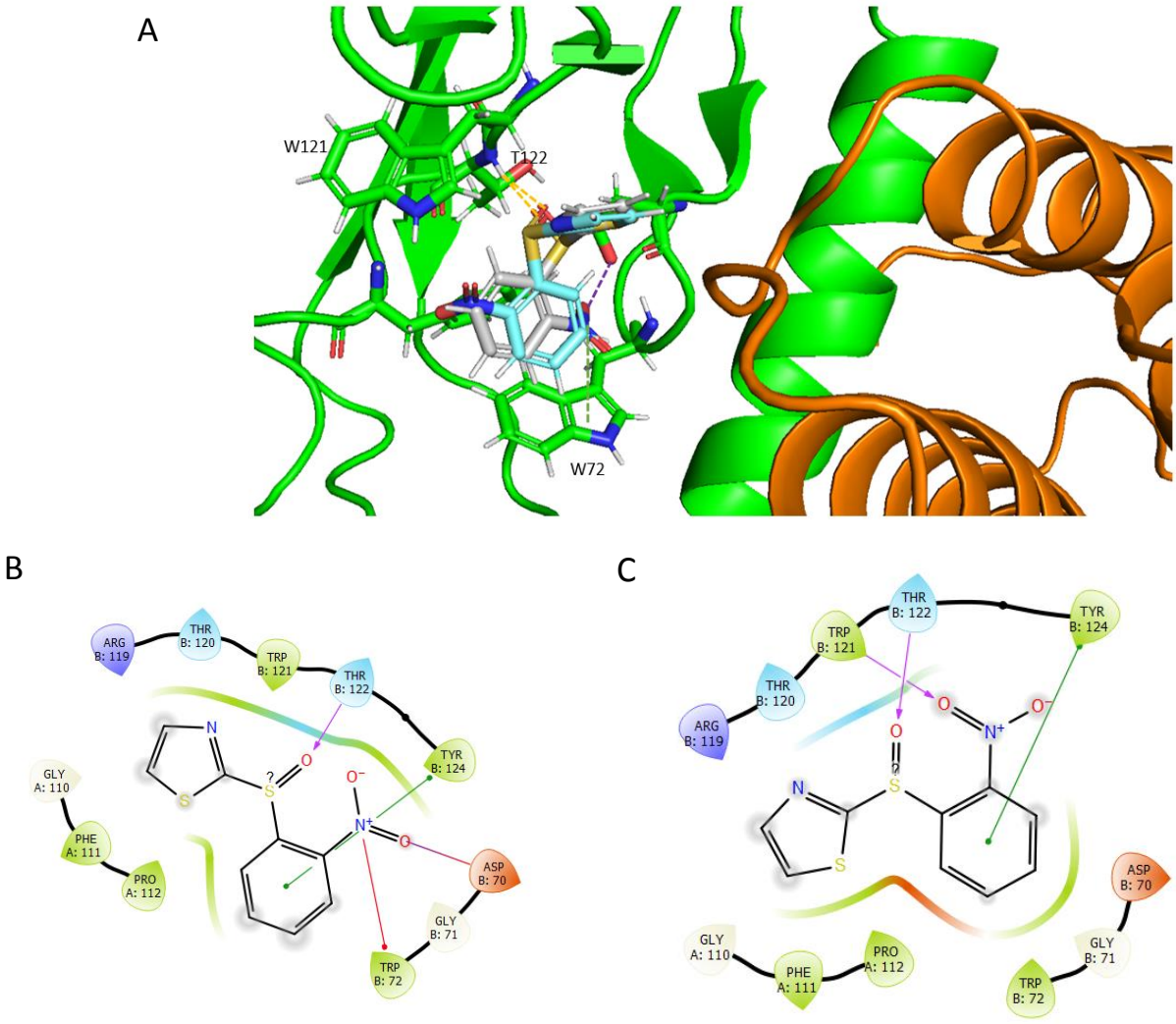

Figure 5.7 - Lowest energy docking pose of SHF1581 bound to the AM_1 receptor (PDB: 3AQF). (A) The 3D image of SHF1581 docked into the AM_1 receptor. The CLR is coloured in green and RAMP2 is coloured in orange. The (*R*) enantiomer is coloured in grey and the (*S*) enantiomer is coloured in light blue. Hydrogen bonds are indicated by yellow dashed lines, ionic interactions are indicated by purple dashed lines and pi-cation interactions are indicated by green dashed lines. Key residues in the binding pocket are shown and labelled. Docking was carried out using Schrodinger (Maestro 13.2) and the image was generated using PyMol Molecular Graphics System, Version 1.7.4.5- Educational Product, Schrodinger. (B) and (C) the 2D ligand interaction diagram of the (*R*) and (*S*) enantiomers respectively. Hydrogen bonds are indicated by purple lines, ionic interactions are indicated by red lines and hydrophobic interactions are indicated by green lines.

Table 5.3 - Docking Scores of SHF1578 and SHF1581 in the AM_1 receptor ECD (PDB: 3AQF). Docking scores generated by Schrodinger (Maestro 13.2)

Compound	Enantiomer	Docking Score (kcal mol^{-1})
SHF1578	(*R*)	-5.0
SHF1578	(*S*)	-5.0
SHF1581	(*R*)	-3.6
SHF1581	(*S*)	-3.6

5.2.2 Synthesis of SHF1572 Analogues

As with SHF1572, SHF1578 was also an intermediate in the SHF1556 enantiomer synthesis (see Chapter 3), meaning a small amount of this compound was easily isolated for *in vitro* testing. SHF1581 was synthesised by Joe Egan, from Compound **53** (Scheme **5.1**) using the standard two step SnAr-oxidation procedure used to synthesise analogues of SHF1556 (see Chapter 4).

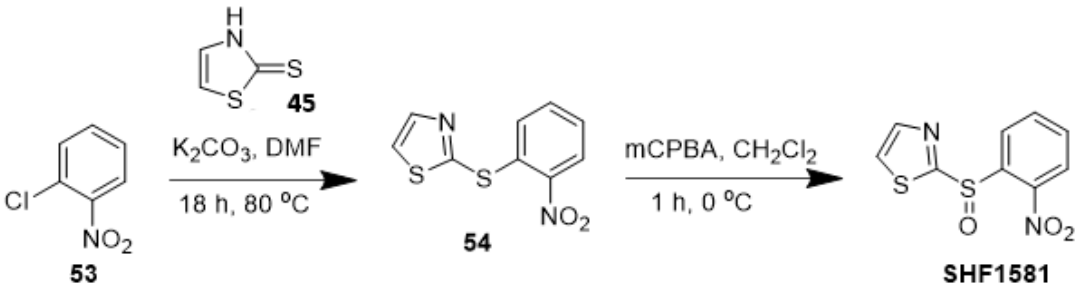

Scheme 5.1 – Synthesis of SHF1581

5.2.3 *In Vitro* Testing of SHF1572 Analogues

With both SHF1578 and SHF1581 in hand, both compounds were subsequently tested for AM_1 potency. Surprisingly, neither compound displayed any significant potency towards the AM_1 receptor in the cAMP assay (Figure **5.8**), with both compounds both showing pIC50 values <4. These data therefore suggest that the nitrile group in SHF1572 plays a key role in the compounds potency towards AM_1.

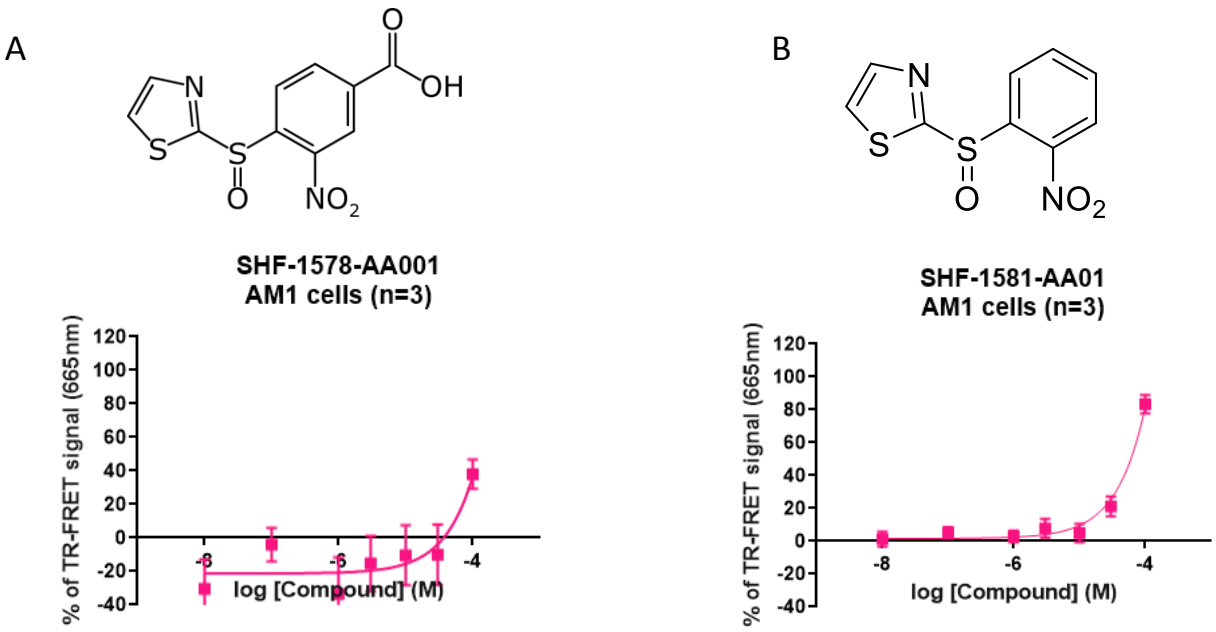

Figure 5.8 - Concentration-response plots of SHF1578 (A) and SHF1581 (B) generated from the cAMP assay. Compound was tested on CLR/RAMP2 overexpressing cells which were subsequently stimulated by the EC50 concentration of AM (1 nM). Data was plotted using GraphPad Prism 9.0.2. Curve fitting was applied but no curve could be fitted

5.3 Investigation of the Effect of Nitrile Substituent Position

Having established that the nitrile group in SHF1572 is clearly important for AM_1 potency, it was next decided to investigate the effect of moving this group to various positions around the phenyl ring. Relative to the sulfoxide, the nitrile in SHF1572 is in the 4-position or *para* position. It was decided to synthesise analogues of SHF1572 with the nitrile group in the 3-position (SHF1588) the 2-position (SH1589) and the 5-position (SHF1591) in order to detect increases or decreases in AM_1 potency and determine the optimal position of the nitrile group (Figure **5.9**). It was also decided to investigate the effect of moving the nitro group in SHF1572 *meta* to the sulfoxide and *ortho* to the nitrile to determine the optimal position of this group.

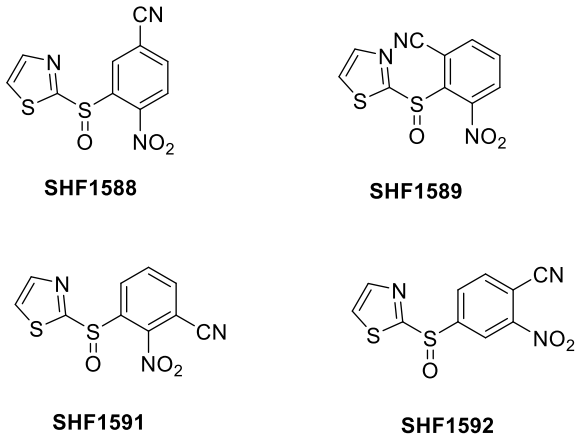

Figure 5.9 – Chemical structures of SHF1588, SHF1589, SHF1591 and SHF1592

5.3.1 Docking of Nitrile Substituent Position Analogues in AM_1

All SHF1572 analogues studied in this section docked in similar positions, in the CLR binding region between CLR Trp72 and Arg119 (Figure **5.10**) (Figure **5.11**). Unlike in SHF1572, the docking poses of SHF1588, SHF1589 and SHF1591 predicted the nitrile group to form interactions, forming hydrogen bonds with CLR Trp121 and Tyr124 amide backbones in SHF1588, the CLR Thr122 amide backbone in SHF1589, and the CLR Arg119 sidechain in SHF1591 (Figure **5.10**). The sulfoxide oxygen atoms in SHF1588 and SHF1591 were predicted to hydrogen bond with CLR Thr122, whilst the nitro group in all three compounds would interact with CLR Trp72. The docking pose of SHF1592, like SHF1572, predicted no interactions between the nitrile group and the protein (Figure **5.11**). Instead, the nitro group pointed towards the Thr122 backbone and formed a hydrogen bond with this residue, whilst the sulfoxide oxygen formed a hydrogen bond with CLR Tyr124 backbone. Overall from the docking poses it was expected all four compounds would display similar potency to SHF1572, with SHF1588 and SHF1589 being slightly more potent due to the presence of interactions with the sulfoxide, nitro and nitrile groups. The docking scores for SHF1588 and SHF1589 were lower than that seen for SHF1572 (Table **5.4**), implying moving the nitrile group to the respective positions could be detrimental for AM1 activity. SHF1591 showed similar docking scores to SHF1572, whilst SHF1592 displayed an increase, suggesting moving the nitro group to this position could have a positive impact on AM1 activity.

Table 5.4 - Docking Scores of nitrile substituent position analogues in the AM_1 receptor ECD (PDB: 3AQF).

Docking scores generated by Schrodinger (Maestro 13.2)

Compound	Enantiomer	Docking Score (kcal mol^{-1})
SHF1588	(*R*)	-3.9
SHF1588	(*S*)	-3.9
SHF1589	(*R*)	-3.7
SHF1589	(*S*)	-3.6
SHF1591	(*R*)	-4.1
SHF1591	(*S*)	-4.3
SHF1592	(*R*)	-4.4
SHF1592	(*S*)	-4.3

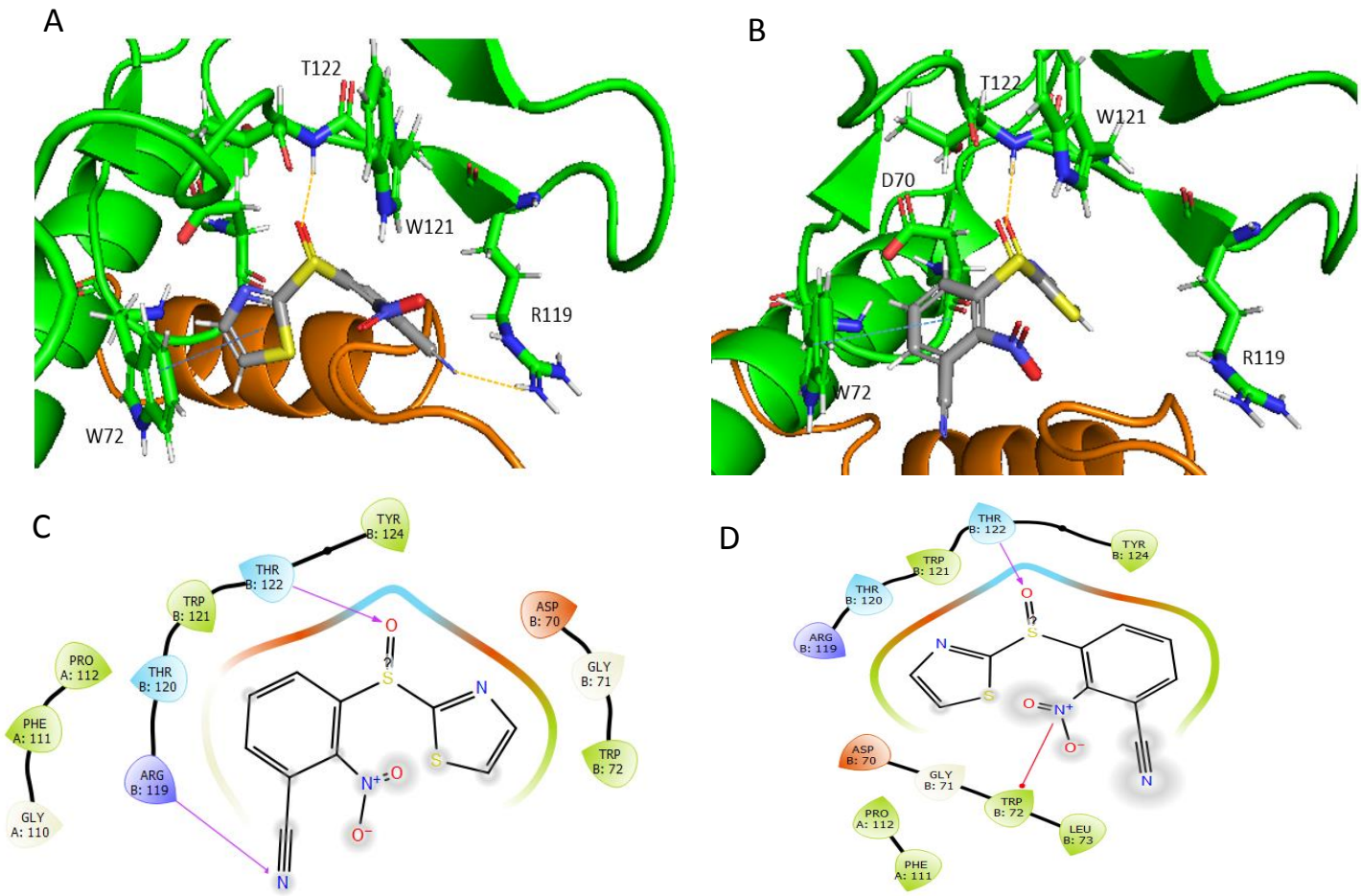

Figure 5.10 - Lowest energy docking pose of SHF1591 (R) enantiomer, (A) and (C), and (S) enantiomer, (B) and (D), bound to the AM_1 receptor (PDB: 3AQF). (A) and (B) show the compound docked to the AM_1 receptor ECD. The CLR is coloured in green and RAMP2 is coloured in orange. Hydrogen bonds are indicated by yellow dashed lines and pi-pi interactions are indicated by blue dashed lines. Key residues in the binding pocket are shown and labelled. Docking was carried out using Schrodinger (Maestro 13.2) and the image was generated using PyMol Molecular Graphics System, Version 1.7.4.5- Educational Product, Schrodinger. (C) and (D) show the corresponding 2D ligand interaction diagrams generated from Maestro 13.2. Hydrogen bonds are indicated by purple lines and hydrophobic interactions are indicated by green lines.

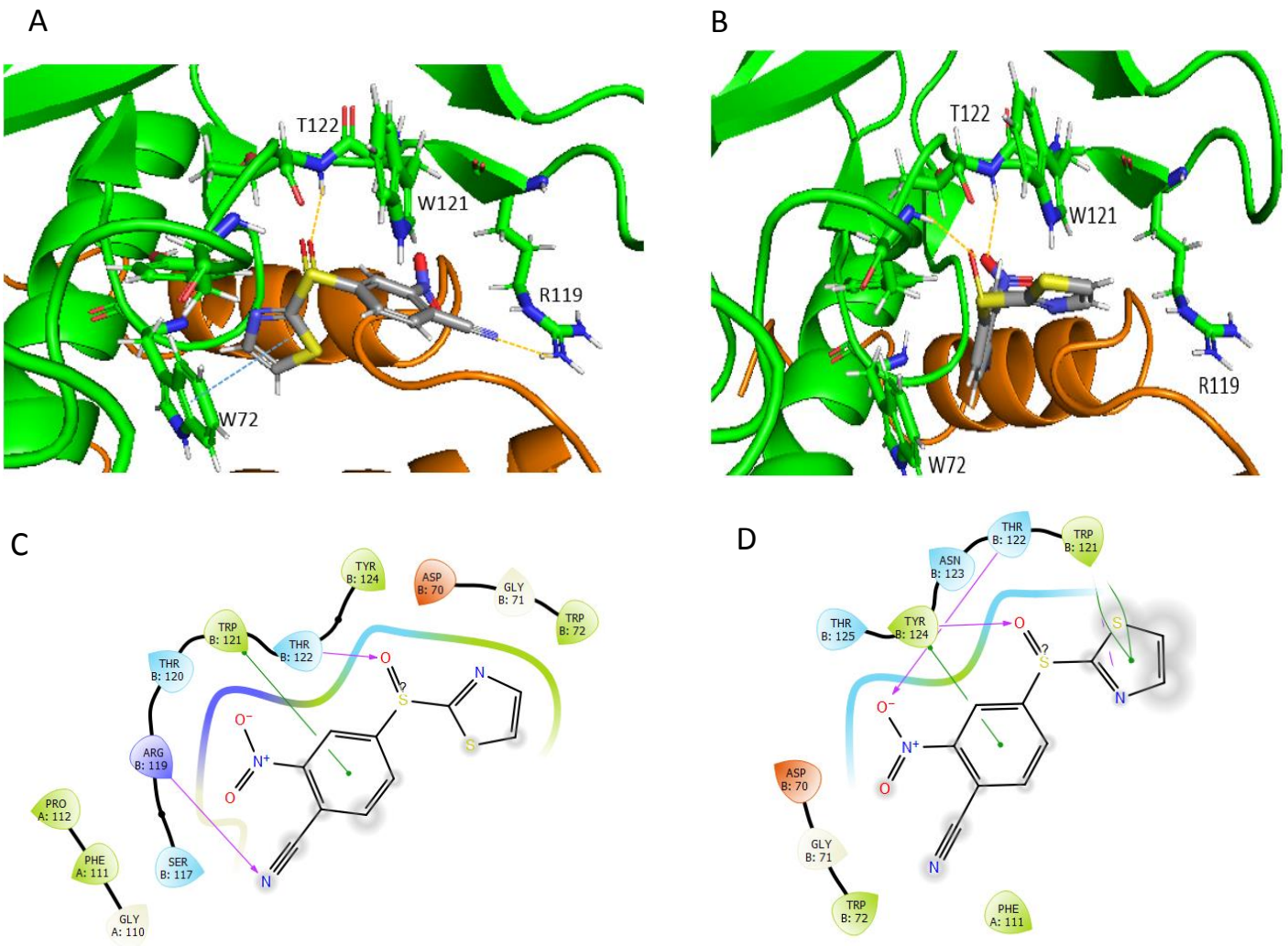

Figure 5.11 - Lowest energy docking pose of SHF1592 (R) enantiomer, (A) and (C), and (S) enantiomer, (B) and (D), bound to the AM_1 receptor (PDB: 3AQF). (A) and (B) show the compound docked to the AM_1 receptor ECD. The CLR is coloured in green and RAMP2 is coloured in orange. Hydrogen bonds are indicated by yellow dashed lines and pi-pi interactions are indicated by blue dashed lines. Key residues in the binding pocket are shown and labelled. Docking was carried out using Schrodinger (Maestro 13.2) and the image was generated using PyMol Molecular Graphics System, Version 1.7.4.5- Educational Product, Schrodinger. (C) and (D) show the corresponding 2D ligand interaction diagrams generated from Maestro 13.2. Hydrogen bonds are indicated by purple lines and hydrophobic interactions are indicated by green lines.

5.3.2 Synthesis of Nitrile Substiuent Position Analogues

SHF1588, SHF1589, SHF1591 and SHF1592 were all synthesised from the corresponding fluoro-nitrobenzonitriles (Scheme **5.2**). Each compound underwent the two step SnAr, oxidation synthetic procedure with compound **45** as described above for SHF1581 (Scheme **5.1**) to form the corresponding SHF1572 analogue.

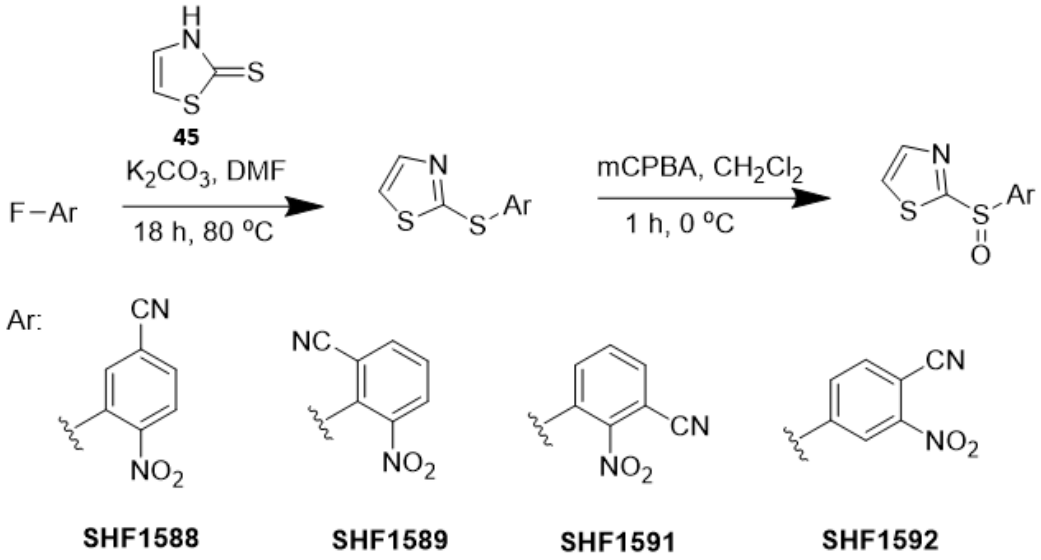

Scheme 5.2 – Synthesis of SHF1572 positional analogues

5.3.3 *In Vitro* Testing of Nitrile Substituent Position Analogues

With the SHF1572 analogues in hand, the next stage was to test the compounds for AM_1 potency using the cAMP assay (Figure **5.12**) (Table **5.5**) (Table **5.6**). Interestingly, changing the position of the nitrile group on the phenyl ring had no significant effect on AM_1 potency compared to SHF1572. SHF1572, with the nitrile group in the 4-position was the most potent of the series. Moving the nitrile to the 3-position (SHF1588) saw a decrease in potency of around 2-fold (pIC50 = 6.08 +/- 0.175) (P = 0.1328), whilst moving to the 2-position (SHF1589) and the 5-position (SHF1591) saw potency decreases of 1.5-fold (pIC50 (SHF1589) = 6.20 +/- 0.117) (P =0.4366), (pIC50 (SHF1591) = 6.16 (+/- 0.153) (P = 0.3808) . These data therefore suggest that the position of the nitrile group in this fragment has no real effect on AM_1 potency. What was also intriguing was that keeping the nitrile group in the 4-position but moving the nitro group from the 6-position to the 5-position (SHF1592) shows a large reduction in AM_1 potency, implying that the nitro group in the 5-position is critical for AM_1 potency of this fragment.

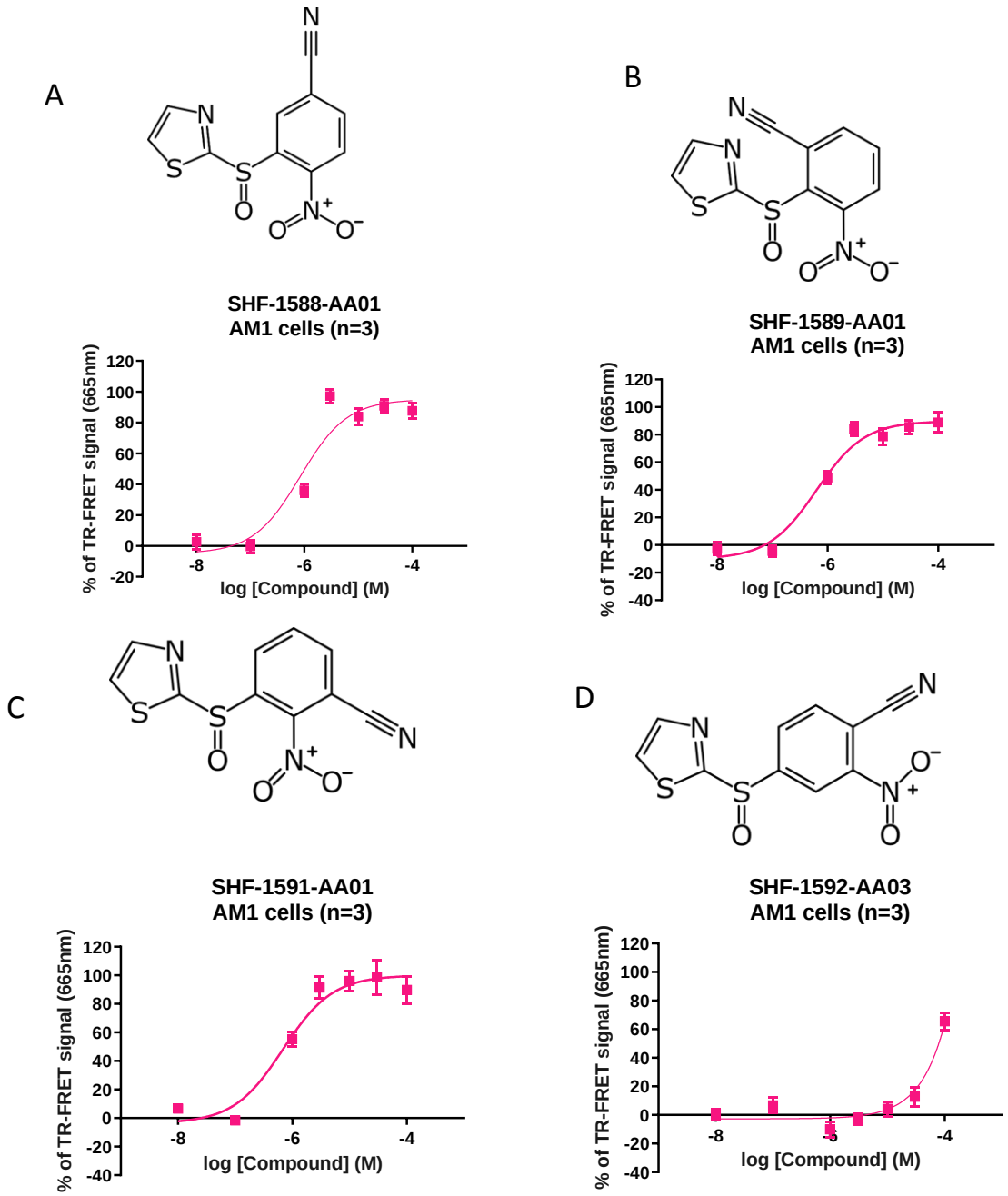

Figure 5.12 - Concentration-response plots of SHF1588, SHF1589, SHF1591 and SHF1592 generated from the cAMP assay. Compounds were tested on CLR/RAMP2 overexpressing cells which were subsequently stimulated by the EC50 concentration of AM (1 nM). Data was plotted using GraphPad Prism 9.0.2 and the IC50 was determined using a non-linear 3-parameter inhibition curve.

Table 5.5 – Best fit data for SHF1572 positional analogues. P values were used to compare the pIC50 values with SHF1572. A P value of <0.05 was considered statistically significant.

	Compound			
Parameter	**SHF1588**	**SHF1589**	**SHF1591**	**SHF1592**
pIC50	6.08	6.20	6.16	n.d
Std Error	0.175	0.117	0.153	-
R Square	0.8388	0.8578	0.7746	-
Best Fit Top	95.04	89.83	100.0	-
Best Fit Bottom	-4.994	-10.23	-3.707	-
P Value	0.1328	0.4366	0.3808	-

Table 5.6 – AM_1 pIC50 data for SHF1572 positional analogues

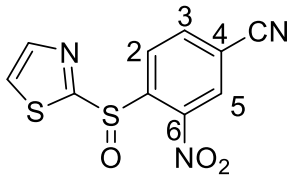

Compound	Nitrile Position	Nitro Position	pIC50 (AM_1) (+/- Std Error)
SHF1572	4	6	6.32 (+/- 0.166)
SHF1588	3	6	6.08 (+/- 0.175)
SHF1589	2	6	6.20 (+/- 0.117)
SHF1591	5	6	6.16 (+/- 0.153)
SHF1592	4	5	n.d

5.4 Counter Screening of SHF1572 Fragment and Analogues

The selectivity of SHF1572 and it's analogues for AM_1 was determined by counter screening against AM_2 and CGRP (Table **5.7**). SHF1572 showed reasonable selectivity for AM_1, displaying 7-fold increase in potency over AM_2 (pIC50 = 5.45 +/- 0.179) (P = 0.0067) and 10-fold selectivity over CGRP (pIC50 = 5.33 +/- 0.142) (P = 0.0369). SHF1578 and SHF1581 meanwhile, both of which were inactive on AM_1 were both inactive on both AM_2 and CGRP.

The analogues in which the nitrile group had changed position on the phenyl ring were also more selective towards AM_1. Moving the nitrile group to the 3-position (SHF1588) sees a 5-fold increase in AM_1 potency over AM_2 (pIC50 = 5.37 +/- 0.102) (P < 0.0001), and a 3-fold increase over CGRP (pIC50 = 5.56 +/- 0.102) (P = 0.0369). Moving the group further to the 2-position reduces AM_1 selectivity further, with SHF1589 displaying 3-fold and 2-fold increase over AM_2 (pIC50 = 5.88 +/- 0.248) (P = 0.0106) and CGRP (pIC50 = 5.74 +/- 0.074) respectively, with the latter not considered statistically significant (P = 0.1130). SHF1591, with the nitrile group positioned in the 5-position, is not significantly selective for AM_1, with potency on all three receptors sitting just below 1 µM (pIC50 (AM_2) = 6.03 +/- 0.168) (P = 0.4979) (pIC50 (CGRP) = 6.06 +/- 0.200) (P = 0.6671). Meanwhile, no significant potency was observed on any of the CLR/RAMP receptors when the nitro group was moved from the 6-position to the 5-position (SHF1592).

Table 5.7 – AM_1, AM_2 and CGRP pIC50 data for SHF1572 analogues

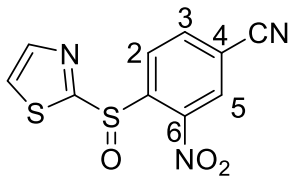

Compound	R-Position	Nitro Position	pIC50 (AM_1) (+/- Std Error)	pIC50 (AM_2) (+/- Std Error)	pIC50 (CGRP) (+/- Std Error)
SHF1572	CN/4	6	6.32 (+/- 0.166)	5.45 (+/- 0.179)	5.33 (+/- 0.142)
SHF1578	COOH/4	6	n.d	n.d	n.d
SHF1581	H/4	6	n.d	n.d	n.d
SHF1588	CN/3	6	6.08 (+/- 0.175)	5.37 (+/-0.102)	5.56 (+/-0.190)
SHF1589	CN/2	6	6.20 (+/- 0.117)	5.88 (+/- 0.248)	5.74 (+/- 0.079)
SHF1591	CN/5	6	6.16 (+/- 0.153)	6.03 (+/- 0.168)	6.06 (+/- 0.200)
SHF1592	CN/4	5	n.d	n.d	n.d

5.5 Docking of SHF1572 and Analogues in CGRP and AM_2

Docking in the CGRP and AM_2 ECDs was carried out in order to get an idea of where these compounds might be binding in the respective receptors. The docking poses of SHF1572 in the CGRP ECD (PDB: 3N7R) predicted the compound to sit at the RAMP1 end of the binding pocket (Figure **5.13**). The sulfoxide oxygen in both enantiomers was predicted to point towards CLR Trp72 and form a hydrogen bond with this residue, whilst the nitro group sat in the space between RAMP1 Trp74 and CLR Arg38, forming a pi-cation interaction and an ionic interaction, respectively. The nitrile group pointed out into the space and was predicted to form no significant interactions.

The docking poses of SHF1578 closely match that of SHF1572 (Figure **5.14**). The compound is predicted to sit in the same area, with the hydrogen bond between the sulfoxide oxygen and CLR Trp72 being retained. In this case the carboxylic acid groups are twisted towards CLR Arg38 and can interact via hydrogen bonds, whilst the nitro group can interact with

both RAMP1 Trp74 and Trp84 via pi-pi and pi-cation interactions. A similar pose is observed for SHF1581, containing neither nitrile nor carboxylic acid groups. It is therefore surprising from these results that both compounds display little potency on CGRP.

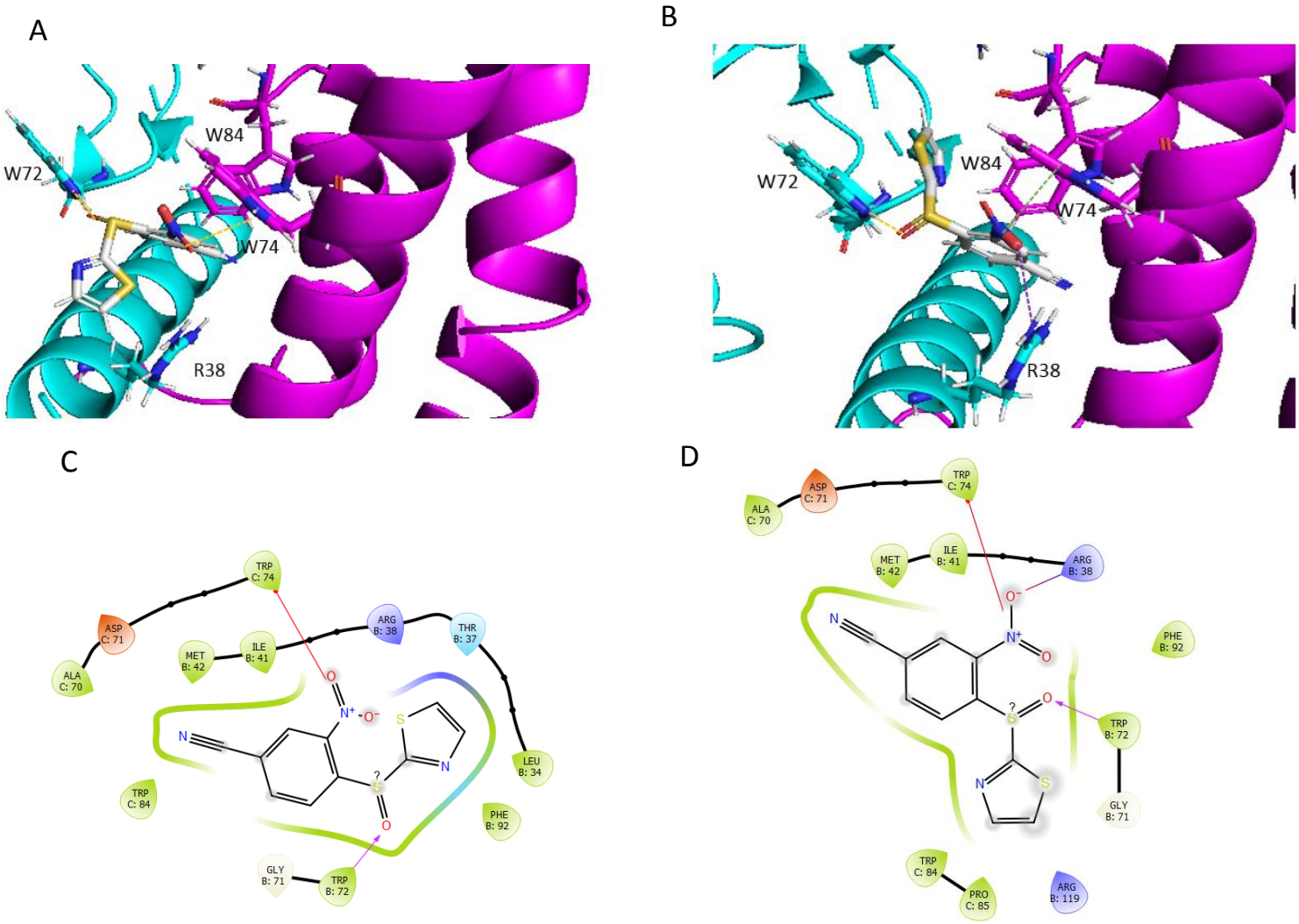

Figure 5.13 - Lowest energy docking pose of SHF1572 (R) enantiomer, (A) and (C), and (S) enantiomer, (B) and (D), bound to the CGRP receptor (PDB: 3N7R). (A) and (B) show the compound docked to the AM_1 receptor ECD. The CLR is coloured in cyan and RAMP1 is coloured in magenta. Hydrogen bonds are indicated by yellow dashed lines, ionic interactions are indicated by purple dashed lines and pi-cation interactions are indicated by green dashed lines. Key residues in the binding pocket are shown and labelled. Docking was carried out using Schrodinger (Maestro 13.2) and the image was generated using PyMol Molecular Graphics System, Version 1.7.4.5- Educational Product, Schrodinger. (C) and (D) show the corresponding 2D ligand interaction diagrams generated from Maestro 13.2. Hydrogen bonds are indicated by purple lines and ionic interactions are indicated by red lines.

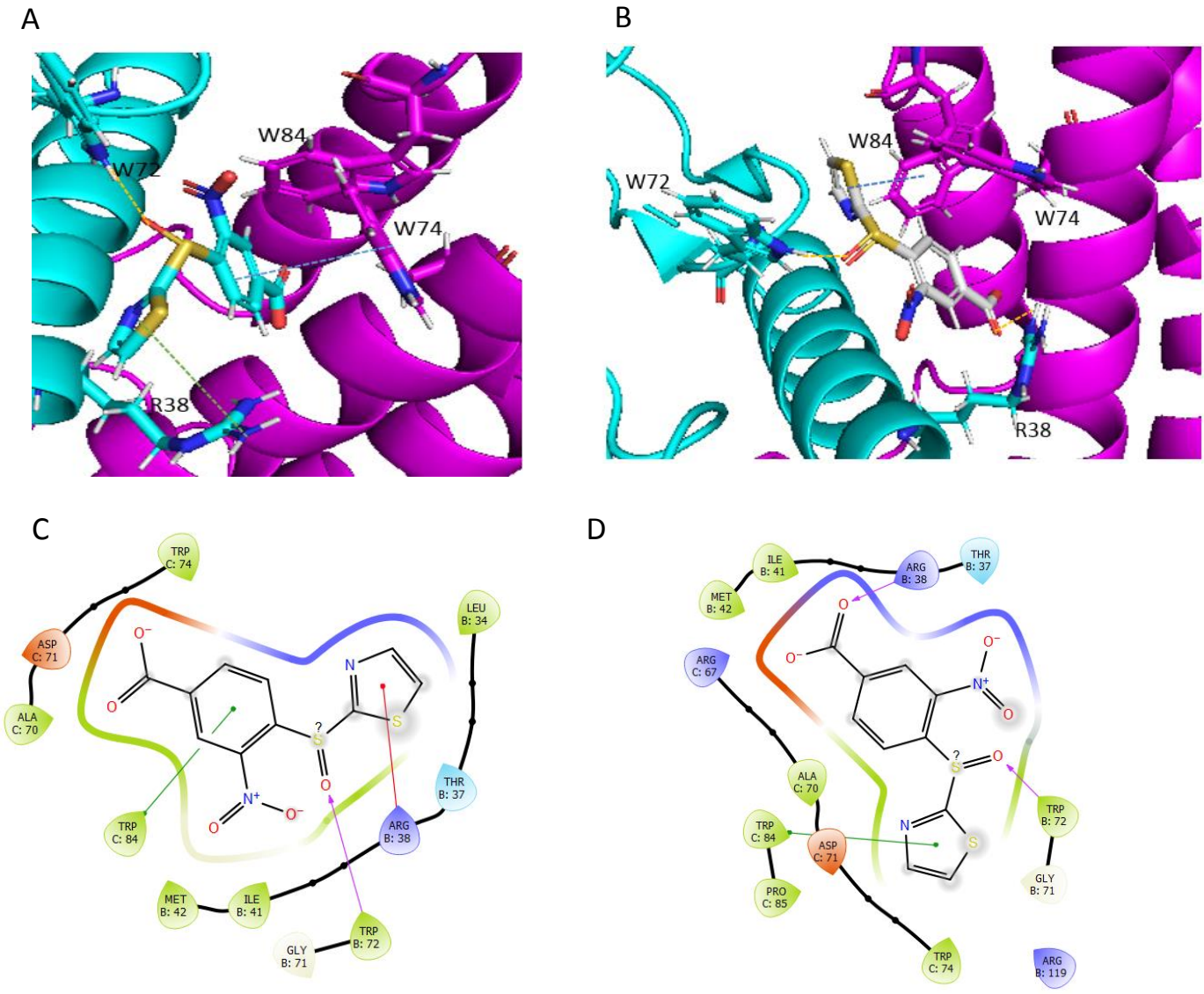

Figure 5.14 - Lowest energy docking pose of SHF1578 (R) enantiomer, (A) and (C), and (S) enantiomer, (B) and (D), bound to the CGRP receptor (PDB: 3N7R). (A) and (B) show the compound docked to the AM_1 receptor ECD. The CLR is coloured in cyan and RAMP1 is coloured in magenta. Hydrogen bonds are indicated by yellow dashed lines, ionic interactions are indicated by purple dashed lines, pi-pi interactions are indicated by blue dashed lines and pi-cation interactions are indicated by green dashed lines. Key residues in the binding pocket are shown and labelled. Docking was carried out using Schrodinger (Maestro 13.2) and the image was generated using PyMol Molecular Graphics System, Version 1.7.4.5- Educational Product, Schrodinger. (C) and (D) show the corresponding 2D ligand interaction diagrams generated from Maestro 13.2. Hydrogen bonds are indicated by purple lines and ionic interactions are indicated by red lines.

The docking pose for SHF1572 was also replicated by positional analogues SHF1588, SHF1589, SHF1591 and SHF1592 (Figure **5.15**) (Figure **5.16**). The sulfoxide groups in all cases

pointed towards CLR Trp72, forming a hydrogen bond with this residue in most cases, whilst, with the exception of SHF1589, the nitrile group pointed towards CLR Arg38, also forming a hydrogen bond with this residue. The nitro group again tended to sit between CLR Arg38 and RAMP1 Trp74, forming interactions with these residues and, in some cases, Trp84 by means of pi-pi or pi-cation interactions. Moving the nitro group *meta* to the sulfoxide substituent appeared to retain these interactions (Figure **5.16**), which was again surprising given the experimental data.

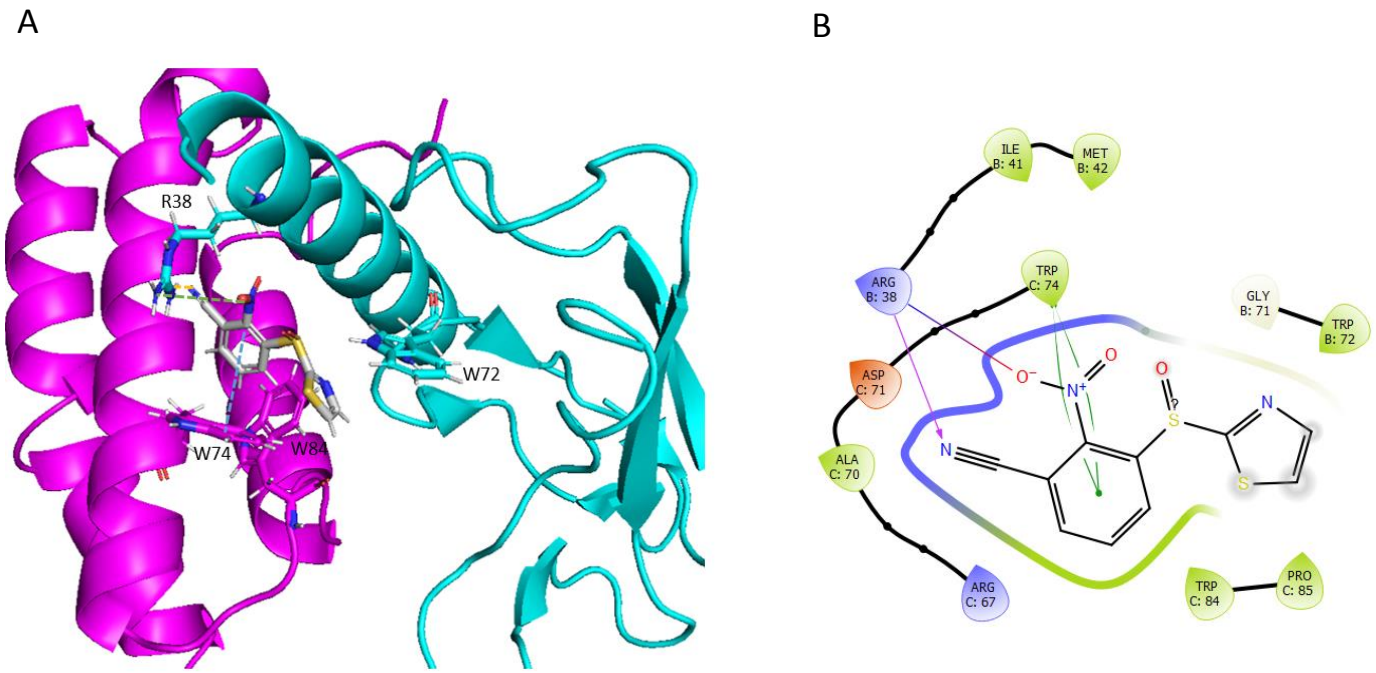

Figure 5.15 - Lowest energy docking pose of the (*R*) enantiomer of SHF1591 bound to the CGRP receptor (PDB: 3N7R). (A) The 3D image of the compound docked into the CGRP receptor ECD. The CLR is coloured in cyan and RAMP1 is coloured in magenta. Hydrogen bonds are indicated by yellow dashed lines, pi-pi interactions are indicated by blue dashed lines and ionic interactions are indicated by green dashed lines. Key residues in the binding pocket are shown and labelled. Docking was carried out using Schrodinger (Maestro 13.2) and the image was generated using PyMol Molecular Graphics System, Version 1.7.4.5- Educational Product, Schrodinger. (B) The 2D ligand interaction diagram generated by Maestro 13.2. Hydrogen bonds are indicated by purple lines, ionic interactions are indicated by red lines and pi-pi interactions are indicated by green lines.

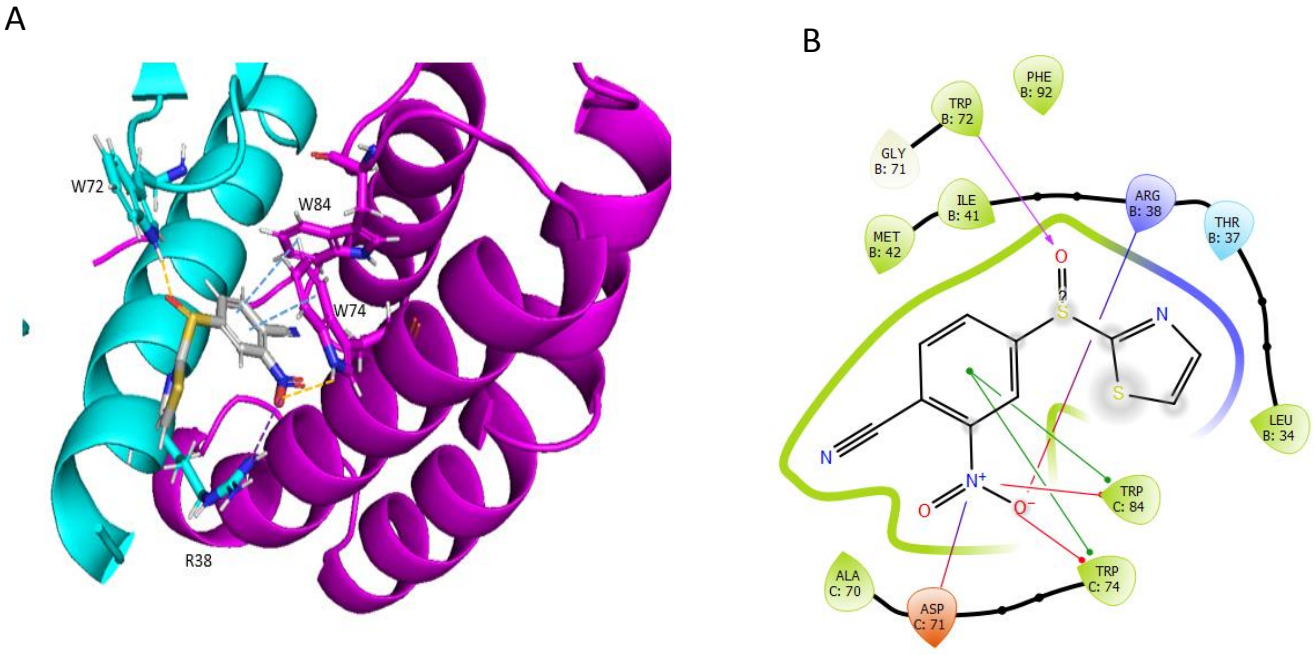

Figure 5.16 - Lowest energy docking pose of the (*R*) enantiomer of SHF1592 bound to the CGRP receptor (PDB: 3N7R). (A) The 3D image of the compound docked into the CGRP receptor ECD. The CLR is coloured in cyan and RAMP1 is coloured in magenta. Hydrogen bonds are indicated by yellow dashed lines, pi-pi interactions are indicated by blue dashed lines and ionic interactions are indicated by green dashed lines. Key residues in the binding pocket are shown and labelled. Docking was carried out using Schrodinger (Maestro 13.2) and the image was generated using PyMol Molecular Graphics System, Version 1.7.4.5- Educational Product, Schrodinger. (B) The 2D ligand interaction diagram generated by Maestro 13.2. Hydrogen bonds are indicated by purple lines, ionic interactions are indicated by red lines and pi-pi interactions are indicated by green lines.

The docking pose of SHF1572 in the AM_2 ECD (PDB: 6UUS) saw the compound sit more towards the CLR binding region, with the thiazole reaching out towards RAMP3 above CLR Trp72 (Figure **5.17**). In this pose, both the nitrile and the nitro group were predicted to hydrogen bond to CLR Thr120 sidechain, with the thiazole forming a pi-pi stacking interaction with Trp72.

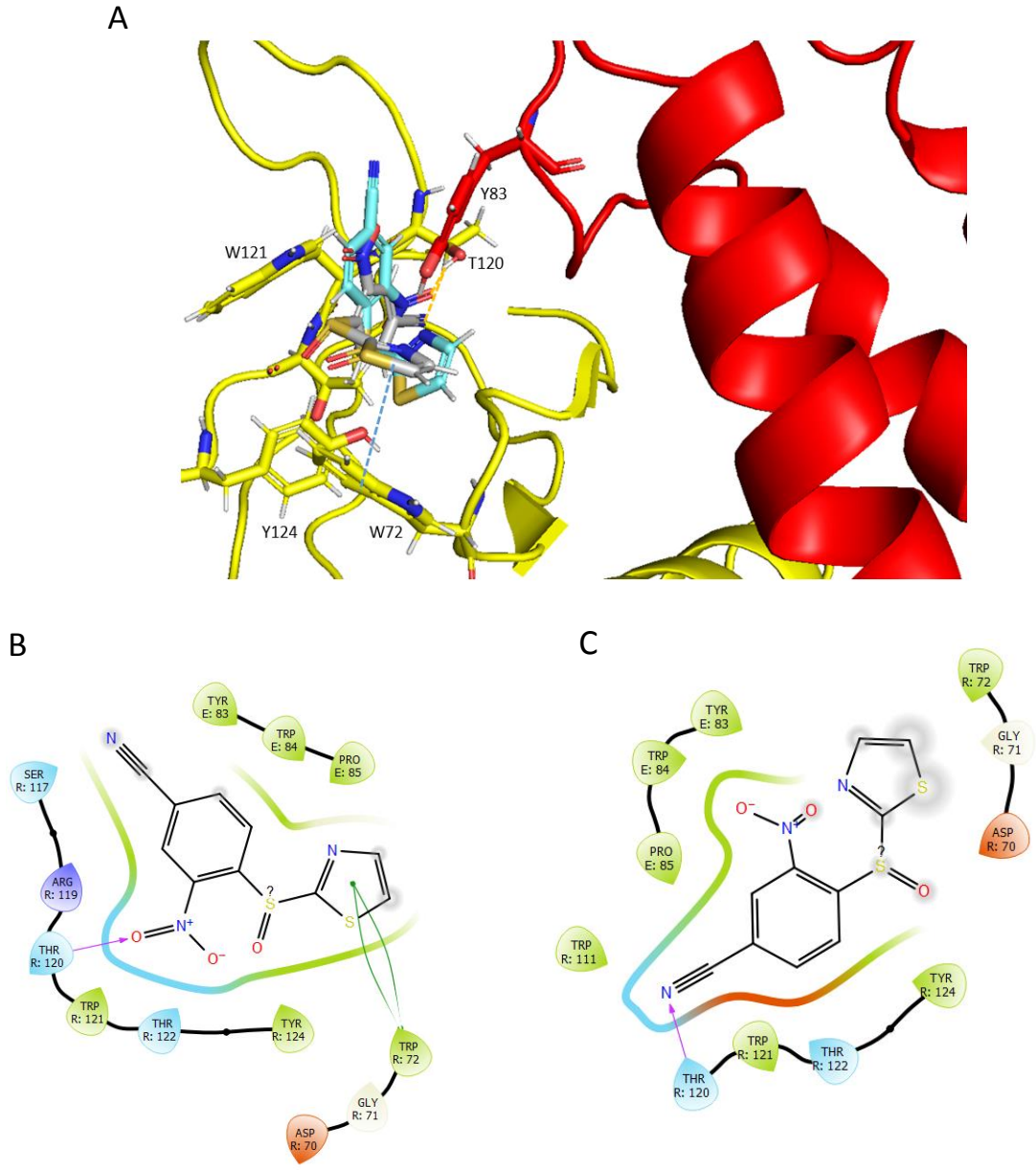

Figure 5.17 - Lowest energy docking pose of SHF1572 bound to the AM_2 receptor (PDB: 6UUS). (A) 3D image of SHF1572 docked into the AM_2 ECD. The CLR is coloured in yellow and RAMP3 is coloured in red. The (*R*) enantiomer is coloured in grey and the (*S*) enantiomer is coloured in light blue. Hydrogen bonds are indicated by yellow dashed lines and pi-pi interactions are indicated by blue dashed lines. Key residues in the binding pocket are shown and labelled. Docking was carried out using Schrodinger (Maestro 13.2) and the image was generated using PyMol Molecular Graphics System, Version 1.7.4.5- Educational Product, Schrodinger. (B) and (C) 2D Interaction diagrams of the (*R*) and (*S*) enantiomers respectively. Hydrogen bonds are indicated by purple lines and hydrophobic interactions are indicated by green lines.

The (*R*) enantiomer of SHF1578 also docked in a similar way, although with the thiazole forming an additional hydrogen bond to RAMP3 Tyr83 and the carboxylic acid group pointing into space (Figure **5.18**). Interestingly, however, the (*S*) enantiomer docked in an alternative region towards the top of the RAMP3 α3 helix. Interactions at this site included hydrogen bonds between the sulfoxide oxygen and CLR N110, the nitro group and CLR N66 and RAMP3 Q90, and the thiazole nitrogen and CLR R113 (Figure **5.18**). Both enantiomers of SHF1581 docked in the same region as (*R*) SHF1578, predicting similar interactions.

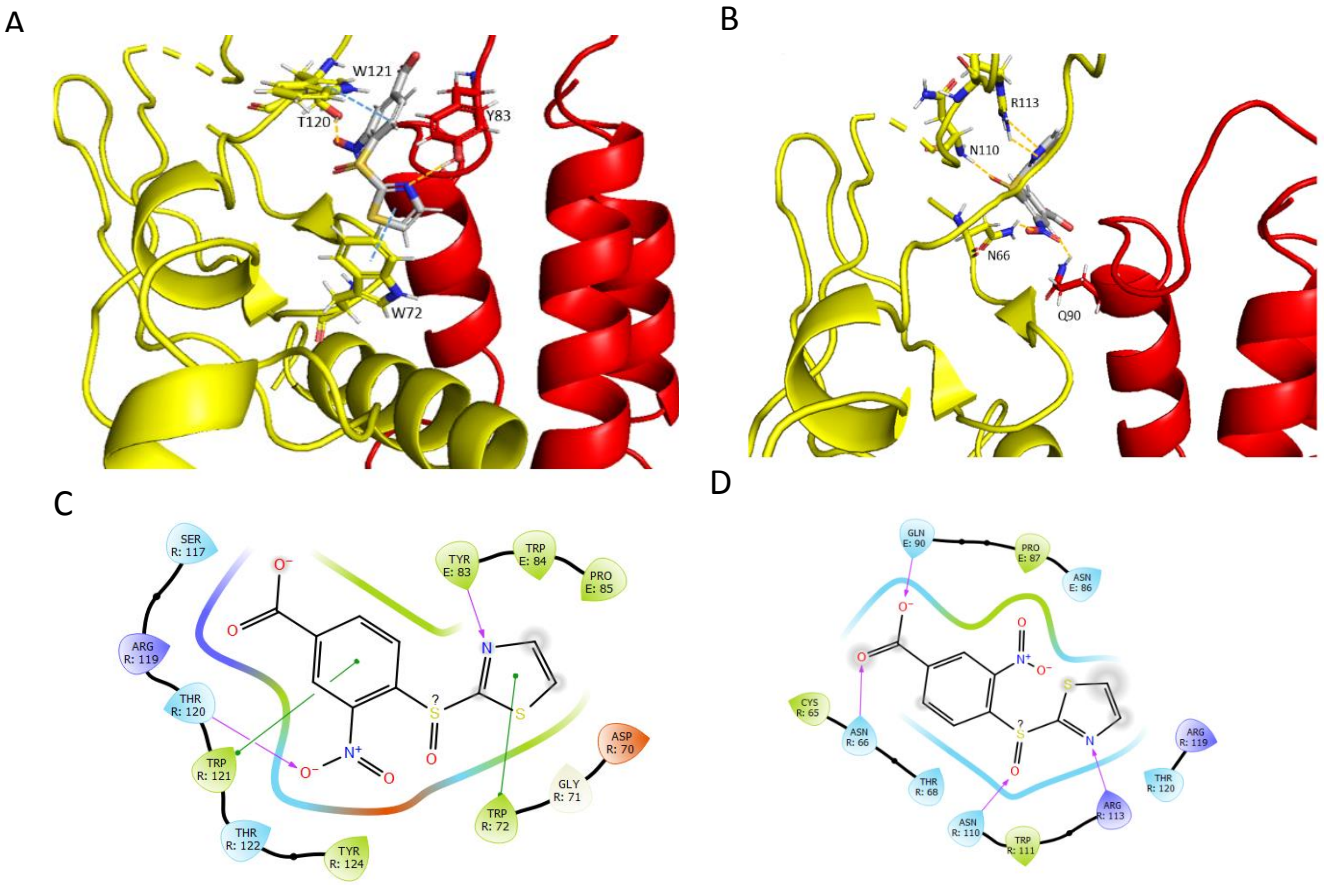

Figure 5.18 - Lowest energy docking pose of SHF1578 (R) enantiomer, (A) and (C), and (S) enantiomer, (B) and (D), bound to the AM_2 receptor (PDB: 6UUS). (A) and (B) show the compound docked to the AM_2 receptor ECD. The CLR is coloured in yellow and RAMP3 is coloured in red. Hydrogen bonds are indicated by yellow dashed lines, pi-pi interactions are indicated by blue dashed lines and pi-cation interactions are indicated by green dashed lines. Key residues in the binding pocket are shown and labelled. Docking was carried out using Schrodinger (Maestro 13.2) and the image was generated using PyMol Molecular Graphics System, Version 1.7.4.5- Educational Product, Schrodinger. (C) and (D) show the corresponding 2D ligand interaction diagrams generated from Maestro 13.2. Hydrogen bonds are indicated by purple lines, ionic interactions are indicated by red lines and hydrophobic interactions are indicated by green lines.

The positional analogues SHF1588, SHF1589, SHF1591 and SHF1592 also all docked in similar positions. Almost all poses predicted the thiazole ring to stretch out towards RAMP3 and stack against CLR Trp72, whilst the phenyl ring would often form pi-pi interactions with CLR Trp121 (Figure **5.19**). CLR Thr120 sidechain was often a key contact point for the compounds, forming hydrogen bonds with the nitrile in SHF1588, SHF1591 and SHF1592, Additional interactions would also be made with RAMP3 in some cases, either by the thiazole nitrogen or the nitro group. SHF1592, in which the nitro group is *meta* to the sulfoxide, only predicts limited contacts with the protein, with only a hydrogen bond between the nitrile and CLR Thr120 observed in the (*S*) enantiomer, and a pi-pi interaction between the phenyl ring and CLR Trp72 in the (*R*) enantiomer (Figure **5.20**). This result seems more consistent with the observed lower potency for SHF1592 from the experimental data.

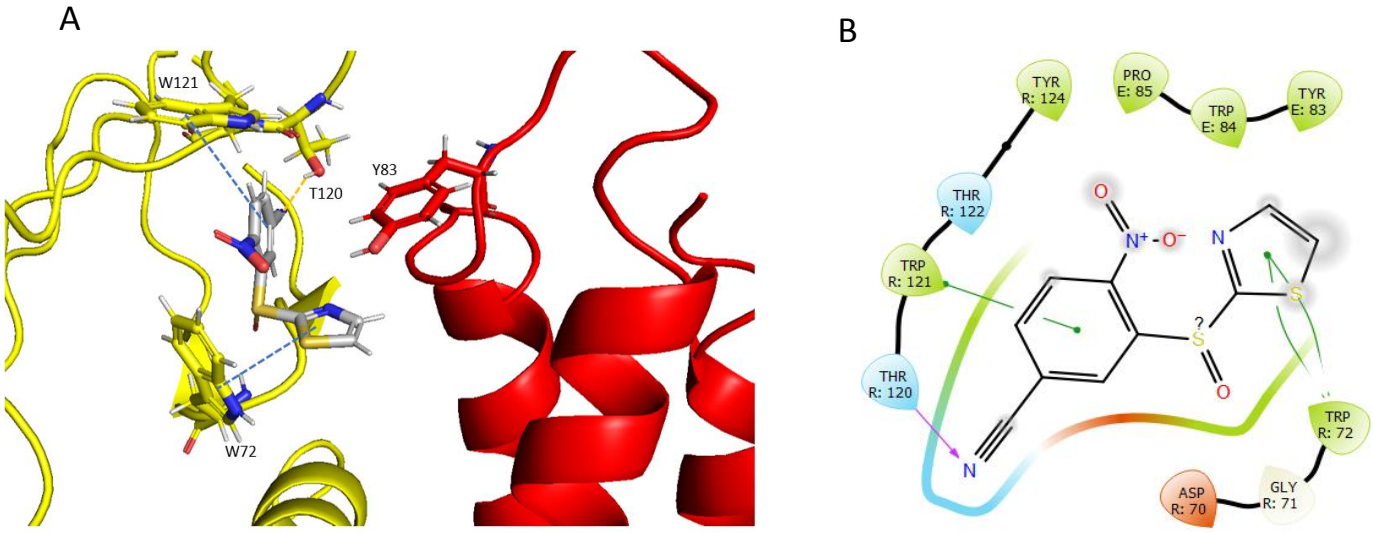

Figure 5.19 - Lowest energy docking pose of the (*R*) enantiomer of SHF1588 bound to the AM_2 receptor (PDB: 6UUS). (A) 3D image of the compound docked into the AM_2 ECD. The CLR is coloured in yellow and RAMP3 is coloured in red. The (*R*) enantiomer is coloured in grey and the (*S*) enantiomer is coloured in light blue. Hydrogen bonds are indicated by yellow dashed lines and pi-pi interactions are indicated by blue dashed lines. Key residues in the binding pocket are shown and labelled. Docking was carried out using Schrodinger (Maestro 13.2) and the image was generated using PyMol Molecular Graphics System, Version 1.7.4.5-Educational Product, Schrodinger. (B) 2D ligand interaction diagram generated from Maestro 13.2. Hydrogen bonds are indicated by purple lines and hydrophobic interactions are indicated by green lines.

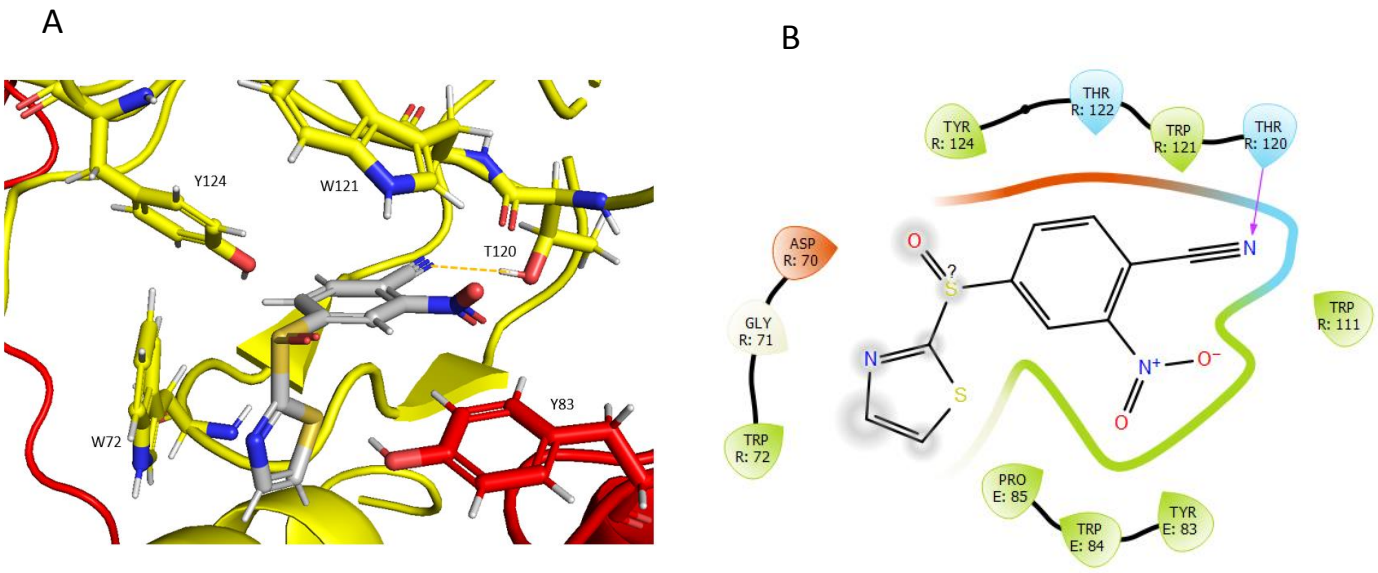

Figure 5.20 - Lowest energy docking pose of the (*S*) enantiomer of SHF1592 bound to the AM_2 receptor (PDB: 6UUS). (A) 3D image of the compound docked into the AM_2 ECD. The CLR is coloured in yellow and RAMP3 is coloured in red. The (*R*) enantiomer is coloured in grey and the (*S*) enantiomer is coloured in light blue. Hydrogen bonds are indicated by yellow dashed lines. Key residues in the binding pocket are shown and labelled. Docking was carried out using Schrodinger (Maestro 13.2) and the image was generated using PyMol Molecular Graphics System, Version 1.7.4.5- Educational Product, Schrodinger. (B) 2D ligand interaction diagram generated from Maestro 13.2. Hydrogen bonds are indicated by purple lines.

5.6 Conclusion

To summarise, SHF1572, a low molecular weight fragment of SHF1556 was found to retain most AM_1 potency compared to SHF1556. SAR studies on this fragment have revealed that hydrolysing or deleting the nitrile kills most of the potency of the compound, whilst varying the nitrile substituent position retains potency. Potency was further found to significantly decrease when the position of the nitro substituent changed, indicating the importance of the nitro group in this position in both SHF1572 and possibly SHF1556. SHF1572 displayed reasonable selectivity for AM_1 over CGRP and AM_2, with this selectivity mostly being matched when the position of the nitrile substituent was changed.

Chapter 6 – General Discussion

Chapter 6: General Discussion

The aim of this study was to discover and develop a class of small molecule antagonist against the AM_1 receptor. A potent AM_1 receptor antagonist has, to our knowledge, yet to be reported in the literature despite the identification of antagonists for the closely related receptors CGRP and AM_2. Based on previous reports of the pharmacology of both AM and it's receptors, it is thought that the AM_1 receptor is heavily linked to AMs role as a potent vasodilator, which is particularly problematic during septic shock. Therefore antagonising the AM_1 receptor could arrest the dramatic blood pressure drop seen in patients with septic shock by raising blood pressure to normal levels before allowing the initial infection to be treated. A potent AM_1 antagonist could also aid further understanding into the role of this receptor in other physiological and pathophysiological processes.

There were two different strategies used in this study to find hit compounds for AM_1. One strategy used the structure of previously discovered CGRP and AM_2 antagonists, as well as some structural features of the AM_1 ECD to find potent compounds, whilst the other strategy was to generate a series of hits using the method of high throughput screening carried out by the European Lead Factory. Although the former strategy failed to yield any potent compounds, the latter generated some promising hit structures which led to the identification of SHF1556 as a lead compound. SAR studies on this compound have identified key functional groups in the structure that are required for potency, whilst also leading to the discovery of a lower molecular weight fragment SHF1572, with this compound retaining the majority of SHF1556 AM_1 potency despite its smaller structure.

6.1 Fragments Containing CLR Binder SHF355 Display No Potency on AM_1

Candidate antagonists for the AM_1 receptor were initially designed based on the structures of previous CGRP and AM_2 antagonists. It was hypothesised that as each receptor contains the same CLR unit but a different RAMP unit, using known CLR binding fragments coupled to various potential RAMP binding fragments would lead to a potent AM_1 antagonist. It was therefore decided to use the known CLR binding fragment SHF355, which is present in the lead AM_2 antagonist (Avgoustou, Jailani et al., 2020) (Zirimwabagabo, Jailani et al., 2021)

and couple this to various carboxylic acids, esters or amines that could serve as potential RAMP2 binding fragments, with particular focus on targeting RAMP2 Ser94 for selectivity. However, despite the presence of SHF355, none of the compounds displayed any significant potency towards AM_1. A variety of functional groups at the RAMP end were screened but to no avail. These data could suggest that this CLR binding fragment may not be optimal in the AM_1 binding pocket.

The crystal structure of the AM_1 ECD has previously been resolved (Kusano, Kukimoto-Niino et al., 2012), enabling molecular docking of compounds in this structure. The crystal structure of previous CGRP antagonist Telcagepant has also been co-crystallised in the CGRP receptor ECD (ter Haar, Koth et al., 2010), allowing a useful comparison between the binding poses of these antagonists with the predicted docking poses of the SHF355 based compounds in the AM_1 ECD.

Telcagepant binds to CGRP such that the carbonyl and amide groups in its azabenzimidazole moiety form hydrogen bonds with the CLR Thr122 main chain, with the compound then extending outwards towards the CLR-RAMP1 interface (ter Haar, Koth et al., 2010). As SHF355 retains these hydrogen bond acceptors in CLR binding region of Telcagepant, it could also be reasoned that this series of compounds would bind to AM_1 in a similar way. However, according to the docking, this binding pose is predicted to be unfavourable in AM_1. This is likely due to the presence of the large RAMP2 Arg97 residue, not conserved in RAMP1 (Kusano, Kukimoto-Niino et al., 2008) (ter Haar, Koth et al., 2010), which effectively obstructs the CLR-RAMP interface of the pocket (Kusano, Kukimoto-Niino et al., 2012) (Figure **6.1**). Docking of compounds in this pose would therefore lead to unfavourable steric clashes with this residue. There is also the additional problem of the salt bridge between Arg97 and E101, which would be difficult to overcome. This could explain why this series of compounds display very little antagonistic potency at the AM_1 receptor.

The equivalent residues on RAMP1 and RAMP3 are Ala70 and Thr70 respectively, meaning this area of the binding pocket in both CGRP and AM_2 is more open. This implies that this series of compounds would be able to bind to these receptors in a similar manner to Telcagepant at CGRP, with the SHF355 end able to interact with CLR Thr122 main chain as designed. This additionally suggests that the shape of the CGRP and AM_2 binding pockets are more similar as compared to that of AM_1, with this being further backed up by the fact

that the lead AM_2 antagonists also show strong potency towards CGRP whilst displaying very little potency for AM_1 (Zirimwabagabo, Jailani et al., 2021). Although not designed for these receptors, it would be interesting to see whether the SHF355 series of compounds displays any potency at CGRP or AM_2.

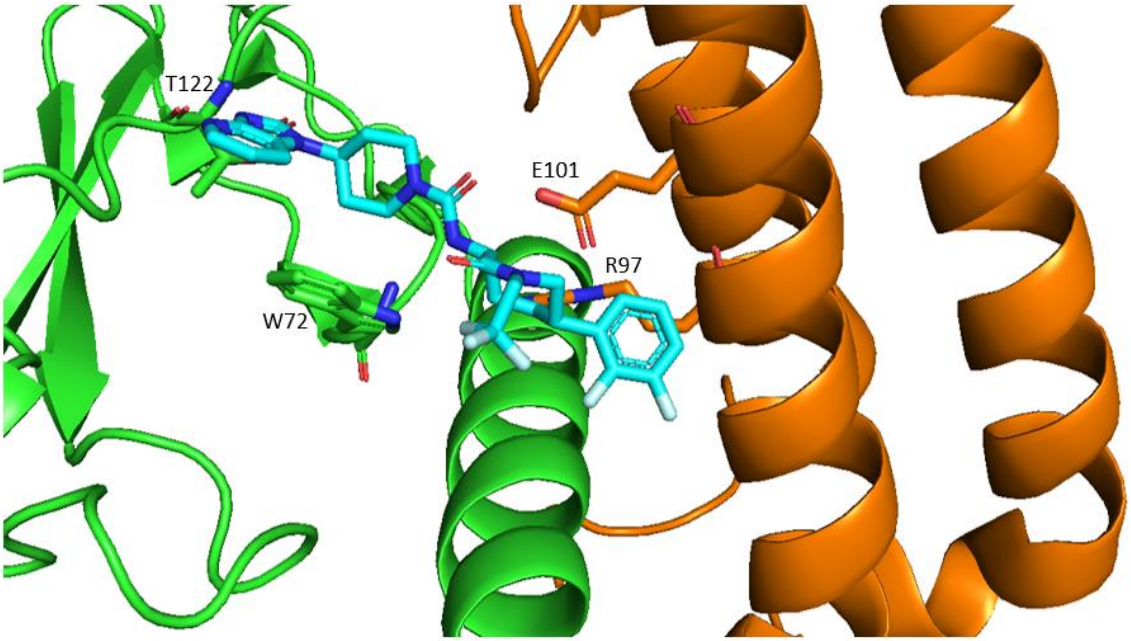

Figure 6.1 – The binding mode of CGRP antagonist Telcagepant superimposed on the AM_1 ECD. Image was created by superimposing the crystal strucuture of Telcagepant bound to CGRP (PDB: 3N7R) with the AM_1 ECD (3AQF) to highlight the potential steric clash between this compounds binding mode and RAMP2 Arg97. CLR is coloured in green and RAMP2 is coloured in orange. Key residues are shown and labelled. Image was generated using PyMol Molecular Graphics System, Version 1.7.4.5- Educational Product, Schrodinger.

6.2 SHF1556 is a Promising Lead AM_1 Antagonist

The high throughput screening results from the European Lead Factory led to the discovery of some interesting hit structures. One such compound was SHF1486, displaying sub micro molar potency on the AM_1 receptor. From this structure, SHF1556 was identified. SHF1556 is the most potent AM_1 antagonist to date, displaying antagonistic potency of around 100 nM. This demonstrates a very promising lead compound for the discovery of further antagonists at this receptor.

SHF1556 was identified from the literature due to the structural similarities with SHF1486 (Aiyar, 2000). Comparing the two structures, one could assume that the thiazole ring in

SHF1556 is equivalent to the phenyl ring in SHF1486, the sulfoxide in SHF1556 is equivalent to the sulfone in SHF1486, whilst the nitro group in SHF1556 could be equivalent to the N-O group on the 5-membered heterocycle in SHF1486 (Figure **6.2**). Intriguingly, replacing the sulfoxide in SHF1556 with a sulfone led to a significant drop in potency, while SHF1486 displays sub micro molar potency (IC50 = 320 nM) despite the presence of a sulfone group (Figure **6.2**). Hence, it would be interesting to see whether replacement of the sulfone with the sulfoxide in SHF1486 boosts the potency of this compound. It is also worth noting that the structures of both SHF1556 and SHF1486 are different to the gepant series of CGRP antagonists (Rudolph, 2005) (Panone, 2007) (ter Haar, Koth et al., 2010) and the current lead AM_2 antagonists (Avgoustou, Jailani et al., 2020) (Zirimwabagabo, 2021) which has therefore led to the discovery of a different class of CLR/RAMP antagonists.

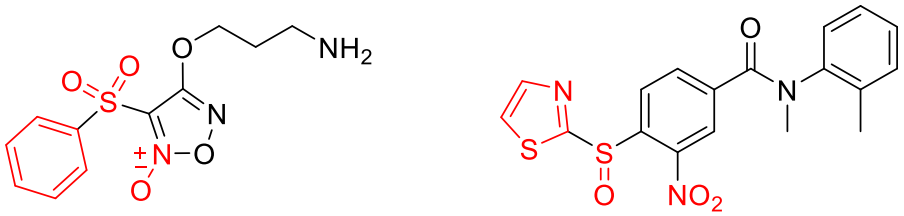

SHF1486 **SHF1556**

Figure 6.2 – Structural comparisons of SHF1486 and SHF1556. Equivalent groups are highlighted in red.

The enantiomers of SHF1556 have also been resolved and separated, with the (*S*) enantiomer proving to be the most potent on AM_1, matching the potency of racemic SHF1556. Interestingly, the (*R*) enantiomer is only around 5-fold less potent than the (*S*) enantiomer, retaining a significant amount of potency. This result is somewhat surprising, given the importance of the sulfoxide group for AM_1 potency, although the docking suggests that this could be compensated for by interactions from both the amide carbonyl and the nitro group in the (*R*) enantiomer. It would be interesting to co-crystallise the AM_1 ECD with each of the enantiomers to view the positions in which the two enantiomers bind in the receptor, as well as to aid future structure based drug design for this compound. The isolation of the separate enantiomers make this compound more ideal for a drug like compound due to the possible pharmacological effects of the two enantiomers.

SHF1556 displays modest selectivity over CGRP and AM_2 (4-fold and 2-fold respectively), with potency for both receptors also in the sub micro molar range. Whilst it would be ideal

for the compound to display greater selectivity for AM_1, the biggest priority for use of the antagonist in the clinical treatment of septic shock would be to raise and maintain blood pressure levels to allow the initial infection to be treated. Therefore the potency of the compound would be of higher priority than the selectivity in this case. It was also found that the (*S*) enantiomer was also the more potent on CGRP, matching that seen for AM_1, whilst the stereochemistry of the more potent enantiomer is reversed for AM_2 with the (*R*) enantiomer exhibiting higher potency than the (*S*) enantiomer.

6.3 Molecular Docking Studies Predict a Unique Binding Mode

The binding mode of SHF1556 to the AM_1 receptor is currently unclear as there is no crystal structure of the compound bound to the receptor available. However, use of molecular docking can aid in prediction and speculation as to how SHF1556 could be binding to the AM_1 ECD. Interestingly, the predicted binding mode of SHF1556 is different to that observed with the gepants at CGRP. The compound is predicted to dock across the CLR, within a region between CLR residues Trp72 and Arg119, containing Trp72, Tyr124, Thr122, Trp121, Thr120 and Arg119 (Figure **6.3**) (Figure **6.4 A**). This is in contrast to Olcegepant and Telcagepant, which bind to the CLR Thr122 main chain and then extend outwards towards the CLR-RAMP interface. The docking poses of the SHF355 analogues suggest that, due to the limited space of the AM_1 binding pocket, compounds are unlikely to bind to AM_1 in the same way as the gepant series of compounds in CGRP. This alternative binding mode could therefore explain why the SHF1556 series of compounds are able to display potent AM_1 antagonism.

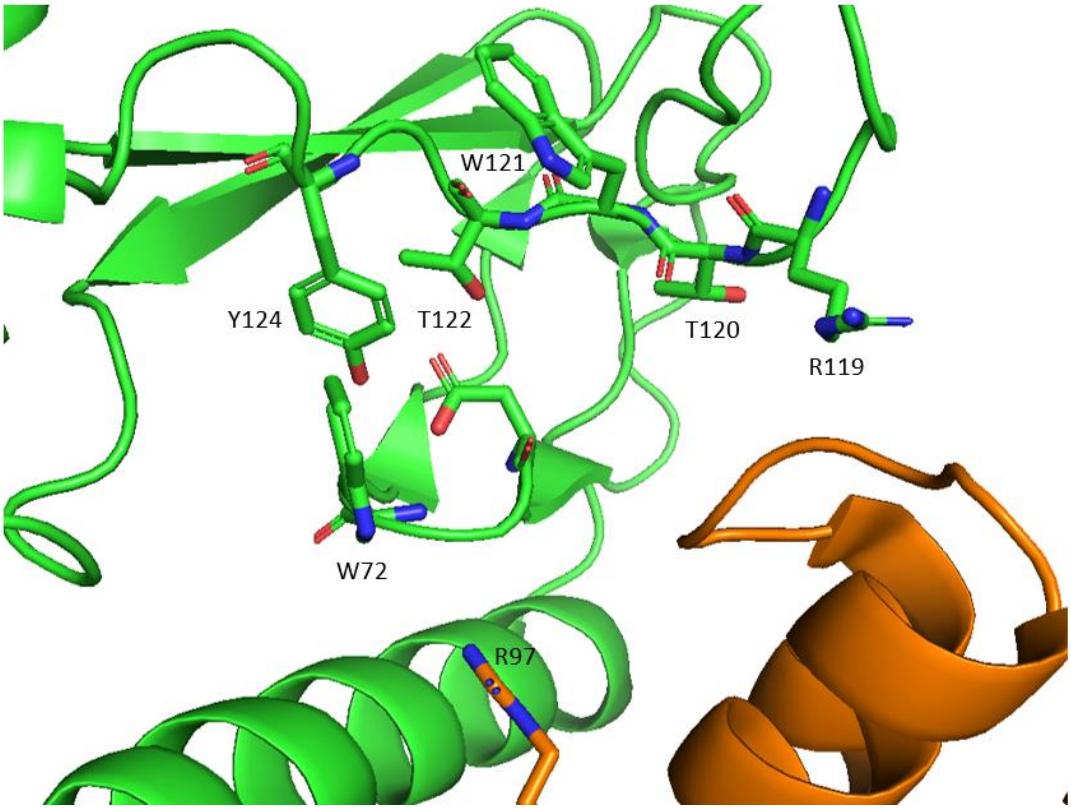

Figure 6.3 – Crystal Structure of the AM_1 ECD (PDB: 3AQF) with specific focus on the SHF1556 binding region. CLR is coloured in green and RAMP2 is coloured in orange. Key residues are shown and labelled. Image was generated using PyMol Molecular Graphics System, Version 1.7.4.5- Educational Product, Schrodinger.

SHF1486 is predicted to dock in a similar manner to SHF1556, across the CLR binding region. Predicted interactions between this compound and the receptor are similar to that predicted for the SHF1556 series of compounds, with the sulfone oxygen and nitro groups interacting with CLR residues Thr122 and Asp70 respectively. An interesting observation of this docking pose is that the extended alkyl amine chain is able to reach down towards RAMP2 and interact with Glu101 and Glu105 via hydrogen bonding. This could suggest a

means of boosting the potency of SHF1556 by adding a similarly flexible amine chain to target these RAMP2 residues.

The docking poses of SHF1556 to the CGRP receptor, on the other hand, more closely resemble that of the gepant family of compounds (Figure **6.4 B**). The potency of SHF1556 on CGRP was around 4-fold lower than on AM_1, suggesting that this alternative pose is less effective for receptor antagonism and could therefore possibly explain the modest selectivity for AM_1 over CGRP. It is surprising that the SHF1556 series of compounds do not dock in the same way in CGRP as in AM_1 due to the presence of the same CLR residues in this region. A possible explanation of this could be due to allosteric modulation of the RAMPs on CLR conformation. Upon superimposing both ligand bound and unbound structures of AM_1 and CGRP, one big difference is the position of the Arg119 residue which forms the border of the SHF1556-AM_1 binding region (Figure **6.5**). In CGRP, this residue points inwards towards the space in this region, therefore decreasing the size of the binding pocket. Consequently, this space would become too small for the compound to bind in, forcing it to adopt the alternative pose observed for CGRP. This same docking pose is also observed for SHF1556 on AM_2, although it is less certain as to why the compound prefers to dock in this way due to the poorly resolved AM_2 ECD.

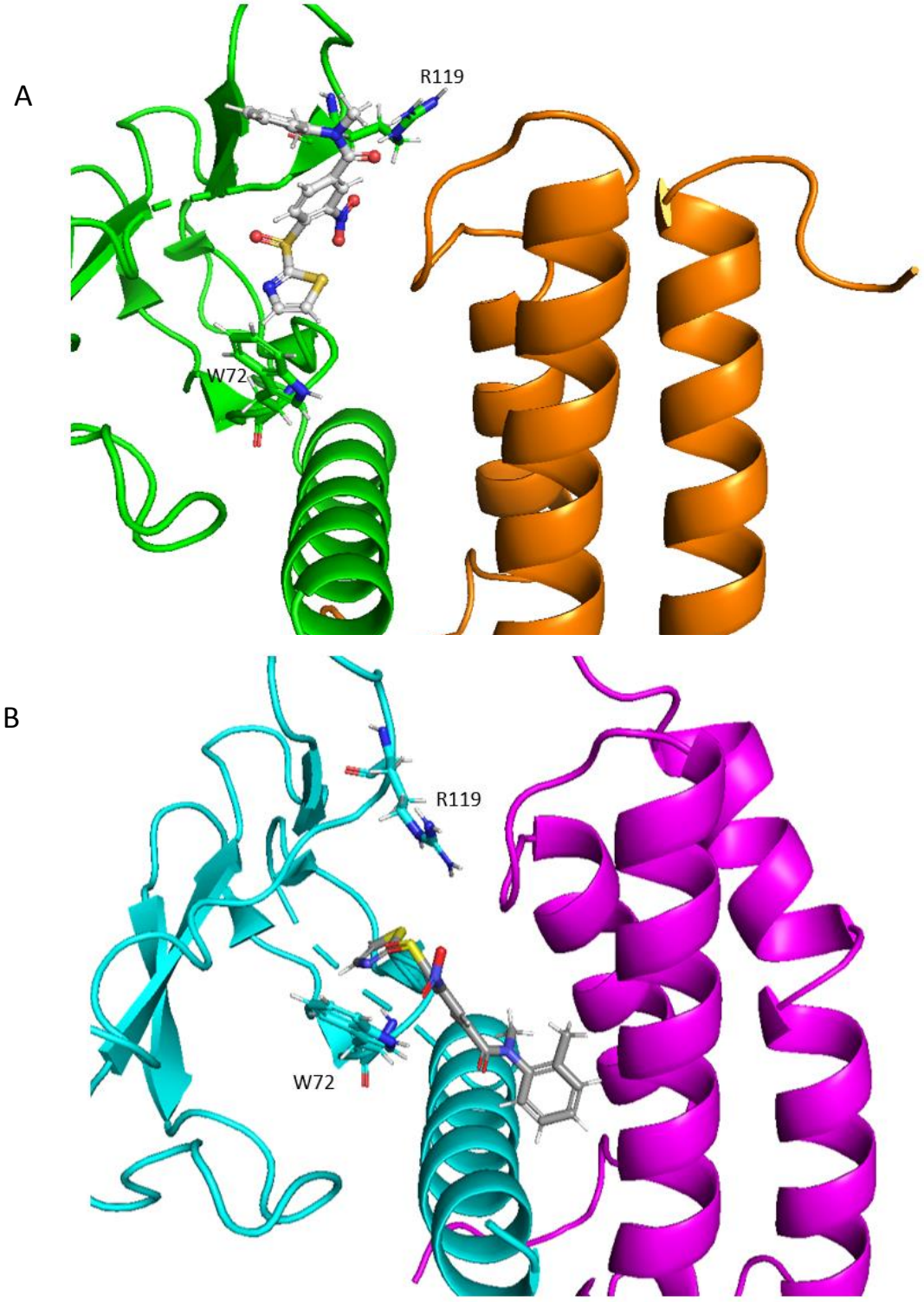

Figure 6.4 – Comparison of the docking poses of SHF1556 on AM_1 ECD (PDB: 3AQF) (A) and CGRP (PDB: 3N7R) (B). For AM_1 (A) CLR is coloured in green and RAMP2 is coloured in orange. For CGRP (B) CLR is coloured in cyan and RAMP1 is coloured in magenta. Compound is coloured in grey in both cases. Image was generated using PyMol Molecular Graphics System, Version 1.7.4.5- Educational Product, Schrodinger.

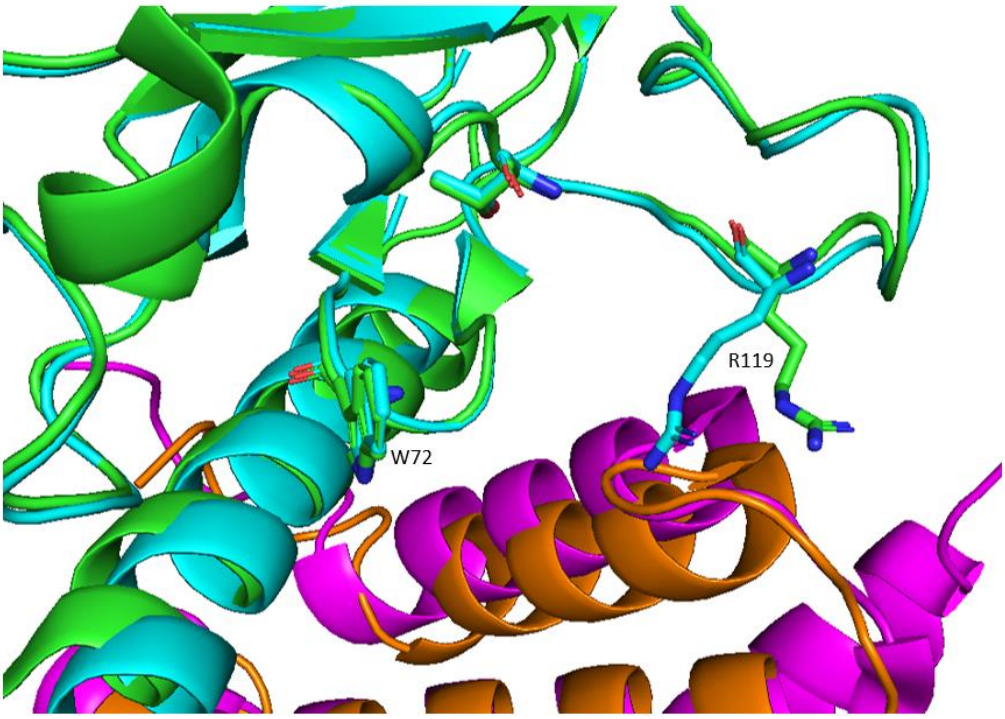

Figure 6.5 – Comparison of the position of Arg119 residue in unbound AM_1 ECD (PDB: 3AQF) and CGRP ECD (PDB: 3N7P). Image was created by superimposing the AM_1 ECD on the CGRP ECD. For AM_1 CLR is coloured in green and RAMP2 is coloured in orange. For CGRP CLR is coloured in cyan and RAMP1 is coloured in magenta. Image was generated using PyMol Molecular Graphics System, Version 1.7.4.5- Educational Product, Schrodinger.

6.4 Drug-like Properties of SHF1556

SHF1556 shows promising properties as a potential drug-like compound. Lipinski's rule of 5 for a drug-like compound states that the compound must have a molecular weight of less than 500, have no more than 5 hydrogen bond donors, have no more than 10 hydrogen bond acceptors and have a log P value of less than 5 (Lipinski, 1996). All criteria of Lipinski's rule of 5 are obeyed in this case, as the compound has a molecular weight of 401 Da, no hydrogen bond donors, 7 hydrogen bond acceptors and a calculated log P value of 3.7. However, as mentioned above, the likely clinical route of admission for this compound would be via intravenous drip due to the urgent need to raise the dangerously low blood pressure levels in patients suffering from septic shock. This means the drug would be likely be introduced straight into the blood stream rather than the oral route. Therefore the key pharmacokinetic considerations would be parameters such as metabolism, plasma protein

binding and excretion. SHF1556 displays good antagonistic potency at the AM_1 receptor and it would be interesting to investigate its efficacy *in vivo* in raising blood pressure from AM induced hypotension.

6.4 SAR Studies on SHF1556 reveal key groups required for potency

Structure activity relationship studies on SHF1556, aided by analogue synthesis, have revealed a key role for the sulfoxide in AM_1 potency. The corresponding sulfide analogue of SHF1556 displays no potency at AM_1, whilst the sulfone analogue sees a significant drop in potency. These observations align well with the observed docking poses of this series of compounds, in which the sulfoxide oxygen forms a hydrogen bond with the protein in most cases. This interaction occurs most frequently with the CLR Thr122 main chain, whilst interactions have also been frequently observed with Tyr124 main chain and Arg119 side chain. All other sulfide analogues of this compound class that were tested exhibited no activity at AM_1, further highlighting the importance of the sulfoxide group on this series.

Despite the lack of AM_1 potency, the corresponding sulphide (SHF1555) shows around 1 µM potency on both AM_2 and CGRP. This makes sense from molecular docking studies, with the docking poses of SHF1556 at CGRP and AM_2 predicting the sulfoxide oxygen to make no significant interactions with the protein. Curiously, every other sulfide analogue tested on AM_2 and CGRP shows no potency at these receptors. It is currently unclear as to why only the sulfide analogue of SHF1556 is the only such analogue to exhibit any AM_2 and CGRP potency.

The nitro group also appears to be significant for SHF1556 AM_1 activity. Reduction of the nitro group to the corresponding aniline completely reduces potency, whilst it also appears that moving the nitro group from the *ortho* to the *meta* position relative to the sulfoxide substituent on the corresponding nitrile compound also dramatically reduces potency. This observation also aligns well with the observed docking poses for these compounds, with the poses frequently predicting the nitro group to associate with CLR Asp70 via ionic interactions, and CLR Trp72 by pi-cation interactions. Such a dramatic drop in potency appears surprising for the aniline analogue SHF1574, due to its ability to form hydrogen bonds with nearby residues. An explanation for this could be the anilines potential ability to form an intramolecular hydrogen bond with the sulfoxide, forming a stable 6-membered

structure. Such an interaction could alter the conformation of the molecule and prevent the key groups from interacting with the protein.

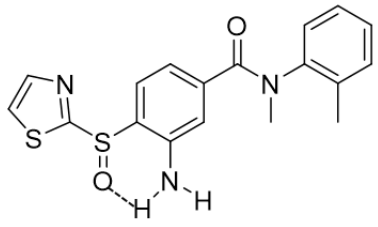

Figure 6.6 – Possible intramolecular hydrogen bonding within the structure of SHF1574. Hydrogen bond is indicated with a dashed line.

Modifications made to the structure of SHF1556 to date have not yielded a compound with greater AM_1 potency. In cases where the molecule increased in size due to factors such as increased aromatic ring size in place of the thiazole, or the introduction of methoxy/ethoxy substituents on the amide side, AM_1 potency appeared to slightly drop whilst leading to higher selectivity for CGRP and/or AM_2. These observations suggest that increases in the size of the compound are less tolerable on AM_1 than CGRP/AM_2, which would imply molecules of smaller sizes are more favourable at this receptor.

6.5 SHF1556 Fragment SHF1572 Retains Majority of AM_1 Potency

SHF1572 is a low molecular weight fragment of SHF1556, with a small nitrile group substituting the amide motif on the right-hand side of the molecule. Notably, this compound maintains the important sulfoxide and nitro groups. This fragment interestingly retained 91% of SHF1556 potency when tested directly against this compound, highlighting the discovery of a small, potent AM_1 antagonist as well as highlighting the importance of the left-hand side fragment of SHF1556.

SHF1572 also appears to show greater selectivity for AM_1 over CGRP, showing a 7-fold and 10-fold decrease in potency for the respective receptors. Molecular docking studies on SHF1572 at AM_1, AM_2 and CGRP receptor ECDs predicted similar binding modes as those seen for SHF1556 at the respective receptor. Whilst SHF1572 could comfortably sit in the same region as seen for SHF1556 at AM_1 (Figure **6.7 A**), the compound was often too small

to occupy the whole binding region seen for CGRP and AM_2 (Figure **6.7 B**), with the compound often docking exclusively either at the RAMP side or the CLR side for these receptors. This could possibly explain the increase in selectivity for AM_1, whilst further implying that a smaller compound would be more beneficial for AM_1 potency.

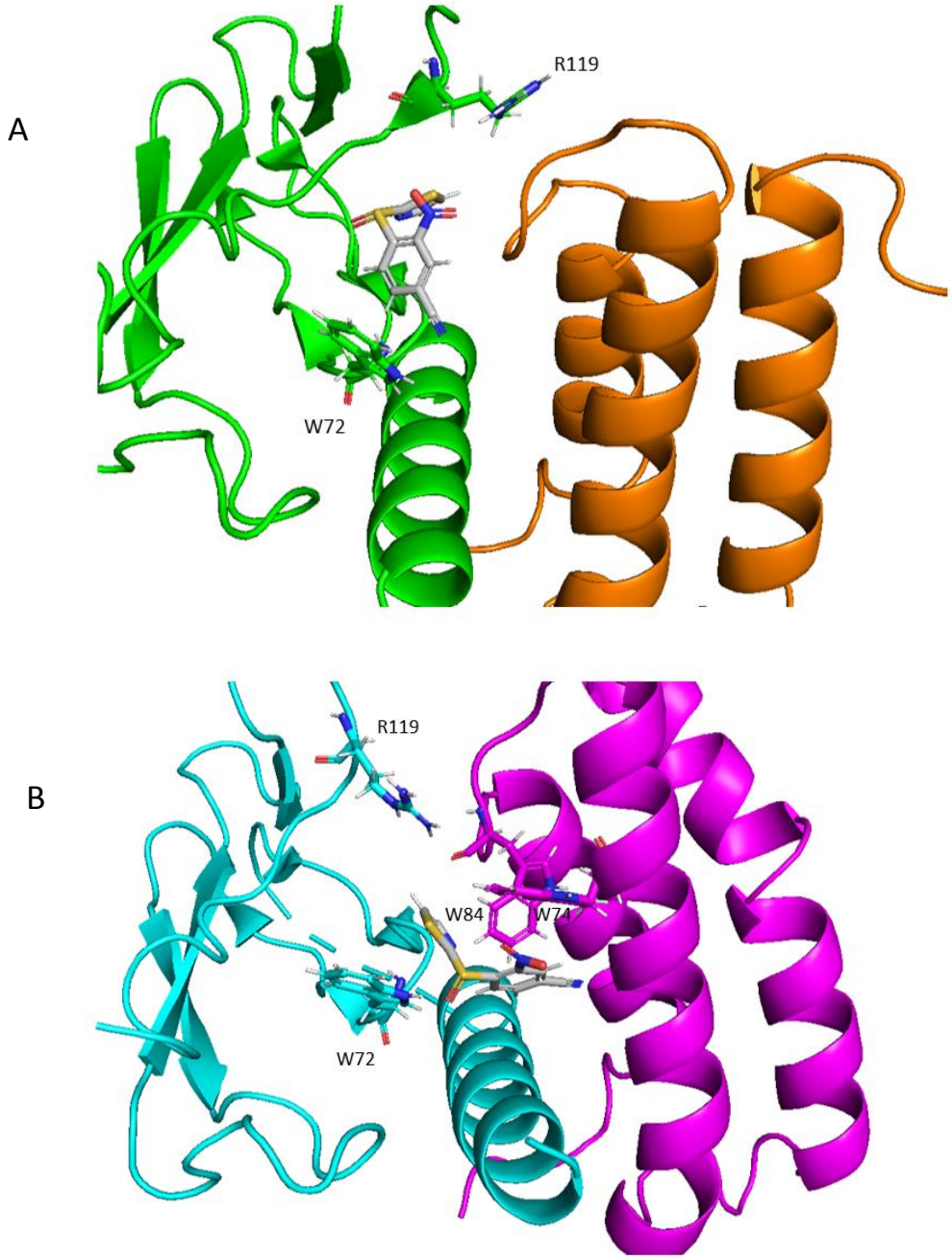

Figure 6.7 - Comparison of the docking poses of SHF1572 on AM_1 ECD (PDB: 3AQF) (A) and CGRP (PDB: 3N7R) (B). For AM_1 (A) CLR is coloured in green and RAMP2 is coloured in orange. For CGRP (B) CLR is coloured in cyan and RAMP1 is coloured in magenta. Compound is coloured in grey in both cases. Image was generated using PyMol Molecular Graphics System, Version 1.7.4.5- Educational Product, Schrodinger.

The SAR of SHF1572 investigated to date has been somewhat complicated. Studies have so far indicated that hydrolysis of the nitrile to the carboxylic acid significantly reduces potency at AM_1 despite the promise of this analogue from molecular docking studies, whilst deleting the nitrile completely also has the same effect. Furthermore, whilst changing the substituent position of the nitrile group broadly retained the potency seen with SHF1572, movement of the nitro group *meta* to the sulfoxide significantly decreased activity. The latter observation could further highlight the importance of the nitro group being *ortho* to the sulfoxide. It would be interesting to further investigate the SAR of this compound class, possibly by replacing the nitrile group with groups also containing hydrogen bond acceptors such as alcohols or amines. Due to the retained activity of SHF1572 analogues arising by changing the position of the nitrile substituent, it could also be interesting to incorporate the amide group seen in SHF1556 and compare the potencies of this amide at different positions (Figure **6.8**).

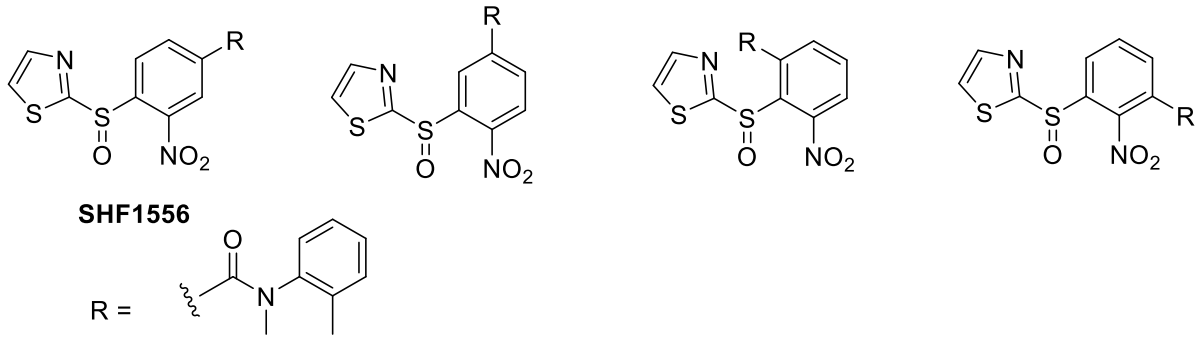

Figure 6.8 – Representation of possible positions on the SHF1572 fragment to incorporate the amide motif present in SHF1556.

6.6 Conclusion and Future Work

To conclude, these data show we have discovered a potent small molecule antagonist, SHF1556, for the AM_1 receptor (IC50 = 100 nM), which has been established as a suitable lead compound in this regard. This compound also displays modest selectivity over the closely related CGRP and AM_2 receptors We have additionally isolated the active enantiomer of this compound and found the stereochemistry of this enantiomer to be (*S*).

We have also established useful SAR for this structure, with the sulfoxide and nitro groups proving to be key to AM_1 activity. From the SAR, we have also established a novel, low molecular weight fragment of SHF1556, namely SHF1572 which retains the majority of the potency of SHF1556 whilst somewhat improving selectivity. The potency of both compounds demonstrates their potential as use as clinical drugs for the treatment of septic shock, whilst also providing plenty of opportunity for structural modification to further optimise potency and selectivity.

Future work could involve investigating the *in vivo* efficacy of SHF1556 as a treatment of septic shock by measuring how effectively it can raise blood pressure from AM induced hypotension. Further SAR studies can also be carried out from the structure of SHF1556, as it would also be interesting to replace the thiazole ring with saturated rings or heterocycles, or alkyl groups to further investigate the importance of this group. From the docking of SHF1486 and SHF1586, it could also be interesting to incorporate the alkyl amine end of SHF1486 onto SHF1556 to determine whether introduction of a more flexible amine-bearing group would be able to reach acidic RAMP2 residues and boost potency. Furthermore SHF1572 has given a promising new direction for the project. SAR of the compound could further investigate the importance of the nitrile group in this compound, with one possible avenue to replace this group with other functional groups containing hydrogen bond acceptors. The co-crystallisation of SHF1556 with the AM_1 ECD could also be attempted to determine the binding mode of this compound. This information could further aid structure based drug design of antagonists targeting the AM_1 receptor.

Chapter 7 – Experimental/Materials and Methods

Chapter 7: Experimental/Materials and Methods

7.1 Chemistry

General Considerations

All reagents, unless otherwise stated, were obtained from commercial sources and used without further purification. ^{1}H NMR spectra were recorded on a Bruker AVIII HD 400 (400 MHz), Bruker AVI 400 (400 MHz) or Bruker AMX 400 (400 MHz) supported by an Aspect 3000 data system and referenced to the residual solvent peak. Signal positions were recorded in δ ppm with the abbreviations s, d, t, q and m representing singlet, doublet, triplet, quintet and multiplet respectively. ^{13}C NMR spectra were recorded on a Bruker AVIII HD 400 (100.6 MHz) or Bruker AVI 400 (100.6 MHz) with complete proton decoupling. Chemical shifts are reported in ppm from tetramethylsilane with the solvent as the internal reference. Infrared (IR) spectra were recorded on a Perkin Elmer Paragon FTIR spectrometer (ν_{max} in cm^{-1}). Samples were recorded neat as thin films. High resolution mass spectra (HRMS) were recorded on an Agilent LC in electrospray mode. Flash chromatography was performed on silica gel (BDH Silica Gel 60 43-60) using head pressure by means of a compressed air line. Thin-layer chromatography (TLC) was performed using aluminium-back plates coated with silica, which were developed using standard visualising agents: UV light or potassium permanganate.

Synthesis of 1-((2-(trimethylsilyl)ethoxy)methyl)-1*H*-pyrrolo[2,3-b]pyridine (17)

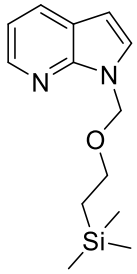

17

A solution of 7-azaindole (4.0 g, 33.9 mmol) in DMF (21 mL) was cooled to 0 ^{o}C before portion wise addition of sodium hydride (80% dispersion in mineral oil) (0.98 g, 40.6 mmol). The resulting suspension was stirred for 1 hour before dropwise addition of 2-(trimethylsilyl)ethoxymethyl chloride (6.8 g, 40.6 mmol). The suspension was warmed to room temperature and left to stir overnight. The resulting mixture was quenched by dropwise addition of water before effervescence ceased, and then further diluted with water (2 x 60 mL). The resulting mixture was extracted with ethyl acetate (2 x 60 mL). Combined organic extracts were washed with water (2 x 40 mL) and brine (2 x 40 mL), dried over magnesium sulphate, filtered and evaporated to provide the title compound (8.2 g, 98%). **^{1}H NMR ($CDCl_3$, 400 MHz):** δ 8.35 (dd, J = 4.5 Hz, 1.5 Hz, 1H, Ar), 7.93 (dd, J = 8.0 Hz, 1.6 Hz, 1H, Ar), 7.34 (d, J = 3.5 Hz, 1H, Ar), 7.10-7.12 (m, 1H, Ar), 6.54 (d, J = 3.5 Hz, 1H, Ar), 5.71 (s, 2H, CH_2), 3.54-3.58 (m, 2H, CH_2), 0.91-0.93 (m, 2H, CH_2), -0.06 (s, 9H, 3 x SiMe); **LCMS** (249.1 $[M-H]^+$). Data consistent with that published by Bell, 2010

Synthesis of 3,3-dibromo-1-((2-(trimethylsilyl)ethoxy)methyl)-1*H*-pyrrolo[2,3-b]pyridin-2(3*H*)-one (18)

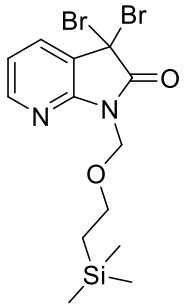

18

A suspension of pyridinium tribromide (38.4 g, 0.12 mol) in 1,4-dioxane (30 mL) was cooled to 10 ^{o}C before dropwise addition of 1-((2-(trimethylsilyl)ethoxy)methyl)-1*H*-pyrrolo[2,3-b]pyridine (6.0 g, 24.1 mmol) in 1,4-dioxane (40 mL). The reaction was warmed to room temperature and stirred for 2 hours. The mixture was then partitioned between water (90 mL) and ethyl acetate (90 mL). The organic layer was washed with water (2 x 70 mL),

saturated sodium bicarbonate (2 x 70 mL), sodium thiosulfate solution (2 x 70 mL) and brine (3 x 70 mL), dried over magnesium sulphate, filtered and evaporated to provide the title compound. (5.7 g, 68%). **^{1}H NMR ($CDCl_3$, 400 MHz):** δ 8.32 (dd, J = 5.0 Hz, 1.5 Hz, 1H, Ar), 7.89 (dd, J = 7.5 Hz, 1.5 Hz, 1H, Ar), 7.16-7.18 (m, 1H, Ar), 5.34 (s, 2H, CH_2), 3.71-3.75 (m, 2H, CH_2), 0.99-1.01 (m, 2H, CH_2), -0.02 (s, 9H, 3 x SiMe). **LCMS** (423.0 $[M-H]^+$). Data consistent with that published by Bell, 2010

Synthesis of 1-((2-(trimethylsilyl)ethoxy)methyl)-1*H*-pyrrolo[2,3-b]pyridin-2(3*H*)-one (19)

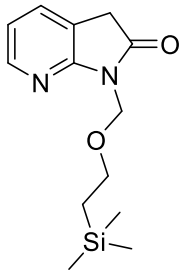

19

To a solution of 3,3-dibromo-1-((2-(trimethylsilyl)ethoxy)methyl)-1*H*-pyrrolo[2,3-b]pyridin-2(3*H*)-one (5.7 g, 14 mmol) in THF (82 mL) was added saturated aqueous ammonium chloride solution (21 mL). The mixture cooled to 0 ^oC before addition of zinc (9.0 g, 0.14 mol) in three portions. The resulting suspension was warmed to room temperature and stirred for 3 hours. The suspension was filtered through a celite pad before washing with ethyl acetate (40 mL). The filtrate was diluted with water (60 mL) before being filtered through a further celite pad. The organic layer was separated from the filtrate and washed with water (40 mL) and brine (2 x 40 mL), dried over magnesium sulphate, filtered and evaporated. Crude product was purified by flash column chromatography, eluting with 0-30% ethyl acetate/petrol to provide the title compound (2.0 g, 54%). **^{1}H NMR ($CDCl_3$, 400 MHz):** δ 8.24 (d, J = 4.0 Hz, 1H, Ar), 7.52 (d, J = 7.5 Hz, 1H, Ar), 6.98-7.00 (m, 1H, Ar), 5.27 (s, 2H, CH_2), 3.69-3.73 (m, 2H, CH_2), 3.60 (s, 2H, CH_2), 0.99-1.01 (m, 2H, CH_2), -0.01 (s, 9H, 3 x SiMe); **LCMS** (265.1 $[M-H]^+$). Data consistent with that published by Bell, 2010

Synthesis of (4-nitro-1,2-phenylene)dimethanol (23)

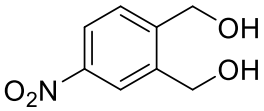

23

A solution of 4-nitrophthalic acid (5.0 g, 24 mmol) in THF (51 mL) was cooled to 0 ^oC before dropwise addition of borane dimethylsulphide complex (9.0 g, 0.12 mol). The reaction warmed to room temperature and left to stir overnight. The resulting mixture was quenched with dropwise addition of methanol before concentration to 25-30 % volume. The mixture was then adjusted to pH 10 with addition of 2M sodium hydroxide before extraction with ethyl acetate (5 x 50 mL). Combined organic layers were dried over magnesium sulphate, filtered and evaporated to obtain the title compound (4.2 g, 95%). **^{1}H NMR ($CDCl_3$, 400 MHz):** δ 8.12-8.16 (m, 2H, 2 x OH), 7.56 (d, J = 7.0 Hz, 1H, Ar), 5.13-5.18 (m, 2H, 2 x Ar), 4.08-4.10 (m, 2 x CH_2); **LCMS** (184.1 $[M-H]^+$). Data consistent with that published by Bell, 2010

Synthesis of 1,2-bis(bromomethyl)-4-nitrobenzene (24)

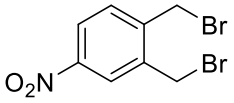

24

A suspension of (4-nitro-1,2-phenylene)dimethanol (4.2 g, 23 mmol) in dioxane (88 mL) was cooled to 0 ^oC before dropwise addition of phosphorus tribromide (6.8 g, 25 mmol). The reaction was warmed to room temperature and left to stir overnight. The resulting mixture was then poured into saturated sodium bicarbonate solution and extracted with ethyl acetate (3 x 40 mL). Combined organic extracts were dried over magnesium sulphate, filtered and evaporated to produce the title compound (3.1 g, 44 %). **^{1}H NMR ($CDCl_3$, 400 MHz):** δ 8.27 (d, J = 2.5 Hz, 1H, Ar), 8.18 (dd, J = 8.5 Hz, 2.4 Hz, 1H, Ar), 7.58 (d, J = 8.5 Hz, !H,

Ar) 4.69 (s, 2H, CH_2), 4.68 (s, 2H, CH_2); **LCMS** (309.6 $[M-H]^+$). Data consistent with that published by Bell, 2010

Synthesis of 5-nitro-1'-((2-(trimethylsilyl)ethoxy)methyl)-1,3-dihydrospiro[indene-2,3'-pyrrolo[2,3-b]pyridin]-2'(1'*H*)-one (20)

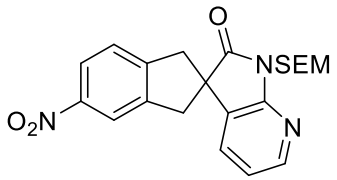

20

To a mechanically stirred solution of 1-((2-(trimethylsilyl)ethoxy)methyl)-1H-pyrrolo[2,3-b]pyridin-2(3*H*)-one (2.0 g, 7.62 mmol) in DMF (50 mL), was added1,2-bis(bromomethyl)-4-nitrobenzene (2.6 g, 8.3 mmol). Ceasium carbonate (6.2 g, 19.1 mmol) was then added in one portion and the reaction was left to stir overnight at room temperature. The resulting suspension was then filtered over a pad of celite, washing with ethyl acetate (60 mL). The filtrate was washed with water (3 x 30 mL) and brine (30 mL), dried over magnesium sulphate, filtered and evaporated to obtain the crude product. The crude was purified by flash column chromatography, eluting with 10-40 % ethyl acetate/petrol to produce the title compound (1.5 g, 49%). **^{1}H NMR ($CDCl_3$, 400 MHz):** δ 8.26 (dd, J = 5.5 Hz, 1.5 Hz, 1H, Ar), 8.18-8.20 (m, 2H, 2 x Ar), 7.45 (d, J = 8.0 Hz, 1H, Ar), 7.10 (dd, J = 7.5 Hz, 1.5 Hz, 1H, Ar), 6.89-6.91 (m, 1H, Ar,) 5.33 (s, 2H, CH_2,) 3.72-3.76 (m, 4H, 2 x CH_2), 3.21 (dd, J = 16.0 Hz, 5.0 Hz, 2H, CH_2), 1.01-1.03 (m, 2H, CH_2), 0.02 (s, 9H, 3 x SiMe); **LCMS** (412.2 $[M-H]^+$). Data consistent with that published by Bell, 2010

Synthesis of 5-amino-1'-((2-(trimethylsilyl)ethoxy)methyl)-1,3-dihydrospiro[indene-2,3'-pyrrolo[2,3-b]pyridin]-2'(1'*H*)-one (21)

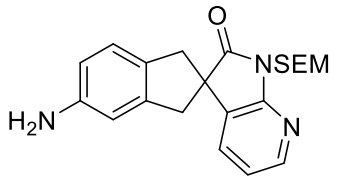

21

To a solution of 5-Nitro-1'-((2-(trimethylsilyl)ethoxy)methyl)-1,3-dihydrospiro[indene-2,3'-pyrrolo[2,3-b]pyridin]-2'(1'*H*)-one (1.0 g, 3.6 mmol) in THF (23 mL), was added saturated aqueous ammonium chloride (8.4 mL) and zinc (2.4 g, 36 mmol). The resulting suspension was left to stir overnight at room temperature. The mixture was then filtered through a celite pad, washing with ethyl acetate (20 mL). The filtrate was washed with water (3 x 20 mL), dried over magnesium sulphate, filtered and evaporated. The crude product was purified by flash column chromatography, eluting with 50 % ethyl acetate/petrol to produce the title compound (810 mg, 59%). **^{1}H NMR ($CDCl_3$, 400 MHz):** δ 8.21 (dd, J = 5.0 Hz, 1.5 Hz, 1H, Ar), 7.12 (dd, J = 7.0 Hz, 1.5 Hz, 1H, Ar), 7.05 (d, J = 8.0 Hz, 1H, Ar), 6.84-6.86 (m, 1H, Ar), 6.61-6.63 (m, 2H, 2 x Ar), 5.32 (s, 2H, CH_2), 3.70-3.74 (m, 4H, 2 x CH_2), 2.94 (d, J = 15.0 Hz, 2H, CH_2), 1.00-1.02 (m, 2H, CH_2), 0.01 (s, 9H, 3 x SiMe); **LCMS** (382.2 $[M-H]^+$). Data consistent with that published by Bell, 2010

Synthesis of 5-aminospiro[1,3-dihydroindene-2,3'-1*H*-pyrrolo[2,3-b]pyridine]-2'-one (SHF355)

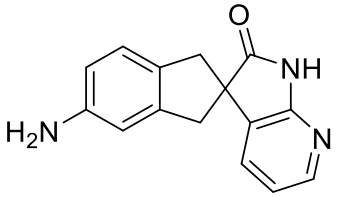

SHF355

A solution of 5-Amino-1'-((2-(trimethylsilyl)ethoxy)methyl)-1,3-dihydrospiro[indene-2,3'-pyrrolo[2,3-b]pyridin]-2'(1'H)-one (435 mg, 1.14 mmol) in freshly prepared hydrogen chloride in methanol (15% concentration (v/w)) was heated to reflux and left to stir overnight. The resulting mixture was then concentrated in vacuo before dilution with water

(20 mL). The pH adjusted to 9 with saturated sodium bicarbonate solution before extraction with dichloromethane (3 x 30 mL) and 9:1 dichloromethane/methanol (3 x 30 mL). Combined organic layers were dried over magnesium sulphate, filtered and evaporated to give the title compound (215 mg, 75%).**^{1}H NMR (MeOD, 400 MHz):** δ 8.06 (dd, J = 5.5 Hz, 1.5 Hz, 1H, Ar), 7.14 (dd, J = 7.5 Hz, 1.5 Hz, 1H, Ar), 7.04 (d, J = 7.5 Hz, 1H, Ar), 6.87-6.91 (m, 1H, Ar), 6.67-6.69 (m, 2H, 2 x Ar), 3.43-3.47 (m, 2H, CH_2), 2.96 (dd, J = 15.0 Hz, 5.5 Hz, 2H, CH_2); **LCMS** (252.1 $[M-H]^+$). Data consistent with that published by Bell, 2010

Synthesis of 2-methyl-*N*-[2'-oxospiro[1,3-dihydroindene-2,3'-1*H*-pyrrolo[2,3-b]pyridine]-5-yl]benzamide (SHF1430)

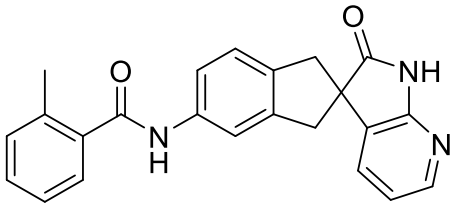

SHF1430

5-aminospiro[1,3-dihydroindene-2,3'-1*H*-pyrrolo[2,3-b]pyridine]-2'-one (6 mg, 0.024 mmol), HATU (12 mg, 0.031 mmol), NMM (2 drops) and *O*-toluic acid (3.5 mg, 0.026 mmol) were dissolved in DMF (1 ml) and stirred at room temperature for 30 minutes before the reaction mixture was quenched using ethanol (10 drops). The crude product was purified by high performance liquid chromatography, using a gradient of 95:5 to 5:95 water/acetonitrile for 20 minutes to form the title compound (3.5 mg, 40%). **^{1}H NMR (MeOD, 400 MHz)** δ 8.08 (dd, J = 5.5 Hz, 1H, Ar), 7.71 (s, 1H, Ar), 7.55 (d, J = 7.5 Hz, 1H, Ar), 7.49 (d, J = 7.5 Hz, 1H, Ar), 7.40 (t, J = 7.0 Hz, 1H, Ar), 7.31 (t, J = 8.0 Hz, 3H, 3 x Ar), 7.23 (d, J = 7.5 Hz, 1H, Ar), 6.92-6.95 (m, 1H, Ar), 3.54-3.61 (m, 2H, CH_2), 3.11-3.17 (m, 2H, CH_2), 2.48 (3, 3H, CH_3); **LCMS** (370.3 $[M-H]^+$).

Synthesis of 2-phenyl-*N*-[2'-oxospiro[1,3-dihydroindene-2,3'-1*H*-pyrrolo[2,3-b]pyridine]-5-yl]propenamide (SHF1437)

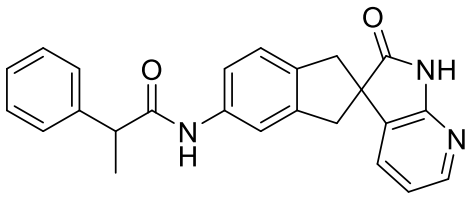

SHF1437

5-aminospiro[1,3-dihydroindene-2,3'-1*H*-pyrrolo[2,3-b]pyridine]-2'-one (6 mg, 0.024 mmol), HATU (12 mg, 0.031 mmol), NMM (2 drops) and 2-phenylpropenoic acid (4.3 mg, 0.026 mmol) were dissolved in DMF (1 ml) and stirred at room temperature for 30 minutes before the reaction mixture was quenched using ethanol (10 drops). The crude product was purified by high performance liquid chromatography, using a gradient of 95:5 to 5:95 water/acetonitrile for 20 minutes to yield to form the title compound (3.7 mg, 40%). **^{1}H NMR (MeOD, 400 MHz):** δ 8.08 (d, J = 5.5 Hz, 1H, Ar), 7.55 (d, J = 21.5 Hz, 1H, Ar), 7.42 (t, J = 9.5 Hz, 3H, 3 x Ar), 7.30-7.36 (m, 3H, 3 x Ar), 7.22-7.28 (m, 2H, 2 x Ar), 7.01-7.05 (m, 1H, Ar), 3.86 (q, J = 7.0 Hz, 1H, CH), 3.50-3.56 (m, 2H, CH_2), 3.09-3.14 (m, 2H, CH_2), 1.53 (d, J = 7.0 Hz, 3H, CH_3); **LCMS**(384.2 $[M-H]^+$).

Synthesis of tert-butyl *N*-[3-oxo-3-[(2'-oxospiro[1,3-dihydroindene-2,3'-1*H*-pyrrolo[2,3-b]pyridine]-5-yl)amino]-2-phenylpropyl]carbamate (SHF143)

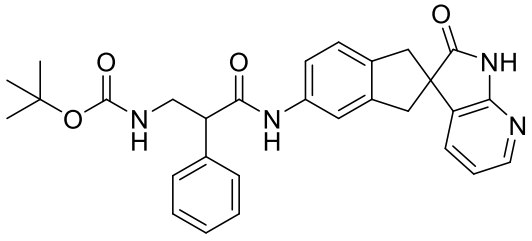

SHF143

5-aminospiro[1,3-dihydroindene-2,3'-1*H*-pyrrolo[2,3-b]pyridine]-2'-one (6 mg, 0.024 mmol), HATU (12 mg, 0.031 mmol), NMM (2 drops) and 3-[(2-methylpropan-2-yl)oxycarbonylamino]-2-phenylpropanoic acid (6.9 mg, 0.026 mmol) were dissolved in DMF

(1 ml) and stirred at room temperature for 30 minutes before the reaction mixture was quenched using ethanol (10 drops). The crude product was purified by high performance liquid chromatography, using a gradient of 95:5 to 5:95 water/acetonitrile for 20 minutes to form the title compound (2.3 mg, 20%); **^{1}H NMR (MeOD, 400 MHz):** δ 8.06 (d, J = 5.0 Hz, 1H, Ar), 7.58 (d, J = 15. 5 Hz, 1H, Ar), 7.44 (t, J = 7.5 Hz, 3H, 3 x Ar), 7.36 (t, J = 7.5 Hz, 2H, 2 x Ar), 7.29 (t, J = 7.0 Hz, 1H, Ar), 7.23 (d, J = 7.5 Hz, 1H, Ar), 7.16 (d, J = 7.0 Hz, 1H, Ar), 6.88-6.92 (m, 1H, Ar), 3.99 (t, J = 7.0 Hz, 1H, CH), 3.64-3.70 (m, 2H, CH_2), 3.43-3.56 (m, 2H, CH_2), 3.04-3.11 (m, 2H, CH_2), 1.44 (s, 9H, 3 x CH_3); **LCMS** (499.2 $[M-H]^+$)

Synthesis of methyl 4-[2-oxo-2-[(2'-oxospiro[1,3-dihydroindene-2,3'-1*H*-pyrrolo[2,3-b]pyridine]-5-yl)amino]ethyl]benzoate (SHF1438)

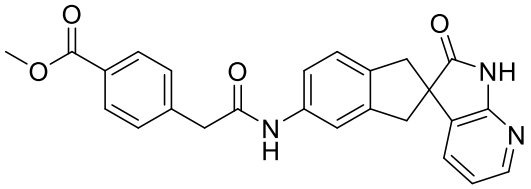

SHF1438

5-aminospiro[1,3-dihydroindene-2,3'-1*H*-pyrrolo[2,3-b]pyridine]-2'-one (6 mg, 0.024 mmol), HATU (12 mg, 0.031 mmol), NMM (2 drops) and 4-methoxycarbonylbenzoic acid (4.7 mg, 0.026 mmol) were dissolved in DMF (1 ml) and stirred at room temperature for 30 minutes before the reaction mixture was quenched using ethanol (10 drops). The crude product was purified by high performance liquid chromatography, using a gradient of 95:5 to 5:95 water/acetonitrile for 20 minutes to form the title compound (2.1 mg, 20%); **^{1}H NMR (MeOD, 400 MHz):** δ 8.07 (d, J = 5.0 Hz, 1H, Ar), 8.02 (d, J = 8.0 Hz, 2H, 2 x Ar), 7.59 (s, 1H, Ar), 7.51 (d, J = 8.5 Hz, 2H, 2 x Ar), 7.42 (d, J = 8.0 Hz, 1H, Ar), 7.25 (d, J = 8.0 Hz, 1H, Ar), 7.19 (dd, J = 7.5 Hz, 1H, Ar), 6.90-6.94 (m, 1H, Ar), 3.92 (s, 3H, OMe), 3.79 (s, 2H, CH_2), 3.51-3.57 (m, 2H, CH_2), 3.07-3.13 (m, 2H, CH_2); **LCMS** (428.1 $[M-H]^+$).

Synthesis of 2-(2-nitrophenyl)-*N*-[2'-oxospiro[1,3-dihydroindene-2,3'-1*H*-pyrrolo[2,3-b]pyridine]-5-yl]acetamide (SHF1447)

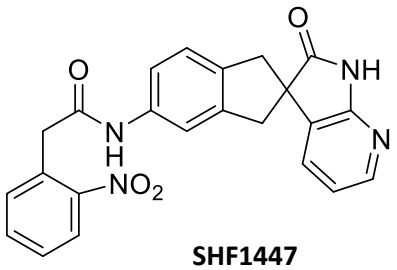

SHF1447

5-aminospiro[1,3-dihydroindene-2,3'-1*H*-pyrrolo[2,3-b]pyridine]-2'-one (6 mg, 0.024 mmol), HATU (12 mg, 0.031 mmol), NMM (2 drops) and 2-nitrophenylacetic acid (4.7 mg, 0.026 mmol) were dissolved in DMF (1 ml) and stirred at room temperature for 30 minutes before the reaction mixture was quenched using ethanol (10 drops). The crude product was purified by high performance liquid chromatography, using a gradient of 95:5 to 5:95 water/acetonitrile for 20 minutes to form the title compound (5.54 mg, 56%)**. ^{1}H NMR (400 MHz, MeOD)** δ 8.12 (d, J = 8.0 Hz, 1H, Ar), 8.07 (dd, J = 5.5 Hz, 1.5 Hz, 1H, Ar), 7.68-7.72 (m, 1H, Ar), 7.56 (t, J = 7.5 Hz, 3H, 3 x Ar), 7.40 (d, J = 8.0 Hz, 1H, Ar), 7.25 (d, J = 8.0 Hz, 1H, Ar), 7.18 (dd, J = 7.0 Hz, 1.5 Hz, 1H, Ar), 6.89-6.92 (m, 1H, Ar), 4.17 (s, 2H, CH_2), 3.50-3.57 (m, 2H, CH_2), 3.06-3.12 (m, 2H, CH_2);′**LCMS** (415.1 $[M-H]^+$).

Synthesis of *N*-[2'-oxospiro[1,3-dihydroindene-2,3'-1*H*-pyrrolo[2,3-b]pyridine]-5-yl]-2-(trifluoromethyl)pyridine-4-carboxamide (SHF1497)

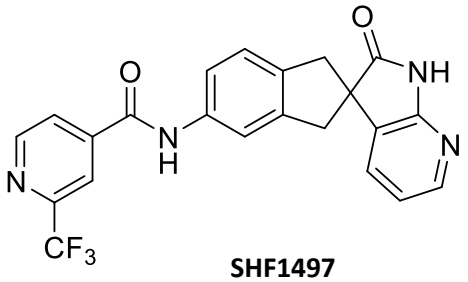

SHF1497

5-aminospiro[1,3-dihydroindene-2,3'-1*H*-pyrrolo[2,3-b]pyridine]-2'-one (6 mg, 0.024 mmol), HATU (12 mg, 0.031 mmol), NMM (2 drops) and 2-(trifluoromethyl)pyridine-4-carboxylic

acid (5.0 mg, 0.026 mmol) were dissolved in DMF (1 ml) and stirred at room temperature for 30 minutes before the reaction mixture was quenched using ethanol (10 drops). The crude product was purified by high performance liquid chromatography, using a gradient of 95:5 to 5:95 water/acetonitrile for 20 minutes to form the title compound (6.9 mg, 68%). **^{1}H NMR (MeOD, 400 MHz)** δ 8.94 (d, J = 5.0 Hz, 1H, Ar), 8.32 (s, 1H, Ar), 8.15 (d, J = 5.0 Hz, 1H, Ar), 8.08 (dd, J = 5.5 Hz, 1.5 Hz, 1H, Ar), 7.76 (s, 1H, Ar), 7.61 (d, J = 8.0 Hz, 1H, Ar), 7.34 (d, J = 8.0 Hz, 1H, Ar), 7.21 (dd, J = 7.5 Hz, 1.5 Hz, 1H, Ar), 6.91-6.93 (m, 1H, Ar), 3.55-3.61 (m, 2H, 2 x CH_2), 3.12-3.19 (m, 2H, 2 x CH_2); **LCMS** (425.1 $[M-H]^+$).

Synthesis of 4-amino-2-chloro-*N*-[2'-oxospiro[1,3-dihydroindene-2,3'-1*H*-pyrrolo[2,3-b]pyridine]-5-yl]benzamide (SHF1448)

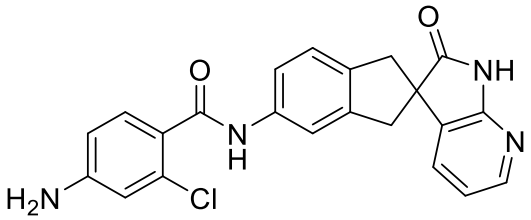

SHF1448

5-aminospiro[1,3-dihydroindene-2,3'-1*H*-pyrrolo[2,3-b]pyridine]-2'-one (6 mg, 0.024 mmol), HATU (12 mg, 0.031 mmol), NMM (2 drops) and 2-amino-4-chlororbenzoic acid (4.5 mg, 0.026 mmol) were dissolved in DMF (1 ml) and stirred at room temperature for 30 minutes before the reaction mixture was quenched using ethanol (10 drops). The crude product was purified by high performance liquid chromatography, using a gradient of 95:5 to 5:95 water/acetonitrile for 20 minutes to form the title compound(2.8 mg, 29%). **^{1}H NMR (MeOD, 400 MHz):** δ 8.08 (dd, J = 5.5 Hz, 1.5 Hz, 1H, Ar), 7.67 (s, 1H, Ar), 7.52 (d, J = 7.5 Hz, 1H, Ar), 7.37 (d, J = 8.5 Hz, 1H, Ar), 7.29 (d, J = 8.0 Hz, 1H, Ar), 7.22 (d, J = 7.0 Hz, 1H, Ar), 6.92-6.96 (m, 1H, Ar), 6.79 (d, J = 2.0 Hz, 1H, Ar), 6.69 (dd, J = 8.5 Hz, 2.0 Hz, 1H, Ar), 3.53-5.60 (m, 2H, CH_2), 3.09-3.15 (m, 2H, CH_2); **LCMS** (405.1 $[M-H]^+$).

Synthesis of 6-bromo-*N*-[(2R)-2'-oxospiro[1,3-dihydroindene-2,3'-1*H*-pyrrolo[2,3-b]pyridine]-5-yl]pyridine-3-carboxamide (SHF1496)

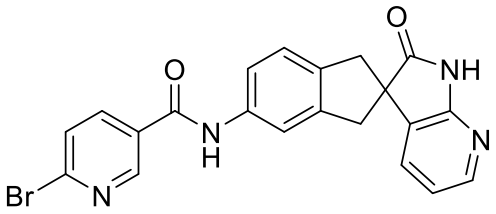

SHF1496

5-aminospiro[1,3-dihydroindene-2,3'-1*H*-pyrrolo[2,3-b]pyridine]-2'-one (6 mg, 0.024 mmol), HATU (12 mg, 0.031 mmol), NMM (2 drops) and 6-bromopiridyne-3-carboxylic acid (5.3 mg, 0.026 mmol) were dissolved in DMF (1 ml) and stirred at room temperature for 30 minutes before the reaction mixture was quenched using ethanol (10 drops). The crude product was purified by high performance liquid chromatography, using a gradient of 95:5 to 5:95 water/acetonitrile for 20 minutes to form the title compound (3.9 mg, 37%). **^{1}H NMR (MeOD, 400 MHz)** δ 8.53 (d, J = 7.0 Hz, 1H, Ar), 8.08 (dd, J = 5.5 Hz, 1.5 Hz, 1H, Ar), 7.66 (t, J = 10.5 Hz, 2H, 2 x Ar), 7.44 (t, J = 8.0 Hz, 1H, Ar), 7.34 (d, J = 8.0 Hz, 1H, Ar), 7.21 (d, J = 7.0 Hz, 1H, Ar), 7.03 (t, J = 7.0 Hz, 1H, Ar), 6.91-6.94 (m, 1H, Ar), 3.55-3.63 (m, 2H, CH_2), 3.12-3.19 (m, 2H, CH_2); **LCMS** (437.2 $[M-H]^+$).

Synthesis of *N*-(2'-oxospiro[1,3-dihydroindene-2,3'-1*H*-pyrrolo[2,3-b]pyridine]-5-yl)imidazo[1,2-a]pyridine-2-carboxamide (SHF1457)

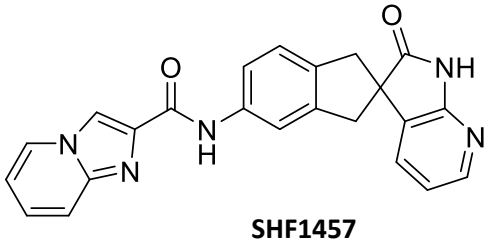

SHF1457

Ethyl imidazo[1,2-a]pyridine-2-carboxylate and LiOH (2 mg) were dissolved in a 3:2:3 mixture of MeOH/H_2O/THF and stirred at room temperature for 3 hours. The solvent was then removed and the crude product taken to the next step without purification. The resulting solid, 5-aminospiro[1,3-dihydroindene-2,3'-1*H*-pyrrolo[2,3-b]pyridine]-2'-one (6 mg, 0.024 mmol), HATU (12 mg, 0.031 mmol), NMM (2 drops) were dissolved in DMF and stirred at room temperature for 30 minutes, before the reaction was diluted to form the title compound (2.7 mg, 29%). **^{1}H NMR (MeOD, 400 MHz)** δ 8.90 (d, J = 2.5 Hz, 1H, Ar), 8.22 (dd, J = 8.5 Hz, 2.5 Hz, 1H, Ar), 8.08 (dd, J = 5.5 Hz, 1.5 Hz, 1H, Ar), 7.79 (d, J = 7.0 Hz, 1H, Ar),

7.72 (s, 1H, Ar), 7.57 (d, J = 7.5 Hz, 1H, Ar), 7.33 (d, J = 8.0 Hz, 1H, Ar), 7.20 (dd, J = 7.5 Hz, 1.5 Hz, 2H, 2 x Ar), 6.91-6.94 (m, 2H, 2 x Ar), 3.50-3.63 (m, 2H, CH_2), 3.12-3.18 (m, 2H, CH_2); **LCMS** (395.1 $[M-H]^+$).

Synthesis of tert-butyl 4-[2'-oxospiro[1,3-dihydroindene-2,3'-1*H*-pyrrolo[2,3-b]pyridine]-5-yl]carbamoyl]piperidine-1-carboxylate (SHF1499)

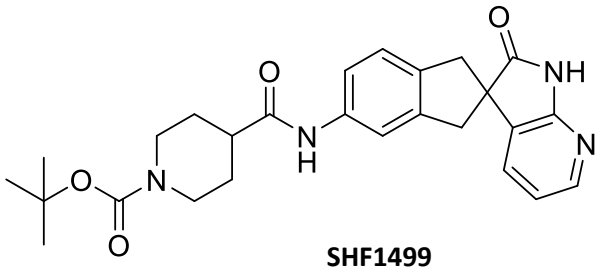

SHF1499

Methyl N-boc-piperidine-4-carboxylate (5.8 mg, 0.026 mmol) and LiOH (2 mg, 0.083 mmol) were dissolved in a 3:2:3 mixture of MeOH/H_2O/THF and stirred at room temperature for 3 hours. The solvent was then removed and the crude product was taken to the next step without purification. The resulting solid, 5-aminospiro[1,3-dihydroindene-2,3'-1*H*-pyrrolo[2,3-b]pyridine]-2'-one (6 mg, 0.024 mmol), HATU (12 mg, 0.031 mmol), NMM (2 drops) were dissolved in DMF and stirred at room temperature for 30 minutes, before the reaction was diluted to form the title compound (1.9 mg, 17%). **^{1}H NMR (MeOD, 400 MHz)** δ 8.07 (dd, J = 5.5 Hz, 2.0 Hz, 1H, Ar), 7.58 (s, 1H, Ar), 7.42 (d, J = 8.0 Hz, 1H, Ar), 7.25 (d, J = 8.0 Hz, 1H, Ar), 7.17 (dd, J = 7.5 Hz, 1.5 Hz, 1H, Ar), 6.89-6.92 (m, 1H, Ar), 4.09-4.19 (m, 4H, 2 x CH_2), 3.51-3.57 (m, 2H, CH_2), 3.07-3.12 (m, 2H, CH_2), 2.55-2.62 (m, 1H, CH_2), 1.83-1.89 (m, 2H, CH_2), 1.64-1.74 (m, 2H, CH_2), 1.49 (s, 9H, 3 x CH_3); **LCMS** (463.2 $[M-H]^+$).

Synthesis of ethyl 5-oxo-5-[2'-oxospiro[1,3-dihydroindene-2,3'-1*H*-pyrrolo[2,3-b]pyridine]-5-yl]amino]pentanoate (SHF1458)

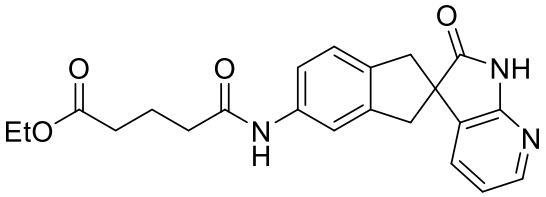

SHF1458

5-aminospiro[1,3-dihydroindene-2,3'-1*H*-pyrrolo[2,3-b]pyridine]-2'-one (20 mg, 0.080 mmol), Glutaric acid monoethyl ester chloride (15 mg, 0.092 mmol) and Et_3N (0.02 mL, 0.24 mmol) were dissolved in dichloromethane (1 mL) and stirred at room temperature for 16 hours. The reaction was quenched with H_2O before DCM was added and the organic layer extracted. The combined organic layers were washed with brine (3 x 20 ml), dried with magnesium sulfate and subsequently filtered. The solvent was removed under reduced pressure, resulting in the crude product. The crude product was purified using flash column chromatography, eluting with 50% to 70% EtOAc-petrol to give the title compound (11.8 mg, 39%) **^{1}H NMR (MeOD, 400 MHz)** δ 8.07 (d, J = 5.0 Hz, 1H, Ar), 7.58 (s, 1H, Ar), 7.41 (d, J = 8.0 Hz, 1H, Ar), 7.25 (d, J = 8.5 Hz, 1H, Ar), 7.18 (dd, J = 7.5 Hz, 1.5 Hz, 1H, Ar), 6.90-6.93 (m, 1H, Ar), 4.15 (q, J = 7.0 Hz, 2H, CH_2), 3.50-5.58 (m, 2H, CH_2), 3.07-3.13 (m, 2H, CH_2), 2.42-2.47 (m, 2H, CH_2), 1.99-2.06 (m, 2H, CH_2), 1.27 (t, 7.0 Hz, 3H, CH_3); **LCMS** (394.2 $[M-H]^+$)

Synthesis of 5-oxo-5-[(2'-oxospiro[1,3-dihydroindene-2,3'-1*H*-pyrrolo[2,3-b]pyridine]-5-yl)amino]pentanoic acid (SHF1501)

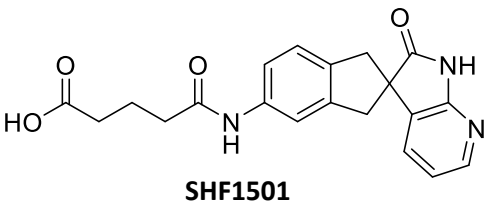

SHF1501

Ethyl 5-oxo-5-[2'-oxospiro[1,3-dihydroindene-2,3'-1*H*-pyrrolo[2,3-b]pyridine]-5-yl]amino]pentanoate (9 mg, 0.026 mmol)and LiOH (2 mg, 0.083 mmol) were dissolved in a 3:2:3 mixture of MeOH/H_2O/THF and stirred at room temperature for 3 hours. The solvent was subsequently removed. The crude product was was purified by high performance liquid chromatography, using a gradient of 95:5 to 5:95 water/acetonitrile for 20 minutes to form the title compound (4.8 mg, 51%). **^{1}H NMR (MeOD, 400 MHz):** δ 8.07 (d, J = 5.5 Hz, 1H, Ar),

7.59, (s, 1H, Ar), 7.41 (d, J = 8.0 Hz, 1H, Ar), 7.24 (d, J = 8.5 Hz, 1H, Ar), 7.17 (dd, J = 7.5 Hz, 1.5 Hz, 1H, Ar), 6.89-6.92 (m, 1H, Ar), 3.51-3.58 (m, 2H, CH_2), 3.06-3.12 (m, 2H, CH_2), 2.44 (t, J = 7.5 Hz, 2H, CH_2), 2.35 (t, J = 7.0 Hz, 2H, CH_2), 1.96-2.04 (m, 2H, CH_2); **LCMS** (366.2 $[M-H]^+$).

Synthesis of 1-(2'-oxospiro[1,3-dihydroindene-2,3'-1*H*-pyrrolo[2,3-b]pyridine]-5-yl)-3-(1-phenylethyl)urea (SHF1462)

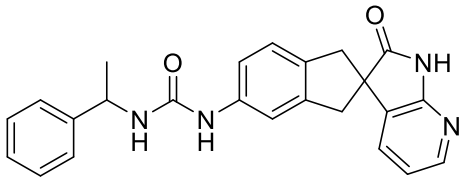

SHF1462

To a solution of 5-aminospiro[1,3-dihydroindene-2,3'-1*H*-pyrrolo[2,3-b]pyridine]-2'-one (20 mg, 0.08 mmol) and pyridine (6 drops) in dichloromethane (0.5 mL) was added triphosgene (30 mg, 0.1 mmol) in dichloromethane (0.5 mL) dropwise. The resulting mixture was left to stir at room temperature for 30 minutes. The solvent was then removed before dissolving in dichloromethane (0.5 mL). A solution of α-methylbenzylamine (9.5 mg, 0.08 mmol) and pyridine (6 drops) in dichloromethane (0.5 mL) and the resulting mixture was stirred at room temperature for 2 hours. The solvent was then evaporated. The crude product was purified by High Performance Liquid Chromatography, using a gradient of 95:5 to 5:95 water/acetonitrile over 20 minutes to yield the title compound (2 mg, 7%) **^{1}H NMR (MeOD, 400 MHz):** δ 8.06 (dd, J = 5.5 Hz, 1.5 Hz, 1H, Ar), 7.33-7.37 (m, 1H, Ar), 7.28-7.32 (m, 4H, 4 x Ar), 7.19-7.24 (m, 1H, Ar), 7.13-7.17 (m, 1H, Ar), 7.03 (d, J = 7.5 Hz, 1H, Ar), 6.87-6.92 (m, 1H, Ar), 6.66-6.70 (m, 1H, Ar), 5.36 (q, J = 5.5 Hz, 1H, CH_3), 3.43-3.50 (m, 2H, CH_2), 3.19-3.24 (m, 2H, CH_2), 1.49 (d, J = 7.0 Hz, 3H, CH_3); **LCMS:** (399.2 $[M-H]^+$)

Synthesis of 1-(2-methoxyethyl)-3-(2'-oxospiro[1,3-dihydroindene-2,3'-1*H*-pyrrolo[2,3-b]pyridine]-5-yl)urea (SHF1468)

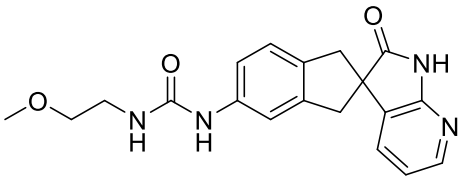

SHF1468

To a solution of 5-aminospiro[1,3-dihydroindene-2,3'-1*H*-pyrrolo[2,3-b]pyridine]-2'-one (20 mg, 0.08 mmol) and pyridine (6 drops) in dichloromethane (0.5 mL) was added triphosgene (30 mg, 0.1 mmol) in dichloromethane (0.5 mL) dropwise. The resulting mixture was left to stir at room temperature for 30 minutes. The solvent was then removed before dissolving in dichloromethane (0.5 mL). A solution of 2-methoxyethanamine (7 mg, 0.08 mmol) and pyridine (6 drops) in dichloromethane (0.5 mL) and the resulting mixture was stirred at room temperature for 2 hours. The solvent was then evaporated. The crude product was purified by High Performance Liquid Chromatography, using a gradient of 95:5 to 5:95 water/acetonitrile over 20 minutes to yield the title compound (2.4 mg, 10%) **^{1}H NMR (400 MHz, MeOD):** δ 8.01-8.08 (m, 1H, Ar), 7.76-7.83 (m, 1H, Ar), 7.62-7.66 (m, 1H, Ar), 7.49-7.54 (m, 1H, Ar), 7.23-7.29 (m, 2H, 2 x Ar), 3.80 (t, J = 5.5 Hz, 2H, CH_2), 3.68 (t, J = 5.0 Hz, 2H, CH_2), 3.50-3.57 (m, 2H, CH_2), 3.40 (s, 3H, OMe), 3.15-3.24 (m, 2H, CH_2); **LCMS:** (353.2 [M-H$^+$])

Synthesis of 1,1-bis(2-hydroxyethyl)-3-(2'-oxospiro[1,3-dihydroindene-2,3'-1*H*-pyrrolo[2,3-b]pyridine]-5-yl)urea (SHF1500)

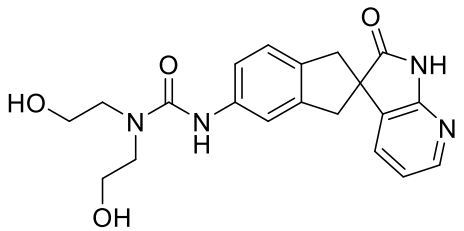

SHF1500

To a solution of 5-aminospiro[1,3-dihydroindene-2,3'-1*H*-pyrrolo[2,3-b]pyridine]-2'-one (20 mg, 0.08 mmol) and pyridine (6 drops) in dichloromethane (0.5 mL) was added triphosgene (30 mg, 0.1 mmol) in dichloromethane (0.5 mL) dropwise. The resulting mixture was left to stir at room temperature for 30 minutes. The solvent was then removed before dissolving in

dichloromethane (0.5 mL). A solution of diethanolamine (8.5 mg, 0.08 mmol) and pyridine (6 drops) in dichloromethane (0.5 mL) and the resulting mixture was stirred at room temperature for 2 hours. The solvent was then evaporated. The crude product was purified by High Performance Liquid Chromatography, using a gradient of 95:5 to 5:95 water/acetonitrile over 20 minutes to yield the title compound (1.7 mg, 6%) **^{1}H NMR (MeOD, 400 MHz):** δ 8.05-8.08 (m, 1H, Ar), 7.46-7.48 (m, 1H, Ar), 7.29-7.32 (m, 1H, Ar), 7.16-7.22 (m, 2H, 2 x Ar), 6.88-6.93 (m, 1H, Ar), 3.81 (t, J = 5.0 Hz, 2H, CH_2), 3.58 (t, J = 5.5 Hz, 2H, CH_2), 3.49-3.53 (m, 2H, CH_2), 3.12-3.16 (m, 2H, CH_2), 3.03-3.09 (m, 4H, 2 x CH_2); **LCMS:** (383.2 [M-H$^+$])

Synthesis of 3-(2'-oxospiro[1,3-dihydroindene-2,3'-1*H*-pyrrolo[2,3-b]pyridine]-5-yl)-1,1-bis(prop-2-enyl)urea (SHF1496)

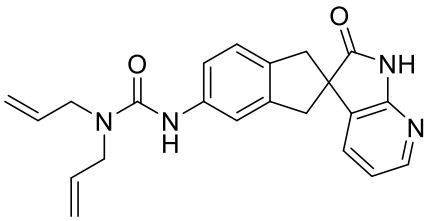

SHF1496

To a solution of 5-aminospiro[1,3-dihydroindene-2,3'-1*H*-pyrrolo[2,3-b]pyridine]-2'-one (20 mg, 0.08 mmol) and pyridine (6 drops) in dichloromethane (0.5 mL) was added triphosgene (30 mg, 0.1 mmol) in dichloromethane (0.5 mL) dropwise. The resulting mixture was left to stir at room temperature for 30 minutes. The solvent was then removed before dissolving in dichloromethane (0.5 mL). A solution of diallylamine (7.8 mg, 0.08 mmol) and pyridine (6 drops) in dichloromethane (0.5 mL) and the resulting mixture was stirred at room temperature for 2 hours. The solvent was then evaporated. The crude product was purified by High Performance Liquid Chromatography, using a gradient of 95:5 to 5:95 water/acetonitrile over 20 minutes to yield the title compound (3.8 mg, 13%) **^{1}H NMR (MeOD, 400 MHz):** δ 8.07 (dd, J = 5.5 Hz, 1.5 Hz, 1H, Ar), 7.25-7.34 (m, 2H, 2 x Ar), 7.22-7.23 (m, 1H, Ar), 7.14-7.18 (m, 1H, Ar), 5.86-5.95 (m, 4H, 2 x C=CH_2), 5.21-5.28 (m, 2H, 2 x C=CH), 4.00-4.04 (m, 4H, 4 x CH_2), 3.49-3.57 (m, 2H, CH_2), 3.04-3.10 (m, 2H, CH_2); **LCMS:** (375.2 [M-H]$^+$)

Synthesis of 4-fluoro-*N*-methyl-*N*-(2-methylphenyl)-3-nitrobenzamide (42)

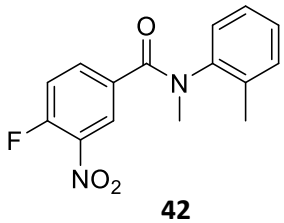

42

To a solution of 4-fluoro-3-nitrobenzoic acid (153 mg, 0.83 mmol) in dichloromethane(10 ml), was added thionyl chloride (0.6 mL, 8.3 mmol) and DMF (3 drops). The reaction mixture was heated under reflux for 1.5 hours. The mixture was cooled to room temperature before being evaporated. The compound was re-dissolved in dichloromethane before dropwise addition of a solution of aniline (100 mg, 0.83 mmol) and triethylamine (0.23 mL, 1.66 mmol) in dichloromethane (30 mL). The resulting mixture was stirred at room temperature for 1 hour. Sodium bicarbonate (20 mL) was then added to the mixture before extracting with dichloromethane (20 mL). The organic layer was washed with saturated potassium carbonate (30 mL) and brine (2 x 30 mL), dried with magnesium sulphate, filtered and evaporated. The crude product was purified by flash column chromatography, eluting with 30-50% ethyl acetate/petrol to provide the title compound (140 mg, 59%). **^{1}H NMR ($CDCl_3$, 400 MHz):** δ 7.98 (dd, J = 7.0 Hz, 2.5 Hz, 1H, Ar), 7.58-7.62 (m, J = 2.0 Hz, 1H, Ar), 7.20 (t, J = 4.5 Hz, 2H, 2 x Ar), 7.08 (t, J = 8.0 Hz, 2H, 2 x Ar), 3.41 (s, 3H, NMe_3), 2.23 (s, 3H, Me); **^{13}C NMR ($CDCl_3$, 101 MHz):** δ 167.1 (C=O), 157.1 (C-Ar), 154.3 (C-Ar), 142.4 (C-Ar), 135.4 (C-Ar), 134.6 (C-Ar), 131.9 (C-Ar), 128.7 (C-Ar), 128.3 (C-Ar), 127.6 (C-Ar), 126.7 (C-Ar), 118.0 (C-Ar), 117.8 (C-Ar), 37.7 (NCH_3), 17.6 (CH_3); **FTIR:** ν_{max}/cm^{-1} (neat) 1643 (C=O), 1535 (N-O), 1348 (N-O); **HRMS (ESI^+):** calculated for $C_{15}H_{13}N_2O_3F$ (ES^+)($+H^+$): 289.0988 Found: 289.0918 (289 [M-H]$^-$).

Synthesis of 2-mercaptothiazole (45)

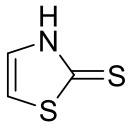

45

A solution of 2-bromothiazole (2 g, 12 mmol) and thiourea (2.8 g, 36 mmol) in methanol (35 mL) was heated under reflux. The reaction was left to stir overnight. The mixture was cooled to room temperature before being evaporated. 0.5M sodium hydroxide (20 mL) was then added and mixture was stirred for 15 minutes at room temperature. The resulting mixture adjusted to pH 4 using acetic acid before extraction with ethyl acetate (30mL). The organic layer was washed with water (2 x 30 mL) and brine (2 x 30 mL), dried with magnesium sulphate, filtered and evaporated to provide the title compound (1.2 g, 85**%). ^{1}H NMR (CDCl$_3$, 400 MHz):** δ 7.00 (d, J = 4.5 Hz, 1H, Ar), 7.30 (d, J = 4.5 Hz, 1H, Ar); **HRMS (ESI$^+$):** calculated for (ES$^+$)(+H$^+$): 117.9785 Found: 117.9784 **LCMS:** (118 [M-H]$^-$). Data consistent with that of Tegtmeier et al, 2005.

Synthesis of *N*-methyl-*N*-(2-methylphenyl)-3-nitro-4-(2-thiazolylthio)benzamide (43)

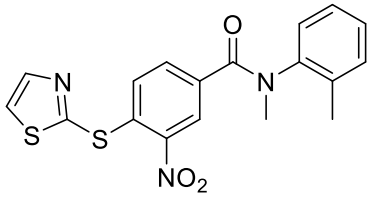

43

To a solution of 4-fluoro-*N*-methyl-*N*-(2-methylphenyl)-3-nitrobenzamide (92 mg, 0.32 mmol) and 2-Mercaptothiazole (56 mg, 0.48 mmol) in DMF (2 mL), was added potassium carbonate (88 mg, 0.64 mmol). The resulting suspension was heated to 40 ^{o}C and left to stir overnight. The resulting suspension was cooled to room temperature before addition of saturated sodium bicarbonate (10 mL), before extraction with ethyl acetate (2 x 20 mL). The combined organic extracts were washed with brine (2 x 20 mL), dried with magnesium sulphate, filtered and evaporated to produce the title compound. (90 mg, 73%). **^{1}H NMR**

($CDCl_3$, 400 MHz): δ 8.08 (dd, J = 16.5 Hz, 2.0 Hz, 2H, 2 x Ar), 7.66 (d, J = 3.5 Hz, 1H, Ar), 7.45 (dd, J = 8.5 Hz, 2.0 Hz, 1H, Ar), 7.20 (d, J = 4.5 Hz, 2H, 2 x Ar) 7.14-7.17 (m, 1H, Ar) 7.06 (d, J = 7.5 Hz, 1H, Ar), 6.84 (d, J = 8.5 Hz, 1H, Ar), 3.40 (s, 3H, NMe), 2.22 (s, 3H, Me); **^{13}C NMR ($CDCl_3$, 101 MHz):** δ 185.1 (C=O), 172.9 (C-Ar), 145.5 (C-Ar), 143.7 (C-Ar), 138.4 (C-Ar), 138.1 (C-Ar), 136.9 (C-Ar), 134.6 (C-Ar), 133.6 (C-Ar), 131.9 (C-Ar), 128.6 (C-Ar), 128.3 (C-Ar), 127.6 (C-Ar), 127.5 (C-Ar), 126.0 (C-Ar), 125.9 (C-Ar), 37.7 (NCH_3), 17.5 (CH_3); **FTIR:** ν_{max}/cm^{-1} (neat) 1609 (C=O), 1544 (N-O), 1463 (N-O); **HRMS (ESI^+):** calculated for (ES^+)($+H^+$): 386.0633 Found: 386.0663.

Synthesis of *N*-methyl-*N*-(2-methylphenyl)-3-nitro-4-(2-thiazolylsulfinyl)benzamide (SHF1556)

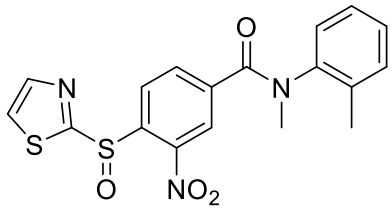

SHF1556

A solution of *N*-methyl-*N*-(2-methylphenyl)-3-nitro-4-(2-thiazolylthio)benzamide (40 mg, 0.1 mmol) in dichloromethane (2 mL) was cooled to 0 ^oC, before addition of mCPBA (20 mg, 0.11 mmol). The resulting mixture was stirred at 0 ^oC for 40 minutes. The mixture was treated with sodium bicarbonate (10 mL) before extraction with dichloromethane (2 x 10 mL). The combined organic layers were washed with brine (2 x 10 mL), dried with magnesium sulphate, filtered and evaporated. The crude was purified by flash column chromatography, eluting with 30-50% ethyl acetate/petrol to yield the title compound. (25 mg, 62%). **^{1}H NMR ($CDCl_3$, 400 MHz):** δ 8.24-8.29 (m, 2H, 2 x Ar), 7.82-7.88 (m, 2H, 2 x Ar), 7.54 (d, J = 3.0 Hz, 1H, Ar), 7.21 (d, J = J= 4.5 Hz, 2H, 2 x Ar), 7.13-7.18 (m, 1H, Ar), 7.08 (t, J = 7.5 Hz, 1H, Ar), 3.46 (s, 3H, NMe), 2.29 (s, 1.5H, Me), 2.27 (s, 1.5H, Me); **^{13}C NMR ($CDCl_3$, 101 MHz):** δ 166.9 (C=O), 144.0 (C-Ar), 142.3 (C-Ar), 142.0 (C-Ar), 140.0 (C-Ar), 134.8 (C-Ar), 134.7 (C-Ar), 134.5 (C-Ar), 131.9 (C-Ar), 129.0 (C-Ar), 128.5 (C-Ar), 127.7 (C-Ar), 127.5 (C-Ar), 126.1 (C-Ar), 125.5 (C-Ar), 125.1 (C-Ar), 37.5 (NCH_3), 17.5 (CH_3); **FTIR:** ν_{max}/cm^{-1} (neat) 1605

(C=O), 1529 (N-O), 1339 (N-O), 1068 (S=O); **HRMS (ESI$^+$):** calculated for (ES^+)($+H^+$): 402.0582 Found: 402.0586.

Synthesis of 3-nitro-4-(1,3-thiazol-2-ylsulfanyl)benzonitrile (49)

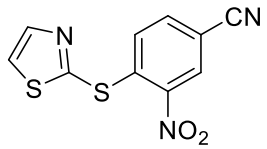

49

To a solution of 4-Fluoro-3-nitrobenzonitrile (1 g, 6.0 mmol) and 2-Mercaptothiazole (776 mg, 6.6 mmol) in DMF (24 ml), was added potassium carbonate (2.5 g, 0.64 mmol). The resulting suspension was heated to 60 ^oC and left to stir overnight. The resulting suspension cooled to room temperature before addition of saturated sodium bicarbonate (40 mL), before extraction with ethyl acetate (2 x 40 mL). Combined organic extracts washed with brine (2 x 40 mL), dried with magnesium sulphate, filtered and evaporated. The product was purified by flash column chromatography, eluting with 30%-50% ethyl acetate/petrol to produce the title compound (1.22 g, 76%). **^{1}H NMR ($CDCl_3$, 400 MHz):** δ 8.58 (d, J = 1.5 Hz, 1H, Ar), 8.15 (d, J = 3.5 Hz, 1H, Ar), 7.75 (d, J = 3.5 Hz, 1H, Ar), 7.67 (dd, J = 8.5 Hz, 1.5 Hz, 1H, Ar), 7.20 (d, J = 8.5 Hz, 1H, Ar); **^{13}C NMR ($CDCl_3$, 400 MHz):** δ 168.3 (C≡N), 145.9 (C-Ar), 144.7 (C-Ar), 142.9 (C-Ar), 135.8 (C-Ar), 129.5 (C-Ar), 129.2 (C-Ar), 126.6 (C-Ar), 116.2 (C-Ar), 110.2 (C-Ar); **FTIR:** v_{max}/cm^{-1} (neat) 2235 (C≡N), 1542 (N-O), 1343 (N-O) **HRMS (ESI$^+$):** calculated for (ES^+)($+H^+$): 263.9901 Found: 263.9921

Synthesis of 3-nitro-4-(1,3-thiazol-2-ylsulfinyl)benzonitrile (SHF1572) (50)

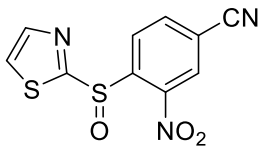

SHF1572 (50)

A solution of 3-nitro-4-(1,3-thiazol-2-ylsulfanyl)benzonitrile (1.79 g, 6.8 mmol) in dichloromethane (136 mL) was cooled to 0 ^oC before portionwise addition of mCPBA (1.76 g,

10.2 mmol). The resulting mixture was stirred at 0 ^{o}C for 1 hour, then warmed to room temperature and stirred for an additional 30 minutes. The reaction mixture was then treated with aqueous saturated sodium bicarbonate solution (100 mL). The organic layer was washed with aqueous saturated sodium bicarbonate (100 mL), and brine (2 x 100 mL), dried over magnesium sulphate, filtered and evaporated. The resulting solid was purified using flash column chromatography, eluting with 30-50% ethyl acetate/hexane to yield the title compound (1.62 g, 85%). **^{1}H NMR ($CDCl_3$, 400 MHz):** δ 8.63-8.65 (m, 2H, 2 x Ar), 8.27 (dd, J = 8.0 Hz, 1.5 Hz, 1H, Ar), 7.84 (d, J = 3.0 Hz, 1H, Ar), 7.63 (d, J = 3.0 Hz, 1H, Ar); **^{13}C NMR (MeOD, 101 MHz);** 171.3 (C≡N), 146.6 (C-Ar), 145.1 (C-Ar), 144.3 (C-Ar), 138.1 (C-Ar), 128.6 (C-Ar), 127.7 (C-Ar), 124.9 (C-Ar), 116.6 (C-Ar), 115.6 (C-Ar); **FTIR:** v_{max}/cm^{-1} (neat) 2237 (C≡N), 1540 (N-O), 1347 (N-O), 1071 (S=O); **HRMS (ESI^+):** calculated for (ES^+)(+H^+): 279.9851 Found: 279.9854

Synthesis of 3-nitro-4-(1,3-thiazol-2-ylsulfinyl)benzoic acid (SHF1578) (46)

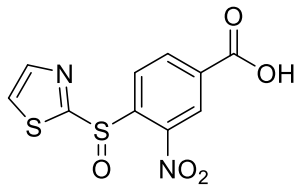

SHF1578 (46)

3-nitro-4-(1,3-thiazol-2-ylsulfinyl)benzonitrile (1.62 g, 5.8 mmol) was dissolved in a 70% mixture of sulphuric acid in water and heated to 120 ^{o}C. The resulting mixture was stirred overnight at 120 ^{o}C. The reaction mixture was then cooled to room temperature before being poured into ice cold water (100 mL). The resulting mixture was extracted with ethyl acetate (2 x 100 mL). The combined organic layers were washed with water (150 mL) and brine (150 mL), dried over magnesium sulphate, filtered and evaporated to yield the title compound (1.24 g, 72%). **^{1}H NMR (MeOD, 400 MHz):** δ 8.93 (d, J = 1.5 Hz, 1H, Ar), 8.70 (dd, J = 8.0 Hz, 1.5 Hz, 1H, Ar), 8.55 (d, J = 8.0 Hz, 1H, Ar), 7.90-7.93 (m, 2H, 2 x Ar); **^{13}C NMR (MeOD, 400 MHz)**; 165.1 (C=O), 143.4 (C-Ar), 135.8 (C-Ar), 132.5 (C-Ar), 129.8 (C-Ar), 129.1 (C-Ar), 127.6 (C-Ar), 126.4 (C-Ar), 125.9 (C-Ar), 125.3 (C-Ar); **FTIR:** v_{max}/cm^{-1} (neat) 3098 (O-

H), 1714 (C=O), 1529 (N-O), 1340 (N-O), 1263 (C-O), 1002 (S=O); **HRMS (ESI$^+$):** calculated for (ES^+)($+H^+$): 298.9796 Found: 298.9798

Synthesis of racemic SHF1556-methylbenzylamine salt (47 ±)

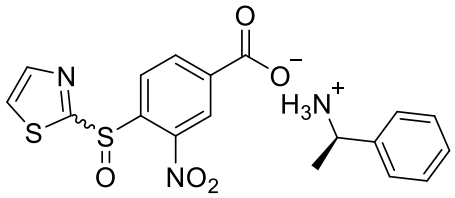

47 ±

A solution of 3-nitro-4-(1,3-thiazol-2-ylsulfinyl)benzoic acid (910 mg, 3.0 mmol) and (*S*)-α-methylbenzylamine (371 mg, 3.0 mmol) in acetonitrile (30 mL) was heated to 60 ^oC and left to stir for 3 hours. The resulting mixture was cooled to room temperature, before removal of the solvent yielded the title compound (1.27 g). **^{1}H NMR (MeOD, 400 MHz);** δ 8.91 (d, J = 1.5 Hz, 1H), 8.61 (dd, J = 8.0 Hz, 1.5 Hz, 1H), 8.44 (d, J = 8.0 Hz, 1H), 7.93 (d, J = 3.0 Hz, 1H), 7.87 (d, J = 3.0 Hz, 1H), 7.39-7.46 (m, 5H), 4.44 (q, J = 7.0 Hz, 1H), 1.63 (d, J = 7.0 Hz, 3H)

Resolution of SHF1556-methylbenzylamine salt diastereomers

Racemic SHF1556-methylbenzylamine salt was recrystallized with ethyl acetate to form the (+) diastereomer (recrystallized solid) (460 mg) and the (-) diastereomer (filtrate) (687 mg).

(+) Diastereomer: **^{1}H NMR (MeOD, 400 MHz):** δ 8.90 (d, J = 1.5 Hz, 1H, Ar), 8.60 (dd, J = 8.0 Hz, 1.5 Hz, 1H, Ar), 8.44 (d, J = 8.0 Hz, 1H, Ar), 7.92 (d, J = 3.0 Hz, 1H, Ar), 7.88 (d, J = 3.0 Hz, 1H, Ar), 7.38-7.49 (m, 5H, 5 x Ar), 4.48 (q, J = 7.0 Hz, 1H, CH), 1.65 (d, J = 7.0 Hz, 3H, CH_3)

(-) Diastereomer: **^{1}H NMR (MeOD, 400 MHz):** 8.89 (d, J = 1.5 Hz, 1H), 8.60 (dd, J = 8.0 Hz, 1.5 Hz, 1H), 8.44 (d, J = 7.0 Hz, 1H), 7.93 (d, J = 3.0 Hz, 1H), 7.88 (d, J = 3.0 Hz, 1H), 7.37-7.48 (m, 5H), 4.46 (q, J = 7.0 Hz, 1H), 1.64 (d, J = 7.0 Hz, 3H)

Synthesis of (*S*) 3-nitro-4-(1,3-thiazol-2-ylsulfinyl)benzoic acid (46 (*S*))

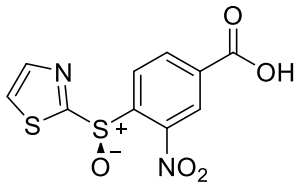

46 (*S)*

To the diastereomer of SHF1556-methylbenzylamine salt from the recrystallized solid (see above) was added 1M HCL (50 mL). The mixture was then extracted with ethyl acetate (50 mL). The organic layer was washed with 1M HCl (50 mL) and brine (2 x 50 mL), dried over magnesium sulfate, filtered and evaporated to yield the title compound (238 mg). **^{1}H NMR (MeOD, 400 MHz);** δ **^{1}H NMR (MeOD, 400 MHz):** δ 8.93 (d, J = 1.5 Hz, 1H, Ar), 8.70 (dd, J = 8.0 Hz, 1.5 Hz, 1H, Ar), 8.55 (d, J = 8.0 Hz, 1H, Ar), 7.90-7.93 (m, 2H, 2 x Ar); **HRMS (ESI$^+$):** calculated for (ES$^+$)(+H$^+$): 298.9796 Found: 298.9792

Synthesis of (*R*) 3-nitro-4-(1,3-thiazol-2-ylsulfinyl)benzoic acid (46 (*R*))

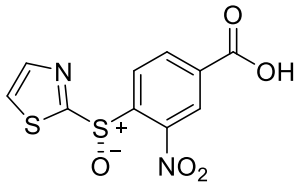

46 (*R*)

To the diastereomer of SHF1556-methylbenzylamine salt from the filtrate (see above) was added 1M HCL (50 mL). The mixture was then extracted with ethyl acetate (50 mL). The organic layer was washed with 1M HCl (50 mL) and brine (2 x 50 mL), dried over magnesium sulfate, filtered and evaporated to yield the title compound (458 mg). **^{1}H NMR (MeOD, 400 MHz);** δ **^{1}H NMR (MeOD, 400 MHz):** δ 8.93 (d, J = 1.5 Hz, 1H, Ar), 8.70 (dd, J = 8.0 Hz, 1.5 Hz, 1H, Ar), 8.55 (d, J = 8.0 Hz, 1H, Ar), 7.90-7.93 (m, 2H, 2 x Ar); **HRMS (ESI$^+$):** calculated for (ES$^+$)(+H$^+$): 298.9796 Found: 298.9791

Synthesis of (*S*) *N*-methyl-*N*-(2-methylphenyl)-3-nitro-4-(2-thiazolylsulfinyl)benzamide (SHF1556 (*S*))

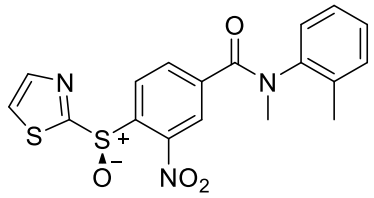

SHF1556 (*S*)

To a solution of 3-nitro-4-(1,3-thiazol-2-ylsulfinyl)benzoic acid (80 mg, 0.27 mmol) and *N*,*N*-dicyclohexylcarbodiimide (50 mg, 0.24 mmol) in dichloromethane was added *N*-methyl toluidine (41 mg, 0.27 mmol) and DMAP (0.1 mg, 0.8 mmol). The resulting mixture was heated to reflux and left to stir overnight. The mixture was then cooled to room temperature and the solvent was removed. The resulting solid was re-suspended in ethyl acetate, filtered and evaporated. The resulting solid was purified by flash column chromatography, eluting with 50%-70% ethyl acetate/hexane. Further purification by trituration with diethyl ether yielded the title compound (20 mg, 20%) **^{1}H NMR ($CDCl_3$, 400 MHz);** δ 8.24-8.28 (m, 2H, 2 x Ar), 7.82-7.87 (m, 2H, 2 x Ar), 7.54 (d, J = 3.0 Hz, 1H, Ar), 7.21 (d, J = 4.5 Hz, 2H, 2 x Ar), 7.13-7.18 (m, 1H, Ar), 7.08 (t, J = 7.5 Hz, 1H, Ar), 3.46 (s, 3H, NMe), 2.29 (s, 1.5H, Me), 2.27 (s, 1.5H, Me); **HRMS (ESI$^+$):** calculated for (ES^+)($+H^+$): 402.0582 Found: 402.0591

Synthesis of (*R*) *N*-methyl-*N*-(2-methylphenyl)-3-nitro-4-(2-thiazolylsulfinyl)benzamide (SHF1556 (*R*))

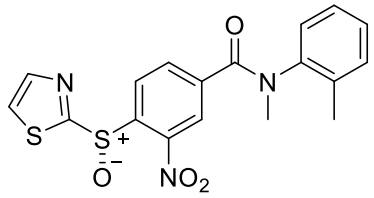

SHF1556 (*R*)

To a solution of 3-nitro-4-(1,3-thiazol-2-ylsulfinyl)benzoic acid (75 mg, 0.25 mmol) and *N*,*N*-dicyclohexylcarbodiimide (46 mg, 0.24 mmol) in dichloromethane was added *N*-methyl toluidine (30 mg, 0.23 mmol) and DMAP (0.1 mg, 0.8 mmol). The resulting mixture was

heated to reflux and left to stir overnight. The mixture was then cooled to room temperature and the solvent was removed. The resulting solid was re-suspended in ethyl acetate, filtered and evaporated. The resulting solid was purified by flash column chromatography, eluting with 50%-70% ethyl acetate/hexane. Further purification by trituration with diethyl ether yielded the title compound (18 mg, 19%) **^{1}H NMR ($CDCl_3$, 400 MHz);** δ 8.24-8.28 (m, 2H, 2 x Ar), 7.82-7.87 (m, 2H, 2 x Ar), 7.54 (d, J = 3.0 Hz, 1H, Ar), 7.21 (d, J = 4.5 Hz, 2H, 2 x Ar) 7.13-7.18 (m, 1H, Ar), 7.08 (t, J = 7.5 Hz, 1H, Ar), 3.46 (s, 3H, NMe), 2.29 (s, 1.5H, Me), 2.27 (s, 1.5H, Me); **HRMS (ESI^+):** calculated for (ES^+)($+H^+$): 402.0582 Found: 402.0589

Synthesis of *N*-methyl-*N*-(2-methylphenyl)-3-nitro-4-(1,3-thiazol-2-ylsulfonyl)benzamide (SHF1558)

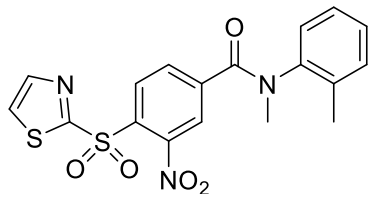

SHF1558

To a solution of *N*-methyl-*N*-(2-methylphenyl)-3-nitro-4-(2-thiazolylsulfinyl)benzamide (20 mg, 0.05 mmol) in dichloromethane (1 mL) was added mCPBA (54 mg, 0.31 mmol). The resulting mixture was stirred at room temperature for 3 hours minutes. The mixture was treated with sodium bicarbonate (10 mL) before extraction with dichloromethane (2 x 10 mL). The combined organic layers were washed with brine (2 x 10 mL), dried with magnesium sulphate, filtered and evaporated. The crude was purified by flash column chromatography, eluting with 30-50% ethyl acetate/petrol to yield the title compound (11 mg, 52%). **^{1}H NMR ($CDCl_3$, 400 MHz):** δ 8.58 (d, J = 2.0 Hz, 2H, 2 x Ar), 8.15 (d, J = 3.5 Hz, 2H, 2 x Ar), 7.78-7.80 (m, 1H, Ar), 7.75 (d, J = 3.5 Hz, 2H, 2 x Ar), 7.65-7.68 (m, 2H, 2 x Ar), 3.44 (s, 3H, NMe), 2.26 (s, 3H, Me); **HRMS (ESI^+):** calculated for (ES^+)($+H^+$): 418.0531 Found: 418.0521

Synthesis of 3-amino-*N*-methyl-*N*-(2-methylphenyl)-4-(1,3-thiazol-2-ylsulfinyl)benzamide (SHF1574)

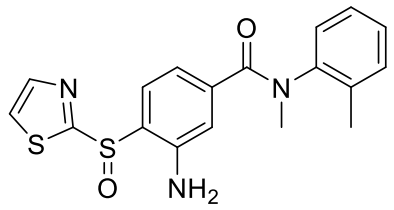

SHF1574

To a solution of *N*-Methyl-*N*-(2-methylphenyl)-3-nitro-4-(2-thiazolylsulfinyl)benzamide (29 mg, 0,072 mmol) in THF (1 mL) was added saturated aqueous ammonium chloride solution (0.1 mL) followed by portionwise addition of zinc (47 mg, 0.72 mmol). The resulting suspension was left to stir overnight at room temperature. The resulting suspension was then filtered through a pad of celite, washing with ethyl acetate (10 mL). The filtrate was washed with water (2 x 10 mL), dried over magnesium sulphate, filtered and evaporated. The resulting product was purified by flash column chromatography, eluting with 30-50% ethyl acetate/petrol to yield the title compound (10 mg, 37%): **^{1}H NMR ($CDCl_3$, 400 MHZ**); δ 8.23 (s, 1H, Ar), 8.08 (dd, J = 16.0 Hz, 2.0 Hz, 1H, Ar), 7.66 (d, J = 3.5 Hz, 1H, Ar), 7.45 (s, 2H, 2 x Ar), 7.20 (d, J = 4.0 Hz, 2H, 2 x Ar), 7.13-7.18 (m, 1H, Ar), 7.06 (t, J = 5.5 Hz, 1H, Ar), 3.48 (s, 3H, NMe), 2.29 (s, 3H, CH_3); **LCMS** (372.1 $[M-H]^-$)

Synthesis of 3-nitro-4-(1,3-thiazol-2-ylsulfanyl)benzoic acid (51)

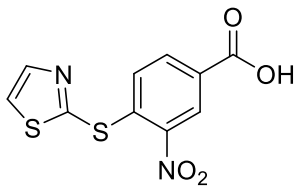

51

A solution of 3-nitro-4-(1,3-thiazol-2-ylsulfanyl)benzonitrile (500 mg, 1.9 mmol) in 70% sulphuric acid/water (8 mL) was heated to 120 ^oC and stirred for 18 hours. The resulting mixture was diluted with ice cold water (80 ml) before extraction with ethyl acetate (2 x 80

mL). The combined organic layers were washed with water (100 mL) and brine (100 mL), dried with magnesium sulfate, filtered and evaporated to produce the title compound (512 mg, 96%). **^{1}H NMR ($CDCl_3$, 400 MHz)**: δ 8.95 (d, J = 2.0 Hz, 1H, Ar), 8.14 (d, J = 3.5 Hz, 1H, Ar), 8.10 (dd, J = 8.5 Hz, 2.0 Hz, 1H, Ar), 7.73 (d, 8.5 Hz, 1H, Ar), 7.15 (d, J = 8.5 Hz, 1H, Ar); **^{13}C NMR (MeOD, 101 MHz)** δ 165.5 (C=O), 156.6 (C-Ar), 145.2 (C-Ar), 140.6 (C-Ar), 133.9 (C-Ar), 128.2 (C-Ar), 127.2 (C-Ar), 126.4 (C-Ar), 78.0 (C-Ar), 53.4 (C-Ar); **FTIR:** ν_{max}/cm^{-1} (neat) 3084 (O-H), 1700 (C=O 1529 (N-O), 1314 (N-O), 1245 (C-O); **HRMS (ESI^+):** calculated for (ES^+)(+H^+): 282.9847 Found: 282.9889

Synthesis of *N*-(2-methylphenyl)-3-nitro-4-(1,3-thiazol-2-ylsulfanyl)benzamide

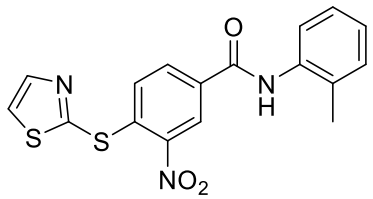

To a solution of 3-nitro-4-(1,3-thiazol-2-ylsulfanyl)benzoic acid (75 mg, 0.27 mmol) in dichloromethane (0.4 M), was added thionyl chloride (0.11 mL, 2.7 mmol) and DMF (2 drops). The resulting mixture was heated under reflux for 1.5 hours. The mixture was cooled to room temperature before being evaporated. The resulting solid was re-dissolved in dichloromethane (0.3 M) before addition of a solution of aniline (37 mg, 0.27 mmol) and triethylamine (0.11 mL, 0.81 mmol). The resulting mixture was stirred at room temperature for 1 hour. Sodium bicarbonate (10 mL) was then added to the mixture before extracting with dichloromethane (10 mL). The organic layer was washed with saturated potassium carbonate (10 mL) and brine (2 x 10 mL), dried with magnesium sulphate, filtered and evaporated. The crude product was purified by flash column chromatography, eluting with 30-50% ethyl acetate/petrol to yield the title compound (76 mg, 76%): **^{1}H NMR ($CDCl_3$, 400 MHz);** δ 8.73 (d, J = 2.0 Hz, 1H, Ar), 8.11 (d, J = 3.5 Hz, 1H, Ar), 7.92-7.97 (m, 2H, 2 x Ar), 7.72 (d, J = 3.5 Hz, 1H, Ar), 7.20-7.24 (m, 2H, Ar), 7.11-7.17 (m, 2H, 2 x Ar), 2.30 (s, 3H, Me); **HRMS (ESI^+):** calculated for (ES^+)(+H^+): 372.0477 Found: 327.0473

Synthesis of *N*-(2-methylphenyl)-3-nitro-4-(1,3-thiazol-2-ylsulfinyl)benzamide (SHF1568)

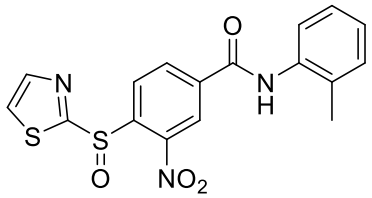

SHF1568

A solution of *N*-(2-methylphenyl)-3-nitro-4-(1,3-thiazol-2-ylsulfanyl)benzamide (75 mg, 0.2 mmol) in dichloromethane (5 mL) was cooled to 0 ^{o}C, before addition of mCPBA (52 mg, 0.03 mmol) The resulting mixture was stirred at 0 ^{o}C for 45 minutes. The resulting mixture treated with sodium bicarbonate (10 mL) before extraction with dichloromethane (2 x 10 mL). The organic layer washed with brine (2 x 10 mL), dried with magnesium sulphate, filtered and evaporated. The product was purified by preparative HPLC, eluting with a gradient of 5% to 80% water/acetonitrile for 20 minutes to form the title compound (33 mg, 42%). **^{1}H NMR ($CDCl_3$, 400 MHz):** δ 8.86 (s, 1H, Ar), 8.65 (d, J = 8.0 Hz, 1H, Ar), 8.48 (d, J = 8.0 Hz, 1H, Ar), 7.86 (d, J = 3.0 Hz, 1H, Ar), 7.61 (d, J = 3.0 Hz, 1H, Ar), 7.30-7.34 (m, 2H, 2 x Ar), 7.20-7.24 (m, 2H, 2 x Ar), 2.39 (s, 3H, Me); **HRMS (ESI^{+}):** calculated for (ES^{+})($+H^{+}$): 388.0426 Found: 388.0434

Synthesis of 3-nitro-*N*-phenyl-4-(1,3-thiazol-2-ylsulfinyl)benzamide (SHF1576)

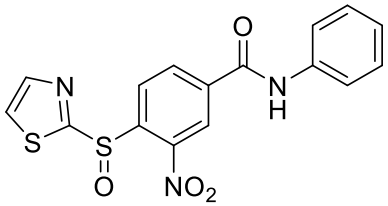

SHF1576

To a solution of 3-nitro-4-(1,3-thiazol-2-ylsulfinyl)benzoic acid (75 mg, 0.25 mmol) in dichloromethane (1 mL) was added thionyl chloride (13 µL, 2.5 mmol) and DMF (2 drops). The resulting mixture was heated to reflux and left to stir for 2 hours. The resulting mixture was cooled to room temperature before being evapourated. To a solution of the resulting acid chloride in dichloromethane (1 mL) was added a solution of aniline (23 mg, 0.25 mmol) and triethylamine (0.1 mL, 0.75 mmol) in dichloromethane (1 mL) dropwise. The resulting mixture was left to stir at room temperature for 2 hours. The reaction mixture was then diluted with dichloromethane (10 mL) before addition of saturated aqueous sodium bicarbonate solution (10 mL). The organic layer was separated and washed with saturated aqueous sodium bicarbonate (10 mL) and brine (2 x 10 mL), dried over magnesium sulphate, filtered and evaporated. The resulting product was purified by flash column chromatography, eluting with 40-60% ethyl acetate/petrol to yield the corresponding amide (20 mg, 21%): **^{1}H NMR ($CDCl_3$, 400 MHz);** δ 8.74 (δ, J = 2.0 Hz, 1H, Ar), 8.13 (d, J = 3.5 Hz, 1H, Ar), 7.98-8.03 (m, 1H, Ar), 7.73 (d, J = 3.5 Hz, 1H, Ar), 7.64 (d, J = 8.0 Hz, 1H, Ar), 7.40 (t, J = 8.0 Hz, 2H, 2 x Ar), 7.15-7.24 (m, 3H, 3 x Ar) **LCMS** (374.1 $[M-H]^+$)

Synthesis of *N*-methyl-3-nitro-*N*-phenyl-4-(1,3-thiazol-2-ylsulfanyl)benzamide

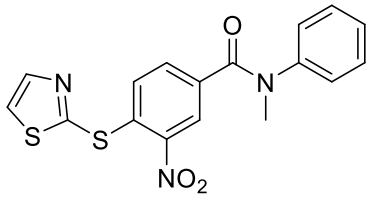

To a solution of 3-nitro-4-(1,3-thiazol-2-ylsulfanyl)benzoic acid (100 mg, 0.35 mmol) in dichloromethane (0.9 mL), was added thionyl chloride (0.15 mL, 1.8 mmol) and DMF (2 drops). The resulting mixture was heated under reflux for 1.5 hours. The mixture was cooled to room temperature before being evaporated. The resulting solid was re-dissolved in dichloromethane (1 mL) before addition of a solution of aniline (37 mg, 0.27 mmol) and triethylamine (0.11 mL, 0.81 mmol) in dichloromethane (1 mL). The resulting mixture was stirred at room temperature for 1 hour. Sodium bicarbonate (10 mL) was then added to the mixture before extracting with dichloromethane (10 mL). The organic layer was washed with saturated potassium carbonate (10 mL) and brine (2 x 10 mL), dried with magnesium

sulphate, filtered and evaporated. The crude product was purified by flash column chromatography, eluting with 50% ethyl acetate/petrol to yield the title compound (67 mg, 52%). **^{1}H NMR ($CDCl_3$, 400 MHz):** δ 8.14 (d, J = 1.5 Hz, 1H, Ar), 8.04 (d, J = 3.5 Hz, 1H, Ar), 7.65 (d, J = 3.5 Hz, 1H, Ar), 7.40 (dd, J = 8.5 Hz, 2.0 Hz, 1H, Ar), 7.27-7.31 (m, 2H, 2 x Ar), 7.22 (t, J = 7.5 Hz, 1H, Ar), 7.06 (d, J = 7.5 Hz, 2H, 2 x Ar), 6.84 (d, J = 8.5 Hz, 1H, Ar), 3.50 (s, 3H, NMe); **HRMS (ESI^+):** calculated for (ES^+)(+H^+): 372.0477 Found: 372.0479

Synthesis of *N*-methyl-3-nitro-*N*-phenyl-4-(1,3-thiazol-2-ylsulfinyl)benzamide (SHF1582)

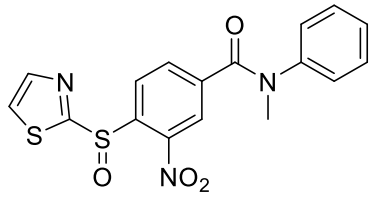

SHF1582

A solution of *N*-methyl-3-nitro-*N*-phenyl-4-(1,3-thiazol-2-ylsulfanyl)benzamide (67 mg, 0.18 mmol) in dichloromethane (4 mL) was cooled to 0 ^oC, before addition of mCPBA (37 mg, 0.22 mmol). The resulting mixture was stirred at 0 ^oC for 45 minutes. The resulting mixture treated with sodium bicarbonate (10 mL) before extraction with dichloromethane (2 x 10 mL). The organic layer washed with brine (2 x 10 mL), dried with magnesium sulphate, filtered and evaporated. The product was purified by preparative HPLC, eluting with a gradient of 5% to 80% water/acetonitrile for 20 minutes to yield the title compound (30 mg, 43%). **^{1}H NMR ($CDCl_3$, 400 MHz):** δ 8.28 (d, J = 8.0 Hz, 2H, 2 x Ar), 7.82-7.85 (m, 2H, 2 x Ar) 7.55 (d, J = 3.0 Hz, 1H, Ar), 7.32 (d, J = 7.0 Hz, 2H, 2 x Ar), 7.25 (d, J = 7.0 Hz, 1H, Ar), 7.09 (d, J = 7.5 Hz, 2H, 2 x Ar), 3.57 (s, 3H, NMe); **HRMS (ESI^+):** calculated for (ES^+)(+H^+): 388.0426 Found: 388.0420

Synthesis of *N*-(4-ethoxyphenyl)-3-nitro-4-(1,3-thiazol-2-ylsulfanyl)benzamide

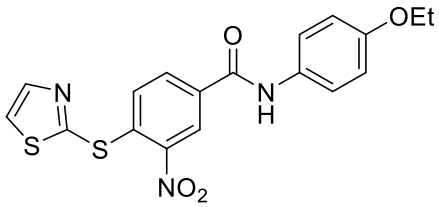

To a solution of 3-nitro-4-(1,3-thiazol-2-ylsulfanyl)benzoic acid (75 mg, 0.27 mmol) in dichloromethane (0.4 M), was added thionyl chloride (0.11 mL, 2.7 mmol) and DMF (2 drops). The resulting mixture was heated under reflux for 1.5 hours. The mixture was cooled to room temperature before being evaporated. The resulting solid was re-dissolved in dichloromethane (0.3 M) before addition of a solution of aniline (37 mg, 0.27 mmol) and triethylamine (0.11 mL, 0.81 mmol). The resulting mixture was stirred at room temperature for 1 hour. Sodium bicarbonate (10 mL) was then added to the mixture before extracting with dichloromethane (10 mL). The organic layer was washed with saturated potassium carbonate (10 mL) and brine (2 x 10 mL), dried with magnesium sulphate, filtered and evaporated. The crude product was purified by flash column chromatography, eluting with 30-50% ethyl acetate/petrol to provide the title compound (80 mg, 73%). **^{1}H NMR ($CDCl_3$, 400 MHz):** δ 8.73 (d, J = 1.5 Hz, 1H, Ar), 8.13 (d, J = 3.5 Hz, 1H, Ar), 7.99 (J = 8.5 Hz, 1H, Ar), 7.72 (d, J = 3.5 Hz, 1H, Ar), 7.53 (d, J = 9.0 Hz, 1H, Ar), 7.19 (d, J = 8.5 Hz, 1H, Ar), 6.94 (d, J = 9.0 Hz, 2H, 2 x Ar), 4.06 (q, J = 6.5 Hz, 2H, CH_2), 1.44 (t, J = 7.5 Hz, 3H, CH_3); **HRMS (ESI^+):** calculated for (ES^+)(+H^+): 402.0586 Found: 402.0593 (402 [M-H]$^-$)

Synthesis of *N*-(4-ethoxyphenyl)-3-nitro-4-(1,3-thiazol-2-ylsulfinyl)benzamide (SHF1564)

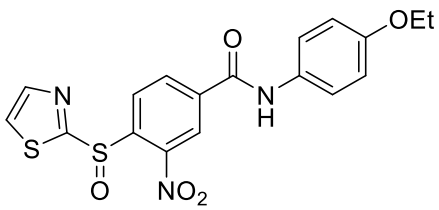

SHF1564

A solution of *N*-(4-ethoxyphenyl)-3-nitro-4-(1,3-thiazol-2-ylsulfanyl)benzamide (15 mg, 0.03 mmol) in dichloromethane (60 mM) was cooled to 0 ^{o}C, before addition of mCPBA (10 mg, 0.05 mmol)). The resulting mixture was stirred at 0 ^{o}C for 45 minutes. The resulting mixture treated with sodium bicarbonate (10 mL) before extraction with dichloromethane (2 x 10 mL). The organic layer washed with brine (2 x 10 mL), dried with magnesium sulphate, filtered and evaporated. The product was purified by preparative HPLC, eluting with a gradient of 5% to 80% water/acetonitrile for 20 minutes to obtain the title compound (12 mg, 58%). **^{1}H NMR ($CDCl_3$, 400 MHz):** δ 8.84 (s, 1H, Ar), 8.63 (d, J = 8.0 Hz, 1H, Ar), 8.48 (d, J = 8.0 Hz, 1H, Ar), 7.86 (d, J = 3.0 Hz, 1H, Ar), 7.60 (d, J = 3.0 Hz, 1H, Ar), 7.54-7.58 (m, 2H, 2 x Ar), 6.96 (d, J = 9.0 Hz, 2H, 2 x Ar), 4.08 (q, J = 7.0 Hz, 2H, CH_2), 1.35 (t, J = 7.5 Hz, 3H, CH_3); **HRMS (ESI^+):** calculated for (ES^+)(+H^+): 418.0531 Found: 418.0543

Synthesis of 3-nitro-4-(1,3-thiazol-2-ylsulfanyl)-*N*-(3,4,5-trimethoxyphenyl)benzamide

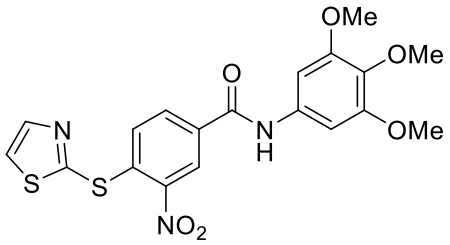

To a solution of 3-nitro-4-(1,3-thiazol-2-ylsulfanyl)benzoic acid (75 mg, 0.27 mmol) in dichloromethane (0.4 M), was added thionyl chloride (0.11 mL, 2.7 mmol) and DMF (2 drops). The resulting mixture was heated under reflux for 1.5 hours. The mixture was cooled to room temperature before being evaporated. The resulting solid was re-dissolved in dichloromethane (0.3 M) before addition of a solution of aniline (37 mg, 0.27 mmol) and triethylamine (0.11 mL, 0.81 mmol). The resulting mixture was stirred at room temperature for 1 hour. Sodium bicarbonate (10 mL) was then added to the mixture before extracting with dichloromethane (10 mL). The organic layer was washed with saturated potassium carbonate (10 mL) and brine (2 x 10 mL), dried with magnesium sulphate, filtered and evaporated. The crude product was purified by flash column chromatography, eluting with 30-50% ethyl acetate/petrol to provide the title compound (81 mg, 67%); **^{1}H NMR ($CDCl_3$,**

400 MHz): δ 8.73 (d, J = 2.0 Hz, 1H, Ar), 8.14 (d, J = 3.5 Hz, 1H, Ar), 8.00 (dd, J = 8.5 Hz, 2.0 Hz, 1H, Ar), 7.73 (d, J = 3.5 Hz, 1H, Ar), 7.20 (d, J = 8.5 Hz, 1H, Ar), 6.97 (s, 2H, 2 x Ar), 3.91 (s, 9H, 3 x OMe); **HRMS (ESI$^+$):** calculated for (ES$^+$)(+H$^+$): 448.0637 Found: 448.0641

Synthesis of 3-nitro-4-(1,3-thiazol-2-ylsulfinyl)-*N*-(3,4,5-trimethoxyphenyl)benzamide (SHF1566)

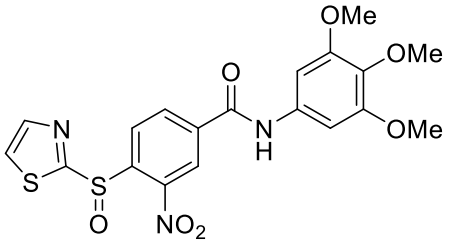

SHF1566

A solution of 3-nitro-4-(1,3-thiazol-2-ylsulfanyl)-*N*-(3,4,5-trimethoxyphenyl)benzamide (80 mg, 0.18 mmol) in dichloromethane (5 mL) was cooled to 0 ^oC, before addition of mCPBA (37 mg, 0.21 mmol). The resulting mixture was stirred at 0 ^oC for 45 minutes. The resulting mixture treated with sodium bicarbonate (10 mL) before extraction with dichloromethane (2 x 10 mL). The organic layer washed with brine (2 x 10 mL), dried with magnesium sulphate, filtered and evaporated. The product was purified by preparative HPLC, eluting with a gradient of 5% to 80% water/acetonitrile for 20 minutes to obtain the title compound (61 mg, 72%) **^{1}H NMR ($CDCl_3$, 400 MHz);** δ 8.85 (d, J = 1.5 Hz, 1H, Ar), 8.63 (d, J = 8.0 Hz, 1H, Ar), 8.49 (dd, J = 8.0 Hz, 1.5 Hz, 1H, Ar), 7.86 (d, J = 3.0 Hz, 1H, Ar), 7.61 (d, J = 3.0 Hz, 1H, Ar), 7.00 (s, 2H, 2 x Ar), 3.92 (s, 9H, 3 x OMe); **HRMS (ESI$^+$):** calculated for (ES$^+$)(+H$^+$): 464.0586 Found: 464.0591

Synthesis of *N*-Methyl-3,4,5-trimethoxyaniline

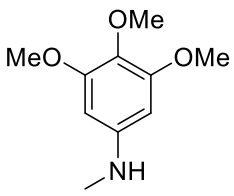

To a solution of 3,4,5-trimethoxyaniline (100 mg, 0.55 mmol) in THF (5 mL) was added formaldehyde (37% wt in water) (54 µL, 0.66 mmol), acetic acid (62 µL, 1.1 mmol) and sodium triacetoxyborohydride (466 mg, 2.2 mmol). The resulting mixture was stirred at room temperature for 20 minutes. The mixture was then quenched with saturated aqueous potassium carbonate solution (10 mL) before extraction with ethyl acetate (20 mL). The organic layer was washed with saturated sodium bicarbonate solution (20 mL) and brine (2 x 20 mL), dried over magnesium sulphate, filtered and evaporated. The resulting oil was purified by flash column chromatography, eluting with 60-80% ethyl acetate/hexane to yield the title compound (52 mg, 48%); ^{1}NMR ($CDCl_3$, 400 MHz); δ 5.86 (s, 2H, 2 x Ar), 3.85 (s, 6H, 2 x OMe), 3.78 (s, 3H, OMe), 2.83 (s, 3H, NMe) **HRMS (ESI$^+$):** calculated for (ES^+)($+H^+$): 198.1130 Found: 198.1133

Synthesis of *N*-methyl-3-nitro-4-(1,3-thiazol-2-ylsulfanyl)-*N*-(3,4,5-trimethoxyphenyl)benzamide

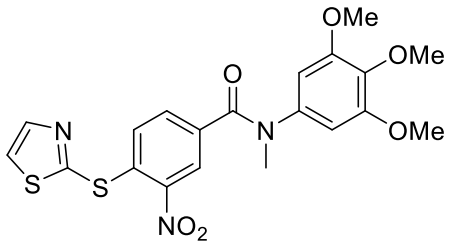

To a solution of 3-nitro-4-(1,3-thiazol-2-ylsulfanyl)benzoic acid (67 mg, 0.24 mmol) in dichloromethane (0.7 mL) was added oxalyl chloride (152 mg, 1.2 mmol) and DMF (2 drops). The resulting mixture was heated to reflux and left to stir for 2 hours. The mixture was then cooled to room temperature and evaporated. The resulting solid was then re-dissolved in dichloromethane (1 mL) and a solution of *N*-methyl-3,4,5-trimethoxyaniline (47 mg, 0.24 mmol) and triethylamine (0.07 mL, 0.62 mmol) in dichloromethane (1 mL) was added dropwise. The resulting mixture was stirred at room temperature for 2 hours. The reaction mixture was then diluted with dichloromethane (10 mL) and washed with saturated sodium

bicarbonate solution (2x 10 mL) and brine (2 x 10 mL), dried over magnesium sulfate, filtered and evaporated. The resulting solid was purified by flash column chromatography, eluting with 70-80% ethyl acetate in hexane to yield the title compound (52 mg, 52%) **^{1}H NMR ($CDCl_3$, 400 MHz);** δ 8.27 (d, J = 2.0 Hz, 1H, Ar), 8.05 (d, J = 3.5 Hz, 1H, Ar), 7.66 (d, J = 3.5 Hz, 1H, Ar), 7.45 (dd, J = 8.5 Hz, 2.0 Hz, 1H, Ar), 6.89 (d, J = 8.5 Hz, 1H, Ar), 6.30 (s, 2H, 2 x Ar), 3.81 (s, 3H, OMe), 3.74 (s, 6H, 2 x OMe), 3.47 (s, 3H, NMe) **HRMS (ESI^+):** calculated for (ES^+)(+H^+): 462.0794 Found: 462.0805

Synthesis of *N*-methyl-3-nitro-4-(1,3-thiazol-2-ylsulfinyl)-*N*-(3,4,5-trimethoxyphenyl)benzamide (SHF1583)

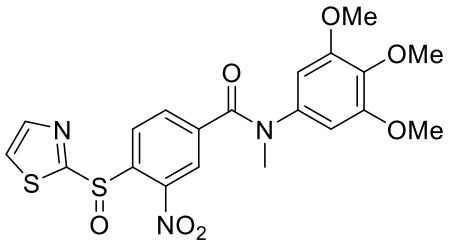

SHF1583

A solution of *N*-methyl-3-nitro-4-(1,3-thiazol-2-ylsulfanyl)-*N*-(3,4,5-trimethoxyphenyl)benzamide (52 mg, 0.11 mmol) in dichloromethane (1 mL) was cooled to 0 ^oC before addition of mCPBA (23 mg, 0.14 mmol). The resulting mixture was stirred at 0 ^oC for 1 hour. The resulting mixture was diluted with dichloromethane (10 mL) and washed with saturated sodium bicarbonate solution (2 x 10 mL) and brine (2 x 10 mL), dried over magnesium sulphate, filtered and evaporated. The resulting solid was purified by preparative HPLC, eluting with a gradient of 5% to 80% acetonitrile/water over 18 minutes to yield compound the tiltle compound (35 mg, 67%) **1H NMR ($CDCl_3$, 400 MHz);** δ 8.31-8.36 (m, 2H, 2 x Ar), 7.97 (d, J = 8.0 Hz, 1H, Ar), 7.82 (d, J = 3.0 Hz, 1H, Ar), 7.55 (d, J = 3.0 Hz, 1H, Ar), 6.30 (s, 2H, 2 x Ar), 3.79 (s, 3H, OMe), 3.72 (s, 6H, 3 x OMe), 3.54 (s, 3H, NMe) **HRMS (ESI^+):** calculated for (ES^+)(+H^+): 478.0743 Found: 478.0756

Synthesis of *N*-methyl-4-ethoxyaniline

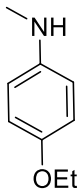

To a solution of 4-ethoxyaniline (100 mg, 0.55 mmol) in THF (5 mL) was added formaldehyde (37% wt in water) (54 µL, 0.66 mmol), acetic acid (62 µL, 1.1 mmol) and sodium triacetoxyborohydride (466 mg, 2.2 mmol). The resulting mixture was stirred at room temperature for 20 minutes. The mixture was then quenched with saturated aqueous potassium carbonate solution (10 mL) before extraction with ethyl acetate (20 mL). The organic layer was washed with saturated sodium bicarbonate solution (20 mL) and brine (2 x 20 mL), dried over magnesium sulphate, filtered and evaporated. The resulting oil was purified by flash column chromatography, eluting with 60-80% ethyl acetate/hexane to yield the title compound (52 mg, 48%); **^{1}H NMR ($CDCl_3$, 400 MHz);** δ 6.82 (dd, J = 7.0 Hz, 2.0 Hz, 2H, 2 x Ar), 6.60 (dd, J = 7.0 Hz, 2.0 Hz, 2H, 2 x Ar), 3.99 (q, J = 7.0 Hz, 2H, CH_2), 2.83 (s, 3H, CH_3), 1.40 (t, J = 7.0 Hz, 3H) **HRMS (ESI^+):** calculated for (ES^+)($+H^+$): 152.1075 Found: 152.1070

Synthesis of *N*-(4-ethoxyphenyl)-*N*-methyl-3-nitro-4-(1,3-thiazol-2-ylsulfinyl)benzamide (SHF1584)

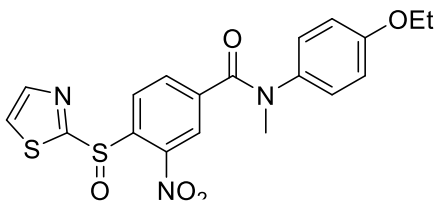

SHF1584

To a solution of 3-nitro-4-(1,3-thiazol-2-ylsulfinyl)benzoic acid (80 mg, 0.27 mmol) and *N*,*N*-dicyclohexylcarbodiimide (66 mg, 0.32 mmol) in dichloromethane was added *N*-methyl-4-ethoxyaniline (41 mg, 0.27 mmol) and DMAP (0.1 mg, 0.8 mmol). The resulting mixture was heated to reflux and left to stir overnight. The mixture was then cooled to room temperature and the solvent was removed. The resulting solid was re-suspended in ethyl acetate, filtered and evaporated. The resulting solid was purified by flash column chromatography, eluting with 50%-70% ethyl acetate/hexane to yield the title compound (35 mg, 30%); **^{1}H NMR ($CDCl_3$, 400 MHz);** δ 8.27-8.30 (m, 2H, 2 x Ar), 7.81-7.83 (m, 2H, 2 x Ar), 7.54 (d, J = 3.0 Hz, 1H, Ar), 6.99 (d, J = 8.5 Hz, 2H, 2 x Ar), 6.77 (d, J = 8.5 Hz, 2H, 2 x Ar), 3.99 (q, J = 7.0 Hz, 2H, CH_2), 3.52 (s, 3H, NMe), 1.41 (t, J = 7.0 Hz, 3H, CH_3) **HRMS (ESI^+):** calculated for (ES^+)(+H^+): 432.0688 Found: 432.0683

Synthesis of 4-nitro-3-(1,3-thiazol-2-ylsulfanyl)benzonitrile

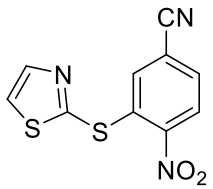

To a solution of 3-flouro-4-nitrobenzonitrile (200 mg , 1.2 mmol) and 2-mercapothiazole (155 mg, 1.3 mmol) in dimethylformide (4.5 mL) was added potassium carbonate (499 mg, 3.6 mmol). The resulting suspension was heated to 60 ^oC and left to stir overnight. The mixture was then treated with aqueous saturated sodium bicarbonate solution (10 mL) before extraction with ethyl acetate (2 x 20 mL). The combined organic layers were washed with aqueous saturated sodium bicarbonate solution (20 mL) and brine (2 x 20 mL), dried over magnesium sulphate, filtered and evaporated. The resulting solid was purified by flash column chromatography, eluting with 40-50% ethyl acetate/hexane to yield the title compound (231 mg, 73%). **^{1}H NMR ($CDCl_3$, 400 MHz):** δ 8.36 (d, J = 8.5 Hz, 1H, Ar), 8.15 (d, J = 3.5 Hz, 1H, Ar), 7.74 (d, J = 3.5 Hz, 1H, Ar), 7.62 (dd, J = 8.5 Hz, 1.5 Hz, 1H, Ar), 7.42 (d, J = 1.5 Hz, 1H, Ar); **HRMS (ESI^+):** calculated for (ES^+)(+H^+): 263.9901 Found: 263.9892

Synthesis of 4-nitro-3-(1,3-thiazol-2-ylsulfinyl)benzonitrile (SHF1588)

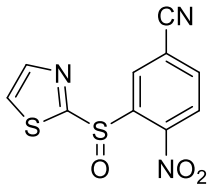

SHF1588

A solution of 4-nitro-3-(1,3-thiazol-2-ylsulfanyl)benzonitrile (225 mg, 0.85 mmol) in dichloromethane (17 mL) was cooled to 0 ^{o}C before portionwise addition of mCPBA (177 mg, 1.02 mmol). The resulting mixture was stirred at 0 ^{o}C for 1 hour, then warmed to room temperature and stirred for an additional 30 minutes. The reaction mixture was then treated with aqueous saturated sodium bicarbonate solution (20 mL). The organic layer was washed with aqueous saturated sodium bicarbonate (20 mL), and brine (2 x 20 mL), dried over magnesium sulphate, filtered and evaporated. The resulting solid was purified using flash column chromatography, eluting with 40% ethyl acetate/hexane to yield the title compound (116 mg, 49%). **^{1}H NMR ($CDCl_3$, 400 MHz):** δ 8.76 (d, J = 2.0 Hz, 1H, Ar), 8.48 (d, J = 8.5 Hz, 1H, Ar), 8.07 (dd, J = 8.5 Hz, 2.0 Hz, 1H, Ar), 7.84 (d, J = 3.0 Hz, 1H, Ar), 7.63 (d, J = 3.0 Hz, 1H, Ar); **HRMS (ESI^{+}):** calculated for (ES^{+})($+H^{+}$): 279.9851 Found: 279.9851

Synthesis of 3-nitro-2-(1,3-thiazol-2-ylsulfanyl)benzonitrile

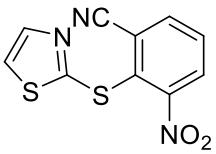

To a solution of 3-flouro-4-nitrobenzonitrile (200 mg , 1.2 mmol) and 2-mercapothiazole (155 mg, 1.3 mmol) in dimethylformamide (4.5 mL) was added potassium carbonate (499 mg, 3.6 mmol). The resulting suspension was heated to 60 ^{o}C and left to stir overnight. The mixture was then treated with aqueous saturated sodium bicarbonate solution (10 mL) before extraction with ethyl acetate (2 x 20 mL). The combined organic layers were washed with aqueous saturated sodium bicarbonate solution (20 mL) and brine (2 x 20 mL), dried

over magnesium sulphate, filtered and evaporated. The resulting solid was purified by flash column chromatography, eluting with 40-50% ethyl acetate/hexane to yield the title compound (210 mg, 66%). **^{1}H NMR ($CDCl_3$, 400 MHz):** δ 8.17 (dd, J = 8.0 Hz, 1.5 Hz, 1H, Ar), 7.96 (dd, J = 8.0 Hz, 1.5 Hz, 1H, Ar), 7.73 (d, J = 3.5 Hz, 1H, Ar), 7.69 (t, J = 8.0 Hz, 1H, Ar), 7.42 (d, J = 3.5 Hz, 1H, Ar); **HRMS (ESI^+):** calculated for (ES^+)($+H^+$): 263.9901 Found: 263.9911

Synthesis of 3-nitro-2-(1,3-thiazol-2-ylsulfinyl)benzonitrile (SHF1589)

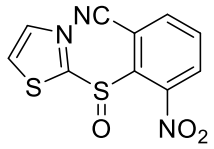

SHF1589

A solution of 3-nitro-2-(1,3-thiazol-2-ylsulfanyl)benzonitrile (210 mg, 0.80 mmol) in dichloromethane (16 mL) was cooled to 0 ^oC before portionwise addition of mCPBA (165 mg, 0.96 mmol). The resulting mixture was stirred at 0 ^oC for 1 hour, then warmed to room temperature and stirred for an additional 30 minutes. The reaction mixture was then treated with aqueous saturated sodium bicarbonate solution (20 mL). The organic layer was washed with aqueous saturated sodium bicarbonate (20 mL), and brine (2 x 20 mL), dried over magnesium sulphate, filtered and evaporated. The resulting solid was purified using flash column chromatography, eluting with 40% ethyl acetate/hexane to yield the title compound (116 mg, 52%). **^{1}H NMR ($CDCl_3$, 400 MHz):** δ 8.49 (dd, J = 8.5 Hz, 1.5 Hz, 1H, Ar), 8.23 (dd, J = 8.0 Hz, 1.0 Hz, 1H, Ar), 7.87-7.92 (m, 2H, 2 x Ar), 7.73 (d, J = 3.0 Hz, 1H, Ar); **HRMS (ESI^+):** calculated for (ES^+)($+H^+$): 279.9851 Found: 279.

Synthesis of 2-nitro-3-(1,3-thiazol-2-ylsulfanyl)benzonitrile

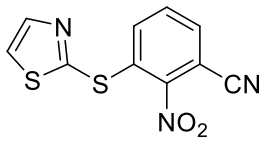

To a solution of 3-flouro-4-nitrobenzonitrile (200 mg , 1.2 mmol) and 2-mercapothiazole (155 mg, 1.3 mmol) in dimethylformamide (4.5 mL) was added potassium carbonate (499 mg, 3.6 mmol). The resulting suspension was heated to 60 ^{o}C and left to stir overnight. The mixture was then treated with aqueous saturated sodium bicarbonate solution (10 mL) before extraction with ethyl acetate (2 x 20 mL). The combined organic layers were washed with aqueous saturated sodium bicarbonate solution (20 mL) and brine (2 x 20 mL), dried over magnesium sulphate, filtered and evaporated. The resulting solid was purified by flash column chromatography, eluting with 40-50% ethyl acetate/hexane to yield the title compound (160 mg, 51%). **^{1}H NMR ($CDCl_3$, 400 MHz):** 8.03 (d, J = 3.5 Hz, 1H, Ar), 7.73-7.75 (m, 1H, Ar), 7.64 (d, J = 3.5 Hz, 1H, Ar), 7.56-7.58 (m, 2H, 2 x Ar); **HRMS (ESI^{+}):** calculated for (ES^{+})($+H^{+}$): 263.9901 Found: 263.9908

Synthesis of 2-nitro-3-(1,3-thiazol-2-ylsulfinyl)benzonitrile (SHF1591)

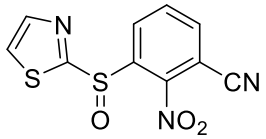

SHF1591

A solution of 2-nitro-3-(1,3-thiazol-2-ylsulfanyl)benzonitrile (113 mg, 0.42 mmol) in dichloromethane (8 mL) was cooled to 0 ^{o}C before portionwise addition of mCPBA (88 mg, 0.96 mmol). The resulting mixture was stirred at 0 ^{o}C for 1 hour, then warmed to room temperature and stirred for an additional 30 minutes. The reaction mixture was then treated with aqueous saturated sodium bicarbonate solution (20 mL). The organic layer was washed with aqueous saturated sodium bicarbonate (20 mL), and brine (2 x 20 mL), dried over magnesium sulphate, filtered and evaporated. The resulting solid was purified using flash column chromatography, eluting with 40% ethyl acetate/hexane to yield the title compound (89 mg, 76%). **^{1}H NMR ($CDCl_3$, 400 MHz):** δ 8.70-8.75 (m, 1H, Ar), 8.11-8.14 (m, 2H, 2 x Ar), 7.86 (d, J = 3.0 Hz, 1H, Ar), 7.63 (d, J = 3.0 Hz, 1H, Ar) **HRMS (ESI^{+}):** calculated for (ES^{+})($+H^{+}$): 279.9851 Found: 279.9856

Synthesis of 2-nitro-4-(1,3-thiazol-2-ylsulfanyl)benzonitrile

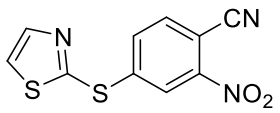

To a solution of 3-flouro-4-nitrobenzonitrile (200 mg , 1.2 mmol) and 2-mercapothiazole (155 mg, 1.3 mmol) in dimethylformamide (4.5 mL) was added potassium carbonate (499 mg, 3.6 mmol). The resulting suspension was heated to 60 ^{o}C and left to stir overnight. The mixture was then treated with aqueous saturated sodium bicarbonate solution (10 mL) before extraction with ethyl acetate (2 x 20 mL). The combined organic layers were washed with aqueous saturated sodium bicarbonate solution (20 mL) and brine (2 x 20 mL), dried over magnesium sulphate, filtered and evaporated. The resulting solid was purified by flash column chromatography, eluting with 40-50% ethyl acetate/hexane to yield the title compound (257 mg, 81%). **^{1}H NMR ($CDCl_3$, 400 MHz):** δ 8.29 (d, J = 2.0 Hz, 1H, Ar), 8.02 (d, J = 3.5 Hz, 1H, Ar), 7.83 (d, J = 8.0 Hz, 1H, Ar), 7.75 (d, J = 8.0 Hz, 2.0 Hz 1H, Ar), 7.63 (d, J = 8.5 Hz, 1H, Ar); **HRMS (ESI^{+}):** calculated for (ES^{+})($+H^{+}$): 263.9901 Found: 263.9899

Synthesis of 3-nitro-4-(1,3-thiazol-2-ylsulfinyl)benzonitrile (SHF1592)

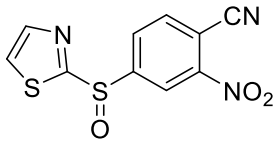

SHF1592

A solution of 2-nitro-4-(1,3-thiazol-2-ylsulfanyl)benzonitrile (210 mg, 0.80 mmol) in dichloromethane (16 mL) was cooled to 0 ^{o}C before portionwise addition of mCPBA (165 mg, 0.96 mmol). The resulting mixture was stirred at 0 ^{o}C for 1 hour, then warmed to room temperature and stirred for an additional 30 minutes. The reaction mixture was then treated with aqueous saturated sodium bicarbonate solution (20 mL). The organic layer was washed with aqueous saturated sodium bicarbonate (20 mL), and brine (2 x 20 mL), dried over magnesium sulphate, filtered and evaporated. The resulting solid was purified using flash column chromatography, eluting with 40% ethyl acetate/hexane to yield the title compound (150 mg, 57%). **^{1}H NMR ($CDCl_3$, 400 MHz):** δ 8.82 (d, J = 1.5 Hz, 1H, Ar), 8.32 (dd,

J = 8.0 Hz, 1.5 Hz, 1H, Ar), 8.10 (d, J = 8.0 Hz, 1H, Ar), 7.98 (d, J = 3.0 Hz, 1H, Ar), 7.70 (d, J = 3.0 Hz, 1H, Ar); **HRMS (ESI^+):** calculated for (ES^+)($+H^+$): 279.9851 Found: 279.9852

7.2 Biology

7.2.1 Tissue Culture

CHO-K1 cells overexpressing the CLR and RAMP2 proteins (AM_1 receptor) were cultured in T175 tissue culture flasks with F-12K Nut Mix supplemented with 10% Foetal Bovine Serum (FBS), 1% Penicillin/Streptomycin mix, Puromycin (2.5 µg/mL), Hygromycin B (300 µg/mL) and G418 (800 µg/mL), at 37 ^oC in a 5% CO_2 incubator. Cells were passaged at around 80% confluency and media was changed at least twice a week.

1321N1 cells overexpressing the CLR and RAMP1 proteins (CGRP receptor), and 1321N1 cells overexpressing the CLR and RAMP3 proteins (AM_2 receptor) were cultured in T175 tissue culture flasks with Dulbecco's Modified Eagle Medium supplemented with 10% FBS, 1% Penicillin/Streptomycin mix, Puromycin (2.5 µg/mL) and G418 (800 µg/mL), at 37 ^oC in a 5% CO_2 incubator. Cells were passaged at around 80% confluency and media was changed at least twice a week.

7.2.2 Cell Splitting

Cell media was discarded from the flasks and washed with 20 mL sterile phosphate buffered saline (PBS) and incubated with 5 mL 1x TrypLE Express Dissociation Enzyme for 10 minutes at 37 ^oC in a 5% CO_2 incubator until cells were detached from the flask. Cell detachment was aided with gentle agitation if necessary. 5 mL of PBS was then added to the flask and the cells were then spun at 1000 rpm for 4 minutes in a 15 mL tube. The supernatant was discarded and the cell pellets were suspended in warm growth medium. 1 mL of cell suspension was added to a new T175 flask containing 20 mL cell media.

7.2.3 Cell Counting and Freezing

Cells were detached from the flasks as stated above. 1 mL of cell suspension was then transferred to a 1.5 mL tube, and 10 µL of cell suspension was mixed with 10 µL 0.4% Trypan Blue Solution. The mixture was then placed into a Countess Chamber Slide and inserted into a Countess Automated Cell Counter. The mean number of cells was calculated from two cell

counts. Cells were frozen in a freezing media consisting of 5% DMSO in cell media, and were frozen in 1 mL aliquots of 2 million cells.

7.2.4 cAMP Assay: Peptide Stimulation in Overexpressing Cells

Serial Dilutions of the peptide ligand and forskolin were made in a 96-well plate in a stimulation buffer (see Table **7.1** for content). Final concentrations of peptides ranged from 1 µM to 0.01 nM (Table **7.2**). Serial dilutions of forskolin with a final concentration range of 100 µM to 1 nM were made for each cell line as a positive control. Blanks were made using Stimulation Buffer only to allow measurement of background signal (0% stimulation). Dilutions were transferred to a 384-well plate (2.5 µL/well) and the plate was spun at 1000 rpm for 1 minute.

Table 7.1 – Reagents used to form Stimulation Buffer and their respective volumes

Reagent	Volume*
Hanks Balanced Salt Solution (HBSS) (Ca^{2+}, Mg^{2+})	14 mL
1 M HEPES (4-(2-hydroxyethyl)-1-piperazineethanesulfonic acid)	75 µL
Stabilizer, 7.5% (BSA)	200 µL
250 mM IBMX (3-isobutyl-1-methylxanthine	30 µL

***This recipe will yield 15 mL of Stimulation Buffer**

Table 7.2 – Peptide ligand serial dilutions in Stimulation Buffer

Column	Initial Concentration	Final Concentration	Stimulation Buffer (µL)	Volume of Dilution
1	2×10^{-6}	1×10^{-6}	58	6 µL of 60 µM
2	6×10^{-7}	3×10^{-7}	70	30 µL of 1
3	2×10^{-7}	1×10^{-7}	60	30 µL of 2
4	6×10^{-8}	3×10^{-8}	70	30 µL of 3
5	2×10^{-8}	1×10^{-8}	60	30 µL of 4
6	6×10^{-9}	3×10^{-9}	70	30 µL of 5
7	2×10^{-9}	1×10^{-9}	60	30 µL of 6
8	6×10^{-10}	3×10^{-10}	70	30 µL of 7
9	2×10^{-10}	1×10^{-10}	60	30 µL of 8
10	6×10^{-11}	3×10^{-11}	70	30 µL of 9
11	$2 \times 10^{--11}$	$1 \times 10^{--11}$	60	30 µL of 10
12	0	0	70	-

1 mL aliquots of frozen cells overexpressing CGRP, AM_1 and AM_2 cells were thawed at 37 ^{o}C in a water bath for approximately 30 seconds. 1 mL of warm Stimulation Buffer was added to the cells and the resulting suspension was transferred to a 15 mL tube and spun at 1000 rpm for 4 minutes. The supernatant was then discarded and the cells were re-suspended in 1 mL warm PBS and spun at 1000 rpm for 4 minutes. The supernatant was discarded and the cells were re-suspended in 1 mL warm Stimulation Buffer. Cells were then counted as stated previously. Cells were subsequently diluted to 2500 cells/5 µL and were added to the 384-well plate. The plate was spun at 1000 rpm for 1 minute and then incubated at room temperature for 30 minutes.

A detection mix was made before addition to the plate. Solutions of Europium cAMP tracer and Ulight in cAMP Detection Buffer (PerkinElmer) were made separately (see Table **7.3** for volumes). The ULight solution was made in the dark and was covered with foil until use. 5 µL/well of each solution was added to the 384-well plate. The plate was then spun at 1000

rpm for 1 minute before incubation in the dark for 1 hour. After incubation, the plate was read using an Ensight multimode plate reader with settings according to Table **7.4**.

Table 7.3 – cAMP detection mix formulation

Reagent	Volumes
Eu cAMP Tracer	1 µL in 49 µL of cAMP Detection Buffer*
Ulight	1 µL in 149 µL of cAMP Detection Buffer**

***This recipe will yield 50 µL Eu cAMP Tracer Solution**

****** This recipe will yield 150 µL of Ulight**

Table 7.4 – Plate reader settings for the cAMP assay

Parameter	Instrument Setup
Excitation Filter	Lamp: 111 (UV2 320)
Emission	615 nm 665 nm
Delay Time	70 µs
Number of Flashes	100
Window Time	100 µs
Total Time	170 µs

7.2.5 cAMP Assay: Determination of Compound IC50 Value

20 mM stocks of compounds in DMSO were diluted stepwise, firstly to 10 mM in DMSO, then to 4 mM in Stimulation Buffer. Compounds were sonicated for 15 minutes after each dilution. 4 mM solutions were then diluted to 400 µM in Stimulation Buffer. 400 µM dilution was made in the first column of a 96-well plate. Serial dilutions of compounds were carried out in the 96-well plate according to Table **7.5**. The final concentrations of compounds in the assay ranged between 100 µM and 10 nM. Blank controls (0% agonist stimulation) and agonist controls (100% stimulation) were made using Stimulation Buffer in the absence of compounds. Compounds were then transferred to a 384-well plate using a high-speed liquid handling dispensation device (Freedom EVO 200, Tecan, Mannerdorf, Switzerland) (2.5 µL/well, 5 µL/well for blank controls) and the plate was spun at 1000 rpm for 1 minute.

Table 7.5 – Compound serial dilutions in Stimulation Buffer

Column	Initial Concentration	Final Concentration	Stimulation Buffer (µL)	Volume of Dilution
1	4×10^{-4}	1×10^{-4}	135	15 µL of 4 mM compound
2	1.2×10^{-4}	3×10^{-5}	140	60 µL of 1
3	4×10^{-5}	1×10^{-5}	120	60 µL of 2
4	1.2×10^{-5}	3×10^{-6}	140	60 µL of 3
5	4×10^{-6}	1×10^{-6}	120	60 µL of 4
6	4×10^{-7}	1×10^{-7}	135	15 µL of 5
7	4×10^{-8}	1×10^{-8}	135	15 µL of 6
8	0	0	135	-

For European Lead Factory compounds tested on CGRP and AM_2, 20 mM compound stocks were diluted to 2 mM in DMSO, and then to 400 µM in Stumulation Buffer. Compounds were sonicated for 15 minutes after each dilution. Compounds were then diluted to 40 µM in Stimulation Buffer in the first column of a 96-well plate. Serial dilutions were carried out according to Table **7.6** resulting in the final assay concentration of compounds ranging between 10 µM and 0.01 nM. Blank and ligand controls were made as described above, and the compounds and controls were transferred to a 384-well plate as described above.

Table 7.6 – Compound serial dilutions in Stimulation Buffer for European Lead Factory on CGRP and AM_2

Column	Initial Concentration	Final Concentration	Stimulation Buffer (µL)	Volume of Dilution
1	4×10^{-5}	1×10^{-5}	135	15 µL of 400 µM compound
2	4×10^{-6}	1×10^{-6}	135	15 µL of 1
3	4×10^{-7}	1×10^{-7}	135	15 µL of 2
4	4×10^{-8}	3×10^{-8}	135	15 µL of 3
5	4×10^{-9}	1×10^{-9}	135	15 µL of 4
6	4×10^{-10}	1×10^{-10}	135	15 µL of 5
7	4×10^{-11}	1×10^{-11}	135	15 µL of 6
8	0	0	135	-

Frozen cells were thawed, washed and counted as described above. Cells were diluted to 2500 cells/5 µL and added to the 384-well plate. The plate was spun at 1000 rpm for 1 minute and incubated at room temperature in the dark for 30 minutes.

The EC50 concentration of AM/ CGRP (determined from dose response experiments) was made in 1 mL Stimulation Buffer from a 2 µM stock. The peptide was then added to the compound and AM control columns of the 384-well plate (2.5 µL/well), and the plate was spun at 1000 rpm for 1 minute and incubated at room temperature in the dark for 20 minutes.

The detection mix was made in the dark as stated above. Eu solution (5 µL/well) and the Ulight solution (5 µL/well) were added separately to the 384-well plate. The plate was spun at 1000 rpm for 1 minute before incubation in the dark at room temperature for 1 hour. The plate was read using an Ensight multimode plate reader using the settings displayed in Table **7.4**.

7.2.6 Data Analysis

TR-FRET data was normalised to the 100% maximum agonist stimulation (wells containing agonist in the absence of compound) and 0% agonist stimulation (wells containing stimulation buffer only). Concentration-response curves were plotted using GraphPad Prism and IC50 values were calculated using a three-parameter non-linear regression inhibition curve.

7.3 Molecular Docking

All molecular docking studies were carried out using Maestro 13.2 (Schrodinger Software). The crystal structures of the AM_1 receptor ECD (3AQF), the Telcagepant-bound CGRP receptor ECD (3N7R) and the full length AM_2 receptor (6UUS) were obtained from the Protein Data Bank. The protein structures for CGRP, AM_1 and AM_2 receptors were prepared for docking using the Protein Preparation Wizard. For protein preparation, the structures were pre-processed to fix structural defects, cleaned up by adding missing hydrogen atoms and side chains, and hydrogen bonds were optimised at pH 7.4. Ligand structures were built using the 2D sketcher before minimisation with using LigPrep. The OPLS4 (Optimised Potential for Liquid Simulations) force field was used to generate the lowest energy conformations of the ligands, whilst all possible stereoisomers and ionisation states at pH 7.4 were generated.

For docking, a receptor grid was initially generated. The grid represents the region that a ligand can occupy during the initial stages of docking. A specific residue in the protein structures was chosen as the centroid of the grid. For the AM_1 receptor structure this was RAMP2 Arg97 and for the CGRP and AM_2 receptor structures the centroid residue was CLR Trp72. The grid was then expanded to cover the whole receptor ECD (20 A, 20 A, 20A). Docking was then carried out with GLIDE, using the generated receptor grids without the application of hydrogen bond constraints. Docked ligands were viewed in Maestro and a GLIDE docking score, a prediction of binding free energy of the docked ligand, for each pose was generated. The poses were visualised using using PyMol Molecular Graphics System, Version 1.7.4.5- Educational Product, Schrodinger.

For (), the Telcagepant-bound CGRP ECD structure, Telcagepant was initially docked into the CGRP receptor ECD for validation of docking procedure. The structures of the CGRP and Telcagepant were split into separate work-spaces and were prepared as stated above. The prepared Telcagepant ligand was then docked and visualised using the receptor grid created for 3N7R and the above procedure.

References

Aiyar, N., Daines, R. A., Disa, J., Chambers, P. A., Sauermelch, Quiniou, M., Khandoudi, N., Gout, B., Douglas, S. A., Willette, R. N. (2000). Pharmacology of SB-273779, A Nonpeptide Calcitonin Gene-Related Peptide 1 Antagonist. *JPET*. 296 768-775.

Aldewachi, H., Al-Zidan, R. N., Conner, M. T., Salman, M. M. (2021). High-Throughput Screening Platforms in the Discovery of Novel Drugs for Neurodegenerative Diseases. *Bioengineering (Basel)* 8(2).

Alexander, S. P. H., Christopoulos, A., Davenport, A. P., Kelly, E., Marrion, N. V., Peters, J. A., Faccenda, E., Harding, S. D., Pawson, A. J., Sharman, J. L., Southan, C., Davies, J. A. (2017). The Concise Guide to Pharmacology 2017-2018: G protein coupled receptors. *Br. J. Pharmacol.* 174 S17-S129.

Allacker, R. P., Zihni, C., and Kapas, S. (1999). An investigation into the antimicrobial effects of adrenomedullin on members of the skin, oral, respiratory tract and gut microflora. *FEMS Microbiol. Immunol.* 23 289-293.

Angus, D. C. and T. van der Poll (2013). Severe sepsis and septic shock. *N Engl J Med* 369(9) 840-851.

Archbold, J. K., Flanagan, J. U., Watkins, H. A., Gingell, J. J., Hay, D. L. (2011). Structural insights into RAMP modification of secretin family G protein-coupled receptors: implications for drug development. *Trends Pharmacol Sci* 32(10) 591-600.

Avgoustou, P., Jailani, A. B. A., Zirimwabagabo, J., Tozer, M. J., Gibson, K. R., Glossop, P. A., Mills, J. E. J., Porter, R. A., Blaney, P., Bungay, P. J., Wang, N., Shaw, A. P., Bigos, K. J. A., Holmes, J. L., Warrington, J. I., Skerry, T. M., Harrity, J. P. A., Richards, G. O. (2020). Discovery of a First-in-Class Potent Small Molecule Antagonist against the Adrenomedullin-2 Receptor. *ACS Pharmacol Transl Sci* 3(4) 706-719.

Barwell, J., Miller, P. S., Donelly, D., Poyner, D. R. (2010). Mapping interaction sites within the N-terminus of the calcitonin gene-related peptide receptor; the role of residues 23-60 of the calcitonin receptor-like receptor. *Peptides* 31(1) 170-176.

Bell, I. M. (2014). Calcitonin gene-related peptide receptor antagonists: new therapeutic agents for migraine. *J Med Chem* 57(19) 7838-7858.

Bell, I. M., Bednar, R. A., Corcoran, H. A., Fay, F. F., Gallicchio, S. N., Johnstone, V. K., Hershey, J. C., Miller-Stein, C. M., Moore, E. L., Mosser, S. D., Roller, S. A., Salvatore, C. A., Theberge, C. R., Wong, B.

K., Zartman, C. B., Kane, S. A., Williams, T. M., Graham, S. L., Vacca, J. P. (2009). The identification of potent, orally bioavailable tricyclic CGRP receptor antagonists. *Bioorg Med Chem Lett* 19(16) 4740-4742.

Bell, I. M., Bednar, R. A., Fay, F. F., Gallicchio, S. N., Hochman, J. H., McMasters, D. R., Miller-Stein, C., Moore, E. L., Mosser, S. D., Pudvah, N. T., Quigley, A. G., Salvatore, C. A., Stump, C. A., Theberge, C. R., Wong, B. K., Zartman, C. B, Zhang, X., Kane, S. A., Graham, S. L., Vacca, J. P., Williams, T. M. (2006). Identification of novel, orally bioavailable spirohydantoin CGRP receptor antagonists. *Bioorg Med Chem Lett* 16(24) 6165-6169.

Bell, I. M., Gallicchio, S. N., Wood, M. R., Quigley, A. G., Stump, C. A., Zartman, C. B., Fay, F. F., Li, C., Lynch, J. J., Moore, E. L., Mosser, S. D., Prueksaritanont, T, Regan, C. P., Roller, S., Salvatore, C. A., Kane, S. A., Vacca, J. P., Selnick, H. G. (2010). Discovery of MK-3207: A Highly Potent, Orally Bioavailable CGRP Receptor Antagonist. *ACS Med Chem Lett* 1(1) 24-29.

Beltowski, J. and Jammroz, A. (2004). Adrenomedullin – What do we know 10 years since it's discovery. *Pol. J. Pharmacol.* 56 5-27.

Booe, J. M., Walker, C. S., Barwell, J., Kuteyi, G., Simms, J., Jamaluddin, M. A., Warner, M. L., Bill, R. M., Harris, P. W., Brimble, M. A, Poyner, D. R., Hay, D. L., Pioszak, A. A. (2015). Structural Basis for Receptor Activity-Modifying Protein-Dependent Selective Peptide Recognition by a G Protein-Coupled Receptor. *Mol Cell* 58(6) 1040-1052.

Booe, J. M., Warner, M. L., Roehrkasse, A. M., Hay, D. L., Pioszak, A. A. (2018) Probing the Mechanism of Receptor Activity-Modifying Protein Modulation of GPCR Ligand Selectivity through Rational Design of Potent Adrenomedullin and Calcitonin Gene-Related Peptide Antagonists. *Mol Pharmacol* 93(4) 355-367.

Burgey, C. S., Stump, C. A., Nguyen, D. N., Deng, J. Z., Quigley, A. G., Norton, B. R., Bell, I. M., Mosser, S. D., Salvatore, C. A., Rutledge, R. Z., Kane, S. A., Koblan, K. S., Vecca, J. P., Graham, S. L., Williams, T. M. (2006). Benzodiazepine calcitonin gene-related peptide (CGRP) receptor antagonists: optimization of the 4-substituted piperidine. *Bioorg Med Chem Lett* 16(19) 5052-5056.

Christopoulos, A., Christopoulos, G., Morfis, M., Udawela, M., Laburthe, M., Couvineau, A., Kuwasako, K., Telakaratne, N., Sexton, P. M. (2003). Novel receptor partners and function of receptor activity-modifying proteins. *J Biol Chem* 278(5) 3293-3297.

Dackor, R. T., Fritz-Six, S., Dunworth, W. P., Gibbons, C. L., Smithies, O., Caron, M. K. (2006). Hydrops fetalis, cardiovascular defects, and embryonic lethality in mice lacking the calcitonin receptor-like receptor gene. *Mol Cell Biol* 26(7) 2511-2518.

Daines R. A., Chambers P. A., *Preparation of 4-sulfinyl benzamides as calcitonin gene-related peptide antagonists*, 1998, WO9856779

Doods, H., Hallermeyer, G., Wu, D., Entzeroth, M., Rudolf, K., Engel, W., Eberlein, W. (2000) Pharmacological profile of BIBN4096BS, the first selective small molecule CGRP antagonist. *Br. J. Pharmacol.* 129 420-423.

Dubowchik, G. M., C. M. Conway and A. W. Xin (2020). Blocking the CGRP Pathway for Acute and Preventive Treatment of Migraine: The Evolution of Success. *J Med Chem* 63(13) 6600-6623.

Eguchi, S., Hirata, Y., Kano, H., Sato, K., Watanabe, Y., Watanabe, T. X., Nakajima, K., Sakakibara, S., Marumo, F. (1994). Specific receptors for adrenomedullin in cultured rat vascular smooth muscle cells. *FEBS Lett* 340(3) 226-230.

Fredriksson, R., Lagerstrom, C., Lundin, L., Schioth, H. (2003). The G-Protein-Coupled-Receptors in the Human Genome Form Five Main Families. Phylogenetic Analysis, Paralogon Groups and Fingerprints. *Mol. Pharmacol.* 63 (6) 1256-1272.

Garayoa, M., Martinez, A., Lee, S., Pio, R., An, W. G., Neckers, L., Trepel, J., Montuenga, L. M., Ryan, H., Johnson, R., Gassmann, M., Cuttitta, F. (2000). Hypoxia-Indicible Factor-1 (HIF-1) Up-Regulates Adrenomedullin Expression in Human Tumour Cell Lines during Oxygen Deprivation: A Possible Promotion Mechanism of Carcinogenesis. *Mol. Endocrinol.* 14(6) 848-862.

Geven, C., M. Kox and P. Pickkers (2018). Adrenomedullin and Adrenomedullin-Targeted Therapy As Treatment Strategies Relevant for Sepsis. *Front Immunol* 9 292.

Gibbons, C., Dackor, R., Dunworth, W., Fritz-Six, K., Caron, K. M. (2007). Receptor Activity-Modifying Proteins: RAMPing up Adrenomedullin Signalling. *Mol. Endocrinol*. 21(4) 783-796.

Gotts, J. E. and M. A. Matthay (2016). Sepsis: pathophysiology and clinical management. *BMJ* 353 i1585.

Golla, R. and Ramakrishna, S. (2002). A Homogeneous Enzyme Fragment Complementation Cyclic AMP Screen for GPCR Agonists. *J. Biomol. Screen.* 7(6) 515-525.

Gurevich, V. V. and E. V. Gurevich (2019). GPCR Signaling Regulation: The Role of GRKs and Arrestins. *Front Pharmacol* 10 125.

Hansen, J. M., Werner Hague, A., Olesen, J., Ashina, M. (2010). Calcitonin gene-related peptide triggers migraine-like attacks in patients with migraine with aura. *Cephalalgia* 30(10) 1179-1186.

Hargreaves, R. and Olesen, J. (2019). Calcitonin Gene-Related Peptide Modulators – The History and Renaissance of a New Migraine Drug Class. *Headache Currents*. 1-20.

Harikumar, K. G., Simms, J., Christopoulos, G., Sexton, P. M., Miller, L. J. (2009). Molecular basis of association of receptor activity-modifying protein 3 with the family B G protein-coupled secretin receptor. *Biochemistry* 48(49) 11773-11785.

Hauser, A. S. (2017). Trends in GPCR drug discovery: new agents, targets and indications. *Nat. Rev. Drug Discov.* 16 829-842.

Hay, D. L., Walker, C. S., and Poyner, D. R. (2011). Adrenomedullin and calcitonin gene-related peptide receptors in endocrine-related cancers: opportunities and challenges. *Endorc. Relat. Cancer.* 18 C1-C14.

Hay, D. L., Garelja, M. L., Poyner, D. R., Walker, C. S. (2018). Update on the pharmacology of calcitonin/CGRP family of peptides: IUPHAR Review 25. *Br J Pharmacol* 175(1) 3-17.

Hay, D. L. and A. A. Pioszak (2016). Receptor Activity-Modifying Proteins (RAMPs): New Insights and Roles. *Annu Rev Pharmacol Toxicol* 56 469-487.

Hoare, S. R. (2005). Mechanisms of peptide and nonpeptide ligand binding to Class B G-protein-coupled receptors. *Drug Discov Today* 10(6) 417-427.

Hyvelin, J., Shan, Q., Bourreau, J. (2001). Adrenomedullin: A Cardiac Depressant Factor in Septic Shock. *J Card Surg.* 17 328-335.

Ince, C., Mayeux, P. R., Nguyen, T., Gomez, H., Kellum, J. A., Ospina-Tascon, G. A., Hernandez, G., Murray, P., De Backer, D. (2016). The Endothelium in Sepsis. *Shock* 45(3) 259-270.

Ishikawa, T., Chen, J., Wang, J., Okada, F., Sugiyama, T., Kobayashi, T., Shindo, M., Higashino, F., Katoh, H., Asaka, M., Kondo, T., Hosokawa, M., Kobayashi, M. (2003). Adrenomedullin antagonist surpresses *in vivo* growth of human pancreatic cancer cells in SCID mice by surpressing angiogenesis. *Oncogene*. 22 1238-1242.

Ishimitsu, T., Kojima, M., Kangawa, K., Hino, J., Matsuoka, H., Kitamura, K., Eto, T., Matsuo, H. (1994). Genomic Structure of the Human Adrenomedullin Gene. *Biochem Biophys Res Comun.* 203 (1) 631-639.

Isumi, Y., Kubo, A., Katafuchi, T., Kangawa, K., Minamino, M. (1999). Adrenomedullin surpresses interleukin-1β-induced tumour necrosis factor-α production in Swiss 3T3 cells. *FEBS. Lett.* 463 110-114.

Kasibhalta, S., Gourdeau, H., Meerovitch, K., Drewe, J., Reddy, S., Qiu, L., Zhang, H., Bergeron, F., Bouffard, D., Yang, Q., Herich, J., Lamothe, S., Cai, S. X., Tseng, B. (2004). Discovery and mechanism of action of a novel series of apoptosis inducers with potential vascular targeting activity. *Mol. Cancer. Ther.* 3(11) 1365-1373.

Kitaruma, K., Kangawa, K., Kawamoto, M., Ichiki, Y., Nakamura, S., Matsuo, H., Eto, T. (1993). Adrenomedullin: A Novel Hypotensive Peptide Isolated From Human Pheochromocytoma. *Biochem Biophys Res Comun*. 192 553-560

Kusano, S., Kukimoto-Niino, M., Akasaka, R., Toyama, M., Terada, T., Shirouzu, M., Shindo, T., Yokoyama, S. (2008). Crystal structure of the human receptor activity-modifying protein 1 extracellular domain. *Protein Sci* 17(11) 1907-1914.

Kusano, S., Kukimoto-Niino, M., Hino, N., Oshawa, N., Okuda, K, Sakamoto, K., Shirouzu, M., Shindo, T., Yokoyama, S. (2012). Structural basis for extracellular interactions between calcitonin receptor-like receptor and receptor activity-modifying protein 2 for adrenomedullin-specific binding. *Protein Sci* 21(2) 199-210.

Kuwasako, K., Kitamura, K., Ito, K., Uemura, T., Yanagita, Y., Kato, J., Sakata, T., Eto, T. (2001). The seven amino acids of human RAMP2 (86) and RAMP3 (59) are critical for agonist binding to human adrenomedullin receptors. *J Biol Chem* 276(52) 49459-49465.

Kuwasako, K., Kitamura, K., Nagata, S., Kato, J. (2008). Functions of the extracellular histidine residues of receptor activity-modifying proteins vary within adrenomedullin receptors. *Biochem Biophys Res Commun* 377(1) 109-113.

Kuwasako, K., Kitamura, K., Nagoshi, Y., Cao, Y., Eto, T. (2003). Identification of the human receptor activity-modifying protein 1 domains responsible for agonist binding specificity. *J Biol Chem* 278(25) 22623-22630.

Lagerstrom, M. C. and Schioth, H. B. (2008). Structural diversity of G protein-coupled receptors and significance for drug discovery. *Nat. Rev. Drug Discov*. 7 339-357.

Lainchbury, J. G., Troughton, R. W., Lewis, L. K., Yandle, T. G., Richards, A. M., Nicholls, M. G. (2000). Hemodynamic, Hormonal, and Renal Effects of ShortTerm Adrenomedullin Infusion in Healthy Volunteers. *J. Clin. Endocrinol. Metab.* 85 1016-1020.

Lenhart, P. M. and K. M. Caron (2012). Adrenomedullin and pregnancy: perspectives from animal models to humans. *Trends Endocrinol Metab* 23(10) 524-532.

Liang, Y. L., Belousoff, M. J., Fletcher, M. M., Zhang, X., Koshouei, M., Deganutti, G., Koole, C., Furness, S. G. B., Miller, L. J., Hay, D. L., Christopoulos, A., Reynolds, C. A., Danev, R., Wootten, D., Sexton, P. M. (2020). Structure and Dynamics of Adrenomedullin Receptors AM(1) and AM(2) Reveal Key Mechanisms in the Control of Receptor Phenotype by Receptor Activity-Modifying Proteins. *ACS Pharmacol Transl Sci* 3(2) 263-284.

Liang, Y. L., Koshouei, M., Deganutti, G., Glukhova, A., Koole, C., Peat, T. S., Radjainia, M., Plitzko, J. M., Baumeister, W., Miller, L. J., Hay, D. L., Christopoulos, A., Reynolds, C. A., Wotten, D., Sexton, P. M. (2018). Cryo-EM structure of the active, G(s)-protein complexed, human CGRP receptor. *Nature* 561(7724) 492-497.

Lipinski, A. C., Lombardo, F., Dominy, B. W., Feeney, P. J. (1997). Experimental and computational approaches to estimate solubility and permeability in drug discovery and development settings. *Adv. Drug Deliv. Rev.* 23 3-25.

Liu, R., X. Li and K. S. Lam (2017). Combinatorial chemistry in drug discovery. *Curr Opin Chem Biol* 38 117-126.

Mallee, J. J., Salvatore, C. A., LeBourdelles, B., Oliver, K. R., Longmore, J., Koblan, K. S., Kane, S. A. (2002). Receptor activity-modifying protein 1 determines the species selectivity of non-peptide CGRP receptor antagonists. *J Biol Chem* 277(16) 14294-14298.

Martis, E. A., Radhakrishnan, R. and Badve, R. R. (2011). High-Throughput Screening: The Hits and Leads of Drug Discovery - An overview. *J. Appl. Pharm. Sci.* 1(1) 2-10.

McLachtie, L. M. et al (1996). RAMPs regulate the transport of and ligand specificity of the calcitonin-receptor-like-receptor. *Nature*. 393 (6683) 333-339.

Michelini, E., Cevenini, L., Mezzanotte, L., Coppa, A., Roda, A. (2010). Cell-based assays: fuelling drug discovery. *Anal Bioanal Chem* 398(1) 227-238.

Miller, P. S., Barwell, J., Poyner, D. R., Wigglesworth, M. J., Garland, S. L., Donnelly, D. (2010). Non-peptidic antagonists of the CGRP receptor, BIBN4096BS and MK-0974, interact with the calcitonin receptor-like receptor via methionine-42 and RAMP1 via tryptophan-74. *Biochem Biophys Res Commun* 391(1) 437-442.

Moad, H. E. and A. A. Pioszak (2013). Selective CGRP and adrenomedullin peptide binding by tethered RAMP-calcitonin receptor-like receptor extracellular domain fusion proteins. *Protein Sci* 22(12) 1775-1785.

Moore, E. L., Burgey, C. S., Panone, D. V., Shaw, A. W., Tang, Y. S., Kane, S. A., Salvatore, C. A. (2009). Examining the binding properties of MK-0974: a CGRP receptor antagonist for the acute treatment of migraine. *Eur J Pharmacol* 602(2-3) 250-254.

Moore, E. L., Gingell, J. J., Kane, S. A., Hay, D. L., Salvatore, C. A. (2010). Mapping the CGRP receptor ligand binding domain: tryptophan-84 of RAMP1 is critical for agonist and antagonist binding. *Biochem Biophys Res Commun* 394(1) 141-145.

Moore, E. L. and C. A. Salvatore (2012). Targeting a family B GPCR/RAMP receptor complex: CGRP receptor antagonists and migraine. *Br J Pharmacol* 166(1) 66-78.

Nagatomo, Y., Kitamura, K., Kangawa, K., Fujimoto, Y., Eto, T. (1996) Proadrenomedullin N-Terminal 20 Peptide is Rapidly Cleaved by Neutral Endopeptidase. *Biochem Biophys Res Commun* 223 539-543

Norskov-Lauritsen, L., A. R. Thomsen and H. Brauner-Osborne (2014). G protein-coupled receptor signaling analysis using homogenous time-resolved Forster resonance energy transfer (HTRF(R)) technology. *Int J Mol Sci* 15(2) 2554-2572.

Olesen, J., Diener, H., Husstedt, I. W., Goadsby, P. J., Hall, D., Meier, U., Pollentier, S., Lesko, L. M. (2004). Calcitonin Gene–Related Peptide Receptor Antagonist BIBN 4096 BS for the Acute Treatment of Migraine. *N. Engl. J. Med.* 350 (11) 1104-1110.

Panone. D. V., Shaw, A. W., Nguyen, D. N., Burgey, C. S., Deng, J. Z., Kane, S. A., Koblan, K. S., Salvatore, C. A., Mosser, S. D., Johnston, V. K., Wong, B. K., Miller-Stein, C. M., Hershey, J. C., Graham, S. L., Vacca, J. P., Williams, T. M. (2007). Potent, Orally Bioavailable Calcitonin Gene-Related Peptide Receptor Antagonists for the Treatment of Migraine: Discovery of *N*-[(3*R*,6*S*)-6-(2,3-Difluorophenyl)-2-oxo-1 (2,2,2-trifluoroethyl)azepan-3-yl]-4-(2-oxo-2,3-dihydro-1*H*-imidazo[4,5-*b*]pyridin-
1-yl)piperidine-1-carboxamide (MK-0974). *J. Med. Chem.* 50 5564-5567

Paone, D. V., Nguyen, D. N., Shaw, A. W., Burgey, C. S., Potteiger, C. M., Deng, J. Z., Mosser, S. D., Salvatore, C. A., Yu, S., Roller, S., Kane, S. A., Selnick, H. G., Vacca, J. P., Williams, T. M. (2011). Orally bioavailable imidazoazepanes as calcitonin gene-related peptide (CGRP) receptor antagonists: discovery of MK-2918. *Bioorg Med Chem Lett* 21(9) 2683-2686.

Passaglia, P., Gonzaga, N. A., Tirapelli, D. P. C., Tirapelli, L. F., Tirapelli, C. R. (2014). Pharmacological characterisation of the mechanisms underlying the relaxant effect of adrenomedullin in the rat carotid artery. *J Pharm Pharmacol* 66(12) 1734-1746.

Poyner, D. R., Sexton, P. M., Marshall, I., Smith, D. M., Quirion, R., Born, W., Muff, R., Fischer, J. A., Foord, S. M. (2002). International Union of Pharmacology. XXXII. The Mammalian Calcitonin Gene-Related Peptides, Adrenomedullin, Amylin, and Calcitonin Receptors. *Pharmacol. Rev.* 54 (2) 233-246.

Prystay, L., Gagne, A., Kasila, P, Yeh, L., Banks, P. (2001). Homogeneous cell-based fluorescence polarization assay for the direct detection of cAMP. *J Biomol Screen* 6(2) 75-82.

Qi, T. and D. L. Hay (2010). Structure-function relationships of the N-terminus of receptor activity-modifying proteins. *Br J Pharmacol* 159(5) 1059-1068.

Roller, S., Cui, D., Laspina, C., Miller-Stein, C., Rowe, J., Wong, B, Preuksaritanont. (2009). Preclinical pharmacokinetics of MK-0974, an orally active calcitonin gene-related peptide (CGRP)-receptor antagonist, mechanism of dose dependancy and species differences. *Xenobiotica*. 39(1) 33-45.

Rudolph, K., Eberlein, W., Engel, W, Pieper, H., Entzeroth, M., Hallermeyer, G., Doods, H. (2005). Development of Human Calcitonin Gene-Related Peptide (CGRP) Receptor Antagonists. 1. Potent and Selective Small Molecule CGRP Antagonists. 1-[*N*2-[3,5-Dibromo-*N*-[[4-(3,4-dihydro-2(1*H*)-oxoquinazolin-3-yl)-1-piperidinyl]carbonyl]-D-tyrosyl]-L-lysyl]-4-(4-pyridinyl)piperazine: The First CGRP Antagonist for Clinical Trials in Acute Migraine. *J. Med. Chem.* 48 5921-5931.

Salvatore, C. A., Hershey, J. C., Corcoran, H. A., Fay, J. F., Johnston, V. K., Moore, E. L., Mosser, S. D., Burgey, C. S., Panone, D. V., Shaw, A. W., Graham, S. L., Vacca, J. P., Williams, T. M., Koblan, K. S., Kane, S. A. (2008). Pharmacological Characterisation of MK-0972 [*N*-[(3*R*,6*S*)-6-(2,3-Difluorophenyl)-2-oxo-1-(2,2,2-trifluoroethyl)azepan-3-yl]-4-(2-oxo-2,3-dihydro-1*H*-imidazo[4,5-b]pyridin-1-yl)piperidine-1-carboxamide], a Potent and Orally Active Calcitonin Gene-Related Peptide Antagonist for the Treatment of Migrane. *JPET*. 324 (2) 416-421.

Schindler, M. and Doods, H. N. (2002). Binding properties of the novel, non-peptide CGRP receptor antagonist radioligand, [^{3}H]BIBN4096BS. *Eur. J. Pharmacol.* 442 187-193.

Shaw, A. W., Panone, D. V., Nguyen, D. M., Stump, C. A., Burgey, C. S., Mosser, S. D., Salvatore, C. A., Rutledge, R. Z., Kane, S. A., Koblan, K. S., Graham, S. L., Vacca, J. P., Williams, T. M. (2007). Caprolactams as potent CGRP receptor antagonists for the treatment of migrane. *Bioorg Med Chem Lett.* 17 4795-4798.

Shimekake, Y., Nagata, K., Ohta, S., Kambayashi, Y., Teraoka, H., Kitamura, K., Eto, T., Kangawa, K., Matsuo, H. (1995). Adrenomedullin Stimulates Two Signal Transduction Pathways, cAMP Accumulation and Ca2 + Mobilization, in Bovine Aortic Endothelial Cells. *J Biol Chem*. 270 (9) 4412-4417.

Simms, J., Hay, D. L., Wheatley, M., Poyner, D. R. (2006). Characterization of the structure of RAMP1 by mutagenesis and molecular modeling. *Biophys J* 91(2) 662-669.

Singer, M., Deutschman, C. S., Seymour, C. W., Shankar-Hari, M., Annane, D., Bauer, M., Bellomo, R., Bernard, G. R., Chiche, J., Coopersmith, C. M., Hotchkiss, R. S., Levy, M. M., Marshall, J. C., Martin, G. S., Opal, S. M., Rubenfeld, G. D., van der Poll, T., Vincent, J., Angus, D. C. (2016). The Third International Consensus Definitions for Sepsis and Septic Shock (Sepsis-3). *JAMA* 315(8) 801-810.

Stump, C. A., Bell, I. M., Bednar, R. A., Bruno, J. G., Fay, J. F., Gallichio, S. N., Johnston, V. K., Moore, E. L., Mosser, S. D., Quigley, A. G., Salvatore, C. A., Theberge, C. R., Blair Zartman, C., Zhang, X., Kane, S. A., Graham, S. L., Vecca, J. P., Williams, T. M. (2009). The discovery of highly potent CGRP receptor antagonists. *Bioorg Med Chem Lett* 19(1) 214-217.

Syrovatkina, V., Alegre, K. O., Dey, R., Huang, X. (2016). Regulation, Signaling, and Physiological Functions of G-Proteins. *J Mol Biol* 428(19) 3850-3868.

Szymanski, P., M. Markowicz and E. Mikiciuk-Olasik (2012). Adaptation of high-throughput screening in drug discovery-toxicological screening tests. *Int J Mol Sci* 13(1) 427-452.

Talele, T. T. (2020). Acetylene Group, Friend or Foe in Medicinal Chemistry. *J Med Chem* 63(11) 5625-5663.

Tegtmeier F., Walter U., Schinzel R., Wingler K., Scheurer P., Schmidt H., Preparation of compounds containing a N-heteroaryl moiety linked to fused ring moieties for the inhibition of NAD(P)H oxidases and platelet activation, 2005, WO2005111041

ter Haar, E., Koth, C. M., Abdul-Manan, N., Swenson, L., Coll, J. T., Lippke, J. A., Lepre, C. A., Garcia-Guzman, M., Moore, J. M. (2010). Crystal structure of the ectodomain complex of the CGRP receptor, a class-B GPCR, reveals the site of drug antagonism. *Structure* 18(9) 1083-1093.

Tsuruda, T., Kato, J., Kitamura, K., Kawamoto, M., Kuwasako, K., Imamura, T., Koiwaya, Y., Tsuji, T., Kangawa, K., Eto, T. (1999). An autocrine or a paracrine role of adrenomedullin in modulating cardiac fibroblast growth. *Cardiovasc. Res.* 43 958-967.

Tuteja, N. (2009). Signaling through G protein coupled receptors. *Plant Signal Behav* 4(10) 942-947.

Veber, D. F., Johnson, S. R., Cheng, H., Smith, B. R., Ward, K. W., Kopple, K. D. (2002). Molecular Properties That Influence the Oral Bioavailability of Drug Candidates. *J. Med. Chem.* 45(12) 2615-2623.

Wang, P., Ba, Z. F., Cioffi, W. G., Bland, K. I., Chaudry, I. H. (1998). The Pivatol Role in Adrenomedullin in Producing Hyperdynamic Circulation During the Early Stages of Septci Shock. *Arch Surg.* 133 1298-1304.

Watkins, H. A., Walker, C. S., Ly, K. N., Bailey, R. J., Barwell, J., Poyner, D. R., Hay, D. L. (2014). Receptor activity-modifying protein-dependent effects of mutations in the calcitonin receptor-like receptor: implications for adrenomedullin and calcitonin gene-related peptide pharmacology. *Br J Pharmacol* 171(3) 772-788.

Weston, C., Lu, J., Li, N., Barkan, K., Richards, G. O., Roberts, D. J., Skerry, T. M., Poyner, D., Pardamwar, M., Reynolds, C. A., Dowell, S. J., Willars, G. B., Ladds, G. (2015). Modulation of Glucagon Receptor Pharmacology by Receptor Activity-modifying Protein-2 (RAMP2). *J Biol Chem* 290(38) 23009-23022.

Weston, C., Winfield, I., Harris, M., Hodgson, R., Shah, A., Dowell, S. J., Mobarec, J. C., Woodlock, D. A., Reynolds, C. A., Poyner, D. R., Watkins, H. A., Ladds, G. (2016). Receptor Activity-modifying Protein-directed G Protein Signaling Specificity for the Calcitonin Gene-related Peptide Family of Receptors. *J Biol Chem* 291(42) 21925-21944.

Williams, T. M., Stump, C. A., Nguyen, D. N., Quigley, A. G., Bell, I. M., Gallicchio, S. N., Blair Zartman, C., Wan, B., Della Penna, K., Kunapuli, P., Kane, S. A., Koblan, K. S., Mosser, S. D., Rutledge, R. Z., Salvatore, C., Fay, J. F., Vacca, J. P., Graham, S. L. (2006). Non-peptide calcitonin gene-related peptide receptor antagonists from a benzodiazepinone lead. *Bioorg Med Chem Lett* 16(10) 2595-2598.

Wood, M. R., Schirripa, K. M., Kim, J. J., Quigley, A. G., Stump, C. A., Bell, I. M., Bednar, R. A., Fay, J. F., Bruno, J. G., Moore, E. L., Mosser, S. D., Roller, S., Salvatore, C. A., Kane, S. A., Vacca, J. P., Selnick, H. G. (2009). Novel CGRP receptor antagonists through a design strategy of target simplification with addition of molecular flexibility. *Bioorg Med Chem Lett* 19(19) 5787-5790.

Wootten, D., Lindmark, H., Kadmiel, M., Willcockson, H., Caron, K. M., Barwell, J., Drmota, T., Poyner, D. R., (2013). Receptor activity modifying proteins (RAMPs) interact with the VPAC2 receptor and CRF1 receptors and modulate their function. *Br J Pharmacol* 168(4) 822-834.

Wu, V., Yeerna, H., Nohata, N., Chiou, J., Harismendy, O., Raimondi, F., Inoue, A., Russell, R. B., Tamayo, P., Silvio Gutkind, J. (2019). Illuminating the Onco-GPCRome: Novel G protein-coupled receptor-driven oncocrine networks and targets for cancer immunotherapy. *J Biol Chem* 294(29) 11062-11086.

Yasi, E. A., N. S. Kruyer and P. Peralta-Yahya (2020). Advances in G protein-coupled receptor high-throughput screening. *Curr Opin Biotechnol* 64 210-217.

Yoshimoto, R., Mitsui-Saito, M., Ozaki, H., Karaki, H. (1998). Effects of adrenomedullin and calcitonin gene-related peptide on contractions of the rat aorta and porcine coronary artery. *Br J Pharmacol* 123(8) 1645-1654.

Zhang, J. H., Guan, N., Li, T., Mais, D. E., Wang, M. (1999). A simple statistical parameter for use in evaluation and validation of high-throughput screening assays. *J. Biomol. Screen.* 4 67-73.

Zirimwabagabo, J. O., Jailani, A. B. A., Avgoustou, P., Tozer, M. J., Gibson, K. R., Glossop, P. A., Mills, J. E. J., Porter, R. A., Blaney, P., Wang, N., Skerry, T. M., Richards, G. O., Harrity, J. P. A. (2021). Discovery of a First-In-Class Small Molecule Antagonist against the Adrenomedullin-2 Receptor: Structure-Activity Relationships and Optimization. *J Med Chem* 64(6) 3299-3319.